

UNIVERSITY OF SOUTHAMPTON
Faculty of Natural and Environmental Sciences

**The Regulatory Mechanisms Controlling Zinc
Content in Wheat**

by

Nicholas Philip Evens

Thesis for the degree of Doctor of Philosophy

January 2017

UNIVERSITY OF SOUTHAMPTON

ABSTRACT

FACULTY OF NATURAL AND ENVIRONMENTAL SCIENCES

Biological Sciences

Doctor of Philosophy

THE REGULATORY MECHANISMS CONTROLLING ZINC CONTENT IN
WHEAT

By Nicholas Philip Evens

Cereals such as wheat serve as staples for a large proportion of the world's population. However, they contain relatively low concentrations of essential micronutrients such as zinc (Zn) in their edible tissues. This is a major issue for human nutrition and food security.

The process of Zn uptake and partitioning in plants is highly controlled, with systems present for sensing and responding to Zn status. In the model plant, *Arabidopsis thaliana*, two transcription factors, bZIP19 and bZIP23, are thought to act as Zn sensors mediating the increased expression of Zn membrane transporters, ZIPs (Zrt/Irt-like proteins), in response to low Zn status. In this thesis the identification and characterisation of homologous *bZIP* transcription factors and *ZIP* transporters in wheat are described. *TabZIP* sequence analysis confirmed the presence of motifs characteristic to the F-group of bZIP transcription factors. Expression of these wheat bZIPs in an *Atbzip19 bzip23* line showed a conservation of function between the *Arabidopsis* and wheat group F bZIPs.

A key question is whether the wheat bZIP transcription factors and ZIP transporters are regulated by Zn. Gene-expression analysis indicated that the wheat transcription factors *TabZIP1, 3a, 3b, 4 & 5*, and the wheat ZIP transporters, *TaZIP1, 4, 5, 6 & 7* are induced by Zn-deficient conditions. The Zn-transport capability of *TaZIP1, 5, 6, 7 & 8* was confirmed using heterologous yeast expression. Additionally, the binding ability of TabZIPs to regulatory-elements in the promoters of *TaZIPs* was demonstrated. This links TabZIPs and TaZIPs in the Zn-regulatory mechanism of wheat.

This research has identified key genes involved in the regulation, uptake and distribution of Zn in wheat. The molecular mechanisms elucidated will be important in the development of Zn biofortified wheat varieties as well as cultivars which maintain high yield in Zn-deficient conditions. These may prove vital in achieving global food security.

Table of Contents

List of Figures	vii
List of Tables	xi
Acknowledgements	xv
Abbreviations	xvii
Chapter 1. Introduction.....	1
1.1 Micronutrient malnutrition.....	1
1.2 The importance of Zn.....	5
1.2.1 Plant Zn nutrition	6
1.2.2 Human Zn nutrition.....	9
1.3 Solutions to combat Zn deficiency.....	11
1.3.1 Dietary supplementation/fortification/diversification	11
1.3.2 Agronomic biofortification	12
1.3.3 Genetic biofortification	13
1.4 An overview of Zn transport from soil to grain	15
1.4.1 Zn uptake from the soil	15
1.4.2 Root epidermis to xylem	21
1.4.3 Loading of phloem	24
1.4.4 Additional factors involved in Zn transport	26
1.4.5 Loading and distribution of Zn in grain	32
1.5 Micronutrient homeostasis/regulation.....	35
1.5.1 Fe homeostasis	36
1.5.2 Zn homeostasis.....	38
1.6 Aims of the project.....	41
Chapter 2. Materials and methods	43
2.1 Plant material and growth	43
2.1.1 Wheat (<i>Triticum aestivum</i>) hydroponic growth	43
2.1.2 <i>Arabidopsis thaliana</i> growth.....	44
2.2 Bioinformatics.....	45
2.2.1 Sequence search strategies	45
2.2.2 Oligonucleotide primer design.....	45
2.3 Molecular biology techniques	49
2.3.1 RNA extraction	49
2.3.2 cDNA synthesis	50
2.3.2 Polymerase Chain Reaction (PCR) amplification of DNA	50
2.3.3 Gel electrophoresis.....	51
2.3.4 Colony PCR	51
2.3.5 Restriction enzyme digestion	52
2.3.6 Sequence analysis	52
2.3.7 Real-time PCR	53
2.4 <i>T. aestivum</i> gene cloning.....	54
2.4.1 Directional TOPO cloning into Gateway Entry Vector	54
2.4.2 Construction of <i>A. thaliana</i> expression vectors	55
2.4.3 pGEM-T Easy cloning	56
2.4.4 Construction of <i>Saccharomyces cerevisiae</i> expression vectors	57

2.5 Transformation and expression of <i>TaZIPs</i> in yeast mutant strains (Chapter 4)	58
2.5.1 <i>S. cerevisiae</i> strains.....	58
2.5.2 <i>S. cerevisiae</i> growth, transformation and drop spot assays	59
2.6 Transformation and expression of <i>TabZIPs</i> in <i>A. thaliana</i> (Chapter 5)	61
2.6.1 Agrobacterium transformation	61
2.6.2 <i>A. thaliana</i> transformation.....	62
2.6.3 Selection of positive transformants	62
2.6.4 Segregation ratio analyses and identification of T3 homozygous lines.....	63
2.6.5 Zn-deficiency phenotype studies of <i>TabZIP</i> transformed <i>A. thaliana</i> lines	63
2.7 Electrophoretic mobility shift assays (Chapter 5)	64
2.7.1 Amplification of PCR-generated <i>bZIP</i> templates.....	64
2.7.2 Coupled transcription/translation of <i>bZIPs</i>	64
2.7.3 Design and annealing of complementary labelled ZDRE probes.....	64
2.7.4 EMSA binding assay	65
2.8 Field sampling (Chapter 6).....	66
2.8.1 WISP donor trial.....	66
2.8.2 Paragon x WC239 mapping population.....	66
2.8.3 QTL analysis	67
2.9 ICP-OES analysis	67
2.10 Statistical analysis	67
Chapter 3. Identification of <i>T. aestivum ZIP</i> and <i>bZIP</i> genes and their spatiotemporal expression responses to Zn-deficiency	69
3.1 Introduction	69
3.1.1 The <i>ZIP</i> transporter family	69
3.1.2 The importance of <i>bZIP</i> transcription factors in Zn-homeostasis	70
3.1.3 The use of hydroponic culture methods to study micronutrient deficiency responses.....	70
3.2 Aims	71
3.3 Results	71
3.3.1 <i>ZIP</i> transporter genes.....	71
3.3.2 <i>bZIP</i> transcription factor genes.....	79
3.3.3 Development of a hydroponic growth system to subject wheat (<i>T. aestivum</i>) to Zn-deficient conditions	85
3.3.4 Three-week Zn starvation experiment	87
3.3.5 One-week Zn starvation experiment.....	96
3.4 Discussion.....	105
3.4.1 Identification of <i>T. aestivum ZIP</i> transporters and <i>bZIP</i> transcription factors	105
3.4.2 Zn starvation impacts wheat growth and mineral concentration	107
3.4.3 <i>TaZIPs</i> are regulated by Zn status in wheat.....	109
3.4.4 Group F <i>TabZIPs</i> are upregulated in response to Zn deficiency	110
Chapter 4. Cloning and functional characterisation of <i>T. aestivum ZIPs</i>	113
4.1 Introduction	113
4.2 Aims	115
4.3 Results	116
4.3.1 Cloning of <i>TaZIPs</i>	116
4.3.2 <i>zrt1/zrt2</i> yeast complementation.....	122
4.3.3 <i>zrc1/cot1</i> yeast complementation	125
4.3.4 <i>fet3/fet4</i> yeast complementation	127

4.4 Discussion.....	131
4.4.1 The role of TaZIPs in the transport of Zn	131
4.4.2 TaZIP1, 5, 6, 7 and 8 seem unable to transport Fe.....	133
4.4.3 Conclusions.....	134
Chapter 5. Cloning and functional characterisation of <i>T. aestivum</i> bZIPs.....	137
5.1 Introduction.....	137
5.2 Aims	139
5.3 Results.....	139
5.3.1 Cloning of TabZIPs.....	139
5.3.2 Complementation analysis of TabZIPs in the <i>A. thaliana bzip19-4bzip23-2</i> mutant line.....	146
5.3.3 Interaction and binding ability of bZIPs with ZDRE motifs.....	151
5.4 Discussion.....	160
5.4.1 TabZIPs have differential abilities to complement the <i>A. thaliana bzip19-4bzip23-2</i> mutant line grown under Zn-deficient conditions	160
5.4.2 The binding ability of bZIPs to ZDRE motifs and the implications for the Zn homeostatic mechanism of <i>T. aestivum</i>	162
Chapter 6. Examining differences in Zn characteristics using a diverse wheat germplasm	167
6.1 Introduction.....	167
6.2 Aims	169
6.3 Results.....	169
6.3.1 General variation in Zn concentration.....	170
6.3.2 Variation in the Zn uptake of total above ground biomass	172
6.3.3 Variation in grain Zn concentration across the germplasm.....	177
6.3.4 The variation in total yield and grain Zn partitioning across the germplasm.....	181
6.3.5 The performance of ten selected lines during the growing season	184
6.3.6 Comparative hydroponics Zn-starvation experiment of Watkins lines WC789 and WC239	188
6.3.7 Using a field grown mapping population (Paragon x WC239) to identify QTL associated with Zn uptake and partitioning.....	193
6.4 Discussion.....	196
6.4.1 Extensive and consistent variation exists in Zn traits across the WISP donor germplasm.....	196
6.4.2 Zn concentrations and expression levels of <i>TaZIP1</i> and <i>TabZIP1</i> during the growing season do not reflect Zn traits at final harvest.....	197
6.4.3 WC239 and WC789 display similar phenotype responses to hydroponic Zn-deficient conditions, but expression of <i>TabZIP1</i> varies between the lines in response to Zn-deficiency	198
6.4.4 QTL analysis of the Paragon x WC239 mapping population leads to the identification of loci associated with differential Zn performance	200
Chapter 7. General discussion	203
7.1 The pressing need to increase wheat Zn content.....	203
7.2 Specific members of the <i>TaZIP</i> family are promising targets for Zn biofortification strategies	204

7.3 Group F <i>TabZIPs</i> are important in the Zn-regulatory mechanism of wheat and regulate <i>TaZIP</i> expression.....	208
7.4 The prospects for future research and wheat improvement.....	212
7.5 Conclusion.....	214
References	215

List of Figures

CHAPTER 1. INTRODUCTION

Figure 1.1.	Worldwide incidence of food crop Zn deficiency.	9
Figure 1.2.	Strategy I and II uptake pathways of Fe.	18
Figure 1.3.	The route of Zn from uptake to xylem loading.	24
Figure 1.4.	The morphology and destination of rice (<i>O. sativa</i>) node vasculature.	26
Figure 1.5.	An overview of key steps in the transport of Zn from soil to grain/seed.	29
Figure 1.6.	Schematic of a wheat grain.	33
Figure 1.7.	Zn distribution in the wheat grain.	33
Figure 1.8.	The loading pathway of Zn in the grain.	35
Figure 1.9.	bZIP structure and DNA binding schematic.	38
Figure 1.10.	Schematic of <i>A. thaliana</i> group F bZIPs.	39
Figure 1.11.	<i>A. thaliana</i> Zn-deficiency sensing and response mechanism.	40

CHAPTER 2. MATERIALS AND METHODS

Figure 2.1.	Design of SP6 forward and Poly-A tail reverse primers for protein synthesis.	48
Figure 2.2.	RNA quality check using TAE-agarose electrophoresis.	50
Figure 2.3.	DNA molecular markers used for gel electrophoresis.	51
Figure 2.4.	pENTR™/D-TOPO vector map.	55
Figure 2.5.	pMDC32 vector map.	56
Figure 2.6.	pGEM®-T Easy vector map.	57
Figure 2.7.	pYES2 vector map.	58

CHAPTER 3. IDENTIFICATION AND EXPRESSION OF *TaZIPs* AND *TabZIPs*

Figure 3.1.	Phylogenetic analysis of ZIPs in cereals and <i>Arabidopsis</i> .	75
Figure 3.2.	Multiple sequence alignment of <i>Arabidopsis</i> , rice and wheat ZIPs.	76
Figure 3.3.	Topology predictions of TaZIP1-2AL and TaZIP5-2AL.	78
Figure 3.4.	Phylogenetic analysis of group F bZIP genes in cereals and <i>Arabidopsis</i> .	82
Figure 3.5.	Phylogenetic analysis of wheat bZIP genes in cereals.	83
Figure 3.6.	Multiple sequence alignment of <i>Arabidopsis</i> , <i>Brachypodium</i> , barley, rice and wheat group F bZIP genes.	84
Figure 3.7.	Visible phenotypic differences between Zn treatments observed in hydroponically grown wheat (<i>T. aestivum</i> cv. Paragon).	86
Figure 3.8.	Hydroponic-induced Zn deficiency significantly reduces wheat (<i>T. aestivum</i> cv. Paragon) root and shoot fresh weights and	86

increases the root to shoot ratio.

Figure 3.9.	Visible phenotypic effects of Zn starvation throughout a three-week period.	87
Figure 3.10.	The effect of Zn starvation on wheat fresh weight throughout a three-week period.	88
Figure 3.11.	Mineral concentration analysis of wheat root and shoot samples throughout a three-week Zn starvation period.	89
Figure 3.12.	Stability of the <i>TaActin3</i> reference gene throughout a three-week Zn starvation period in root and shoot material.	90
Figure 3.13.	Gene expression analysis of <i>TaZIPs</i> in wheat root material throughout a three-week Zn starvation period.	92
Figure 3.14.	Gene expression analysis of <i>TaZIPs</i> in wheat shoot material throughout a three-week Zn starvation period.	93
Figure 3.15.	Gene expression analysis of <i>TabZIPs</i> in wheat root material throughout a three-week Zn starvation period.	94
Figure 3.16.	Gene expression analysis of <i>TabZIPs</i> in wheat shoot material throughout a three-week Zn starvation period.	95
Figure 3.17.	Visible phenotypic effects of Zn starvation throughout a one-week period.	96
Figure 3.18.	The effect of Zn starvation on wheat fresh weight throughout a one-week period.	97
Figure 3.19.	Mineral concentration analysis of wheat root and shoot samples throughout a one-week Zn starvation period.	98
Figure 3.20.	Stability of the <i>TaActin3</i> and <i>TaSuccDH</i> reference genes throughout a one-week Zn starvation period in root and shoot material.	100
Figure 3.21.	Gene expression analysis of <i>TaZIPs</i> in wheat root material throughout a one-week Zn starvation period.	101
Figure 3.22.	Gene expression analysis of <i>TaZIPs</i> in wheat shoot material throughout a one-week Zn starvation period.	102
Figure 3.23.	Gene expression analysis of <i>TabZIPs</i> in wheat root material throughout a one-week Zn starvation period.	103
Figure 3.24.	Gene expression analysis of <i>TabZIPs</i> in wheat shoot material throughout a one-week Zn starvation period.	104

CHAPTER 4. CLONING AND FUNCTIONAL CHARACTERISATION OF

TaZIPs

Figure 4.1.	Cloning of TaZIP1-2AL into pYES2 yeast expression vector.	116
Figure 4.2.	Amino acid alignment of cloned TaZIP1-2AL with the predicted sequence.	117
Figure 4.3.	Cloning of TaZIP5-2BL, TaZIP6-1BS, TaZIP7-1DS and TaZIP8-2BS into pYES2 yeast expression vector.	118
Figure 4.4.	Amino acid alignments of cloned TaZIP5-2BL, TaZIP6-1BS,	120

	TaZIP7-1DS and TaZIP8-2BS with the predicted sequences.	
Figure 4.5.	Colony PCR confirmation of pYES2TaZIP transformation into the <i>zrt1/zrt2</i> mutant yeast strain.	123
Figure 4.6.	Complementation of the yeast Zn-uptake mutant <i>zrt1/zrt2</i> with <i>TaZIP</i> genes.	124
Figure 4.7.	Colony PCR confirmation of pYES2TaZIP transformation into the <i>zrc1/cot1</i> mutant yeast strain.	125
Figure 4.8.	Complementation of the yeast Zn-sensitive mutant <i>zrc1/cot1</i> with <i>TaZIP</i> genes.	126
Figure 4.9.	Colony PCR confirmation of pYES2TaZIP transformation into the <i>fet3/fet4</i> mutant yeast strain.	127
Figure 4.10.	Complementation of the yeast Fe-uptake mutant <i>fet3/fet4</i> with <i>TaZIP</i> genes.	128
Figure 4.11.	Multiple sequence alignment of <i>TaZIPs</i> cloned from cv. Paragon used in yeast heterologous expression studies.	130

CHAPTER 5. CLONING AND FUNCTIONAL CHARACTERISATION OF

TabZIPs

Figure 5.1.	Cloning of TabZIP1-7DL into pMDC32 <i>Arabidopsis</i> expression vector.	140
Figure 5.2.	Amino acid alignment of cloned TabZIP1-7DL with the predicted sequence.	141
Figure 5.3.	Cloning of TabZIP3b-7BL, TabZIP4-7AL, TabZIP4-7DL and TabZIPG-5DL.	143
Figure 5.4.	Amino acid alignments of cloned TabZIP3b-7BL, TabZIP4-7AL, TabZIP4-7DL and TabZIPG-5DL with the predicted sequences.	144
Figure 5.5.	Multiple sequence alignment of cloned group F TabZIPs, AtbZIP19 and AtbZIP23.	146
Figure 5.6.	Confirmatory PCR of pMDC32TabZIP transformed <i>Arabidopsis</i> lines.	147
Figure 5.7.	Functional complementation of the <i>Arabidopsis bz19-4bz19-23-2</i> mutant with group F TabZIPs.	149
Figure 5.8.	EMSA of AtbZIP19 with ZDRE containing probes.	158
Figure 5.9.	Composite of five EMSAs using different wheat bZIPs.	159

CHAPTER 6. WHEAT GERMPLASM Zn VARIATION

Figure 6.1.	Extensive variation in Zn concentration exists across the WISP donor germplasm.	171
Figure 6.2.	Total biomass Zn uptake increases with total yield in 2011 and 2012 field grown germplasm datasets.	173
Figure 6.3.	Residual values (differences between trendline predictions and actual measurements of total Zn uptake) for 2011 and 2012.	174
Figure 6.4.	Total biomass Zn uptake increases with total yield in 2013 and 2014 field grown germplasm datasets.	175

Figure 6.5.	Residual values of total biomass Zn uptake vs total yield from four years of field-grown WISP germplasm.	176
Figure 6.6.	Grain Zn concentration reduces with increasing grain yield across four years of field-grown germplasm datasets.	178
Figure 6.7.	Residual values of grain Zn concentration vs grain yield from four years of field-grown WISP germplasm.	180
Figure 6.8.	Four-year mean total biomass across the field-grown WISP germplasm.	182
Figure 6.9.	Four-year mean Zn harvest index across the field-grown WISP germplasm.	183
Figure 6.10.	Zn concentrations of ten field-grown wheat lines during the growing season.	185
Figure 6.11.	Zn concentrations and total biomass yield of ten field-grown wheat lines at final harvest across four years of field trials.	186
Figure 6.12.	Absolute quantification of <i>TaZIP1</i> and <i>TabZIP1</i> gene expression levels in root samples obtained from ten field grown wheat lines.	188
Figure 6.13.	Visible phenotypic effects of Zn starvation on two Watkins Collection wheat lines.	189
Figure 6.14.	Fresh weights, SPAD value and Zn concentration of wheat root and shoot samples from two differentially Zn-performing Watkins Collection lines throughout a 12-day Zn starvation period.	190
Figure 6.15.	Absolute quantification of <i>TaZIP1</i> and <i>TabZIP1</i> gene expression levels in root and shoot samples of two contrasting Watkins Collection wheat lines throughout a 12-day Zn starvation period.	192
Figure 6.16.	Frequency distribution of yield and Zn traits across the Paragon x WC239 mapping population.	194

CHAPTER 7. GENERAL DISCUSSION

Figure 7.1.	Model of Zn regulation in wheat (<i>T. aestivum</i>).	211
-------------	---	-----

List of Tables

CHAPTER 1. INTRODUCTION

Table 1.1.	Variation in Zn and Fe concentrations within and between widely consumed foodstuffs.	3
Table 1.2.	Plant nutrients that are mineral elements lacking in human diets, their bodily functions and the effects of their deficiency.	5
Table 1.3.	The functional role of Zn in crucial plant enzymes.	6
Table 1.4.	Experiments demonstrating the effect of Zn levels in plant infection resistance.	8
Table 1.5.	A selection of clinical studies showing the beneficial effects of Zn on human health.	10
Table 1.6.	Summary of key transporter families involved in plant Zn uptake, subsequent transport and vacuolar sequestration.	30

CHAPTER 2. MATERIALS AND METHODS

Table 2.1.	Constituents and concentrations of the modified Letcombe solution used in the hydroponic culture system.	43
Table 2.2.	Timeframes of hydroponic experiments.	44
Table 2.3.	Oligonucleotide primer sequences used in real-time PCR expression analysis.	46
Table 2.4.	Oligonucleotide primer sequences used for the amplification of full length CDS for TOPO [®] cloning.	47
Table 2.5.	Oligonucleotide primer sequences used for the amplification of full length CDS with EcoRI and XhoI restriction sites.	48
Table 2.6.	Oligonucleotide primer sequences used for the amplification of full length bZIP CDS with an SP6 promoter, Kozak region and Poly A tail for use in protein expression kit.	49
Table 2.7.	Backbone oligonucleotide primer sequences used in colony PCR and sequencing reactions.	52
Table 2.8.	SC medium composition for <i>S. cerevisiae</i> culture (<i>zrt1/zrt2</i> and <i>zrc1/cot1</i> strains).	60
Table 2.9.	SC medium composition for <i>zrt1/zrt2</i> and <i>zrc1/cot1</i> strain drop spot assays.	60
Table 2.10.	SC medium composition for <i>S. cerevisiae</i> culture (<i>fet3/fet4</i> strain).	61
Table 2.11.	SC medium composition for <i>S. cerevisiae</i> culture (<i>fet3/fet4</i> strain).	61
Table 2.12.	Sequences of complementary oligonucleotides used in EMSAs.	65

CHAPTER 3. IDENTIFICATION AND EXPRESSION OF *TaZIPs* AND *TabZIPs*

Table 3.1.	Wheat <i>ZIP</i> gene identification details.	73
Table 3.2.	Wheat <i>bZIP</i> gene identification details.	81

CHAPTER 4. CLONING AND FUNCTIONAL CHARACTERISATION OF

TaZIPs

Table 4.1.	Overview of <i>TaZIP</i> complementation ability across three mutant yeast strains.	129
------------	---	-----

CHAPTER 5. CLONING AND FUNCTIONAL CHARACTERISATION OF

TabZIPs

Table 5.1.	Overview of ZDREs.	153
Table 5.2.	ZDRE probe overview.	155

CHAPTER 6. WHEAT GERMPLASM Zn VARIATION

Table 6.1.	The effect and interactions of line, treatment and time point on fresh weight, SPAD value and Zn concentration of root and shoot samples from two differentially Zn-performing Watkins Collection lines throughout a 12-day Zn starvation period.	189
Table 6.2.	The effect and interactions of line, treatment and time point on the absolute quantification of <i>TaZIP1</i> and <i>TabZIP1</i> from root and shoot cDNA samples from two differentially Zn-performing Watkins Collection lines throughout a 12-day Zn starvation period.	192
Table 6.3.	Phenotypes of parents and the mapping population.	193
Table 6.4.	QTLs identified using the Paragon x WC239 mapping population for yield and Zn traits.	195

Academic Thesis: Declaration of Authorship

I, Nicholas Evens declare that this thesis and the work presented in it are my own and has been generated by me as the result of my own original research.

The Regulatory Mechanisms Controlling Zinc Content in Wheat

I confirm that:

1. This work was done wholly or mainly while in candidature for a research degree at this University;
2. Where any part of this thesis has previously been submitted for a degree or any other qualification at this University or any other institution, this has been clearly stated;
3. Where I have consulted the published work of others, this is always clearly attributed;
4. Where I have quoted from the work of others, the source is always given. With the exception of such quotations, this thesis is entirely my own work;
5. I have acknowledged all main sources of help;
6. Where the thesis is based on work done by myself jointly with others, I have made clear exactly what was done by others and what I have contributed myself;
7. None of this work has been published before submission.

Signed:

Date:

Acknowledgements

First and foremost, I am extremely grateful to my supervisors, Dr Lorraine E. Williams, Dr Peter Buchner and Dr Malcolm J. Hawkesford for giving me the opportunity to do this PhD. It has been a long journey, but your continued support and mentoring have allowed me to develop as both a scientist and a person.

My thanks go to Peter for his help and guidance in the lab; your patience and expertise were invaluable. Thank you to Andrew Riche for providing the germplasm datasets and also sharing his mastery of Excel spreadsheets. I would like to thank Saroj Parmar for conducting the ICP-OES mineral analysis of all my samples over the past four years. I have had the privilege of working with many colleagues throughout this project and I would like to thank all the members of both the LEW lab and Malcolm's Plant Nutrition group that I have been fortunate enough to work alongside.

I am grateful to the BBSRC for funding this Food Security Doctoral Training Partnership. I also extend my gratitude to the Forestry Commission for hosting my PIP internship, which was a varied and valuable three months.

I would like to thank my family and close friends for your continued support. Today I find myself writing an acknowledgements section...something which, at times over the last four years, has seemed unreachable! Without you all, it may have been. I am forever thankful to my parents, your unwavering encouragement and support throughout my life allows me to reach my full potential. Thanks to my brother, Alex; I couldn't have done this without you and our adventures...roll-on our never-ending stream of over-ambitious races, rides and undertakings, they truly are the best!

Most importantly, thank you Sylvie. I'm not really sure how you've done it, but thank you for bearing with me through this. Without you, nothing I achieve would mean anything. Now, let's live!

Abbreviations

A	Adenine
ANOVA	Analysis of variance
At	<i>Arabidopsis thaliana</i>
ATP	Adenosine triphosphate
BBSRC	Biotechnology and Biological Sciences Research Council UK
Bd	<i>Brachypodium distachyon</i>
bHLH	Basic helix-loop-helix
BLAST	Basic local alignment search tool
bp	Base pair
BSA	Bovine serum albumin
bZIP	Basic leucine zipper
C	Cytosine
CA	Carbonic anhydrase
CaMV	Cauliflower mosaic virus
Cd	Cadmium
CDF	Cation diffusion facilitator
cDNA	Complementary DNA
CDS	Coding DNA sequence
CIAP	Calf intestinal alkaline phosphatase
CIM	Composite interval mapping
Co	Cobalt
contig	Contiguous DNA consensus region
Cu/Zn SOD	Cu/Zn superoxide dismutase
cv.	Cultivar
D	Day
DALY	Disability-adjusted life year
d.f.	Degrees of freedom
DEPC	Diethylpyrocarbonate
DM	Double-mutant (or) Dry matter
DMA	Deoxymugeneic acid
DNA	Deoxyribonucleic acid
DTT	Dithiothreitol
DTZ	Diphenyl thiocarbazon
DVB	Diffuse vascular bundle
EDTA	Ethylene diaminetetraacetic acid

EGTA	Ethylene glycoltetraacetic acid
EMSA	Electrophoretic mobility shift assay
ENA	Efflux transporter of NA
ER	Endoplasmic reticulum
EV	Empty vectors
EVB	Enlarged vascular bundle
FAO	Food and Agricultural Organization of the United Nations
Fe	Iron
FIT	FER-like iron deficiency induced transcription factor
G	Guanine
GFP	Green fluorescent protein
Gpc-B1	Grain protein content B1 locus
GUS	β -glucuronidase
HI	Harvest index
HMA	Heavy metal transporting ATPase
HPYT	HarvestPlus yield trial
Hr	Hour
Hv	<i>Hordeum vulgare</i>
IAA	Indole-3-acetic acid
IAA	Isoamyl alcohol
ICP-OES	Inductively coupled plasma optical emission spectrometry
IDE	Iron-deficiency response element
IPTG	Isopropyl β -D-1-thiogalactopyranoside
IRT	Iron regulated transporter
LB	Lysogeny broth
Log	Logarithmic
LR	Likelihood ratio
LSD	Least significant difference (calculated at $P < 0.05$ throughout thesis)
MA	Mugineic acid
MES	Morpholinoethanesulfonic acid
MFS	Major facilitator superfamily
Min	Minute
miRNAs	Micro RNAs
Mn	Manganese
mRNA	Messenger RNA
MS	Murashige and Skoog
MTP	Metal tolerance protein

NA	Nicotianamine
NAC	No apical meristem, <i>Arabidopsis</i> transcription activation factor, cup-shaped cotyledon
NC	Not complete
NCBI	National Centre for Biotechnology Information
NF	Non-functional
NIAB	National Institute of Agricultural Botany
NPK	Nitrogen, phosphorus, potassium fertiliser mix
NRQ	Normalised relative quantification
Os	<i>Oryza sativa</i>
PCR	Polymerase chain reaction (or) Plant cadmium resistance
ppm	Parts per million
PS	Phytosiderophore
QTL	Quantitative trait loci/locus
RNA	Ribonucleic acid
RNAi	RNA interference
RNA-seq	RNA-sequencing
RNI	Reference nutrient intake
ROS	Reactive oxygen species
RSL	Recombinant chromosome substitution line
SC	Synthetic complete
SD	Standard deviation
SEM	Standard error of the mean
SHW	Synthetic hexaploid wheat
SNP	Single nucleotide polymorphism
SOC	Super optimal broth with catabolite repression
SPAD	Soil plant analysis development
ssp.	Subspecies
T	Thymine
Ta	<i>Triticum aestivum</i>
TAE	Tris acetate EDTA
TBE	Tris borate EDTA
T-DNA	Transfer DNA
TE	Tris EDTA
TEM-EDX	Transmission electron microscopy and energy-dispersive X-ray
TGAC	The Centre for Genome Analysis
TM	Transmembrane domain

TOM	Transporter of mugineic acid
Tris	Tris (hydroxymethyl) aminomethane
UK	United Kingdom
Ura	Uracil
URGI	Unité de Recherche Génomique Info
US	United States
UTR	Untranslated region
UV	Ultraviolet
VIT	Vacuolar iron transporter
WGIN	Wheat Genetic Improvement Network
WHO	World Health Organisation
WISP	Wheat Improvement Strategic Programme
WT	Wild-type
YPD	Yeast peptone dextrose
YSL	Yellow-stripe like proteins
ZDRE	Zn-deficiency response element
ZIF	Zn-induced facilitator
ZIP	ZRT/IRT-like protein
Zm	<i>Zea mays</i>
Zn	Zinc
ZRT	Zn-regulated transporter

Chapter 1. Introduction

The ultimate goal of modern agriculture is to produce nutritious and safe food in sufficient quantities for the burgeoning global population. By 2050, it is predicted that the world population will be in excess of nine billion people (Godfray et al., 2010). The land available for crop cultivation is unlikely to increase and further pressures from limited water supply and global climate change will only exacerbate the challenge of providing food security for the world's population (Foley et al., 2011). However, it is not simply just an increase in calories that is required by the growing population, but an increase in food quality; the improved micronutrient concentration of many staple crops is of paramount importance.

1.1 Micronutrient malnutrition

Cereals such as wheat (*Triticum aestivum*), barley (*Hordeum vulgare*) and rice (*Oryza sativa*) are cultivated widely for their edible grains and are relied upon as staple foods throughout the world. Whilst cereals offer a valuable source of calories, they are found lacking from a nutritional perspective. Cereal grains have a tendency to be low in elements such as Zinc (Zn), Iron (Fe) and Manganese (Mn) (Cakmak, 2008). These elements are termed micronutrients, because they are only required in relatively low concentrations in plant tissues (5-100 mg/kg) (Alloway, 2008). Humans require more than 22 mineral elements (White and Broadley, 2005), which are supplied in sufficient quantities through the consumption of a nutritionally balanced and diverse diet (see Tables 1.1 and 1.2).

A major problem arises when populations rely upon food sources with poor micronutrient content, such as cereal grains, for the bulk of their daily calorie intake. For example, The Food and Agricultural Organization of the United Nations (FAO) have calculated that populations in a range of countries obtain up to 63% of their daily calorie intake from wheat (FAO database, 2003 data compiled by H.J. Braun-CIMMYT Turkey, published in Alloway, 2008). This is likely to be even higher in rural areas of developing countries (Cakmak 2007). It is unsurprising that in areas with low dietary diversification, micronutrient malnutrition is prevalent.

The World Health Organization (WHO) originally coined the term 'hidden hunger' to describe the many effects micronutrient malnutrition has on humans that are not immediately obvious to the naked eye (Parr and Fjeld, 1994). It is estimated that billions of people around the world are not getting access to the essential micronutrients they require from their diets, the vast majority of those affected are in developing countries (Harvestplus, 2010). Dietary deficiencies lead to increased susceptibility to many diseases and afflictions (see Table 1.2). Ultimately these illnesses kill sufferers and get wide publicity, but the origin of the problem is often the lack of micronutrients in the diets of the affected. Zn, Fe and Vitamin A deficiencies have been ranked

Chapter 1. Introduction

respectively as the 5th, 6th and 7th most significant contributors to illness and disease in the developing world (WHO, 2002). Globally, the number of people at risk of Zn deficiency was estimated to be 1.1 billion in 2011 (Kumssa et al., 2015). This estimate was calculated using a food systems analysis, synthesising data for food supply, food composition, demography and estimated average nutrient requirements. However, it is not solely populations in developing countries that are at risk of micronutrient malnutrition: the National Diet and Nutrition Survey (Public Health England, 2014) calculated that in the UK 17% of 11-18 year olds and 6.6% of the total UK population over 18 years old have an average daily Zn intake below the Lower Reference Nutrient Intake ((LRNI) between 4 and 9.5 mg Zn/day depending on age and sex). The UK population acquires between 31 and 36% of total energy intake from cereals; the largest proportion from all the major food groups (Public Health England, 2014). Furthermore, between 24 and 31% of total Zn intake of the UK population is obtained from cereals and cereal products. It is therefore vital that we have an understanding of the factors contributing to Zn content in cereals as they are an important dietary component for many populations throughout the world.

This project will specifically investigate the regulation of Zn and the mechanisms controlling the uptake and partitioning of Zn in the plant, with the ultimate goal of improving the grain Zn content of wheat (*T. aestivum*).

Table 1.1. Variation in Zn and Fe concentrations within and between widely consumed foodstuffs.

Foodstuff	Trial type	Accessions	Zinc (mg kg ⁻¹)	Iron (mg kg ⁻¹)	Grain fraction tested	Fertiliser regime used	References
<u>Plant-based foods</u>							
Wheat (<i>Triticum</i> spp.) grain							
Selected bread wheat (<i>T. aestivum</i>) genotypes	Field	150	14-35	29-51	Wholemeal milled flour	80 kg/Ha N,P,K	(Zhao et al., 2009)
Selected durum wheat (<i>T. turgidum</i> var <i>durum</i>) genotypes	Field	10	14-27	30-36	Wholemeal milled flour	80 kg/Ha N,P,K	(Zhao et al., 2009)
Selected einkorn wheat (<i>T. monococcum</i> var <i>monococcum</i>) genotypes	Field	5	20-28	38-56	Wholemeal milled flour	80 kg/Ha N,P,K	(Zhao et al., 2009)
Selected emmer wheat (<i>T. turgidum</i> var <i>dicoccum</i>) genotypes	Field	5	16-30	31-40	Wholemeal milled flour	80 kg/Ha N,P,K	(Zhao et al., 2009)
Selected spelt wheat (<i>T. aestivum</i> var <i>spelta</i>) genotypes	Field	5	17-28	38-44	Wholemeal milled flour	80 kg/Ha N,P,K	(Zhao et al., 2009)
Selected bread wheat (<i>T. aestivum</i>) genotypes	Field	243	14-43	18-58	Whole grain samples	'Nitrogen fertilization fitted to high yield objectives'	(Oury et al., 2006)
Selected (<i>Triticum</i> spp.) genotypes	Field	66	20-39	25-56	Whole grain samples	Not given for the sites used	(Morgounov et al., 2006)
Selected (<i>Triticum</i> spp.) genotypes	Field	324	25-92	25-73	Whole grain samples	Not given for the sites used	(Monasterio and Graham, 2010)
Emmer wheat varieties from the Fertile Crescent (<i>T. turgidum</i> var <i>dicoccum</i>)	Field	714	32-100	15-109	Whole grain samples	Not given for the sites used	(Cakmak et al., 2004)
Emmer wheat varieties from the Fertile Crescent (<i>T. turgidum</i> var <i>dicoccum</i>)	Glasshouse	111	14-190	21-91	Whole grain samples	Tuff, vermiculite and peat enriched with Osmocote slow release fertiliser	(Cakmak et al., 2004)
Selected bread wheat (<i>T. aestivum</i>) cultivars from major wheat production areas of China	Field	320	14-57	23-79	Whole grain samples	Not given for the sites used	(Liu et al., 2014)

Chapter 1. Introduction

Rice (<i>Oryza sativa</i>) grain							
Core collection	Field	1138	14-58	6-24	Brown rice	Not given for the sites used	(Gregorio et al., 2000)
Selected varieties of Chinese rice	Field	56	13-39	9-45	Brown rice	Not given for the sites used	(Liang et al., 2007)
Maize (<i>Zea mays</i>) grain							
Core collection	Field	1814	13-58	10-63	Whole kernel	Not given for the site used	(Banziger and Long, 2000)
Selected lines from varying altitudes	Field	109	11-95	14-159	Hand shelled kernels	Not given for the site used	(Maziya-Dixon et al., 2000)
Bean (<i>Phaseolus vulgaris</i>) seed							
Core collection	Field	1072	21-59	34-92	Ground bean seed	Not given for the sites used	(Islam et al., 2002)
Almond (<i>Prunus dulcis</i>) kernel							
Varieties grown commercially in California	Field	7	20-40	26-45	Raw, whole kernel	'Independent orchard management practices'	(Yada et al., 2013)
Animal products							
Cow (<i>Bos taurus</i>)							
Cooked Sirloin samples taken from food retailers	N/A	N/A	57.4±0.3	31.1±0.4	N/A	N/A	(Lombardi-Boccia et al., 2005)
Pastirma (cured meat) samples from various turkish regions	N/A	N/A	159±2.8	136.2±1.8	N/A	N/A	(Demirezen and Uruç, 2006)
Milk (whole)	N/A	N/A	3.7±0.6	0.2±0.03	N/A	N/A	(Pennington and Young, 1990)
Chicken (<i>Gallus gallus domesticus</i>)							
Cooked Leg samples taken from food retailers	N/A	N/A	24±0.1	12±0.2	N/A	N/A	(Lombardi-Boccia et al., 2005)
Mackerel (<i>Micromesistius poutassou</i>)							
Fillet sampled from various fishery locations in Turkey	N/A	N/A	20±3.1	92±11	N/A	N/A	(Demirezen and Uruç, 2006)

Table 1.2. Plant nutrients that are mineral elements lacking in human diets, their bodily functions and the effects of their deficiency. UK adult Reference Nutrient Intakes (RNI) are given (Buttriss, 2000).

Plant nutrient	RNI	Human bodily function	Effects of deficiency in humans
Iron (micronutrient)	8.7-15 mg/d	Oxygen carrier in Haemoglobin, electron acceptor in various metabolic enzymes	Impaired immune function, lowered work capacity, anaemia (McDermid and Lonnerdal, 2012)
Zinc (micronutrient)	7-9.5 mg/d	Essential component in hundreds of enzymes, stabilises molecular structure of many cellular components and membrane transporters	Reduced immune system functioning, stunting, delayed sexual and bone maturation, impaired neonatal development (Huang et al., 2015). Increased susceptibility to malaria pneumonia and diarrhoea (Caulfield et al., 2004)
Selenium (beneficial nutrient)	60-75 µg/d	Component in selenoproteins with roles including defence against oxidative stress and thyroid hormone regulation and production	Keshan disease (a cardiomyopathy) and Kashin-Beck (a form of arthritis) (Rayman, 2000)
Calcium (macronutrient)	700 mg/d	Calcium salts give skeletal rigidity, calcium ions are required in a range of metabolic processes	Decreased bone mass, osteoporotic fracture, rickets (Weaver and Peacock, 2011)
Magnesium (macronutrient)	270- 300 mg/d	Enzymes involved in energy metabolism, protein, RNA and DNA synthesis as well as membrane potential maintenance	Weight loss, lethargy, cardiac arrhythmia and pulmonary oedema (FAO and WHO, 2001b)
Manganese* (micronutrient)	>1.4 mg/d	Component of several enzyme families required in amino acid, lipid, protein and carbohydrate metabolism	Skeletal abnormalities, impaired growth and reproductive function, disruption of lipid and carbohydrate metabolism (Aschner and Aschner, 2005)
Copper (micronutrient)	1.2 mg/d	Required for normal utilisation of dietary iron. Important in bone, brain and red blood cell development	Myelodysplastic syndrome, anaemia, bone abnormalities (Collins and Klevay, 2011; Huff et al., 2007)

* Human Mn deficiency is not common

1.2 The importance of Zn

Zn is an essential element for all organisms; it acts as a catalytic or structural cofactor in a large number of enzymes and regulatory proteins (Sinclair and Krämer, 2012). Zn is a strong

Chapter 1. Introduction

and efficient Lewis acid catalyst giving it a high binding affinity to a variety of ligands. Zn has extensive utilisation in proteins and is the only metal represented in all six enzyme classes (oxidoreductases, transferases, hydrolases, lysases, isomerases and ligases) (Maret, 2009, 2013). It has been estimated that from prokarya to eukarya between 4% and 10% of the total genomes encode proteins that contain putative Zn binding patterns (Andreini et al., 2006b). It has also been calculated that humans alone contain over 3000 Zn-containing proteins (Andreini et al., 2006a). It is the critical structural and functional role in multiple enzyme systems that makes Zn so important to the nutrition of humans, plants and all other organisms (see Table 1.3).

Table 1.3. The functional role of Zn in crucial plant enzymes.

Zn containing enzyme	Function in plants	Reference
Carbonic Anhydrase (CA)	CA is required in both C3 and C4 plants. In C3 plants it facilitates the diffusion of CO ₂ to carboxylation sites and the intracellular interconversion of CO ₂ and HCO ₃ ⁻ .	(Sandmann and Boger, 1983)
Cu/Zn Superoxide Dismutase	This enzyme is required in the antioxidant defence of cells exposed to superoxides (O ₂ ⁻).	(Abreu and Cabelli, 2010)
Alcohol dehydrogenase	Catalyses the reduction of acetaldehyde to ethanol. Especially important in plants grown in anaerobic conditions such as waterlogged soils.	(Moore and Patrick, 1988)
RNA polymerase	Synthesis of RNA.	(Prask and Plocke, 1971)
Stromal processing peptidase	Catalyses the removal of transit peptides from a variety of precursor proteins imported into chloroplasts.	(Richter and Lamma, 2003)
Matrix metalloproteinases (MMPs)	A family of endoproteinases that degrade extracellular matrix substrates.	(Maidment et al., 1999; Marino and Funk, 2012)
Peptide deformylases	A family of enzymes essential to the N-terminal protein processing pathway.	(Giglione et al., 2000)
Zn finger transcription factors	Transcriptional regulation of key genes to a vast array of signals ranging from heat, salinity and oxidative stress responses to stamen and carpel development.	(Davletova et al., 2005; Zhao et al., 2014)

1.2.1 Plant Zn nutrition

Zn is vital to the normal functioning of multiple, key plant physiological pathways and is important in providing structural and functional integrity to cellular membranes within plants (Cakmak & Marschner 1988). Zn is essential in plants for growth regulation (Norvell and Welch, 1993), enzyme activation (see Table 1.3), phytohormone activity (Cakmak & Marschner 1989), fertility and seed production (Sharma et al., 1990), photosynthesis (Randall and Bouma, 1973) as well as defence against disease (see Table 1.4). If Zn is not available to a plant in sufficient quantities, a reduction in growth, yield and crop quality can occur (Brown et al., 1993).

Zn is involved in at least three separate processes that are fundamental to the production of photoassimilates: 1) carbonic anhydrase activity (Ohki, 1976), 2) chlorophyll content (Hu and Sparks, 1991) and 3) chloroplast structure (Chen et al., 2008). The importance of Zn in photoassimilate production has been shown in wheat with higher Zn levels resulting in an increased final yield (Yilmaz et al., 1998). Zn has been experimentally shown to be of importance in the maintenance of yield when plants are under drought stress (Bagci et al., 2007). The widespread irregularity in rainfall across much of the world's crop growing regions makes the drought tolerance provided by elevated Zn levels in the plant very appealing for yield protection (Sadeghzadeh and Rengel, 2011). It is thought that Zn is involved in the inhibition of photooxidative damage that occurs from reactive oxygen species (ROS) which are formed within the plant under drought conditions (Wenzel and Mehlhorn, 1995). Zn is a structural component of anti-oxidative enzymes that detoxify these ROS such as Cu/Zn superoxide dismutase. Additionally, Zn is required in the production of Zn-finger proteins (such as Zat12) that act as transcription factors, upregulating a suite of drought stress response genes (amongst other abiotic stresses) (Davletova et al., 2005).

Zn may have important roles in the protection of plants from pathogen attack. Under Zn-deficient conditions, the structural integrity of cell membranes is reduced (Cakmak & Marschner 1989). This causes the cell membranes to become leaky and increases the release of a pathogen-attracting root exudate containing amino acids, sugars and phenolics, into the rhizosphere (Cakmak & Marschner 1986). This increased root exudation has been shown in wheat by measuring the increased leakage of ^{32}P and ^{36}Cl from root cells in Zn-deficient plants (Welch et al. 1982). Cakmak and Marschner (1988) also showed that leakage of K^+ , amino acids, sugars and phenolics from roots of cotton (*Gossypium hirsutum*), wheat, tomato (*Solanum lycopersicum*) and apple (*Malus domestica*) increased in response to Zn deficiency, thus supporting the role of Zn in the structural integrity of cell membranes. Experiments conducted under both controlled and field conditions have shown an increased susceptibility of plants to various pathogens when grown under Zn-deficient conditions. This is thought to be due in part to an increased leakage of root exudates (see Table 1.4).

Table 1.4. Experiments demonstrating the effect of Zn levels in plant infection resistance.

Reference	Disease	Brief description
(Al-Fahdawi et al 2013)	<i>Fusarium pseudograminearum</i>	5 durum wheat varieties (<i>Triticum trugidum</i> spp. <i>Durum</i>) were grown under two Zn treatments. Reduced Zn gave a greater biomass penalty with infection and increased the extent of crown rot symptoms. Plant growth penalty differences were observed between different genotypes.
(Brennan, 1992)	<i>Gaeumannomyces graminis</i> var. <i>tritici</i> (<i>Ggt</i>)	Wheat plants were field grown- under varying Zn fertiliser treatments. Zn-deficient plants were more severely infected by <i>Ggt</i> .
(Streeter et al., 2001)	Root-rotting fungus <i>Rhizoctonia solani</i>	<i>Medicago truncatula</i> tolerance to infection was increased through Zn fertiliser addition. This was supported by controlled environment studies.
(Siddiqui et al., 2002)	<i>Microphamina phaseoline</i> , <i>Fusarium solani</i> and <i>Rhizoctonia solani</i>	Soil Zn addition in combination with disease-suppressive strains of fluorescent pseudomonads reduced the nematode root penetration rate in three tomato varieties.
(Sparrow and Graham, 1988)	<i>Fusarium graminearum</i>	Wheat grown at three levels of Zn nutrition showed a significant reduced infection rate with increased Zn supply.

Zn has also been shown to be important in the establishment of seedlings. Plants emerging from seeds with low Zn concentrations have been shown in both the field (Yilmaz et al., 1998) and under glasshouse conditions (Rengel & Graham, 1995a) to have poor seedling vigour and field establishment. Thus, not only will it be beneficial for human nutrition to increase the Zn content of grains, but it may reduce the seeding requirements in Zn-deficient soils. Seeds with higher Zn concentrations will have improved initial root and shoot growth, thus aiding plant establishment. In principle, this is similar to the agronomic method of seed priming, where seeds are soaked in a 'nutrient primed' solution before sowing to enhance micronutrient availability (such as Zn) in the critical life stage of seedling emergence (Farooq et al., 2012). However, if seeds with inherently higher levels of Zn are available, this seed priming would not be required.

1.2.2 Human Zn nutrition

Estimating the number of humans suffering from Zn malnourishment is not easy; the lack of reliable, sensitive bioindicators in human health compared to other human micronutrient deficiencies such as Fe (indicated by anaemia) make Zn deficiency difficult to accurately quantify (Hotz and Brown, 2004). However, it is estimated that between 16 and 33% of the world's population is at risk of inadequate Zn intake (Hotz and Brown, 2004; Wessells and Brown, 2012; Kumssa et al., 2015). The distribution of this human malnutrition is widespread, but is particularly prevalent in developing countries, such as areas of Sub-Saharan Africa and Southern Asia. Unsurprisingly, there is a strong correlation between areas with Zn-deficient soil and areas where Zn deficiency in humans is widespread (Alloway 2008). Figure 1.1 shows the global distribution of regions where Zn deficiency in food crops has been reported.

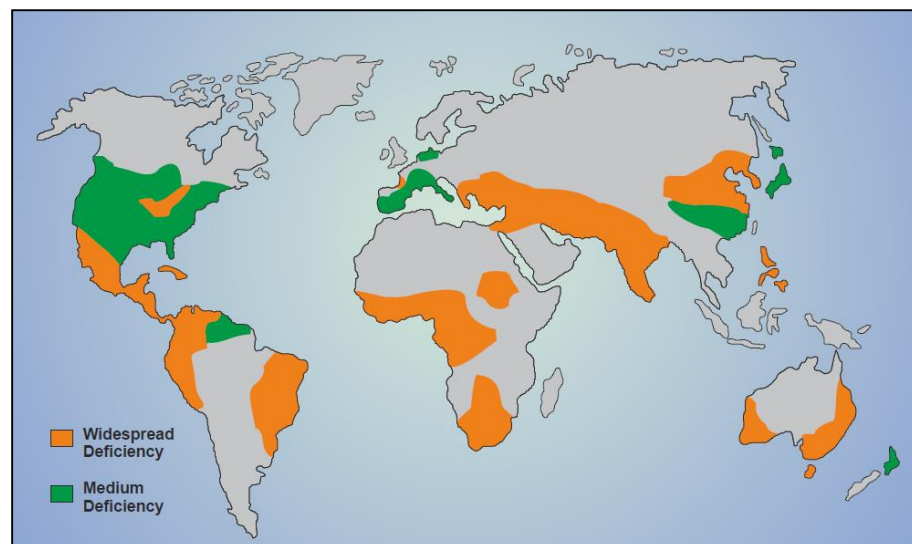


Figure 1.1. Worldwide incidence of food crop Zn deficiency. Reproduced from Alloway 2008.

Zn deficiency is known to impair neurobehavioural development, affect physical growth, reduce reproductive health and increase susceptibility to highly publicised killers such as malaria, diarrhoea and pneumonia (Black et al., 2008; Hess et al., 2009). Clinical studies in which Zn-malnourished communities were given Zn supplementation have shown dramatic decreases in the incidence of diarrhoea and pneumonia in young children (Black et al. 1999). Stark differences have been seen on multiple occasions across diverse regions, studying various afflictions (Table 1.5.). These studies leave little doubt as to the extreme importance of adequate Zn within the human diet.

Table 1.5. A selection of clinical studies showing the beneficial effects of Zn on human health.

Study Reference	Experimental design	Results
(Baqui, 2002)	8070 children in Bangladesh were split into placebo and intervention groups. Intervention group received 20 mg Zn for 14 days	The intervention group showed reduced incidence and duration of diarrhoea, reduced incidence of acute lower respiratory infection and a reduced rate of non-injury deaths
(Bhatnagar et al., 2012)	700 infants with probable serious bacterial infection in three New Delhi hospitals received 10 mg of Zn or placebo daily	Significantly fewer treatment failures occurred in the Zn group. 10 infants receiving Zn died compared to 17 given the placebo
(Duchateau et al., 1981)	2 groups of elderly people (all over 70 years old) administered placebo or 220 mg Zn sulphate twice daily for 1 month	Increase in T lymphocytes and improved immunoglobulin G (IgG) antibody response to tetanus vaccine in the Zn treatment group
(Merialdi et al., 1999)	Mothers (32-36 weeks gestation) were given folate and iron tablets with or without 15 mg of Zn for 4 weeks	Increased movement bouts, and time spent moving in the +Zn group. Also increase in number of heart rate accelerations and increase in foetal heart range in the +Zn group. All of above are considered signs of improved neonatal development
(Ruel et al., 1997)	Infants (6-9 months) from rural Guatemala were given 10 mg Zn or placebo	The non-placebo group showed a significant reduction in incidence of diarrhoea
(Shankar et al., 2000)	274 children in a malaria (<i>P. falciparum</i>) endemic region of Papua New Guinea were given placebo or 10 mg Zn 6 days a week for 6 weeks	Significant reduction in incidence of fever from malaria was seen in the Zn administered group

1.3 Solutions to combat Zn deficiency

Current solutions to combat Zn deficiency fall roughly into three categories: dietary supplementation/fortification/diversification, agronomic biofortification and genetic biofortification and are discussed below.

1.3.1 Dietary supplementation/fortification/diversification

Traditionally, strategies to alleviate micronutrient malnutrition have focused on more direct approaches such as dietary supplementation, food fortification and dietary diversification (White and Broadley, 2005). *Dietary supplementation* consists of supplying a required micronutrient in a readily absorbable form through the use of tablets. Although the efficacy of direct Zn supplementation has been proven in various clinical trials (Table 1.5), this approach relies on numerous human factors; these are unfortunately lacking in many of the principal areas suffering from Zn malnourishment. The infrastructure to deliver Zn supplements in pharmaceutical form is lacking in many affected areas and the continued financial support for implementing and sustaining such a programme may not be available. Unstable governments are unlikely to facilitate adequate distribution throughout their respective regions (Timmer, 2003).

Food fortification is another approach to the alleviation of micronutrient deficiencies. It consists of the direct addition of beneficial minerals into widely consumed foods (usually at the point of processing) that increases the concentration of a particular element. Food fortification programmes have had some success in the past for various micronutrients, especially Fe (Hurrell, 1997). Fe deficiency has experienced a steady drop in both the United States and Sweden since the 1970s thanks to successful food fortification programmes (Cook et al., 1986). In these countries, foods such as infant formula milk, white bread, pasta and breakfast cereals were all fortified with Fe. There are several on-going mass flour fortification programmes that include the addition of Zn (countries include Indonesia, Mexico, Jordan and South Africa) (Brown et al., 2010). Little data is available on the efficacy of these fortification programmes, but initial results from a cereal flour fortification programme in China reveal small, yet statistically significant increases in Zn serum concentrations among women of childbearing age exposed to the Zn-fortified flour, when compared to similar women not given the fortified flour (unpublished data presented in Brown et al. (2010)). Although this success seems promising, food fortification programmes are much less effective in developing countries, especially in rural areas. Again this is mainly due to a lack of appropriate infrastructure, an absence of political commitment and insufficient funding (Hurrell, 1997).

Dietary diversification is the ultimate solution to widespread micronutrient malnutrition. The diversification of dietary intake to include a varied range of food groups to offer the full suite

of required micronutrients (including Zn) is a completely effective strategy that in the developed world is often taken for granted. This however has very little possible application to remote areas of developing countries, where incidence rates of Zn deficiency are high. If fortified flour, or pharmaceutical Zn supplements cannot reach those in need there is no realistic hope of supplying micronutrient-rich foods such as meat, fish and dairy.

In the present state of global development, none of the aforementioned strategies to enhance worldwide Zn nutrition appear feasible in isolation; we must explore alternative solutions.

1.3.2 Agronomic biofortification

Crop fertilisation is widely used as a means of increasing the availability of macronutrients such as nitrogen, phosphorus and potassium (NPK) to the crop. The use of these nutrients increases overall plant growth (both root and shoot) which subsequently enhances the uptake of all available nutrients from the soil, including Zn (Sadeghzadeh and Rengel, 2011). Furthermore, macroelement fertilisers can be used as a convenient vehicle to provide additional micronutrients that may not be readily available in the soil. Fertiliser application could correct soil Zn deficiency, ensuring optimum yields as well as an increased Zn concentration in the edible grain. Fertilisers can be applied to the soil and/or foliage of the crop. A variety of Zn sources are being utilised in fertilisers including ZnSO_4 , ZnCO_3 , ZnO , $\text{Zn}(\text{NO}_3)_2$ and ZnCl_2 (Shuman, 1998). Zn can be added into NPK fertilisers by incorporating it into granules during manufacture, coating Zn onto granular compound fertiliser, or simply bulk blending Zn fertilisers with granular NPK fertiliser. The efficiency of Zn application varies with crop development stage (Ozturk et al., 2006), site of application on the plant (Paterson et al., 1991) and the form in which Zn is incorporated into the fertiliser (Martens and Westerman, 1991). Cost-benefit analyses have shown the potential benefit of Zn fertiliser application at a macroeconomic scale; the costs of application are outweighed by savings from reduced healthcare costs and improved productivity (Joy et al., 2015, 2016). However, per disability-adjusted life year (DALY) lost, genetic approaches to alleviating Zn deficiency are likely to be more economical (Joy et al., 2016).

In the short term, agronomic biofortification is essential, however long-term sustainability in providing Zn-enriched grains to the world is questionable (Cakmak 2008). Zn fertiliser application to the soil must occur every two to three years; this is problematic to farmers in rural areas of developing countries who may not have access to Zn-enriched fertilisers due to financial or logistical constraints. There is even the possibility of Zn toxicity occurring in the soil if Zn-enriched fertilisers are applied year after year. Perhaps the most compelling evidence for agronomic fortification not being the best single approach are provided by the analysis of long-term experiments. Fan et al. (2008) showed that over the past 160 years, grain Zn concentrations

have decreased, predominantly since the 1960s and coinciding with the introduction of semi-dwarf cultivars. Conversely, the soil concentrations of micronutrients including Zn have remained stable, or even increased due to Zn present in the increased rates of NPK fertiliser being applied. The findings from this analysis are supported by Garvin et al. (2006) who conducted a similar analysis in the US. This reduction in grain Zn concentration is in part due to what has been termed the dilution effect (Oury et al., 2006). The dilution effect is the reduction in micronutrient concentration of grain, due to the increase in grain size that accompanies the use of higher yielding cultivars.

The diminishing grain Zn concentration observed in wheat is not fully explained by the dilution effect of an increasing grain yield. Fan et al. (2008) showed that even in unfertilized plots of the Broadbalk long-term continuous wheat experiment at Rothamsted Research, diminishing Zn grain concentrations are shown across time despite yields remaining constant. Zn and Fe concentration trends have shown negative trends when plotted against year of cultivar registration (Zhao et al., 2009). These micronutrient declines are particularly evident from the point of semi-dwarf wheat cultivar introduction onwards (1960s to present). Shewry et al. (2016) have proposed that the semi-dwarf phenotype likely has a direct impact on mineral status either by a reduced root system (and a reduced ability to scavenge minerals from the soil), or a reduced capacity to store minerals in the vegetative tissues prior to redistribution to the grain.

These results show that the necessary breeding strategies used in the past to increase yield have been at the expense of micronutrient concentration in the grain. It is clear that agronomic approaches to maintaining soil Zn concentration (or even increasing Zn in low soil Zn areas) will be necessary, but they are unlikely to provide the drastic increase needed to sustain the necessary improvement in Zn grain concentration. Agronomic biofortification strategies are likely to be a complementary solution to a more advanced, genetic approach.

1.3.3 Genetic biofortification

Breeding approaches

There is genetic variation across wheat germplasm with regards to Zn concentrations in the grain (Gregorio, 2002). For example, measurements of grain Zn concentration in samples of 132 bread wheats ranged from 25.2-53.3 mg/kg (Graham et al., 1999). A striking variation has also been shown in more wild and primitive wheat accessions collected from the Fertile Crescent. Grain Zn concentrations of these were shown to vary from 14 to 190 mg/kg (Cakmak et al., 2004) (for details of variations in wheat grain concentrations across several germplasm see Table 1.1). This variation across lines shows the potential available to enhance the grain Zn concentration of wheat. Indeed, a global initiative is underway to increase Zn content in several staple crops

(including wheat) (www.harvestplus.org). The wheat Zn biofortification aspect of this initiative began in 2000 with the screening of germplasm collections, including wild species and landraces (Velu et al., 2011). By 2006-2007 the Zn variation across genotypes had been used to develop varieties with an 8-12 mg/kg increase in grain Zn concentration through conventional breeding techniques. Multi-location testing in target areas has led to the development of 7 'lead varieties' with grain Zn concentrations above the baseline 33 mg/kg (Velu et al., 2012; Guzmán et al., 2014). One of these 'lead varieties': 'ZincShakthi' has undergone rigorous multi-location testing in India through the dissemination of 1000 mini-kit seed bags to farmers and is now marketed and released throughout India (Velu et al., 2015). Two efficacy trials are currently underway to test the potential of biofortified wheat varieties in combatting Zn malnutrition; one trial with schoolchildren in Bangalore and the other among preschool children and their mothers in the slum areas of New Delhi (Moursi, 2015). This will allow the real-world applicability of these biofortified varieties to be assessed in terms of addressing population wide Zn deficiencies.

QTL (Quantitative Trait Loci/Locus) analyses have been conducted to try and establish the chromosomal location of genes involved in the increased grain concentration of Zn. A QTL analysis carried out by Olmos et al. (2003) using *Triticum diccoides* (wild emmer wheat), originally tried to locate a locus affecting grain protein content. A locus named *Gpc-B1* (*Grain Protein Content B1*) on chromosome 6B was identified as a candidate. This locus, encodes a NAC transcription factor in ancestral wheat, which also contributes to Zn and Fe concentrations by accelerating senescence and increasing nutrient remobilisation from leaves to the developing grain (Uauy et al., 2006; Distelfeld et al., 2007). Another QTL analysis examining grain Zn concentration using a double haploid population derived from a cross between RAC875-2 (Zn-inefficient line) and Cascades (moderately Zn-efficient line) identified QTL on chromosomes 3D, 4B, 6B and 7A that mapped well to grain Zn concentration (Genc et al., 2009). The integration of the alleles underlying these loci into commercial wheat cultivars may provide an option to increase the micronutrient concentration of the grain.

It is clear that considerable variation in grain Zn content exists both between and within primitive and modern wheat varieties. However, there is very little information available at the molecular level providing information as to why certain cultivars are more efficient in their Zn uptake and partition more Zn to the grain than others. Perhaps with a better molecular understanding of the mechanisms underlying these variations in grain Zn content, a more targeted, genetic approach could be deployed to breed future cultivars with increased grain Zn content. Addressing the knowledge gap of the regulatory mechanisms that control grain Zn content may allow a complementary genetic solution to be explored in the development of biofortified crop varieties.

Genetic modification approaches

Genetic modification techniques offer the chance of a more focused approach to increasing grain Zn content. However, this approach relies on a detailed understanding of the molecular basis underlying Zn uptake from the soil and partitioning to the grain. Unfortunately the physiological processes controlling Zn uptake and the subsequent micronutrient accumulation in seeds are not fully understood (Cakmak, 2008; Rengel, 2011). Aspects of the Zn transport pathway have been elucidated in several crop species including rice (*O. sativa*) (Ishimaru et al., 2005; Bashir et al., 2013), maize (*Zea mays*) (Li et al., 2013, 2016) and barley (*H. vulgare*) (Pedas et al., 2009; Tiong et al., 2013, 2015) as discussed in the following sections. However, more research is needed in order to augment our understanding of these Zn acquiring processes. Further knowledge of Zn uptake and partitioning throughout the plant will be essential for developing breeding programmes and biofortification strategies to generate wheat lines with increased performance in Zn-deficient conditions as well as higher Zn-accumulating wheat cultivars.

1.4 An overview of Zn transport from soil to grain

This section seeks to explain the mechanisms known to be of importance in the uptake, transport and partitioning of Zn in plants.

1.4.1 Zn uptake from the soil

The primary route for plants to obtain Zn is through root absorption in the soil. The total concentration of Zn in the soil is determined predominantly by the composition of parental rock material (Chesworth, 1991). Typically, agricultural soils contain 10 to 300 mg Zn kg⁻¹ with an average around 55 mg Zn kg⁻¹ (Barber, 1995). In a global study by Sillanpää (1982), soil samples were examined from 190 field trials across 15 countries. Results showed that Zn deficiency was the most frequent soil micronutrient deficiency with 49% of all soils sampled being classed as Zn-deficient (DTPA extractable value ≤ 0.5 mg/l). Zn-deficient soils are prevalent the world over and vast areas of China, Australia, India and Eastern Europe are all badly affected (Alloway, 2008). However, soil Zn concentration is not always a reliable measure of Zn availability to the plant. The availability of Zn in the soil is governed by a complex interplay of edaphic factors. Temperature (Brennan et al. 1993), pH (Wang et al., 2006), moisture levels (Haldar and Mandal, 1979) and the interaction with other nutrients (Loneragen & Webb 1993) are the primary biophysical factors that influence availability of Zn in the soil to the plant. Often Zn may be present in the soil, but its accessibility to the plant is low due to constraints by one or more of these edaphic influences.

Zn reaches the root surface by root interception (Goos et al., 2000), diffusion (Tinker and Nye, 2000) and mass flow (Strebel and Duynisveld, 1989). Zn uptake occurs from the soil directly in the form of Zn^{2+} (Marschner 1995). Cations such as Zn^{2+} are unable to diffuse across the selectively permeable plasma membrane. Instead they must be transferred across the membrane by transport proteins. A key membrane transporter family involved in the uptake and subsequent transport of Zn throughout the plant is the ZIP (ZRT, IRT-related Protein) transporter protein family, named after the yeast ZRT1 protein and the *A. thaliana* IRT1 protein (Grotz et al., 1998; Guerinot, 2000).

ZIPs (ZRT, IRT-related proteins)

Most ZIP family members are predicted to have eight transmembrane (TM) domains, with their amino- and carboxyl-terminal ends situated on the outer surface of the plasma membrane (Guerinot, 2000). These proteins vary in size (309-476 amino acids) due to the variable region they possess between TM domains 3 and 4. Little is known about the exact transport mechanism of the ZIPs. A study of the human ZIP transporter hZIP2 showed Zn transport was not energy dependent, however it was stimulated by HCO_3^- treatment suggesting a Zn^{2+}/HCO_3^- symport mechanism (Gaither and Eide, 2000), although there is no supporting evidence for this in the literature. Conflicting results have been observed for yeast ZIPs: ZRT1 and ZRT2 which both show a strict energy dependence for Zn transport (Zhao and Eide, 1996a, 1996b). Furthermore, it has been proposed that Zn transport through ZIPs may be driven simply by the concentration gradient of unbound Zn that exists across the cell membrane (Eide, 2005) or perhaps more likely the negative membrane potential maintained by the plasma membrane drawing cations into the cell (Olsen and Palmgren, 2014). Despite the mechanism of Zn transport by members of the ZIP family currently being unresolved, the substrate specificity shown by members of this family is indicative of function through the carrier model.

Eide et al. (1996) demonstrated the ability of the *AtIRT1* gene to rescue a mutant yeast strain lacking in Fe uptake capacity (*fet3fet4*), demonstrating a likely role in plant Fe transport for this protein. Later, it was shown that *AtIRT1* (the founding ZIP family member) also had the ability to rescue a *zrt1zrt2* mutant yeast strain lacking in Zn uptake capacity (strain defective in both the high-affinity transporter *ZRT1*, and low-affinity transporter, *ZRT2*); demonstrating the ability of this protein to also transport Zn (Korshunova et al., 1999). Around the same time, Grotz et al. (1998) identified four closely related genes (*AtZIP1*, *AtZIP2*, *AtZIP3* and *AtZIP4*) using an *A. thaliana* cDNA expression library. *AtZIP1*, *AtZIP2* and *AtZIP3* were shown to complement the *zrt1zrt2* Zn mutant yeast strain. Comparisons of the cDNA sequences that rescued the *zrt1zrt2* mutant yeast strain in this study showed these cDNAs each encoded proteins similar to the products encoded by *ZRT1* and *ZRT2* genes of *S. cerevisiae* and the *IRT1* gene of *A. thaliana*

hence the ZIP nomenclature (ZRT, IRT-related Protein). For clarification, the ZIP family encompasses known IRT proteins as well as ZIP proteins. The suite of ZIP genes known to be involved in plant Zn transport is increasing. Recently Milner et al. (2013) discovered that *AtZIP7*, *AtZIP10*, *AtZIP11* and *AtZIP12* also have the ability to complement the *zrt1zrt2* mutant yeast strain.

Localisation studies of the *AtIRT1* gene (a ZIP family member), using a GUS reporter gene revealed interesting *in-planta* expression patterns (Vert et al., 2002). Strong expression of this gene was observed in the root hairs and epidermis when seedlings were grown under Fe-deficient conditions. Given that *AtIRT1* has been shown to transport Zn in yeast complementation assays (Korshunova et al., 1999) it seems possible that these root periphery localised transporters may be involved in Zn uptake from the soil, although they are likely more important in Fe transport.

Milner et al. (2013) used real-time PCR and GUS expression techniques to examine *in-planta* expression patterns of *AtZIP1* and *AtZIP2*. The results showed higher *AtZIP1* root stele expression when plants were grown under Zn-deficient conditions and shoot vasculature expression reduced under Zn deficiency. They observed that *AtZIP2* had higher root and shoot transcript abundance under Zn-replete conditions and GUS expression was only ever seen in the root of the plant. These expression studies indicate distinct roles of these two *AtZIP* transporters, but the lack of root hair or epidermal expression suggests a limited role in Zn uptake from the soil, but importance in Zn transport throughout the plant vasculature.

Evidence from the range of ZIP family genes investigated in the literature suggests that individual ZIP genes may have very distinct roles in terms of plant localisation (Li et al., 2013). Further characterisation will help unravel the role of specific ZIP family transporters and reveal which are directly associated with Zn (as well as other micronutrient) uptake from the rhizosphere.

Do Zn and Fe share aspects of their uptake mechanisms?

The most studied of all plant micronutrient uptake mechanisms is that of Fe. Plants have evolved two strategies for the uptake of Fe from the soil when faced with deficiency. Strategy I is classically thought to be employed by all higher plants except the gramineae (grass family) (Hell and Stephan, 2003; Marschner and Romheld, 1994). Strategy I plants employ an uptake mechanism whereby membrane-localized H⁺-ATPase pumps, extrude protons into the rhizosphere, acidifying it. This acidification of the rhizosphere drives more Fe(III) into solution, which is in turn reduced to Fe(II) by the FRO2 membrane protein (Ferric Reductase-Oxidase 2) (Robinson et al., 1999) and then transported across the plasma membrane by a ZIP family member; IRT1 (Iron Regulated Transporter 1) (see Figure 1.2).

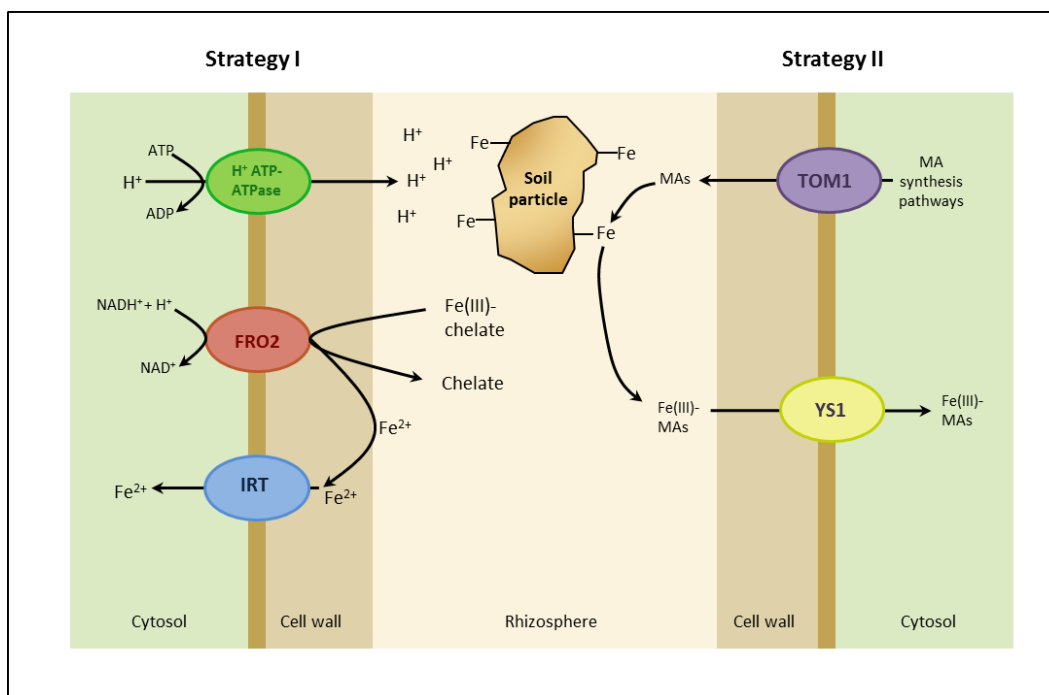


Figure 1.2. Strategy I and II uptake pathways of Fe. Coloured ovals indicate plasma membrane transporters. Abbreviations: FRO, ferric reductase-oxidase; IRT, iron-regulated transporter; MA, mugineic acid; TOM, transporter of MA; YS1, yellow stripe-like protein 1. Figure adapted from Hell and Stephan (2003), Kobayashi and Nishizawa (2012) and Jones et al. (2013)

Members of the grass family (such as wheat) are broadly classified as strategy II plants due to their ability to take up certain metals from the soil in a form bound by chelators. These chelators are excreted by plants and termed phytosiderophores (PS). One class of phytosiderophore, the mugineic acids (MAs), have been shown to be particularly important in the uptake of Fe from the rhizosphere (Ishimaru et al., 2006). These low molecular mass MAs are pumped into the soil by TOM transporters (Transporter Of Mugineic acid) (Nozoye et al., 2011) where they bind soluble Fe that is then taken up in an Fe-phytosiderophore complex through specific complex transporters, the YSLs (Yellow Stripe-Like proteins) (Suzuki et al., 2006) (see Figure 1.3). Although this chelation-based strategy is more important in terms of Fe uptake, there is strong evidence that suggests it plays a role in Zn uptake from the soil. In mutant maize (*Z. mays*) plants (*ys1*), lacking a *YS1* gene that codes for a known YSL Fe-phytosiderophore transporter, a lower amount of Zn was measured in the roots when compared to wild-type plants (Von Wiren et al., 1996). This experiment was supported by expression of *ZmYS1* in yeast and *Xenopus* oocytes which showed transport of both Fe-phytosiderophore and Zn-phytosiderophore complexes (Schaaf et al., 2004).

Evidence of the importance of this phytosiderophore-mediated strategy in Zn uptake is also given by Suzuki et al. (2006). Suzuki et al. (2006) showed that Zn-deficient barley upregulated genes involved in the biosynthesis pathways of MAs and increased secretion of MAs from the roots. They also demonstrated the uptake of Zn-MA complexes by barley using

radiolabelled techniques. The barley plants investigated were proven to be Fe sufficient; thus, these results give compelling evidence for the use of this MA secretion approach by graminaceous species in Zn uptake. This is further supported by evidence obtained from a comparative study of two barley cultivars; Tarm-92 (a Zn-efficient cultivar) and Hamidiye-79 (a Zn-inefficient cultivar) (Erenoglu et al., 2000). Root exudate analysis of these two cultivars showed there was no difference in the increase of phytosiderophore release levels between the two cultivars when they were grown under Fe-deficient conditions, but when grown under Zn-deficient conditions the Zn-efficient cultivar (Tarm-92) released higher amounts than Hamidiye-79. This further indicates the importance of this uptake mechanism, and that a differential level of phytosiderophore release under Zn-deficient conditions may explain a proportion of the varietal differences of Zn-efficiency in barley.

A similar study has been carried out in wheat (*T. aestivum* and *T. durum*) genotypes that differ in Zn-efficiency (Cakmak et al. 1996). Root exudation analysis showed that phytosiderophore release was increased to a greater extent when plants were grown under Zn-deficient conditions by the Zn-efficient bread wheat (*T. aestivum*) cultivars Aroona and Gerek-79, compared to the Zn-inefficient bread wheat (*T. aestivum*) genotype Kirkpinar. Interestingly, despite there being a clear variation in the Zn-efficiency of the durum wheat (*T. durum*) genotypes studied, there was either a very low increase or no change in phytosiderophore release under Zn-deficient conditions. This suggests that variation in phytosiderophore exudation may go some way towards explaining differential Zn-efficiency in bread wheat (*T. aestivum*), however it is likely to be only one of a suite of causal factors due to the results of the durum wheat (*T. durum*) genotypes tested in this study.

Until recently it was thought that the two Fe uptake strategies were distinct, in that all higher plants except the Poaceae family employed strategy I while the Poaceae family exclusively used strategy II. Recently this consensus has been challenged. In rice, the presence of two functional Fe²⁺ transporters which are expressed in the roots under Fe deficiency suggests rice most likely uses a combined approach with phytosiderophore release and subsequent Fe(III)-PS uptake through OsYSL15 while also uptaking Fe²⁺ using IRT transporters (Walker and Connolly, 2008; Ishimaru et al., 2006). A rice mutant line with a mutation in a key enzyme involved in phytosiderophore synthesis (nicotianamine aminotransferase) lacks the ability to extrude phytosiderophores, but when supplied with Fe²⁺ is able to grow (Cheng et al., 2007). This suggests rice has a combined strategy for Fe uptake. Ricachenevsky and Sperotto, (2014) have proposed that the most likely evolutionary route for this is an ‘ancient combined strategy’ whereby an ancestor of rice most likely developed strategy II whilst also keeping the strategy I ability, rather than losing strategy I and rice then reversing the evolutionary loss and re-evolving strategy I back again. Li et al. (2016) have also proposed that maize utilises a combined Fe uptake strategy. The

ability of *ZmIRT1* and *ZmZIP3* to increase the levels of Fe and Zn in *A. thaliana* supports the presence of a strategy I uptake system in maize and also suggests this is an uptake route for Zn as well as Fe. Due to the evolutionary relatedness of wheat with maize and rice it appears most likely that wheat also most likely uses a combined strategy for Fe and Zn uptake.

How could knowledge of Zn transport mechanisms be utilised for improved uptake and biofortification?

With a better understanding of the key transporters involved in the uptake a distribution of Zn throughout the plant, as well as the regulatory mechanisms that control these processes, it may be possible to improve the Zn content of wheat through four interlinked strategies: 1) improvement of Zn uptake efficiency, thus increasing the total amount of Zn in the plant. 2) altering the distribution of Zn in the plant, perhaps by manipulating translocation ratio from root to shoot plant portions. 3) increase the efficiency of Zn remobilisation at senescence, an increase in Zn remobilisation from vegetative tissue to the grain. 4) increase Zn harvest index, improving the proportion of Zn in the above ground plant matter that is in the grain relative to the vegetative tissue. The available evidence provided across a range of plant species discussed in this chapter suggests the ZIP transporters are promising candidates for this objective, however information of their role in wheat is currently lacking.

The roles of the ZIP transporters are well illustrated in a group of plants known as the hyperaccumulators. This small group of species are able to accumulate certain heavy metals (including Zn) to extremely high, normally toxic concentrations in their shoots (Baker and Proctor, 1990). These plants have evolved to occupy the niche created by either natural or anthropogenic high metal containing soils, such as those near ore mining projects or those naturally found in the Harz mountains for example (Macnair et al., 1999). Studies of hyperaccumulator species (notably *Nocceae caerulescens*, *Arabidopsis halleri* and *Nocceae japonica*) have shown an elevated expression of various ZIP family metal transporters (Assunção et al., 2001), expression of these ZIPs is often notably higher in the roots of the hyperaccumulators studied (Wu et al., 2009). The elevated shoot tissue Zn concentrations of the hyperaccumulators shows a prospective route for the biofortification of crop species by selectively enhancing root metal transporters to achieve a higher shoot tissue concentration that could then be genetically diverted to the edible parts of the plant.

Indeed, a study in *H. vulgare* (barley) showed that overexpressing the *AtZIP1* gene by means of a ubiquitin promoter, increased Zn uptake and ultimately led to an increase in grain Zn content (Ramesh et al., 2004). The increase in Zn content in the grain shown was, however, accompanied by a reduction in average grain weight of 27% which is not desirable in terms of yield maintenance. The Zn content per grain was increased in the transgenic *H. vulgare* lines,

indicating that the increase in grain Zn concentration was not due to the dilution effect of smaller grain size. Interestingly Fe content per grain was also increased in the transgenic lines.

ZIP transporters have been identified and studied in a variety of crop species including; maize (*Z. mays*) (Li et al., 2013, 2015a), rice (*O. sativa*) (Ramesh et al., 2003; Bashir et al., 2012; Kavitha et al., 2015), soybean (*Glycine max*) (Moreau et al., 2002), tomato (*S. lycopersicum*) (Eckhardt et al., 2001), barley (*H. vulgare*) (Tiong et al., 2013, 2015), grape (*Vitis vinifera*) (Gainza-Cortés et al., 2012), navel orange (*Citrus sinensis*) (Xing et al., 2016) and bean (*Phaseolus vulgaris*) (Astudillo et al., 2013). A consistent trend across these studies is the upregulation of ZIP genes under Zn-deficient conditions. Most relevant for wheat research is the information of ZIP expression and characterisation in barley; *HvZIP3*, 5, 7, 8, 10 and 13 are all upregulated in response to Zn-deficient conditions (Pedas et al., 2009; Tiong et al., 2013, 2015). Furthermore, HvIRT1, HvZIP3, 5 and 8 have all been shown to rescue the *zrt1/zrt2* Zn mutant yeast strain, indicating Zn transport ability (Pedas et al., 2008, 2009).

At present, there is only one study in which a ZIP transporter has been investigated in a wheat species (Durmaz et al., 2011); wild emmer wheat (*T. turgidum* ssp. *dicoccoides*) a tetraploid relative of modern bread wheat (*T. aestivum*). This emmer wheat ZIP transporter (*TdZIP1*) was shown to be upregulated in the roots of plants grown under low Zn conditions and through complementation assays, the Zn-transporting capabilities of this protein were confirmed (Durmaz et al., 2011). This project seeks to address the existing knowledge gap of the role (and regulation) of ZIP transporter genes in bread wheat (*T. aestivum*) in aid of biofortification.

Although the Zn accumulation methods outlined in this section pose a valuable genetic route for manipulating plant Zn content, it is important to be wary of cadmium (Cd) accumulation. Cd is termed a Zn mimic; its structure is analogous to Zn yet it has negative consequences to both plants and animals (Martelli et al., 2006). This inadvertent uptake of Cd by plants may pose a problem for enhanced Zn containing crop production. This potential problem must be acknowledged and addressed in any genetic biofortification programme due to the low maximum proposed permissible levels of Cd (0.2 mg/kg) in wheat and rice grain (FAO and WHO, 2001a).

1.4.2 Root epidermis to xylem

In order for Zn to travel to the above ground parts of the plant it must travel inwards, from the epidermal cells of the root, to the stele where it is loaded into the xylem for long-distance transport. Initially, Zn can travel through both the symplastic and apoplastic pathways of the plant, towards the stele. However, upon meeting the Casparian strip situated in the endodermis, all transport must switch to symplastic pathways taking a route through the cell-adjointing plasmodesmata in order to penetrate this suberin layer (Sinclair and Krämer, 2012) (see Figure 1.3). No information is available as to what membrane transporters facilitate this necessary

Chapter 1. Introduction

switching from apoplast to symplast, however ZIPs are possible candidates for this given the GUS localisation to the root stele of *AtZIP1* and *AtZIP2* previously observed (Milner et al., 2013). Once past the Casparian strip, the next major obstacle for Zn transport is the loading of the xylem from the adjacent pericycle/xylem parenchyma cells.

At the interface between the xylem parenchyma and the xylem, all components destined for further transport must leave the symplasm (see Figure 1.3). This is a potential bottleneck for Zn accumulation in the above ground edible tissues (the grain in wheat) (Palmgren et al., 2008). A phenotypic study using mutant *A. thaliana* plants carrying defective *hma2* and *hma4* (Heavy Metal Transporting ATPase family) genes produced plants that exhibited stunted growth and chlorosis through an inadequate Zn supply to the leaves (Hussain et al., 2004). In the same study, a GUS-construct was used to report the spatial expression of these two genes in transgenic *A. thaliana* plants. The GUS reporter was expressed strongly in xylem parenchyma cells as well as the vasculature of leaves and the outer cells of immature anthers. Mills et al. (2003 & 2005) showed through the use of heterologous expression with *E. coli* and yeast strains that AtHMA4 is also important in conferring resistance at higher Zn concentrations. This led to the deduction that AtHMA4 possibly plays a dual role in the plant, pumping Zn across the xylem parenchyma under normal concentrations and, at high concentrations of Zn, it could serve to beneficially export Zn from the root either to the shoot or the rhizosphere possibly through alternative cell expression locations (Mills et al., 2005). An overexpression study of *AtHMA4* has revealed that *A. thaliana* overexpressing lines show increased shoot concentrations of Zn (as well as Cd) (Verret et al., 2004). This further supports the evidence that members of the HMA family are key translocation proteins for Zn movement into the xylem.

Research in rice (*O. sativa*) has provided evidence that the function of OsHMA2 is in the xylem loading of Zn (Sato-Nagasawa et al., 2012). T-DNA rice insertion mutants showed a reduction in Zn (as well as Cd) translocation ratio (high concentration of Zn in the root compared to shoot), indicating that Zn was prevented from translocating from the root at the point of xylem loading (Sato-Nagasawa et al., 2012). Barley (*H. vulgare*) *HvHMA2* has been isolated and shown to transport both Zn and Cd in heterologous expression studies with *S. cerevisiae* (Mills et al., 2012). *HvHMA2* also rescues the Zn-deficient phenotype of the *Arabidopsis hma2hma4* mutant indicating it functions as a Zn pump *in-planta* (Mills et al., 2012).

A recent study in wheat (*T. aestivum*) has isolated and characterized *TaHMA2* (Tan et al., 2013). *TaHMA2* over-expression in rice (*O. sativa*), tobacco (*Nicotiana tabacum*) and wheat (*T. aestivum*) increased the translocation ratio (increase in Zn/Cd transport to the shoot from the root). Interestingly, it was observed that overexpression of *TaHMA2* had no effect on seed Zn content of tobacco (*N. tabacum*), but in wheat (*T. aestivum*) and rice (*O. sativa*) an overall decrease in grain Zn concentration was measured. The distribution of this grain Zn concentration reduction

differed between rice (*O. sativa*) and wheat (*T. aestivum*), with all parts of the transgenic rice seeds decreasing in Zn concentration yet only the endosperm of the wheat grain was reduced with the surrounding embryo and aleurone layers actually increasing in Zn concentration. This suggests that TaHMA2 may have a specific role in the Zn loading of the embryo and aleurone. Recently, mutant studies in *Arabidopsis* have revealed the important role of AtHMA2 and AtHMA4 in loading Zn from the seed coat into the *Arabidopsis* seed (Olsen et al., 2016). Further analysis of these HMA genes, particularly those of crop species may provide opportunities for their use in breeding programmes to aid the goal of biofortification.

Another candidate membrane protein proposed to be involved in the loading of xylem is *AtPCR2* (Plant Cadmium Resistance). Through the use of mutant phenotype studies it was shown that the roots of *Arabidopsis pcr2* plants accumulated more Zn than control plants, whilst the roots of plants overexpressing *AtPCR2* contained less Zn, indicating an important role in Zn translocation of *AtPCR2* (Song et al., 2010). Interestingly *Arabidopsis pcr2* mutant lines showed sensitivity to both Zn deficiency and excess, suggesting a dual function of *AtPCR2* with xylem loading under Zn-deficient conditions and efflux via the epidermal cells under conditions of Zn-excess. *OsPCR1* has been identified in rice, overexpression causes an increase in total Zn content of rice grain, suggesting a role in Zn partitioning in rice (Song et al., 2015).

FRD3 (Ferric-Reductase Defective 3) has also been implicated in the translocation of Zn from roots to shoots, achieved through the transport of citrate into the xylem. Although it is hypothesised that this citrate transporter is primarily used to maintain the mobility of Fe in the xylem, it is thought that FRD3 provides high Zn tolerance by alleviating the competition between Fe and Zn in the root to shoot transport system, thus preventing Fe deficiency in conditions of Zn excess (Pineau et al., 2012). FRD3 orthologues are highly expressed (16-fold in roots) in the Zn hyperaccumulator *A. halleri* compared to *A. thaliana* confirming their role in metal homeostasis (Talke, 2006). The distribution of Zn speciation in the xylem sap of the hyperaccumulator *T. caerulescens* shows that 21% of Zn is bound to citrate (Salt et al., 1999); this suggests that the citrate transported by FRD3 may be important in providing a ligand for Zn transport in the xylem as well as Fe.

In addition to the aforementioned HMAs, PCRs and FRD3, ZIPs may also have a role in xylem loading. In the GUS-reporter studies carried out with *AtZIP1* and *AtZIP2*, Milner et al. (2013) observed increased expression in the root stele. Also in this study the *Arabidopsis zip2* knockout lines showed a significant increase in root Zn concentration suggesting a possible role for this transporter in the Zn translocation from root to shoot. This suggests that members of the ZIP family may also be involved in loading of the xylem from xylem parenchyma cells.

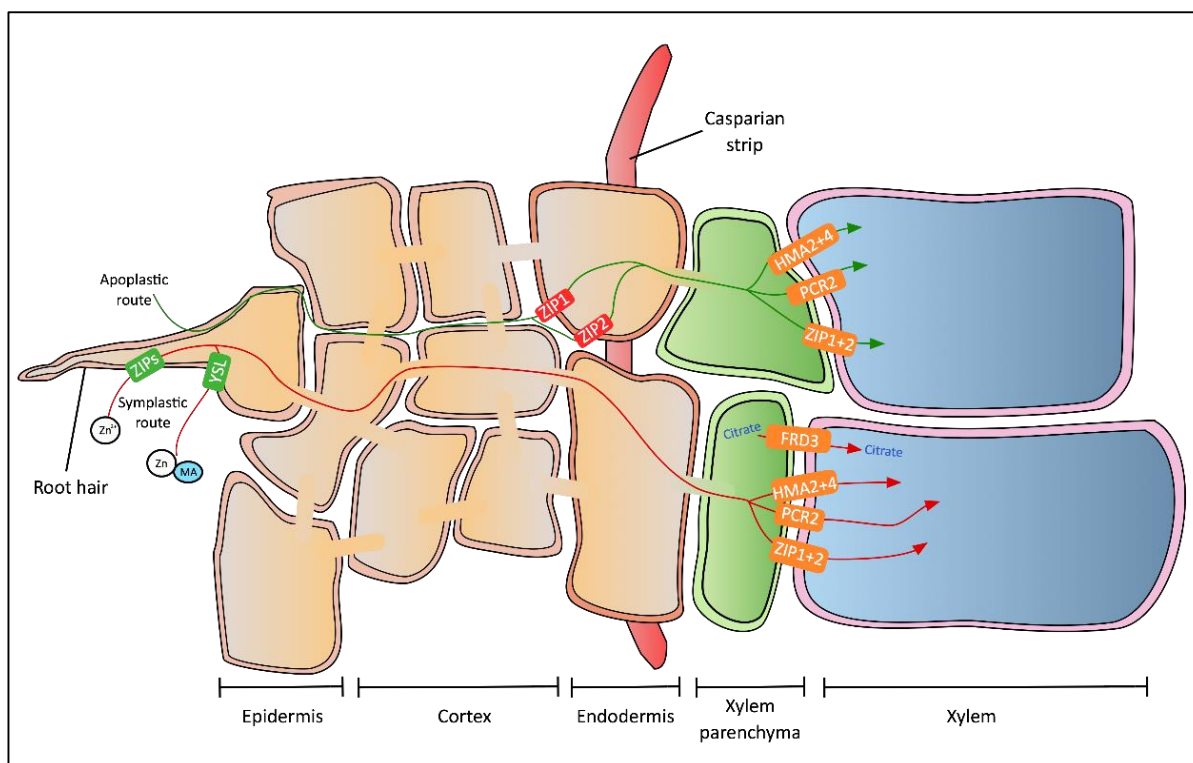


Figure 1.3. The route of Zn from uptake to xylem loading. Both the symplastic and apoplastic pathways are shown (depicted with a red and green arrow respectively). The metal transporters proposed to be involved in the process are shown in green (epidermis uptake proteins), red (for endodermis loading proteins) and in orange (for xylem loading proteins). Abbreviations: FRD, ferric reductase defective; HMA, heavy metal transporting ATPase; MA, mugineic acid; PCR, plant cadmium resistance; YSL, yellow stripe-like protein; ZIP, ZRT IRT-related protein. Root schematic adapted from Jones et al. (2013).

1.4.3 Loading of phloem

Thus far, the likely mechanisms that plants use to transport Zn from the rhizosphere to the xylem have been outlined. However, with regards to biofortification, the goal is to increase the concentration of micronutrients in the edible parts of the plant; in the case of wheat, increasing the Zn content of the grain. The only vasculature to reach the grain is the phloem (Oparak and Gates, 1984). Therefore, the unloading of Zn from the xylem and the loading of the phloem is a key step.

In graminaceous species, nodes play a key role in the distribution of elements throughout the above-ground biomass. Nodes are junctions below the panicles on the stems of plants. Each node has a leaf branching from it, that is connected via the leaf sheath, and a peduncle which has the rachis and grains above (Yamaji and Ma, 2014) (see Figure 1.4). The morphology and research into the importance of nodes is advanced in rice (*O. sativa*) when compared to other graminaceous species. The profile of wheat straw and node morphology have only recently been reported (Ghaffar and Fan, 2015). However, the following findings in rice (*O. sativa*) suggest the nodes of wheat (*T. aestivum*) are promising research topics in terms of plant mineral nutrition.

The nodes are key junctions containing vasculature that ultimately determines the destination of water and mineral elements. Nodes are an important connection point where vascular bundles linked with the roots, leaves and panicles are interconnected. Nodes contain vascular bundles destined for the flag leaf as well as the panicle. The vascular bundles joined to the flag leaf become enlarged and elliptical as they reach the node, hence they are named the enlarged vascular bundles (EVBs). The diffuse vascular bundles (DVBs) are joined to the EVB in the node by the xylem parenchyma cells (the parenchymal cell bridge). The destination of the DVB is the panicle, which contains the rice grains (Yamaguchi et al., 2012) (see Figure 1.4). Although previously suggested to have a role in root to shoot translocation (Sato-Nagasawa et al., 2012), *OsHMA2* has also been shown to be highly expressed in the nodes at the reproductive growth stage of rice (*O. sativa*) (Yamaji et al., 2013). Using immunohistochemical staining, it was observed that *OsHMA2* localised to the plasma membrane of the phloem of both the EVBs and DVBs suggesting an involvement in the transfer of Zn from the xylem to the vascular bundles of the phloem (Yamaji et al., 2013).

OsZIP3 has also been shown to be important in the movement of Zn in the nodes of rice (*O. sativa*). *OsZIP3* is highly expressed in the nodes regardless of Zn status and localised to the xylem transfer cells situated between the EVBs and DVBs. RNAi knockdown *OsZIP3* lines showed a reduced Zn partitioning to the internodes of the developing panicle but an increase in Zn distribution to leaves one (flag leaf), two and three (Sasaki et al., 2015). *OsZIP3* has been shown to transport Zn through yeast complementation studies (Ramesh et al., 2003) further supporting the role of this ZIP member in the above ground distribution of Zn within the plant. Additionally, *OsZIP4* has been suggested to be involved in phloem loading (Ishimaru et al., 2005). *OsZIP4* was shown to be upregulated under Zn-deficient conditions in both the root and the shoot, and through the use of GFP constructs, it was shown that there is a high level of expression in the phloem cells of rice. This shows yet another potential role for a member of the ZIP family in the transport of Zn from soil to grain.

In *A. thaliana*, members of the YSL family have been implicated in phloem loading. Waters & Grusak (2008) showed that an *Arabidopsis* double mutant *ysl1ysl3* exhibited low seed Zn and high leaf Zn concentrations. Thus it seems likely that either or both of these YSL proteins may well be important in the loading of Zn-complexes into the phloem.

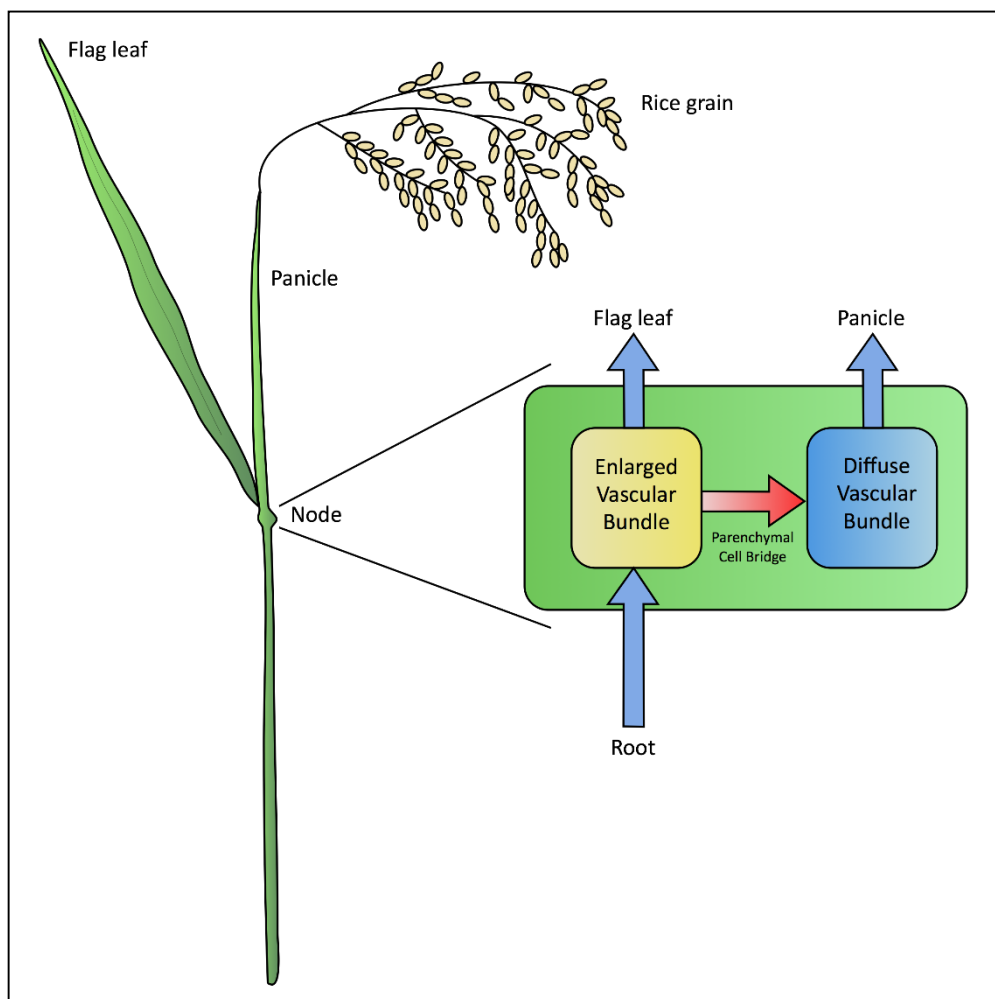


Figure 1.4. The morphology and destination of rice (*O. sativa*) node vasculature. An enlarged schematic of the node is shown with the vasculature origin and destination labelled. Figure adapted from Yamaguchi et al. (2012).

1.4.4 Additional factors involved in Zn transport

Zn partitioning within the whole plant as well as within individual cells must be regulated. An excess of Zn ions in the cell would prove deleterious to the plant, due to the adventitious binding to proteins and displacement of other metal ions such as Fe from their binding sites (Arrivault et al., 2006). Compartmentation of Zn in the vacuole of cells until nutritionally required is a solution to this partitioning dilemma. Understanding and manipulating this compartmentation could provide possible routes for biofortification. Members of the Cation Diffusion Facilitator (CDF) family of proteins, the plant Metal Tolerance Proteins (MTPs), have been put forward as likely candidates for this compartmentation role. Across the plant MTP family, substrate specificity appears to be conserved in phylogenetically related MTP proteins (Ricachenevsky et al., 2013).

Functional complementation studies in yeast, supported by fusion construct expression analysis in *A. thaliana* have shown the ability of AtMTP1 and AtMTP3 to transport Zn and that

both are expressed in the vacuolar membrane (Desbrosses-Fonrouge et al., 2005; Arrivault et al., 2006). Analysis of a mutant *Arabidopsis* line (*mtp1-1*) showed Zn sensitivity of *mtp1-1* seedlings; root growth of mutants was inhibited on high-Zn MS medium (500 μ M) (Kawachi et al., 2009). Upon closer inspection, transmission electron microscopy and energy-dispersive X-ray (TEM-EDX) revealed that wild-type roots accumulated Zn in vacuolar-like organelles, whereas mutant roots did not (Kawachi et al., 2009). The use of RNA interference (RNAi) to silence *AtMTP3* produced a hypersensitive phenotype with increased shoot Zn concentrations and a reduced biomass (Arrivault et al., 2006). This evidence suggests that *AtMTP1* and *AtMTP3* have non-redundant functions in Zn tolerance, most likely through partitioning to the vacuole (Ricachenevsky et al., 2013).

Recent research in rice has shown that *OsMTP1* functionally complements the *Arabidopsis mtp1-1* mutant, indicating conservation of function (Menguer et al., 2013). Complementation of the *zrc1/cot1* yeast mutant (lacking in the Zn and Cobalt (Co) transporters, ZRC1 and COT1) showed that *OsMTP1* can rescue the Zn-sensitive phenotype of this yeast strain. Through the expression of *OsMTP1*-GFP in yeast and *Arabidopsis mtp1-1*, *OsMTP1* was shown to localise to the tonoplast (Menguer et al., 2013). Additionally, research in barley (*H. vulgare*) has identified *HvMTP1*, which has been shown to transport Zn and Co through heterologous yeast complementation (Podar et al., 2012). The roles of MTP proteins in these crop species could provide a target for biofortification strategies. It has been proposed that endosperm specific overexpression of these MTPs could increase the grain Zn content of crops (Palmgren et al., 2008; Ricachenevsky et al., 2013).

AtZIF1 (Zn-Induced Facilitator) is a further membrane transporter proposed to be important in vacuolar Zn partitioning. *AtZIF1* is localised to the tonoplast, overexpression enhances vacuole partitioning of nicotianamine (a metal chelator) in roots and is accompanied by a vacuolar build-up of Zn and an overall increase in root Zn concentration whilst shoot Zn concentrations are reduced (Haydon et al., 2012). *AtZIF2* has also been identified in *Arabidopsis* and shown to rescue the *zrc1/cot1* yeast mutant, (Remy et al., 2014). *Arabidopsis zif2* mutants are hypersensitive to Zn whilst *AtZIF2* overexpression enhances Zn tolerance in *Arabidopsis*. *AtZIF2* was shown to localise to the tonoplast, primarily in root cortical cells and was proposed to transport a small Zn chelator or Zn binding organic acid. Intriguingly Remy et al. (2014) discovered the presence of two different *AtZIF2* transcripts with alternate intron retention in the 5' UTR region of the transcripts. *AtZIF2.2* had a 229 nucleotide long intron in the 5' UTR compared to *AtZIF2.1*. Through luciferase assays it was shown that the intron retention in *AtZIF2.2* doubles the translation efficiency compared to *AtZIF2.1*. It was also shown that alternative splicing was Zn-regulated; higher Zn growth concentrations resulted in higher levels of the longer, more efficiently translated *AtZIF2.2* transcript. This is a post-transcriptional

mechanism that means under high Zn conditions the translational efficiency of this transporter associated with vacuolar Zn sequestration ability is higher, enhancing plant tolerance to Zn at higher levels.

In graminaceous species the Transporters Of Mugineic acids (TOMs) (discussed previously) share conserved motifs with the *AtZIFs*, both are members of the Major Facilitator Superfamily (MFS). For example, OsTOM1 shares 55% amino acid similarity to AtZIF1 (Haydon et al., 2012). The TOMs are expressed in the roots highly under Fe deficiency and in the shoots to a lesser extent, they facilitate Fe uptake by transporting mugineic acids into the soil but are also thought to efflux mugineic acid to the phloem and xylem for internal Fe transport (Nozoye et al., 2011). Deoxymugineic acid (DMA), the primary member of the phytosiderophore family also chelates Zn, thus the TOMs may be important proteins in the transport of Zn throughout the plant as well as the chelation of Zn in the soil (Suzuki et al., 2008). Genes closely related to the rice TOMs have been identified that transport nicotianamine (NA) rather than DMA. These have been named ENA1 and ENA2 (Efflux transporter of NA) (Nozoye et al., 2011). OsENA1 is similar to AtZIF1, and is also predicted to localise to the tonoplast (Nozoye et al., 2011). It has been proposed that OsENA1 may participate here in metal detoxification by transporting NA to the vacuole (Nozoye et al., 2011).

The VITs (Vacuolar Iron Transporters) are another family of transporters that may be of interest in terms of Zn biofortification. In rice (*O. sativa*), OsVIT1 and OsVIT2 can transport Fe and Zn and have been shown to localize to the vacuole. Rice *vit1* and *vit2* T-DNA insertion mutants showed a significant accumulation of Fe and Zn in rice seeds and a corresponding decrease in the flag leaves. This led to the deduction that OsVITs have a role controlling the amount of Fe and Zn that is translocated from source to sink (Zhang et al., 2012). Zhang et al. (2012) postulated that rice plants may control Fe and Zn translocation to the seeds by setting a 'buffering pool' level in flag leaves. The manipulation of this level through targeted knockout of VIT genes could be a potential strategy for Fe and Zn biofortification.

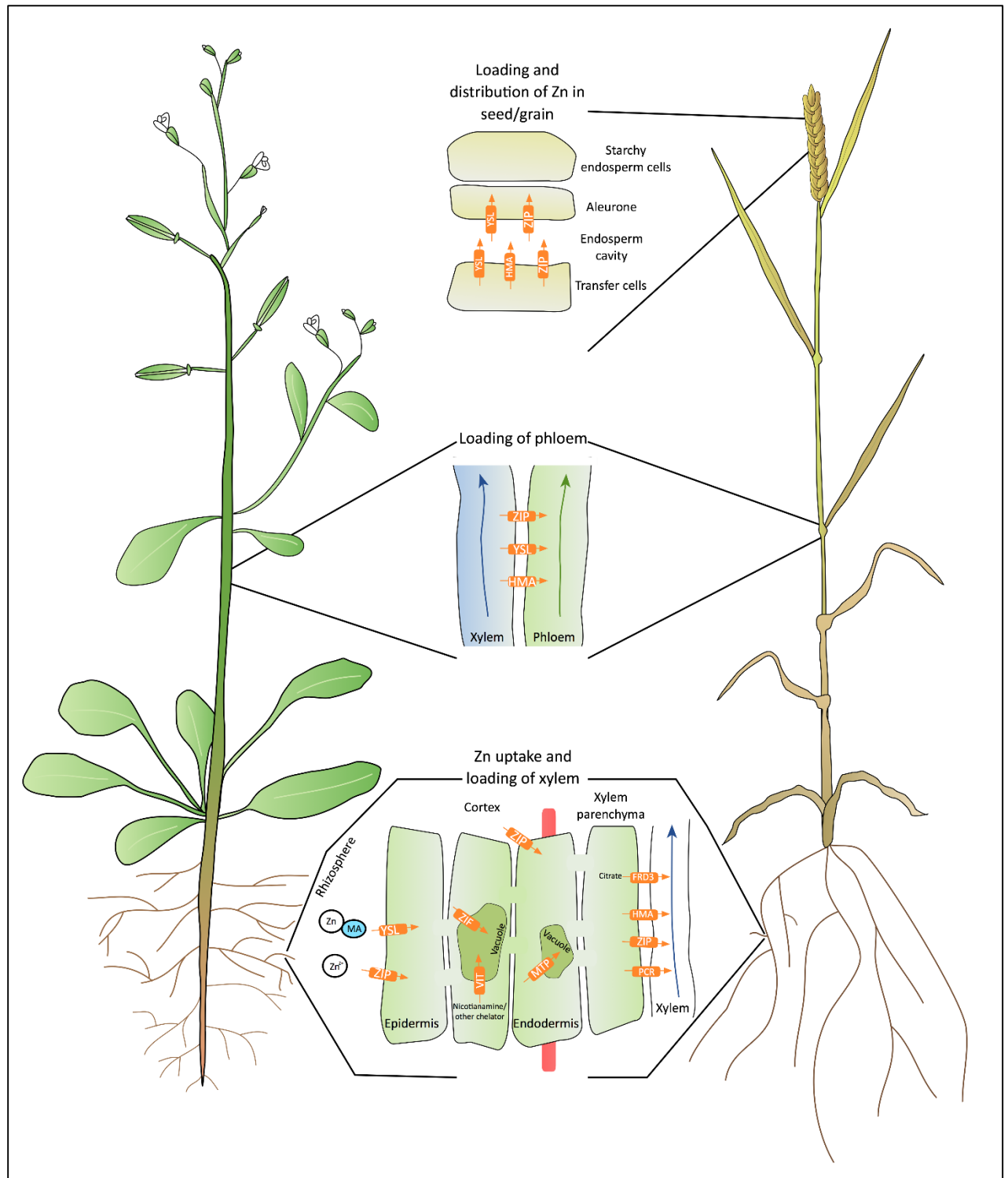


Figure 1.5. An overview of key steps in the transport of Zn from soil to grain/seed. Orange boxes in enlarged sections indicate key metal transporter families involved in the journey of Zn from soil to seed, with the transporter family annotated within. Each of these steps of Zn uptake, loading and translocation are covered in-depth throughout Section 1.4. Abbreviations: FRD, ferric reductase defective; HMA, heavy metal transporting ATPase; MA, mugineic acid; MTP, metal tolerance protein; PCR, plant cadmium resistance; VIT, vacuolar iron transporter; YSL, yellow stripe-like protein; ZIF, Zn-induced facilitator; ZIP, ZRT IRT-related protein. Plants in figure represent dicotyledon (left) and monocotyledon (right).

Table 1.6. Summary of key transporter families involved in plant Zn uptake, subsequent transport and vacuolar sequestration. Key transporter families are listed along with brief summaries of the role in the plant, where possible the transport mechanisms of the transporter families are given.

Transporter family	Role in plant Zn transport	Transport mechanism	References
ZIP (ZRT, IRT-related Protein)	Proposed to be involved in Zn uptake from the rhizosphere, loading of the xylem and loading of the phloem.	Transport mechanism unconfirmed, as discussed in Section 1.4.1	(Grotz et al., 1998; Milner et al., 2013; Ramesh et al., 2004; Durmaz et al., 2011; Pedas et al., 2009; Tiong et al., 2015)
HMA (Heavy Metal Transporting ATPase)	Xylem loading of Zn, important in the translocation from root to shoot.	Subgroup of the large superfamily of P-type ATPases which use ATP to pump charged substrates across membranes against the concentration gradient, forming a phosphorylated intermediate during the reaction cycle.	(Axelsen and Palmgren, 1998; Hussain et al., 2004; Mills et al., 2003, 2005; Verret et al., 2004; Mills et al., 2012; Tan et al., 2013)
PCR (Plant Cadmium Resistance)	Proposed to be involved in xylem loading under Zn-deficient conditions and efflux via epidermal cells under Zn-excess.	Likely forms homooligomers of the two putative membrane-spanning α -helices and predicted to act as secondary active transporters.	(Song et al., 2010, 2015)
FRD3 (Ferric Reductase Defective 3)	FRD3 transports citrate into the xylem which is likely most important for Fe mobility, however may have a role in Zn transport through the xylem.	Multidrug and toxin efflux transporter (MATE) transporter likely to be proton-dependent efflux transporters, as antiporters using existing proton gradients.	(Pineau et al., 2012; Talke, 2006; Eckardt, 2001)
YSL (Yellow Stripe-Like proteins)	Fe-phytosiderophore and likely Zn-phytosiderophore uptake from the rhizosphere. Additionally implicated in phloem loading of Zn-complexes.	Proton coupled symporter for phytosiderophore- and nicotinamine-chelated metals.	(Von Wiren et al., 1996; Schaaf et al., 2004; Waters and Grusak, 2008)
MTP (Metal Tolerance Proteins)	Sequestration of Zn into the vacuole under high Zn conditions.	Members of the Cation Diffusion Facilitator (CDF) family. Unknown transport mechanism in plants.	(Desbrosses-Fonrouge et al., 2005; Arrivault et al., 2006; Menguer et al., 2013; Ricachenevsky et al., 2013)

Table 1.6. continued

Transporter family	Role in plant Zn transport	Transport mechanism	References
ZIF (Zn-Induced Facilitator)	Vacuolar sequestration of Zn either via nicotianamine transport or direct Zn transport.	Members of the Major Facilitator Superfamily (MFS), proposed to act as a proton-coupled antiporter of a metal chelator or metal chelate complex into the vacuole.	(Haydon et al., 2012; Remy et al., 2014)
TOM (Transporter Of Mugineic acids)	Efflux of phytosiderophores into the soil as well as phloem and xylem which subsequently binds Zn.	Members of the MFS, unknown mechanism of transport, however likely to be proton coupled antiporters.	(Nozoye et al., 2011)
ENA (Efflux transporter of NA)	Efflux of NA into the vacuole which may aid in Zn sequestration.	Closely related to the TOMs, likely to be proton coupled antiporters.	(Nozoye et al., 2011)
VIT (Vacuolar Iron Transporter)	Vacuolar transporters capable of Zn transport.	Transport mechanism unknown though likely to be proton coupled antiporter.	(Zhang et al., 2012)

1.4.5 Loading and distribution of Zn in grain

For cereal biofortification, the required destination of Zn is the grain, specifically the edible components. The grain itself consists of several distinct regions. The testa, or pericarp surrounds the grain. Beneath this protective sheath is the aleurone (the outermost layer of the endosperm), the endosperm (the major starch storage region) and the embryo (see Figure 1.6). Currently, research efforts are striving to understand the molecular mechanisms underlying Zn transport across and within these distinct grain regions, various studies have allowed the distribution of Zn in the grain to be elucidated. DTZ (diphenyl thiocarbazon) stain forms a red complex with Zn and has been used to give a low resolution distribution map of Zn in the seed (Ozturk et al., 2006) (Figure 1.7A.). More advanced imaging techniques using an X-ray synchrotron technique have also been employed to generate higher resolution fluorescence heat maps of mineral distributions within the grain (Neal et al., 2013) (Figure 1.7B.). Both imaging techniques have shown that a high concentration of Zn is accumulated in the embryo and the aleurone. A proposed explanation for this accumulation is that the Zn present in the embryo and aleurone is complexed with phytate. This phytate-Zn complex may either not be recognised by metal transporters (Tauris et al., 2009) or is too large to be transported efficiently (Neal et al., 2013). This is unfortunate as both of these Zn rich fractions are lost in the milling process, thus going some way to explaining the low Zn concentration of milled grain.

The grains of wheat are symplastically isolated from the phloem (Patrick and Offler, 1996). In order for nutrients to reach the developing grain they must exit the phloem. Unfortunately relatively little is known with regards to the role of specific transporters in this rate limiting process (Zhang et al., 2007). In order for Zn to enter the endosperm of the developing grain several membranes must be crossed. Firstly, Zn must be transported across the membrane of the maternal transfer cell into the apoplastic space, the endosperm cavity. These transfer cells have characteristic ingrowths that increase their surface area up to 22-fold (Wang et al., 1994). Once in the endosperm cavity, Zn is transported into the filial tissue portion of the grain, by membrane transport into the aleurone cells (Zhang et al., 2007). From the aleurone cells Zn must be transported symplastically into the starchy endosperm, which is the target of any biofortification strategy (see Figure 1.8).

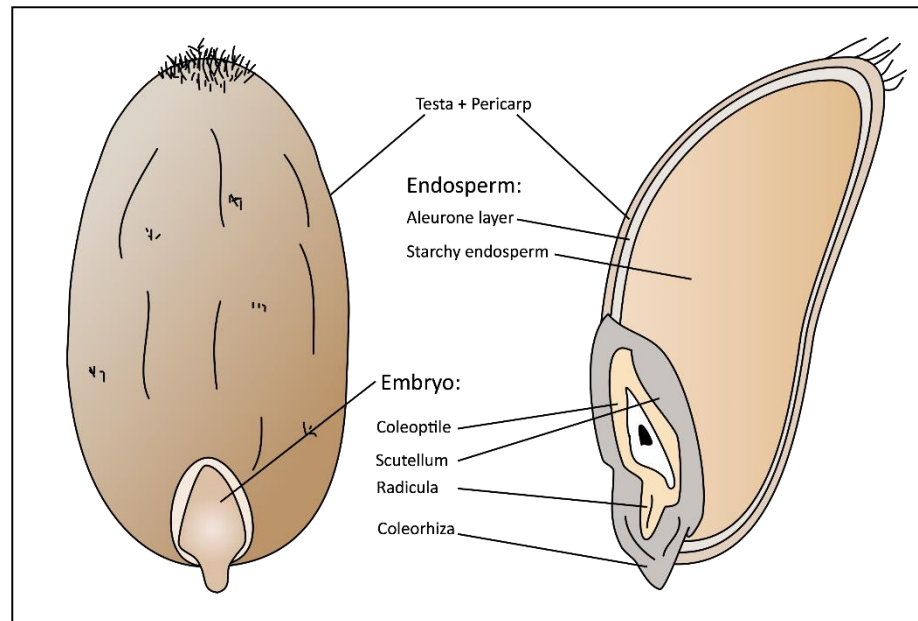


Figure 1.6. Schematic of a wheat grain. Key regions labelled. The right hand diagram shows a transverse section which intersects the embryo.

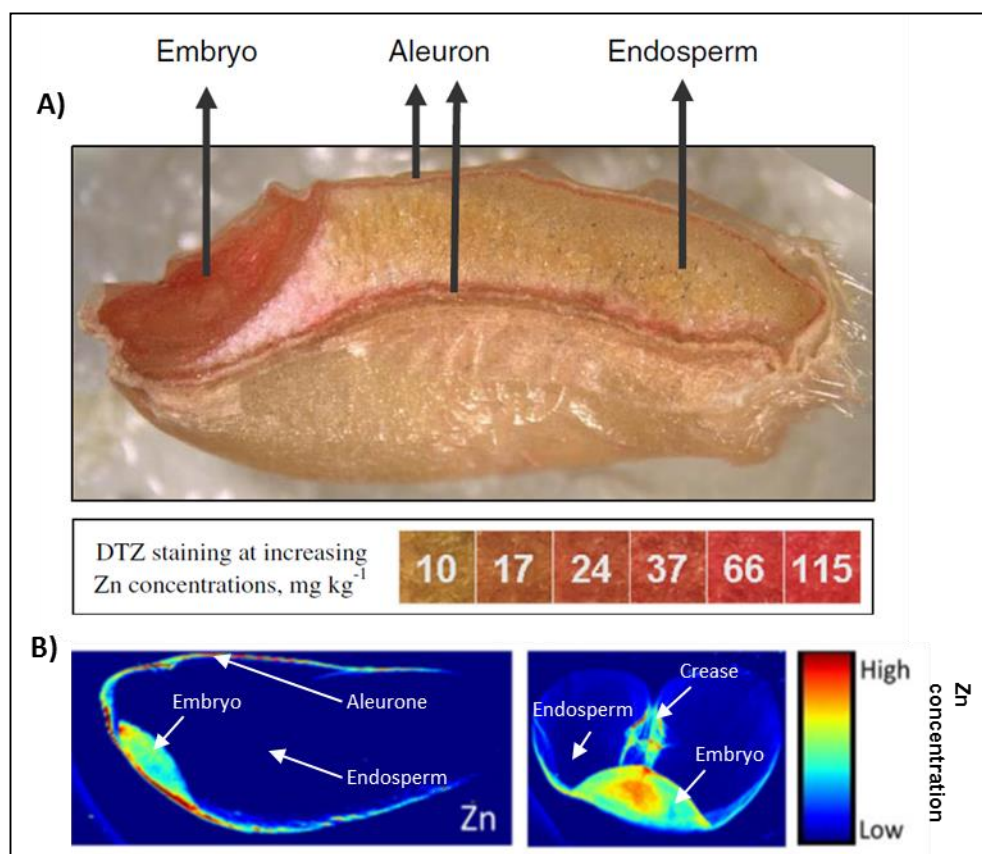


Figure 1.7. Zn distribution in the wheat grain. **A)** Wheat grain showing staining through the use of Diphenyl thiocarbazon (DTZ). Image taken from Ozturk et al. (2006). **B)** X-ray fluorescence heat map of cv. Bobwhite wheat grain (longitudinal section left, transverse section right) showing Zn distribution, red indicates high Zn concentrations, blue indicates low. Images adapted from Neal et al. (2013). Both **A)** and **B)** show the high Zn concentrations present in both the embryo, the aleurone and the crease.

An interesting approach to elucidate key proteins in the transport pathway through the seed has been conducted in barley (*H. vulgare*) (Tauris et al., 2009). Tauris et al. (2009) used laser capture microdissection to selectively isolate key regions of the developing barley (*H. vulgare*) grain (transfer cells, aleurone, endosperm and embryo). The RNA from these regions was extracted and hybridized to an Affymetrix 22K Barley GeneChip to investigate gene expression levels. Results indicated expression profiles for specific metal transporter genes. The results are annotated on Figure 1.8. *HvZIP* gene expression suggests a role in the loading of the endosperm cavity from the transfer cells and also the loading of the aleurone and embryo. Tauris et al. (2009) observed that an overall trend for reduced gene expression of transporter and sequestration genes was evident in the endosperm, this is in agreement with the low Zn concentrations found in the endosperm compared to the aleurone and embryo. Further understanding of the key transporters involved in the loading of micronutrients from the phloem to the grain (and specific regions therein) as well as the regulatory mechanisms involved in nutrient remobilisation will be essential for the development of future biofortification strategies.

As well as the low Zn content in the edible parts of the grain, there is another limiting factor. Wheat grain is inherently rich in substances that limit the absorption of Zn by the human digestive tract, such as polyphenols and phytate (Welch and Graham, 2004). Phytate (myo-inositol-1,2,3,4,5,6-hexakisphosphate) is the major storage compound of phosphorus in the grain, however phytate is also a strong chelator of divalent cations such as Zn which limits the bioavailability of this essential micronutrient. It has been shown through the use of community based studies that phytate reduction in corn tortillas successfully increases human calcium uptake (a divalent cation like Zn), demonstrating its efficacy as a potent antinutrient (Hambidge et al., 2005). An interesting approach to alleviating the reduced bioavailability phytate causes to Fe and Zn has been tested in rice and wheat (Lucca et al., 2001; Brinch-Pedersen et al., 2006). The transgenic expression of heat stable phytase enzymes from *Aspergillus fumigatus* (a saprotrophic fungus) targeted to the grain of rice and wheat has been shown to reduce the phytate concentration in dehusked rice seeds (Lucca et al., 2001) and wheat grains by 45% compared to untransformed lines (Brinch-Pedersen et al., 2006). However there is evidence to suggest that a certain level of phytate is important due to the suggested potential health benefits including cholesterol reduction, reduced lipid serum content (Jenab & Thompson, 2006) and potential inhibition of different cancer types (Somasundar et al., 2005). More research into the levels of phytate required for these potential health benefits is needed before breeding varieties with reduced phytate or even transgenic approaches to incorporate phytase enzymes from other species can be seen as a solution to micronutrient deficiency.

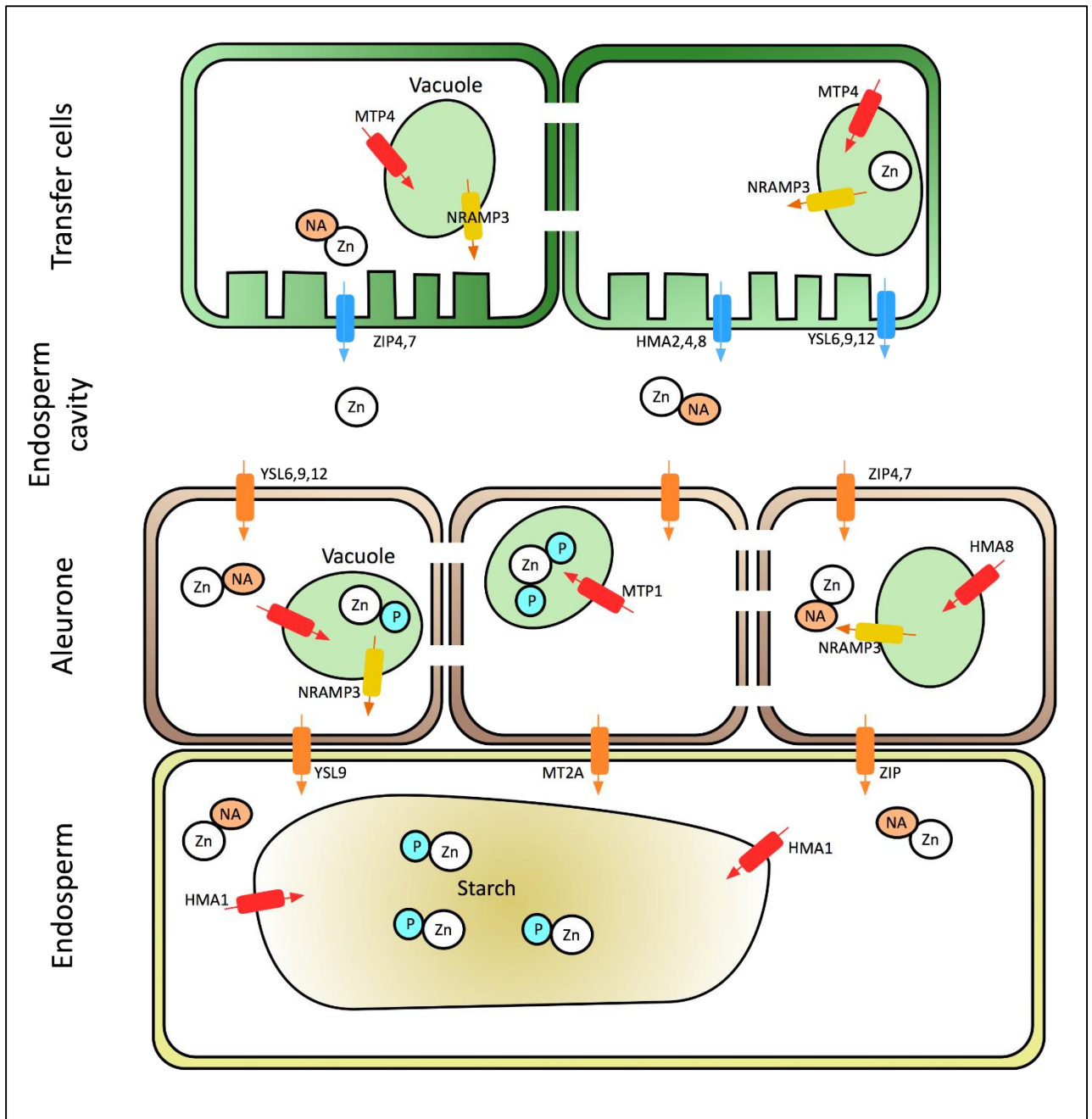


Figure 1.8. The loading pathway of Zn in the grain. Key transporters shown from data presented in (Tauris et al., 2009). This data was generated using barley (*H. vulgare*). Orange boxes indicate cellular importing transporters, blue boxes indicate cellular efflux transporters, red boxes indicate vacuolar uptake transporters, yellow cylinders indicate vacuolar efflux transporters. Abbreviations: HMA, heavy metal transporting ATPase; MTP, metal tolerance protein; NA, nicotianamine; NRAMP, natural resistance-associated macrophage protein; P, phytate; YSL, yellow stripe-like protein; ZIP, ZRT IRT-related protein. Figure based on information given in (Tauris et al., 2009).

1.5 Micronutrient homeostasis/regulation

Gene regulation is crucial for plant adaptation to fluctuating environments. The controlled expression of genes at the transcriptional level is vital in many of the plant stress and defence

responses (Singh, 2002). Transcriptional control allows the temporal and spatial control of gene expression. It has been shown that plants devote a large proportion of their genome to transcription factors (in *A. thaliana* in excess of 1500 transcription factors are encoded) (Riechmann, 2000). Transcription factors bind to relevant *cis*-acting elements and facilitate the binding of other components of transcriptional machinery including RNA polymerase to initiate mRNA synthesis. Transcriptional control is key in the homeostasis of *in-planta* micronutrient concentrations (Pilon et al., 2009).

1.5.1 Fe homeostasis

Fe homeostasis is the most studied of all the micronutrient homeostatic mechanisms in higher plants. A key regulatory transcription factor involved in the Fe-deficiency response, *T3238FER* was identified in tomato (*S. lycopersicum*) (Ling et al., 2002). Through the use of mutant studies, this basic helix-loop-helix (bHLH) transcription factor was shown to be essential in the Fe-deficiency response of tomato. In *A. thaliana* the ortholog of *FER*; *FIT* (FER-like Iron deficiency-induced Transcription factor) has been shown to be vital in the response to Fe-deficient conditions. *Arabidopsis fit1* mutant seedlings exhibit characteristic chlorotic phenotypes and die early in development (Colangelo and Gueriot, 2004). Additional Fe supplementation rescues the seedlings, and using a microarray approach a suite of 59 genes that were shown to be Fe-dependent lost their Fe-regulated expression. Interestingly it was shown that overexpression (35S promoter) of *AtFIT* had no effect on the tolerance of *A. thaliana* to Fe deficiency, Fe-dependent genes were not induced and no obvious phenotype was observed (Colangelo and Gueriot, 2004). A combination approach, overexpressing *AtFIT* with the closely related bHLH genes, *AtbHLH38* and *AtbHLH39* proved effective in the induction of *IRT1* and *FRO2*. The *Arabidopsis* overexpressing *FIT+bHLH38* and *FIT+bHLH39* plants showed enhanced tolerance to Fe-deficient conditions and higher Fe concentration in the shoots, even under Fe-replete conditions (Yuan et al., 2008). A yeast two-hybrid assay showed that *AtFIT* interacts with both *AtbHLH38* and *AtbHLH39* in yeast cells, this interaction was also shown in *Arabidopsis* cells using the bimolecular fluorescence complementation approach. This indicates that the formation of transcription factor heterodimers is essential for the successful implementation of a Fe-deficiency response in *A. thaliana*.

In graminaceous species, important Fe deficiency-responsive elements in the promoter of various Fe-deficiency induced genes have been identified: Iron Deficiency-response Element 1 (IDE1) and IDE2 (Kobayashi et al., 2003). Two transcription factors have been discovered that bind specifically to the *cis*-acting elements IDE1 and IDE2, called IDE-binding Factor 1 (IDEF1) (Kobayashi et al., 2007) and IDEF2. IDEF1 and IDEF2 regulate separate subsets of Fe-deficiency-inducible genes (Kobayashi and Nishizawa, 2012). *IDEF1* expression in Fe-deficient

rice plants has been shown to correlate positively with *OsIRT1*, *OsNAS1-3* (Nicotianamine-synthase) and *OsIRO2* (an Fe deficiency induced bHLH transcription factor) (Kobayashi et al., 2009). *OsIDEF2* RNAi rice (*O. sativa*) lines exhibited less induction of *OsYSL2* (a Fe(II)-nicotianamine transporter gene) (Ogo et al., 2007). Further research in rice (*O. sativa*) using a microarray analysis revealed that among others *OsIRO2* was upregulated under Fe deficiency. This gene codes a bHLH factor that has 32% and 39% homology to *AtbHLH38* and *AtbHLH39* respectively (Ogo et al., 2006). When overexpressed (35S) in rice (*O. sativa*), *OsIRO2* lines show increased MA secretion (Ogo et al., 2007), have improved tolerance to low Fe available calcareous soils and increased Fe uptake and transport to the grain under Fe-deficient conditions (Ogo et al., 2011). RNAi silenced *OsIRO2* plants are hypersensitive to Fe deficiency and have lower MA secretion levels (Ogo et al., 2007).

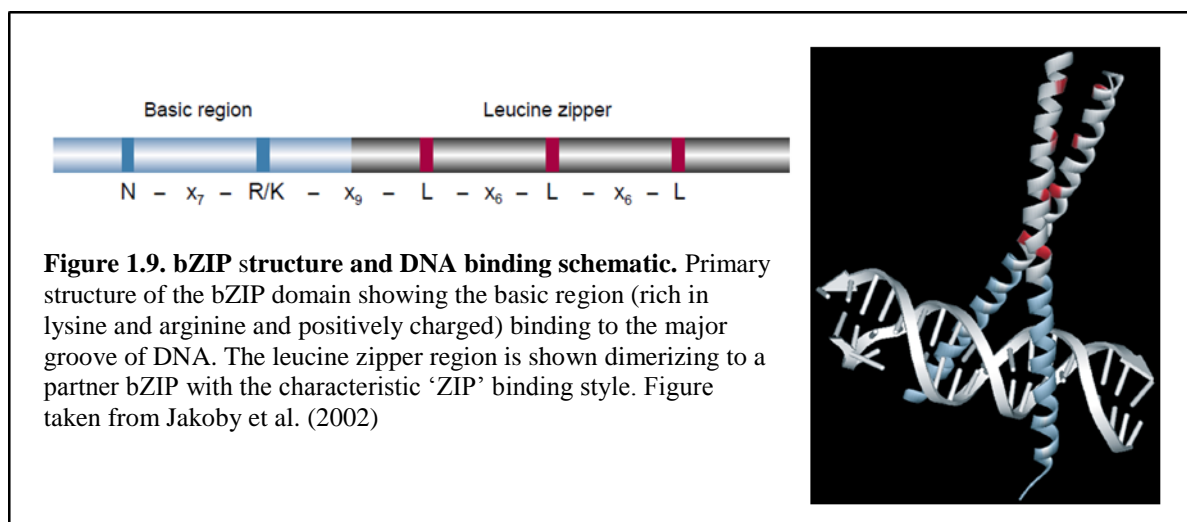
Kobayashi et al. (2012), have experimentally shown that *OsIDEF1* is able to bind Fe and other divalent metals such as Zn and Ni. The binding of these metals was found to be reliant upon a histidine-asparagine rich region and a proline-rich region in the bHLH. An overexpressing rice *idef1* lacking these regions was unable to activate downstream genes during early stages of Fe deficiency (Kobayashi et al., 2012). A homolog in barley (*H. vulgare*) was also identified in this study and shown to contain similar metal binding domains indicating a similar mechanism exists in closely related species. The evidence suggests *IDEF1* could be an Fe sensor, that controls downstream homeostatic responses in accordance with the cellular Fe concentration. Along with its counterpart *OsIRO2*, as well as *OsIRO3* and *OsBHLH133* (involved in Fe-deficiency response repression (Zheng et al., 2010; Wang et al., 2013; Kobayashi et al., 2010) an elaborate Fe-homeostatic mechanism exists, allowing rice to sense and respond to changes in Fe deficiency and bring about gene expression responses to cope with fluctuating Fe conditions.

In addition to the aforementioned transcriptional regulatory mechanisms for Fe nutrition, post-transcriptional regulation also appears to be used by plants in Fe homeostasis. Kong and Yang (2010) showed that eight microRNAs (miRNAs) were upregulated in response to Fe deficiency in *Arabidopsis*. miRNAs are a class of non-coding small RNAs around 22 nucleotides in length that play important roles in the regulation of gene expression by binding to their mRNA targets and inducing gene repression through cleavage (Bartel, 2004). Interestingly Kong and Yang, (2010) found that *IDE1* and *IDE2* elements were present in the promoters upstream of the eight *Arabidopsis* miRNAs. These miRNAs have been shown to act upon a variety of pathways including root development and auxin signalling and it seems plausible that in response to Fe-deficient conditions the plant upregulates these miRNAs which in turn downregulate and help economise Fe usage by repressing various growth processes.

1.5.2 Zn homeostasis

The numerous Zn transport steps described in Section 1.4 shows the multitude of options available for strategic breeding or genetic modification that may enhance both the performance of wheat in Zn-deficient soils and/or the grain Zn content of wheat. But, the possibility may exist to affect more than one of these key transporters at once, through the manipulation of the Zn homeostatic mechanisms used by plants.

The physiological range between Zn deficiency and Zn toxicity in plants is narrow (Yu and Rengel, 1999), for instance the typical leaf Zn concentration requirement for most crop plants is 15-30 mg Zn kg⁻¹ DW, with growth inhibited at leaf Zn concentrations greater than 100-700 mg Zn kg⁻¹ DW (Marschner, 1995; White and Broadley, 2011). Thus the importance of a tight homeostatic network in plants (and also all other organisms for that matter) is clear. Ground-breaking research by Assunção et al. (2010) has shown the importance of two bZIP transcription factors in *A. thaliana* that are vital in the regulation of adaptation to Zn deficiency. bZIP transcription factors have been found in all eukaryotes analysed to date (Jakoby et al., 2002). bZIPs are so-called due to the basic region/leucine zipper (bZIP) domain that they contain (Hurst, 1995). This basic region/leucine zipper domain consists of a basic region comprising 15 residues rich in lysine and arginine which is positively charged and a leucine zipper region which is 16 amino acids long, with leucine residues every seventh amino acid (Jakoby et al., 2002). These leucine residues dimerise with the same region on a partner bZIP, forming a zip-like structure through van der Waals interactions (see Figure 1.9).



The bZIP transcription factor family in *A. thaliana* consists of 75 distinct members, which can be divided into 10 subgroups through common domains (Jakoby et al., 2002). Their functions are varied and wide-ranging including: abiotic stress, seed maturation, flower development and pathogen defence (Jakoby et al., 2002; Alves et al., 2013). Through the use of

mutant studies in *A. thaliana*, Assunção et al. (2010) have shown that the transcription factors, AtbZIP19 and AtbZIP23, are essential in bringing about a Zn-deficiency response. These two bZIP transcription factors (along with AtbZIP24 which has been shown to be a regulator of salt response in *A. thaliana* (Yang et al., 2009a)) are found in group F of the *Arabidopsis* bZIP family (Jakoby et al., 2002). Group F bZIPs share the basic/leucine zipper domain in common with all bZIPs however unique to this group are two upstream domains, 13 and 10 amino acids in length, rich in cysteine and histidine (see Figure 1.10).

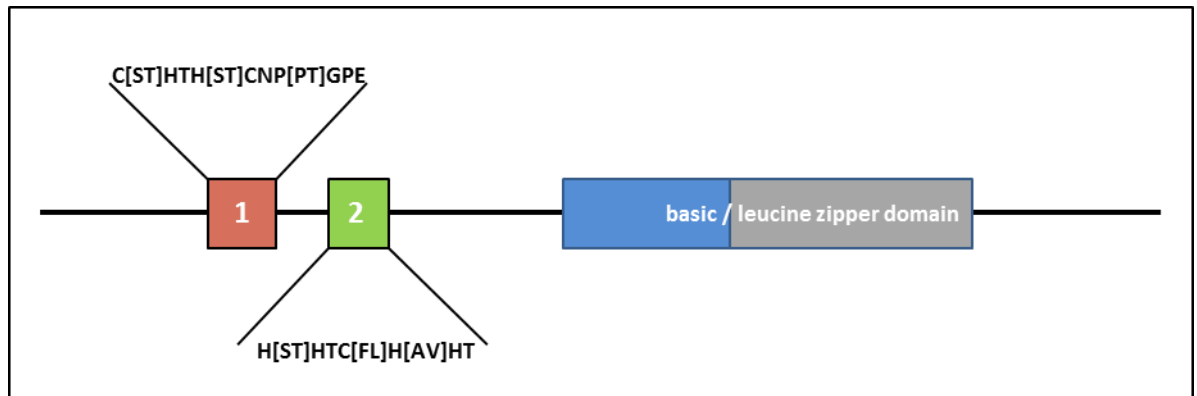


Figure 1.10. Schematic of *A. thaliana* group F bZIPs. The two characteristic cysteine-histidine rich motifs upstream of the bZIP domain are shown in red and green

Mutant *A. thaliana* lines *bzip19-1* and *bzip19-1 bzip23-1* (mutated in *bzip19* and *bzip19+23* respectively) showed Zn-deficiency phenotypes at much higher Zn media concentrations than wild-type plants. This indicates a regulatory role of these two bZIP transcription factors in the Zn network of *A. thaliana*. These bZIPs were initially identified as Zn-regulation candidates through a yeast-one-hybrid screen using overlapping *AtZIP4* promoter fragments as bait. The interaction of bZIP19 and bZIP23 with the *AtZIP4* promoter was confirmed and further investigated using electrophoretic mobility shift assays (EMSAs). EMSAs are an affinity electrophoresis technique that allow protein-DNA interactions to be investigated. The *Arabidopsis* bZIP19 and bZIP23 transcription factors were shown to bind to a unique *cis*-element in the promoter of *AtZIP4*; this 10 bp palindrome motif (RTGTCGACAY) has thus been termed the Zn-deficiency response element (ZDRE). The binding of the transcription factor to the *cis*-element brings about the recruitment of the polymerase machinery that in turn initiates and carries out transcription of the mRNA. This transcriptional regulation has been predicted to occur in all *A. thaliana* ZIP genes that contain a ZDRE motif; this includes *ZIP1*, *ZIP3*, *ZIP4*, *ZIP5*, *ZIP9*, *ZIP12* and *IRT3* (Assunção et al. 2010) (see Figure 1.11). Interestingly in their bioinformatics search Assunção et al. (2010) also found putative ZDREs in the promoter of nicotianamine synthase genes: *AtNAS2*, *AtNAS3* and *AtNAS4*.

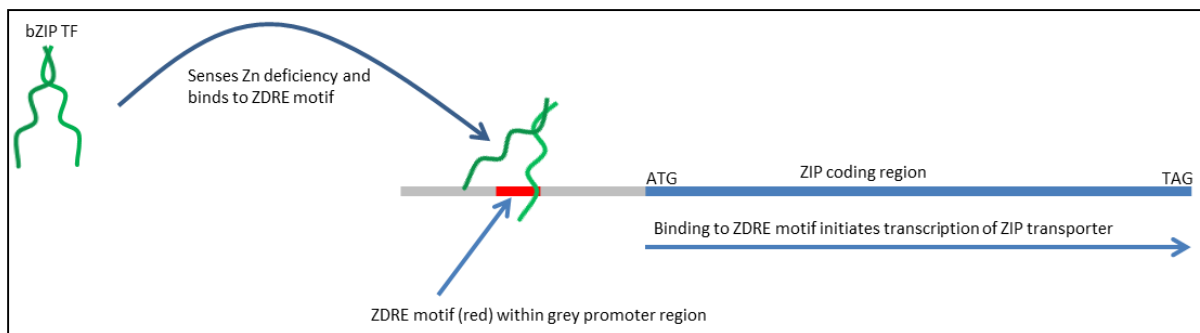


Figure 1.11. *A. thaliana* Zn-deficiency sensing and response mechanism. Schematic representation of *A. thaliana* bZIP19 and bZIP23 regulatory mechanism in response to Zn deficiency. Under Zn-deficient conditions, bZIP19 and bZIP23 bind to ZDRE motifs in Zn membrane transporter gene promoter, bring about recruitment of transcription machinery and initiate transcription of mRNA.

Following the discovery of bZIPs in the Zn-deficiency response of *Arabidopsis*, Claus & Chavarría-Krauser (2012) used mathematical models to deduce the most likely upregulation mechanism. Three scenarios were modelled; activator only model (regulation by one Zn-dependent transcription factor), dimerization model (bZIP19 and bZIP23 dimerize in absence of Zn leading to upregulation) and an activator/inhibitor model (inhibitor prevents upregulation in presence of Zn). Across reasonable parameter ranges they found the activator/inhibitor model the most robust of the three.

Assunção et al. (2013), recently proposed a new model for how this Zn-deficiency sensing system may be facilitating the upregulation of Zn transporters containing a ZDRE motif in their promoter. They propose that under normal Zn supply, bZIP19 and bZIP23 transcription factors present in the cytosol have a Zn^{2+} ion bound at the cysteine-histidine rich motifs. When Zn^{2+} ions are bound, these bZIPs are rendered non-functional, however when low Zn supplies exist in the cytosol, the Zn^{2+} bound to the motif is released and conformational changes make the bZIPs functional. This then leads to the binding of bZIPs to the ZDRE regions of Zn-regulatory genes, causing an upregulation, thereby initiating the Zn-deficiency response of the plant. Although the mechanisms by which Zn deficiency, bZIP sensing and subsequent upregulation are yet to be fully elucidated, it is clear that the upregulation of such a multi-faceted transporter family as the ZIPs could hold great promise for increasing the Zn content of plants. In the model grass species *Brachypodium distachyon* a group F bZIP transcription factor has been investigated; *BdbZIP10* (Glover-Cutter et al., 2014). *BdbZIP10* was reported to have a role in response to Zn deficiency but also more generally in response to oxidative stress.

Further research is required to identify and characterise the role of bZIPs involved in the Zn-deficiency responses of key crop plants such as wheat. By advancing our knowledge of the molecular mechanisms controlling Zn uptake, partitioning and regulation in wheat the development of varieties more adept at sustaining yield on Zn-poor soils as well as Zn-biofortified

cultivars may be possible. This project seeks to address this by investigating the Zn regulatory pathway of bread wheat (*T. aestivum*).

1.6 Aims of the project

The main focus of this project was to investigate the regulatory mechanisms that control Zn content in wheat. The specific aims of the project were:

1. To identify genes present in the wheat genome that are homologous to the *ZIPs* and *bZIPs* which have been shown to be important in Zn regulation of other plant species. Furthermore, to assess whether the *TaZIPs* and *TabZIPs* identified are Zn regulated in expression and examine the spatiotemporal nature of any existing transcriptional regulation (Chapter 3).
2. To determine the Zn-transport ability of *TaZIPs* identified (Chapter 4).
3. To investigate the role of *TabZIPs* in the Zn-deficiency response and determine both the binding ability and location of *TabZIPs* to any *ZDREs* found in the promoters of *TaZIPs* (Chapter 5).
4. To assess the variation in Zn uptake and partitioning ability across a diverse wheat germplasm. Additionally, to investigate the mechanistic basis of this Zn variation (Chapter 6).

Chapter 2. Materials and methods

2.1 Plant material and growth

2.1.1 Wheat (*Triticum aestivum*) hydroponic growth

Seeds from a spring wheat variety (*T. aestivum* cv. Paragon) were surface-sterilised by a 15 minute (min) immersion in a 1% (v/v) sodium hypochlorite (NaOCl) solution, rinsed afterwards several times in sterile water and incubated overnight (>10 hours (hr)) at 4°C. After seven days of germination on sterile water-soaked paper tissue, uniform seedlings were transferred to a controlled environment facility: 16 hr day length with a photon flux rate of 500 $\mu\text{mol photons m}^{-2} \text{s}^{-1}$, day conditions of 20°C/70% humidity, night conditions of 16°C/80% humidity. Seedlings were grown individually in aerated 1 litre hydroponic culture pots (Azlon, Cambridge, UK). Pots were filled with a Letcombe nutrient solution modified for wheat growth (Drew and Saker, 1984). This was replaced every third day (see Table 2.1 for nutrient solution details).

Table 2.1. Constituents and concentrations of the modified Letcombe solution used in the hydroponic culture system. The two concentrations given for ZnCl_2 correspond respectively to the +Zn and -Zn treatments.

Constituents	Final concentration in modified	
	Letcombe	
$\text{Ca}(\text{NO}_3)_2$	1.5 mM	
KNO_3	5 mM	
NaNO_3	2 mM	
MgSO_4	1 mM	
KH_2PO_4	0.5 mM	
FeEDTA	25 μM	
$\text{CuCl}_2 \times 2 \text{H}_2\text{O}$	0.2 μM	
H_3BO_3	1 μM	
$\text{MnCl}_2 \times 4 \text{H}_2\text{O}$	0.6 μM	
$\text{Na}_2\text{MoO}_4 \times 2 \text{H}_2\text{O}$	0.1 μM	
KCl	5 μM	
ZnCl_2	8 μM or 0 μM	
HEDTA	75.5 μM	
MES Buffer	2.56 mM	

Upon harvesting, plants were separated into root and shoot material. Roots were washed with three 5 second soaks in deionized water and dried briefly on paper towel before freezing in liquid nitrogen and storage at -80°C . Samples were either ground with a pestle and mortar in liquid nitrogen or using a freezer mill (Spex sample prep 6870, Metuchen, USA) depending on sample quantity. 1 g of frozen material was aliquoted into a 2 ml microtube and used for subsequent analysis. Four different hydroponic experiments were conducted. Zn-deficiency was initiated by the replacement of +Zn culture solution with zero Zn culture solution. Details are given in Table 2.2.

Table 2.2. Timeframes of hydroponic experiments. The different length of hydroponic growth in +Zn conditions prior to zero Zn treatment at D0 are given. Sampling points are given relative to D0.

Experiment	Germination phase	Hydroponic +Zn growth period	D0 (Split point)	Sampling points
Protocol test experiment	7 days	0 days	↓	D14
Three-week Zn starvation	7 days	7 days		D0 D7 D14 D21
One-week Zn starvation	7 days	14 days		D0 D1 D3 D5 D7
Cultivar comparison experiment	6 days	10 days		D0 D1 D7 D12

2.1.2 *Arabidopsis thaliana* growth

Mature *A. thaliana* plants were grown with a 16 hr day length, photon flux rate of $120 \mu\text{mol photons m}^{-2} \text{s}^{-1}$, day conditions of 23°C and night conditions of 18°C in Fitotron Plant Growth Chambers (Weiss Gallenkamp, UK). Four *Arabidopsis* seeds were sown per pot (DESCH7B black pots; Desch, UK), containing a 1/1/1 ratio of Levington (Green-Tech, UK), John Innes No. 2 (John Innes, UK) and Sinclair Vermiculite Medium Grade (Scots Plants Direct, UK). To each 10 kg of soil, 3 ml of Intercept-5 GR insecticide (Bayer Environmental Sciences, UK) was added. The pots were covered with clear film which, following germination, was removed and the four seedlings were reduced to one per pot. As the first inflorescences emerged, plants were bagged in 50 x 30 x 10 cm clear, micropunched, cut flower sleeves (Geerings, Kent, UK). This prevented cross pollination and the unwanted spread of seed to different plant lines. After 8-10 weeks of growth, siliques were harvested and seed transferred to 30 ml Sterilin Universal containers (Thermo Fisher Scientific, UK), with the lid loosely screwed on for one week allowing seeds to dry completely.

2.2 Bioinformatics

2.2.1 Sequence search strategies

Initially, *ZIP* and *bZIP* sequences from *A. thaliana* were obtained from the NCBI *Arabidopsis* genome database. These sequences were then used as input to BLAST the existing rice genome (*Oryza sativa* cv. Japonica) using the Rice Genome Annotation Project database (<http://rice.plantbiology.msu.edu/>). Using these rice sequences the *Brachypodium distachyon* orthologous genes/sequences were identified, using the brachypodium genomic resources available at http://plants.ensembl.org/Brachypodium_distachyon. Barley (*H. vulgare*) homologs were also identified using the BLAST search function of the barley genomic resources available at http://plants.ensembl.org/Hordeum_vulgare. Finally, the barley, brachypodium, rice and *Arabidopsis* were BLASTED against the IWGSC (International Wheat Genome Sequencing Consortium) wheat (*Triticum aestivum* cv. Chinese Spring) survey sequence databanks at URGI (<http://wheat-urgi.versailles.inra.fr/Seq-Repository>) and the TGAC (The Centre for Genome Analysis) assembly sequence available at http://plants.ensembl.org/Triticum_aestivum. Putative contigs were identified and intron-exon structure in the wheat genome sequences were predicted using alignments with coding sequences of homologous genes identified in related species as discovered in previous steps. Phylogenies based on coding sequences and portions of 5' and 3' ends were created using alignments in Geneious version 8.1.3 (www.geneious.com, Kearse et al., 2012) with the Muscle algorithm (Edgar, 2004) and putative genes were named accordingly. Neighbour joining trees were generated using MEGA (v5.2) software, evolutionary distances were computed using the p-distance method and 1000 bootstrap replicates were conducted for each phylogeny. Previously identified wheat genes and their gene names are shown in Tables 3.1 and 3.2 in Chapter 3. Transmembrane (TM) domains of ZIP amino acid sequences were predicted using HMMTOP (Tusnády and Simon, 2001) and subsequently the topology predictions in Figure 3.3 were generated using Protter version 1.0 (<http://wlab.ethz.ch/protter>).

2.2.2 Oligonucleotide primer design

2.2.2.1 Gene expression real-time PCR primers

Oligonucleotide primer pairs for real-time PCR gene expression analysis were designed to amplify all homeologous copies of an individual gene (Table 2.3). Primer pairs were designed manually, to comply with the following parameters: length 20-25 bases, GC content 45-60%, T_m 63-65°C (based on salt adjusted predictions), T_m difference 5°C maximum between primer pairs and a maximum of two degenerate bases. Amplicon position was selected to be located in the 3' end of the genes, as this allowed sufficient specificity to amplify from a single set of homeologs

whilst not amplifying any other regions from homologous genes. The T_m , hairpin formation and GC content was predicted using the Oligonucleotide Properties Calculator available at (<http://www.basic.northwestern.edu/biotools/oligocalc.html>).

Table 2.3. Oligonucleotide primer sequences used in real-time PCR expression analysis. Primers are given in 5' to 3' orientation. Amplicon sizes of the resulting real-time fragment amplified are shown, along with their amplification efficiency. Primer amplification efficiencies were calculated using LinRegPCR Version 11.0 (Ruijter et al., 2009).

Primer name	Primer sequence (5' to 3')	Amplicon size	Amplification efficiency
TaZIP1rts	GGGAAATGGAGAACYCCTGGATG	97 bp	96%
TaZIP1rtas	GGCATAGAGATCTTGAAAGCAATTGC		
TaZIP4rts	AGTTTCGCCTCAAGTCTGTCTTG	109 bp	99%
TaZIP4rtas	GGCTATTCTCGTCGTAAGCAGAG		
TaZIP5rts	CGCAAGCSTACAACATGAAACAGT and CGCGAGCCTACAACCTTGAAACAG	126 bp	97%
TaZIP5rtas	CTTYAGACACGCTACTGGGTTGG		
TaZIP6rts	GTCATCATCTCTGAAACTGAAGAAGG	111 bp	95%
TaZIP6rtas	CCCTCTATACATTTCACTATGRCC		
TaZIP7rts	ACAGGCAGTATGTTSGGACGTAG	129 bp	97%
TaZIP7rtas	CAGCAAGTGATGGCCTATGTCTG		
TabZIP1rts	CAAGGTGCYGGTGACTCTATGG	93 bp	96%
TabZIP1rtas	TCCTCGACCTGTTTACAGCATTG		
TabZIP3arts	TCTSAGAAGGCAACGTATCCARAG	117 bp	96%
TabZIP3artas	CATGATGAGCTCATGTGGCTTCGT		
TabZIP3brts	TGCCCAGGTTATGAGCTCATGTG	95 bp	98%
TabZIP3brtas	TTCTCCATTGCATAGATCTGCTCTG		
TabZIP4rts	CGAGSTGTTGGGTCAAGSTGC	76 bp	96%
TabZIP4rtas	CCTCTTTACATCATCKGGCAAACC		
TabZIPGrts	CTTAAAGATGAAGTGAGCCGGATC	125 bp	98%
TabZIPGrtas	AGCTTATTGTCAAGTCCTGCCTCA		
TaActinrts	GACGCACAACAGGTATCGTGTTG	108 bp	98%
TaActinrtas	CAGCGAGGTCAAGACGAAGGATG		
TaSuccDHrts	TTTGCTCTCCGTGGTGCCTTTGG	104 bp	104%
TaSuccDHrtas	GAAGATGTGTAGCTCCTTGCTTGC		

2.2.2.2 Full length coding sequence TOPO cloning primers

TabZIP and *TaZIP* TOPO primers were designed to amplify the full length coding DNA sequence (CDS) of the genes of interest, with the CACC (5'-3') sequence at the 5' end of the forward primer to facilitate directional cloning into pENTR entry vectors of the TOPO[®] cloning system (Invitrogen, CA, USA). All TOPO primers include the stop codon of the corresponding CDS. Primer pairs and their respective product sizes are given in Table 2.4.

2.2.2.3 Full length coding sequence pGEM cloning primers

In addition to the TOPO cloning system, the pGEM[®]-T Easy Vector system (Promega, Madison, USA) was also utilised to clone *TaZIPs*. In some cases, genes were amplified directly from cDNA using the primers outlined in Table 2.4 and subsequently ligated into the pGEM-T Easy vector, then upon EcoRI restriction they were ligated into the pYES2 yeast expression vector. However, in the case of *TaZIP7*, the gene was sub-cloned into pYES2 directly from existing TOPO entry vectors using amplifications with EcoRI and XhoI restriction sites as outlined in Table 2.5. Full details are given for each plasmid produced in the relevant results chapter of this thesis.

Table 2.4. Oligonucleotide primer sequences used for the amplification of full length CDS for TOPO[®] cloning.

Primer name	Primer sequence (5' to 3')	Amplicon size
TaZIP1TOPOF	CACCATGGGCGCCACCAATC	1087 bp
TaZIP1TOPOS	CTATGCCCATATGGCAAGCATGGA	
TaZIP5TOPOF	CACCATGAAGCCGAGCGCCG	1147 bp
TaZIP5TOPOS	CTAGGCCCATTTGGCGAGCA	
TaZIP6TOPOF	CACCATGTCCGGCAAGGGTTG	1192 bp
TaZIP6TOPOS	CTATGCCCAGAGAGCTAATATCGACA	
TaZIP7TOPOF	CACCATGATGATCGGTGTCGC	1165 bp
TaZIP7TOPOS	TCAGGCCCAAACGCAAGCG	
TabZIP1TOPOF	CACCATGGACGACGGGGACATC	757 bp
TabZIP1TOPOS	TTACAGCATTGCCCCCACG	
TabZIP3bTOPOF	CACCATGGACGACGGGAACCTC	571 bp
TabZIP3bTOPOS	TTAAAGAAAACACGTATGAGGTTGTT	
TabZIP4TOPOF	CACCATGGACGACGGGGACATA	712 bp
TabZIP4TOPOS	TCACCTCTTTACATCATCTGGCAAA	
TabZIPGTOPOF	CACCATGGGAAGCAGTGAAGC	1176 bp
TabZIPGTOPOS	ATAGCTCAATTAGTGTCTCTCTGG	

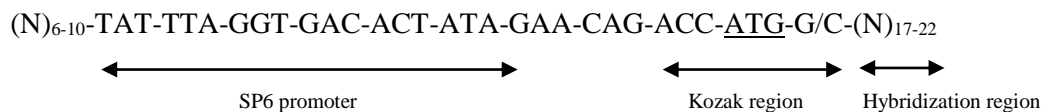
Table 2.5. Oligonucleotide primer sequences used for the amplification of full length CDS with EcoRI and XhoI restriction sites. These primers were used to subclone *TaZIP7* from TOPO entry vectors to pYES2 yeast expression vectors.

Primer name	Forward primer (5' to 3')	Amplicon size
TaZIP7EcoRI	GAATTCATGATGATCGGTTGTCGCAGGC	1172 bp
TaZIP7XhoI	CTCGAGTCAGGCCCAAACCTGCAAG	

2.2.2.4 TNT[®] SP6 protein expression system primers

For the synthesis of bZIP proteins using the TNT[®] SP6 high-yield wheat germ system (Promega, Madison, USA) (see Section 2.7.2), primers with an SP6 promoter, Kozak region and a Poly-A tail were designed in accordance with the manufacturer's instructions (see Figure 2.1). Primer sequences are given in Table 2.6.

5' primer:



3' primer:

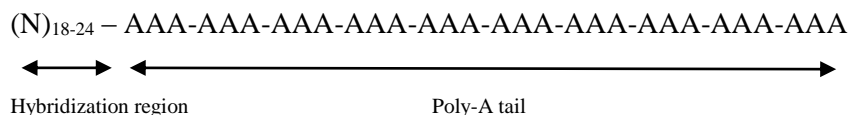


Figure 2.1. Design of SP6 forward and Poly-A tail reverse primers for protein synthesis.

Table 2.6. Oligonucleotide primer sequences used for the amplification of full length bZIP CDS with an SP6 promoter, Kozak region and Poly A tail for use in protein expression kit.

Primer name	Primer sequence (5' to 3')	Amplicon size
TabZIP1SP6F	GACTCATATTTAGGTGACACTATAGAACAGACCACCAT GGACGACGGGGA	819 bp
TabZIP1polyAR	TTTTTTTTTTTTTTTTTTTTTTTTTTTTTTTTTACAGCA TTTGGCCCCC	
TabZIP3bSP6	GACTCATATTTAGGTGACACTATAGAACAGACCACCAT GGACGACGGGAA	594 bp
TabZIP3bpolyAR	TTTTTTTTTTTTTTTTTTTTTTTTTTTTTTAAAGAAAAC ACGTATGAGGT	
TabZIP4SP6	GACTCATATTTAGGTGACACTATAGAACAGACCACCAT GGACGACGGGGA	746 bp/772 bp
TabZIP4polyAR	TTTTTTTTTTTTTTTTTTTTTTTTTTTTTTCACCTCTTT ACATCATCTGG	
TabZIPGSP6	GACTCATATTTAGGTGACACTATAGAGACCACCATGGG AAGCAGTGAAGC	1231 bp
TabZIPGpolyAR	TTTTTTTTTTTTTTTTTTTTTTTTTTTTTTTGCTCAATTA GTGTCCCTTCTGG	
AtbZIP19SP6	GACTCATATTTAGGTGACACTATAGAAGACCACCATGG AAGACGGTGAG	845 bp
AtbZIP19polyAR	TTTTTTTTTTTTTTTTTTTTTTTTTTTTTTTCAAACCTG CTCTTGATGCAC	

2.3 Molecular biology techniques

2.3.1 RNA extraction

Total RNA was isolated from 1 g aliquots of frozen material using a modified protocol based on Verwoerd et al. (1989). The extraction is performed by addition of 1 ml hot (80°C) 1/1 phenol/extraction buffer solution [extraction buffer: 0.1 M Tris/HCl, 0.1 M LiCl, 1% (w/v) SDS, 10 mM EDTA, pH 8] and 500 µl chloroform/IAA (24/1) (Sigma-Aldrich, St. Louis, USA). Samples were vortexed until homogenous, then centrifuged at 6200 g (15000 rpm) for 5 min. A second extraction of the aqueous phase was performed in a new microtube by adding 1 ml chloroform/IAA (24/1) (Sigma-Aldrich, St. Louis, USA), vortexing for 30 seconds and a 5 min centrifugation at 6200 g (15000 rpm). The aqueous phase was again transferred to a new microtube and after the addition of 1 Vol 4 M LiCl, the solution was mixed and the RNA was precipitated overnight at 4°C (Sigma-Aldrich, St. Louis, USA). RNA was collected by a 20 min centrifugation at 6200 g (15000 rpm) and washed with 70% (v/v) ethanol. Pellets were subjected to a DNase treatment consisting of 5 µl RNase free DNase (Promega, Madison, USA), 15 µl DNase buffer (Promega, Madison, USA) and 130 µl H₂O_{DEPC} (diethyl pyrocarbonate-treated water), pellets were solved on ice and incubated for 30 min at 37°C. Following this, 150 µl H₂O_{DEPC} was added and another extraction using 300 µl chloroform/IAA was performed. The

RNA in the aqueous phase was then precipitated at -80°C for 2 hr through the addition of 1/10 volume of 3 M NaOAc and 2.5 x volume of ethanol. The RNA was collected by a 20 min centrifugation at 6200 g (15000 rpm) and washed with 70% (v/v) ethanol. The final air dried pellet was dissolved in an appropriate volume of $\text{H}_2\text{O}_{\text{DEPC}}$.

The RNA concentration was measured using 2 μl of each sample with a NanoDropTM spectrophotometer (ND-1000 V3 3.0; Thermo Scientific, Wilmington, USA). RNA quality was checked by TAE-agarose electrophoresis (1% w/v; 60 V; 40 min) using 1 μg of total RNA. See Figure 2.2 for an example of an RNA quality check.

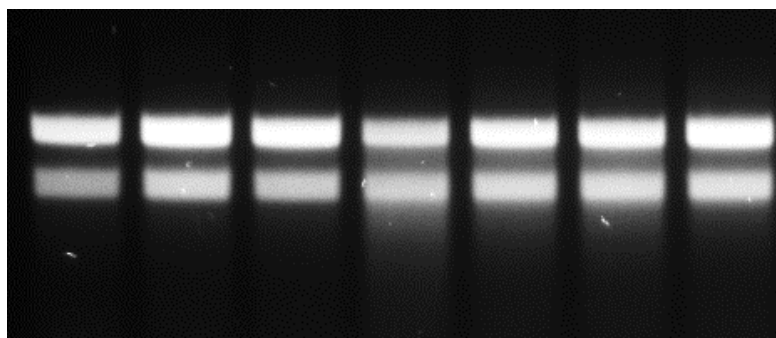


Figure 2.2. RNA quality check using TAE-agarose electrophoresis. 7 hydroponic grown wheat root RNA samples are shown. Two crisp bands are observed indicating good RNA quality. The upper band is the 28S ribosomal RNA (rRNA), the lower band is the 18S rRNA.

2.3.2 cDNA synthesis

cDNA was synthesised using Superscript III Reverse Transcriptase (Invitrogen, Carlsbad, USA). 2 μg of total RNA, 1 μl of 10 mM dT-adaptor primer and an appropriate volume of $\text{H}_2\text{O}_{\text{DEPC}}$ to make a total volume of 13 μl was mixed and incubated at 70°C for 10 min to denature the template RNA. Following this, the reaction mixture was cooled briefly on ice before the addition of 4 μl 5x first strand buffer, 1 μl 0.1 M DTT, 1 μl 10 mM dNTP mix and 1 μl Superscript III Reverse Transcriptase. The sample was then mixed and incubated for 5 min at 20°C , followed by 60 min at 50°C to initiate the cDNA synthesis. A final cycle of 15 min at 70°C terminated the reverse transcription and the synthesised cDNA was stored at -20°C .

2.3.2 Polymerase Chain Reaction (PCR) amplification of DNA

PCR reactions were used to amplify full length CDS prior to TOPO[®] and pGEM-T easy[®] cloning using cDNA material from wheat (*T. aestivum* cv. Paragon) grown under both +Zn and – Zn conditions (see Section 2.1.1). PCR reactions were conducted in thin-walled PCR tubes (STARLAB Ltd, UK) and cycled in a peqSTAR 96-well Universal Gradient PCR machine (peqLAB, DE). Primer tests were conducted using BiomixTM (Bioline, MA, USA) or REDTaq[®] ReadyMixTM (Sigma-Aldrich, St. Louis, USA) both of which contain ultra-stable *Taq* DNA

polymerase. Successful amplifications were then repeated using *Pfu* DNA polymerase (Promega, WI, USA) or Q5[®] High-Fidelity DNA Polymerase (New England Biolabs, MA, USA) which both exhibit 3' to 5' exonuclease (proofreading) activity.

2.3.3 Gel electrophoresis

PCR and restriction enzyme digestion products were visualised using gels containing 1% (w/v) agarose/TAE (40 mM Tris/acetate, 1 mM EDTA, pH 8.0). DNA staining was achieved using either 2 µl/100 ml Nancy-520 (Sigma-Aldrich, St. Louis, USA) or 10 µl/100 ml SYBR[®] Safe (Thermo Fisher Scientific, UK). Samples were loaded with 5x DNA loading buffer (Bioline, MA, USA) added to a final concentration of 1x depending on the amount of sample electrophoresed. Hyperladder 1 kb (Bioline, MA, USA) and Generuler 1kb (Thermo Fisher Scientific, UK) were used to assess product size; in 8 well combs, 15 µl was used, in 12-24 well combs 5 µl was used. Gels were run at 100 V using a Power Pac 200/2.0 (Bio-Rad, CA, USA) for 1-1.5 hr in 1x TAE buffer before visualising using a Gel-Doc UV viewer (Bio-Rad, CA, USA).

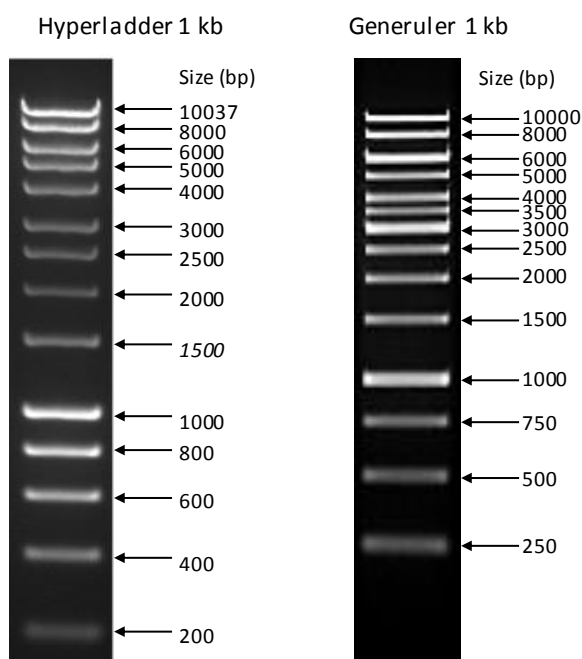


Figure 2.3. DNA molecular markers used for gel electrophoresis. A. Hyperladder 1 kb and **B.** Generuler 1 kb.

2.3.4 Colony PCR

Following successful growth of bacterial colonies, the insert of the plasmid they contain was checked using colony PCR. A sterile P10 sized pipette tip was lightly touched on the surface of a colony before swirling into a 10 µl PCR reaction mix as described in Section 2.3.2. Additional ‘backbone’ primers specific to the cloning vectors used in the checking of plasmid insert sizes are

given in Table 2.7. These backbone primers were used in combination with the specific wheat (*T. aestivum*) primers given in Tables 2.4 and 2.5 to amplify the insert and some of the backbone to check for the presence and the orientation of the insert within the plasmid.

Table 2.7. Backbone oligonucleotide primer sequences used in colony PCR and sequencing reactions.

Primer name	Primer sequence (5' to 3')
pMDC35S	CATTTGGAGAGGACCTCGACTCT
MDCnosR	AAGACCGGCAACAGGATTC
M13 Forward	GTAAAACGACGGCCAG
M13 Reverse	CAGGAAACAGCTATGAC
Gallp Forward	CATTTTCGGTTTGTATTACTT
CycTerm Reverse	GACTTCAGGTTGTCTAACTCCTTC
M13 uni (-21)	TGTAAAACGACGGCCAGT
M13 uni (-43)	AGGGTTTTCCCAGTCACGACGTT
M13 rev (-29)	CAGGAAACAGCTATGACC
T7	TAATACGACTCACTATAGGG
SP6	CATTTAGGTGACACTATAG

2.3.5 Restriction enzyme digestion

In-silico plasmids were created using pDRAW 32 for Windows 8 (freeware available at www.acaclone.com) and Geneious version 8.1.3 (www.geneious.com, Kearse et al., 2012). Using the enzyme selection tool, restriction enzymes were selected based on their ability to produce digestions of empty vectors and vectors with the correct insert that were easily distinguishable. Restriction digests were subsequently conducted according to manufacturer's instructions (Promega, WI, USA). Digests contained at least 100 ng of DNA in a 10 µl reaction including the appropriate 10x restriction enzyme buffer, 1 µl of (1 µg/µl) acetylated bovine serum albumin and 0.5 µl of restriction enzyme(s) (single or double digestion) made to final volume with sterile deionized H₂O. Reactions were incubated at 37°C for 4 hr with a denaturation step of 65°C for 15 min to terminate the digestion. The reactions were then visualised using gel electrophoresis as outlined in Section 2.3.3.

2.3.6 Sequence analysis

Plasmids were sequenced using Source Biosciences UK and Eurofins Genomics Germany. 15 µl of plasmids were sent for sequencing at a concentration of 75 ng/µl. Primers used are shown in Table 2.7. When possible primers provided by the sequencing companies were selected, however when sequencing with non-stock primers they were added to the sequencing sample tubes at a final concentration of 1.2 pM/µl. Sequences received were visually analysed using BioEdit version 7.2.5 (<http://www.mbio.ncsu.edu/bioedit/bioedit.html> Hall et al., 2011) and

aligned using Clustal Omega (<http://www.ebi.ac.uk/Tools/msa/clustalo/>) and Geneious version 8.1.3 (www.geneious.com, Kearse et al., 2012).

2.3.7 Real-time PCR

2.3.7.1 Relative quantification

1.1 µl of sample cDNA was added to: 11 µl H₂O_{DEPC}, 0.7 µl 10 µM forward primer, 0.7 µl 10 µM reverse primer, 0.25 µl ROX reference dye, 13.75 µl SYBR Green Jumpstart Taq ReadyMix™ (Sigma-Aldrich, St. Louis, USA). After mixing, 25 µl of this was loaded onto a white, semi-skirted 96-well plate (4titude, Surrey, UK). An Applied Biosystems 7500 Real Time PCR system (Life Technologies, Paisley, UK) was used to run the plates on a standard 7500 run mode (2 min 50°C, 10 min 95°C, 15 sec 95°C – 1 min 60°C for 40 cycles) with an added dissociation stage. Results were analysed using the associated 7500 software, version 2.0.5. Rn values were exported and mean primer efficiencies were calculated by analysing the linear phase of reaction amplification curves using LinregPCR (Ruijter et al., 2009).

Analysis was carried out using the Normalized Relative Quantification (NRQ) method (Rieu and Powers, 2009). NRQ results are reported as this method was deemed most accurate due to the use of individual primer efficiencies and normalizations within the fold change calculations. The NRQ of expression was calculated in relation to the Ct values and the primer efficiency (E) of the target gene (X) and the normalizing reference gene (N): $NRQ = (E_X)^{-Ct, X} / (E_N)^{-Ct, N}$. The Ct results from the three-week Zn starvation experiment were normalized to Ct averages obtained from two *TaActin3* housekeeping gene runs per cDNA batch. The Ct results from the one-week Zn starvation experiment were normalized to Ct averages obtained from two *TaActin3* and two *TaSuccDH* housekeeping gene runs per cDNA batch.

2.3.7.2 Absolute quantification

In order to examine gene expression patterns between varieties, absolute quantification real-time PCR was used. Real-time amplification fragments (using real-time primers detailed in Table 2.3) were cloned into the pGEM-T easy vector (as described in Section 2.4.3) and confirmed through sequencing. A dilution series of the confirmed fragment containing vector was created consisting of the following concentrations (100 pg/µl, 10 pg/µl, 1 pg/µl, 500 fg/µl, 100 fg/µl, 10 fg/µl, 1 fg/µl and 0.1 fg/µl). Real-time PCR reactions were then set up as detailed in Section 2.3.7.1 using either 1 µl of sample cDNA or 1 µl of the fragment containing pGEM-T vector dilution series. The standard curve linear relationship of the Ct values versus log fg amounts of the fragment containing pGEM-T vector dilution series was calculated. Following normalisation of the sample Ct values to a *TaActin3* housekeeping gene run, sample Ct values

were converted to fg cDNA quantities using the best fit formula obtained from the dilution series/log fg standard curve. cDNA molecules per 1 μ l of cDNA for each sample was then calculated based on the molecular weights of vector-fragment DNA.

2.4 *T. aestivum* gene cloning

2.4.1 Directional TOPO cloning into Gateway Entry Vector

Following the amplification of DNA fragments using the TOPO® primers described in Section 2.2.2.2, fragment sizes in-keeping with CDS length predictions were excised using a scalpel blade and DNA was purified from the slice of 1% (w/v) agarose gel using the QIAquick gel extraction kit (Qiagen, CA, USA) according to the manufacturer's instructions. DNA was quantified using a NanoDrop™ spectrophotometer (ND-1000 V3 3.0; Thermo Scientific, Wilmington, USA).

The *T. aestivum* genes examined were cloned into the TOPO® pENTR/D entry vector (Invitrogen, CA, USA) according to the manufacturer's instructions (see Figure 2.4). A molar ratio of PCR product to entry vector of 2/1 was calculated using the online ligation calculator (http://www.insilico.uni-duesseldorf.de/Lig_Input.html). DNA purified from the gel slice was combined with 0.5 μ l of TOPO® pENTR/D entry vector and 0.5 μ l of salt solution (1.2 M NaCl and 60 mM MgCl₂) in a thin walled PCR tube. This was then made up to 3 μ l with the addition of sterile deionized H₂O. The reaction was incubated at room temperature for 30 min, 2 μ l of this was then added to 25 μ l of thawed One Shot® TOP10 chemically competent *E. coli* cells whilst gently stirring the reaction with the pipette tip. Cells were incubated on ice for 30 min, heat-shocked for 30 seconds at 42°C and chilled on ice for a further 2 min. 250 μ l of SOC medium (Invitrogen, CA, USA) was added to the cells and then incubated in an orbital shaker at 37°C (225 rpm) for 1 hr. Cells were then spread onto LB agar plates containing 100 μ g/ml kanamycin and incubated for ~14 hr at 37°C.

Colonies that had grown after 14 hr were subjected to colony PCR (see Section 2.3.4), and any positive colonies were inoculated in 5 ml LB broth containing 100 μ g/ml kanamycin in a 30 ml Sterilin Universal container (Thermo Fisher Scientific, UK) and incubated for ~14 hr in an orbital shaker at 37°C (225 rpm). Following successful growth of the inoculum, plasmid DNA was extracted using the Qiagen Mini-prep kit (Qiagen, CA, USA) as described in the manufacturer's instructions. Diagnostic restriction enzyme digestions were conducted to confirm the presence of the insert of interest and its correct orientation (see Section 2.3.5).

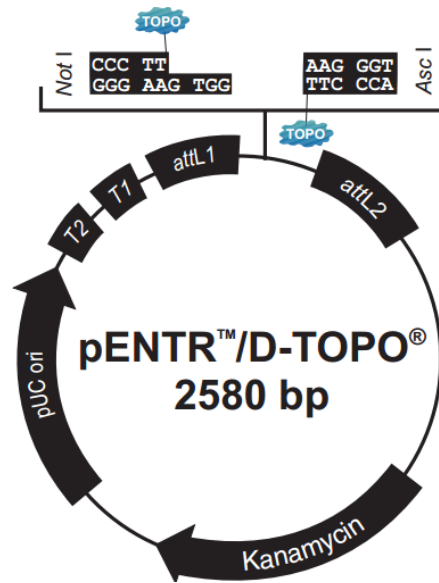


Figure 2.4. pENTR™/D-TOPO vector map. Image taken from Invitrogen pENTR™ Directional TOPO® cloning kit manual (Invitrogen, CA, USA).

2.4.2 Construction of *A. thaliana* expression vectors

Following the plasmid purification of entry vectors and *TabZIP* insert confirmation through diagnostic restriction digest, 500 ng of the entry vector was digested with 1 µl of a restriction enzyme that cuts once only, within the kanamycin resistance gene of the vector. This restriction enzyme was selected using pDRAW 32 for Windows 8 and the restriction digestion was carried out as described in Section 2.3.5. An LR Clonase™ reaction was carried out according to the manufacturer's instructions (Invitrogen, CA, USA) to shuttle the gene flanked by the *attL* sites in the entry vector (see Figure 2.4) to the *attR* sites within the pMDC32 destination vector. pMDC32 is a Gateway-compatible *Agrobacterium* sp. binary vector (Curtis and Grossniklaus, 2003). pMDC32 allows agrobacterium-mediated transformation of genes under the constitutive expression of a dual cauliflower mosaic virus (CaMV) 35S promoter (see Figure 2.5).

75 ng of the linearised entry vector was combined with 75 ng of pMDC32 destination vector and TE buffer, pH 8.0 to a final volume of 8 µl in a thin walled PCR tube. 2 µl of LR Clonase II enzyme™ (Invitrogen, CA, USA) was added to the reaction mix, the reaction was vortexed briefly and incubated at 25°C for 8-10 hr. Following this incubation, 1 µl of proteinase K enzyme (Invitrogen, CA, USA) was added and the reaction was terminated by a 10 min incubation at 37°C. 1 µl of this LR reaction was added to a 50 µl vial of homemade chemically competent *E. coli* DH5a cells and incubated on ice for 30 min. Cells were heat-shocked for 30 seconds at 42°C and transferred to ice for 2 min. 800 µl of SOC medium (Invitrogen, CA, USA)

was added to the cells and then incubated in an orbital shaker at 37°C (225 rpm) for 1 hr. Cells were then spread onto LB agar plates containing 100 µg/ml kanamycin and incubated for ~14 hr at 37°C.

Colonies that had grown after 14 hr were subjected to colony PCR (see Section 2.3.4), and any positive colonies were inoculated in 5 ml LB broth containing 100 µg/ml kanamycin in a 30 ml Sterilin Universal container (Thermo Fisher Scientific, UK) and incubated for ~14 hr in an orbital shaker at 37°C (225 rpm). Following successful growth of the inoculum, plasmid DNA was extracted using the Qiagen Mini-prep kit (Qiagen, CA, USA) as described in the manufacturer's instructions. Diagnostic restriction enzyme digestions were conducted to confirm the presence of the insert of interest and its correct orientation (see Section 2.3.5). Promising pMDC32 destination vector constructs were then sent for sequence analysis (see Section 2.3.6).

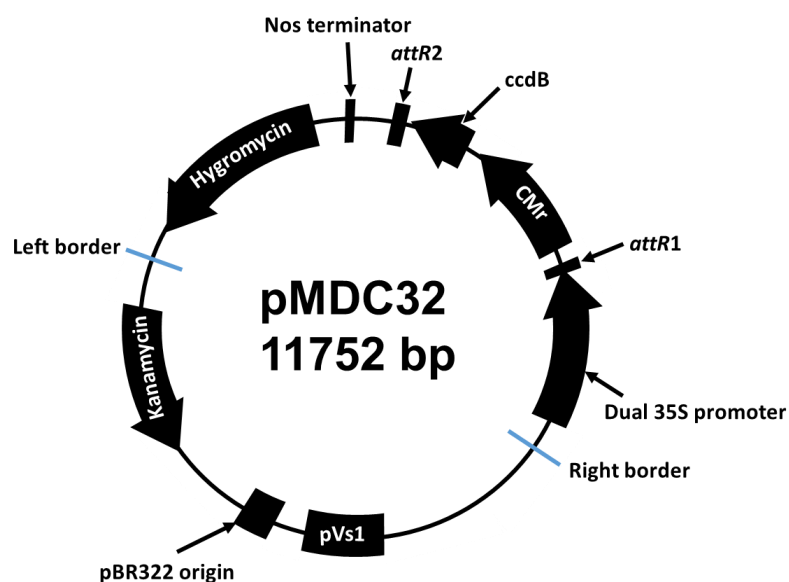


Figure 2.5. pMDC32 vector map.

2.4.3 pGEM-T Easy cloning

Following the initial amplification of blunt ended products as outlined in Section 2.3.2 using proofreading DNA polymerase, 1 µl of GoTaq® DNA polymerase (Promega, Madison, USA) was added to the 50 µl reaction and incubated at 72°C for 5 min in order to add an adenine base to each end of the amplicon. Amplicons were visualised as outlined in Section 2.3.3 and subsequently recovered using the Wizard® SV Gel and PCR Clean-Up System (Promega, Madison, USA) according to manufacturer's instructions. pGEM-T Easy cloning was carried out using a 10 µl reaction volume containing 3.5 µl H₂O_{DEPC}, 1 µl T4-DNA ligase, 2 µl 5x ligation

buffer (containing 250 mM Tris-HCl (pH 7.6), 50 mM MgCl₂, 5 mM ATP, 5 mM DTT, 25% (w/v) polyethylene glycol-8000 (Invitrogen, CA, USA)) with PCR fragment and pGEM-T Easy Vector in a molecular weight ratio of 3/1 and incubated at 20°C for 1 hr and at 16°C for 8 hr. 50 µl of homemade chemically competent DH5α *E. coli* cells were transformed with 5 µl of the ligation product as outlined in Section 2.4.2 and 200 µl was plated on a YT-plate containing ampicillin (50 mg ml⁻¹), IPTG (100mM) and X-Gal (40ng mL⁻¹). Positive transformants were detected using white-blue screening and colony PCR verification (see Section 2.3.4).

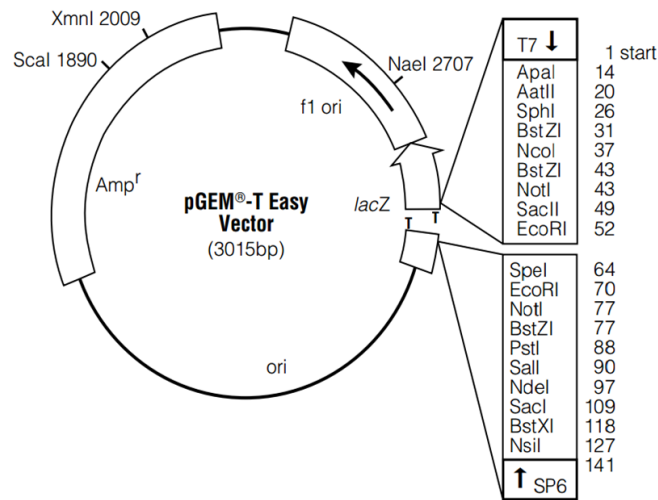


Figure 2.6. pGEM®-T Easy vector map. Image taken from Promega pGEM® Vector systems technical manual (Promega, Madison, USA)

2.4.4 Construction of *Saccharomyces cerevisiae* expression vectors

Following sequencing confirmation of pGEM-T Easy vectors, the *TaZIP* genes were subcloned to the pYES2 yeast expression vector (Invitrogen, CA, USA) using EcoRI digestion and subsequent ligation. 3 µg of the *TaZIP* containing pGEM vector was digested in a 50 µl reaction containing 5 µl Buffer H, 5 µl BSA, 2 µl EcoRI made up to 25 µl using H₂O_{DEPC} at 37°C for 8 hr. This fragment was then visualised on a gel, excised and purified using the Wizard® SV Gel and PCR Clean-Up System (Promega, Madison, USA) according to manufacturer's instructions. To avoid self-ligation the EcoRI linearized pYES2 purified fragment (55 µl) was dephosphorylated in a reaction containing 2 µl alkaline phosphatase, calf intestinal (CIAP) (Promega, Madison, USA), 10 µl of 10x alkaline phosphatase buffer made up to 100 µl using H₂O_{DEPC}. This was incubated at 37°C for 30 min, a further 1.5 µl of CIAP was added and incubated at 37°C for a further 30 min. After a further PCR purification step using the Wizard® SV Gel and PCR Clean-Up System (Promega, Madison, USA), the EcoRI cut *TaZIP* DNA fragment was

ligated into the dephosphorylated, EcoRI cut pYES2 vector using a 10 µl reaction volume containing 3.5 µl H₂O_{DEPC}, 1 µl T4-DNA ligase, 2 µl 5x ligation buffer (containing 250 mM Tris-HCl (pH 7.6), 50 mM MgCl₂, 5 mM ATP, 5 mM DTT, 25% (w/v) polyethylene glycol-8000 (Invitrogen, CA, USA)) with a 3/1 molar ratio of vector to insert.

50 µl of homemade chemically competent *E. coli* DH5α cells were transformed with 5 µl of the ligation product as outlined in Section 2.4.2 and 200 µl was plated on a YT-plate containing ampicillin (50 mg ml⁻¹). Positive transformants were detected using colony PCR verification (see Section 2.3.4).

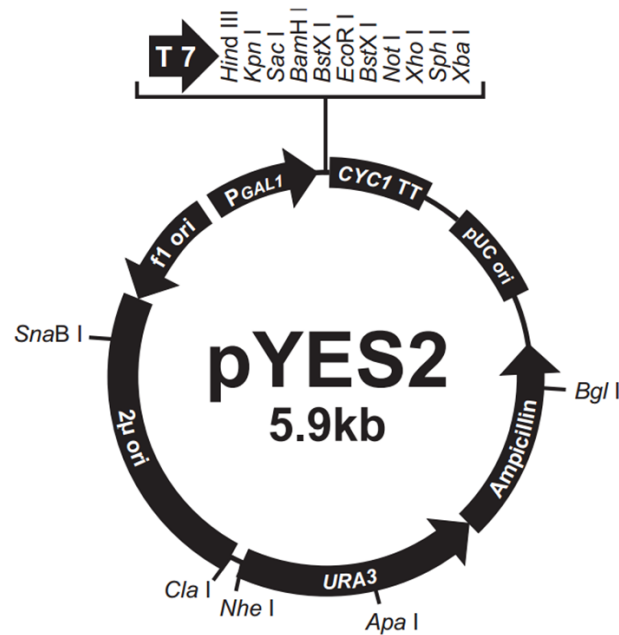


Figure 2.7. pYES2 vector map. Image taken from Invitrogen pYES2 user manual (Invitrogen, CA, USA).

2.5 Transformation and expression of *TaZIPs* in yeast mutant strains (Chapter 4)

2.5.1 *S. cerevisiae* strains

Yeast strains used in this thesis are as follows:

- Wild-type DY1457 (wt for *zrt1/zrt2* and *fet3/fet4*) (MATa, *ade1*/⁺ *can1*, *his3*, *leu2*, *trp1*, *ura3*)
- *zrt1/zrt2* (DY1457 + *zrt1*::LEU2, *zrt2*::HIS3)
- *fet3/fet4* (DY1457 + *fet3-2*::HIS3, *fet3-1*::LEU2)

- Wild-type BY4741 (wt for *zrc1/cot1*) (MATa, his3-1, leu2-0, met15-0, ura3-0). Obtained from Euroscarf, Frankfurt, Germany.
- *zrc1/cot1* double mutant (BY4741 + *zrc1::natMX cot1::kanMX4*). Provided by Dr U. Kramer (Ruhr University, Bochum).

2.5.2 *S. cerevisiae* growth, transformation and drop spot assays

2.5.2.1 *zrt1/zrt2* and *zrc1/cot1* strains

zrt1/zrt2 and *zrc1/cot1* yeast strains were maintained on yeast peptone dextrose (YPD) until introduction of either the gene of interest or the empty pYES2 vector. YPD was composed of 2% (w/v) peptone, 2% (w/v) glucose, 1% (w/v) yeast extract and 2% (w/v) agar (if preparing plates). Yeast cells were transformed using the *S. c.* EasyComp™ Transformation Kit (Thermo Fisher Scientific, UK) according to manufacturer's instructions. 150 µl of the transformed cells were plated on Synthetic Complete (SC) glucose minus uracil plates (see Table 2.8) and incubated at 30°C for 2-4 days. Colony PCR was used to confirm presence of the vector (see Section 2.3.4).

Single, PCR-confirmed colonies were inoculated overnight in 10 ml of SC-glucose minus uracil at 30°C (200 rpm). Inoculums were centrifuged at 1300 g (2500 rpm) for 3 min at room temperature, the supernatant was removed and the pellet suspended in 10 ml of SC-galactose minus uracil. This was incubated at 30°C (200 rpm) for 4 hr to allow gene induction. Inoculums were then centrifuged at 1300 g (2500 rpm) for 3 min at room temperature, then resuspended in SC-galactose minus uracil minus Zn (see Table 2.8) to remove any excess Zn from the pellet. Following resuspension in SC-galactose minus uracil minus Zn the OD₆₀₀ of the cultures was set to 0.39-0.41 and inoculate dilutions of 1/2, 1/10, 1/100 and 1/1000 were made using SC-glucose minus uracil minus Zn (see Table 2.8). 7 µl of the dilutions were dropped onto SC-galactose minus uracil plates (12 cm x 12 cm square petri dish (Sigma-Aldrich, St. Louis, USA)) supplemented as outlined in Table 2.9 and incubated at 30°C. Photographs were taken to document growth at regular intervals, incubation durations are provided alongside photographs in Chapter 4.

Table 2.8. SC medium composition for *S. cerevisiae* culture (*zrt1/zrt2* and *zrc1/cot1* strains).

Reagents	Supplier and reference	SC-glucose minus ura	SC-galactose minus ura	SC-galactose minus ura minus Zn
Yeast nitrogen base w/o amino acids	Sigma Y0626	0.68% (w/v)	0.68% (w/v)	-
Yeast nitrogen base w/o amino acids and w/o Zn	ForMedium CYN2301	-	-	0.69% (w/v)
Drop-out medium w/o uracil	Sigma Y1501	0.192% (w/v)	0.192% (w/v)	0.192% (w/v)
D-Glucose	Sigma G7520	2% (w/v)	-	-
Galactose	Euromedex 1042-B	-	2% (w/v)	2% (w/v)
Agar	Oxoid LP0028	2% (w/v)	2% (w/v)	2% (w/v)
pH	pH set with KOH	5.3	5.3	5.3

Table 2.9. SC medium composition for *zrt1/zrt2* and *zrc1/cot1* strain drop spot assays.

<i>zrt1/zrt2</i>	<i>zrc1/cot1</i>
SC-galactose minus ura minus Zn with the following additions:	SC-Galactose minus ura minus Zn with the following additions:
200 μ M ZnSO ₄	0 mM ZnSO ₄
0 mM EGTA	0.25 mM ZnSO ₄
2 mM EGTA	1 mM ZnSO ₄
5 mM EGTA	
7.5 mM EGTA	

2.5.2.2 *fet3/fet4* strain

The *fet3/fet4* strain was maintained and transformed as the *zrt1/zrt2* and *zrc1/cot1* strains, however, following transformation 150 μ l of the transformed cells were plated on SC-glucose minus uracil + 10 μ M FeCl₃ (pH 4.0) plates (see Table 2.10) and incubated at 30°C for 2-4 days. Colony PCR was used to confirm presence of the vector (see Section 2.3.4).

Single, PCR-confirmed colonies were inoculated overnight in 10 ml of SC-glucose minus uracil + 10 μ M FeCl₃ (pH 4.0) at 30°C (200 rpm). Inoculums were centrifuged at 1300 g (2500 rpm) for 3 min at room temperature, the supernatant was removed and the pellet suspended in 10 ml of SC-galactose minus uracil + 10 μ M FeCl₃ (pH 4.0). This was incubated at 30°C (200 rpm) for 4 hr to allow gene induction. The OD₆₀₀ of the cultures was then set to 0.39-0.41 and inoculate dilutions of 1/2, 1/10, 1/100 and 1/1000 were made using SC-glucose minus uracil + 10 μ M FeCl₃ (pH 4.0) to dilute. 7 μ l of the dilutions were dropped onto SC-galactose minus uracil minus Fe (pH 4.0) plates (12 cm x 12 cm square petri dish (Sigma-Aldrich, St. Louis, USA)) supplemented

as outlined in Table 2.11 and incubated at 30°C. Photographs were taken to document growth at regular intervals, incubation durations are provided alongside photographs in Chapter 4.

Table 2.10. SC medium composition for *S. cerevisiae* culture (*fet3/fet4* strain).

Reagents	Supplier and reference	SC-glucose minus ura + 10 μ M FeCl ₃	SC-galactose minus ura + 10 μ M FeCl ₃	SC-galactose minus ura minus Fe
Yeast nitrogen base w/o amino acids	Sigma Y0626	0.68% (w/v)	0.68% w/v)	-
Yeast nitrogen base w/o amino acids and w/o Fe	ForMedium CYN1101	-	-	0.69% (w/v)
Drop-out medium w/o uracil	Sigma Y1501	0.192%(w/v)	0.192% (w/v)	0.192% (w/v)
D-Glucose	Sigma G7520	2% (w/v)	-	-
Galactose	Euromedex 1042-B	-	2% (w/v)	2% (w/v)
FeCl ₃		10 μ M	10 μ M	-
Agar	Oxoid LP0028	2% (w/v)	2% (w/v)	2% (w/v)
pH	pH set with HCl	4.0	4.0	4.0

Table 2.11. SC medium composition for *S. cerevisiae* culture (*fet3/fet4* strain).

SC-galactose minus ura minus Fe pH (4.0) with the following additions:
0 μ M FeCl ₃
0.74 μ M FeCl ₃
10 μ M FeCl ₃

2.6 Transformation and expression of *TabZIPs* in *A. thaliana* (Chapter 5)

2.6.1 Agrobacterium transformation

1 μ l of the pMDC32 vectors (see Section 2.4.2) were added to 50 μ l of homemade electro-competent GV3850 *Agrobacterium tumefaciens* cells. After gently mixing with pipette tip, the cells were transferred to a pre-cleaned and pre-chilled 0.2 cm gap electroporation cuvette (Bio-Rad, CA, USA). The cells were then pulsed at 1.8 V for 5 milliseconds using a Biorad MicroPulser™ Electroporator (Bio-Rad, CA, USA). 1 ml of LB medium was then added to the cuvette and the bacterial suspension was transferred to a chilled 15 ml Falcon™ tube (Thermo Fisher Scientific, UK), this was then incubated in an orbital shaker for 2 hr at 37°C (225 rpm).

Chapter 2. Materials and methods

Following incubation the culture was spread on LB agar plates containing 50 µg/ml carbenicillin, 50 µg/ml rifampicin and 50 µg/ml kanamycin; these were cultured at 30°C for 3 days.

Colonies that had grown after 3 days were subjected to colony PCR (see Section 2.3.4), and a single positive colony was inoculated in 5 ml LB broth containing 50 µg/ml carbenicillin, 50 µg/ml rifampicin and 50 µg/ml kanamycin in a 30 ml Sterilin Universal container (Thermo Fisher Scientific, UK) and incubated for ~14 hr in an orbital shaker at 30°C (160 rpm).

2.6.2 *A. thaliana* transformation

A. thaliana plants (*bzip19-4bzip23-2* double mutants described in Chapter 5) were transformed with the pMDC32 *TabZIP* vector construct containing *Agrobacterium tumefaciens* cells using a floral dip method adapted from Clough and Bent (1998). Healthy *A. thaliana* plants with primary inflorescences of ~15 cm (~6 weeks old) were clipped 8-10 days before the transformation was conducted to encourage the proliferation of numerous bolts.

The 5 ml LB broth inoculum (see end of Section 2.6.1) was poured into 500 ml of LB broth containing 50 µg/ml carbenicillin, 50 µg/ml kanamycin and 50 µg/ml rifampicin in a sterile 2 litre conical flask and incubated in an orbital shaker at 30°C (225 rpm) overnight. Acetosyringone (3',5'-dimethoxy-4'-hydroxyacetophenone) was added to a final concentration of 100 µM and incubated for a further 3 hr. The culture was subsequently centrifuged in sterilised centrifugation bottles at 3700g for 15 min. The supernatant was removed and the cells re-suspended in 250 ml of sterile distilled water containing 5% (w/v) sucrose. The surfactant, Silwet L-77 (van Meuwen Chemicals, BV, Netherlands), was added to the *Agrobacterium* cells to a final concentration of 0.05% (v/v) and mixed thoroughly.

The aerial parts of the previously clipped *A. thaliana* plants were dipped in the *Agrobacterium* culture for 30 seconds with a gentle swirling action. The dipped plants were then sealed in their flower sleeves to create a humid environment and placed in dim lighting for 24 hr. Following this 24 hr period the flower sleeves were reopened and plants grown under normal conditions, as outlined in Section 2.1.2. Seeds were subsequently partially harvested at the onset of the first flush of dry siliques and harvested fully when all siliques were ripe.

2.6.3 Selection of positive transformants

Seed collected from plants subjected to the transformation procedure (Section 2.6.2) were surface sterilised by a 15 min immersion in a 2% (v/v) bleach solution and rinsed thoroughly afterwards in sterile distilled water. Seeds were then plated on 0.5x Murashige and Skoog basal salt mixture (MS) (Murashige and Skoog, 1962) (Sigma-Aldrich, St. Louis, USA) media containing 1% (w/v) sucrose and 1% (w/v) agar with an antibiotic selection of 50 µg/ml hygromycin (amoxicillin sodium) and 200 µg/ml augmentin (clavulanate potassium) (Melford

Laboratories Ltd., UK). Plates were subjected to a stratification period of 48 hr, at 4°C in the dark. Plates were then transferred to a controlled environment cabinet (Intellus environmental controller, Percival Scientific Inc., IA, USA) and grown under long day white light conditions as described in Section 2.1.2. After ~10 days of growth, positive transformants (T1) were visible. These T1 seedlings were transferred to soil pots as described in Section 2.1.2 and allowed to self-fertilise.

2.6.4 Segregation ratio analyses and identification of T3 homozygous lines

Following the self-fertilisation of T1 plants, T2 seed was collected and segregation ratio analyses were conducted. 50 seeds from each line were plated on two hygromycin MS selection plates (see Section 2.6.3) and one no selection MS plate. Seeds were stratified and grown on the plates as previously described. Eight seedlings from positive transformant seed lines with a hygromycin resistance ratio of 75% ($\pm 5\%$) were transferred to soil and allowed to self-fertilise.

T3 seed was subsequently collected from these T2 plants and a final segregation ratio analysis was conducted. 50 seeds from each line were plated on two hygromycin MS selection plates and one no selection MS plate. Any lines that showed 100% resistance were deemed homozygous and were used in subsequent phenotype experiments.

2.6.5 Zn-deficiency phenotype studies of TabZIP transformed *A. thaliana* lines

Two independent T3 homozygous lines from each transformation were selected to use for phenotype assays. Seeds were surface sterilised as previously described (Section 2.6.3) and plated onto six 12 cm x 12 cm square petri dishes (Sigma-Aldrich, St. Louis, USA) of 0.5x MS media containing 1% (w/v) sucrose and 0.8% (w/v) agarose containing 15 μM ZnSO_4 (+Zn) and 0 μM ZnSO_4 (-Zn). Within each plate, four seedlings from each of four *Arabidopsis* lines (wt, dm and two transformant lines) were grown in different arrangements. This resulted in six replicates of each treatment with four seedlings per replicate. Following a stratification period of 48 hr at 4°C in the dark, plates were transferred to growth cabinets and grown in a vertical position under conditions outlined in Section 2.6.3. After 18 days of growth plates were photographed and root and shoot fresh weights were measured. Individual fresh weights were obtained by calculating the average from the combined weight of the four seedlings prior to statistical analysis. A two-way analysis of variance (ANOVA) was used for the statistical analysis of each complementation experiment (the four TabZIPs investigated) to test for the main effects and interaction between the Zn treatment and *Arabidopsis* line.

2.7 Electrophoretic mobility shift assays (Chapter 5)

2.7.1 Amplification of PCR-generated *bZIP* templates

bZIP DNA fragments were amplified from existing, sequenced vector stocks using primers described in Section 2.2.2.4 in a 50 μ l reaction volume with Q5[®] High-Fidelity DNA Polymerase (New England Biolabs, MA, USA) according to manufacturer's instructions. Following the PCR 5 μ l of the solutions was visualised on a 1% (w/v) agarose/TAE (40 mM Tris/acetate, 1 mM EDTA, pH 8.0) gel. Upon confirmation of correctly sized amplicons, the remaining 45 μ l PCR reaction was purified using the Wizard[®] SV Gel and PCR Clean-Up System (Promega, Madison, USA) according to manufacturer's instructions with two 20 μ l elution steps.

2.7.2 Coupled transcription/translation of *bZIPs*

Following the amplification of *bZIPs* with SP6 promoters, Kozak sequences and poly-A tails, *bZIP* proteins were synthesised *in-vitro* using the TNT[®] SP6 High-Yield Wheat Germ Protein Expression System. 690 ng of DNA was added to 18 μ l of the wheat germ master mix and made up to 30 μ l using nuclease-free water. Reactions were gently pipette mixed and incubated in a PCR machine at 25°C for 2 hr. Additionally, a smaller 6 μ l reaction (3.6 μ l wheat germ master mix and 2.4 μ l nuclease-free water) was incubated alongside the main reaction to allow for two control lanes containing the protein synthesis mix but no template to test for the binding of endogenous proteins to the ZDRE probes.

2.7.3 Design and annealing of complementary labelled ZDRE probes

Complementary oligonucleotide pairs containing the putative Zn-deficiency response elements (ZDREs) present in the promoters of the *TaZIP* genes were designed to determine the binding ability of *bZIPs* to these elements (see Table 2.12). ZDREs were positioned adjacent to one another in the oligonucleotides designed and the same non-native flanking sequences at the 5' and 3' ends were used as in Assunção et al. (2010). In addition to the oligonucleotides containing the wheat ZDREs, the three sets of complementary oligonucleotides used by Assunção et al. (2010) to investigate the *AtbZIP* binding were also synthesised (Ass3Z to Ass2Z). The forward strand oligonucleotides were biotin labelled at the 5' end. Oligonucleotides were synthesised and biotin labelled by Eurofins Genomics (Ebersberg, Germany).

Complementary oligonucleotides were annealed by mixing at a molar ratio of 1/1, in 1.5 ml microtubes. 100 μ l annealing reactions containing 10 mM Tris, 1 mM EDTA, 50 mM NaCl and complementary oligonucleotides, each at a final concentration of 1 pmol/ μ l, were mixed and heated in a water bath for 5 min at 95°C. The water bath was then switched off and left to cool to

room temperature slowly overnight, allowing annealing of the oligonucleotides. These annealed oligonucleotides were stored in 30 μ l aliquots at -20°C and were not refrozen after initial thawing.

Table 2.12. Sequences of complementary oligonucleotides used in EMSAs.

Probe	Forward (5' to 3')	Reverse (5' to 3')
Ass3Z	biotinAATTCATGTCGACATATGTCGACA TATGTCGACACGAGCT	AGCTCGTGTGTCGACATATGTCGACAT ATGTCGACATGAATT
Ass3Zmut	biotinAATTCATGTAGACATATGTAGAC ATATGTAGACACGAGCT	AGCTCGTGTCTACATATGTCTACAT ATGTCTACATGAATT
Ass2Z	biotinAATTCATGTCGACATATGTCGACA CGAGCT	AGCTCGTGTGTCGACATATGTCGACAT GAATT
TaZIP1 ZDRE	biotinGACCGATGACGACATTGTGTCAA CACTGCAC	GTGCAGTGTGACACAATGTCGTCA TCGGTC
TaZIP4 ZDRE	biotinAATTCGTGTCGACACGTGTCGAC ACATGTTGACATGAGCT	AGTCATGTCAACATGTGTCGACAC GTGTCGACACGAATT
TaZIP5 ZDRE	biotinAATTCGTGTCGTCATATGTCGTCA CGAGCT	AGCTCGTGACGACATATGACGACA CGAATT
TaZIP6 ZDRE	biotinAATTCATGTCGAGACATGTCGAG ACGAGCT	AGCTCGTCTCGACATGTCTCGACAT GAATT
TaZIP7 ZDRE	biotinAATTCATGTCGACATATGACGAC ACGAGCT	AGCTCGTGTGTCGTCATATGTCGACAT GAATT

2.7.4 EMSA binding assay

In-vitro translated proteins (3 μ l of the 30 μ l reaction) were added to make a 20 μ l binding solution containing 20 mM Tris.HCl (pH 7.5), 10 mM KCl, 1 mM EDTA, 0.25 μ g/ μ l BSA, 1mM DTT, 0.25 μ g/ μ l salmon sperm DNA and 4 μ l of the annealed oligonucleotide solution. The solution was incubated on ice for 5 min prior to the addition of the probe, then incubated in a PCR machine at 28°C for 30 min. 5 μ l of 5x Novex Hi-Density TBE sample buffer (Thermo Fisher Scientific, UK) was added to the 20 μ l binding reaction and pipette mixed. 20 μ l of the samples were run on a 6% (w/v), 12 well, DNA Retardation Gel (Thermo Fisher Scientific, UK). Gel wells were flushed with 0.5x TBE before use and the gels were pre-run for 1 hr at 100 V before samples were loaded. Gels were run in XCell Surelock™ Mini-Cell tanks (Thermo Fisher Scientific, UK) using 0.5x TBE buffer at 100 V for 1 hr 15 min.

For each gel, the following controls were used:

- Control 1 – Translated protein (whichever is being investigated) and no probe
- Control 2 – No protein (no TNT wheat germ mix) with Ass3Z probe
- Control 3 – TNT wheat germ mix (no template) with Ass3Z probe.

After electrophoresis, the gel was blotted onto Amersham Hybond-N⁺ membrane (GE Healthcare, UK) using the XCell II™ Blot module (Thermo Fisher Scientific, UK) in 0.5x TBE for 1 hr at 200 mA. The membrane was then crosslinked using a Stratalinker® UV Crosslinker 2400 at 120 mJoules/cm² for 1 min with the nucleic acid side of the membrane facing upwards.

The biotin-labelled DNA was detected by chemiluminescence using the Chemiluminescent nucleic acid detection module kit (Thermo Fisher Scientific, UK) according to manufacturer's instructions. The membrane was visualised using the Odyssey[®] FC imaging system (Li-Cor, USA), with a 2 min exposure on the chemiluminescent function.

2.8 Field sampling (Chapter 6)

2.8.1 WISP donor trial

The Wheat Improvement Strategic Programme (WISP) donor trial was utilised in this project. The WISP donor trial is planted annually and consists of a randomised block design, with three replicate blocks of 166 wheat varieties. All plots receive 200 kg N/ha. 2013 field-season samples were collected from the WISP donor trial, planted in November 2012 and located at Black Horse field site, Rothamsted Research, Harpenden, UK. Sampling was conducted at two time points: Time point 1 (06/06/2013 and 07/06/2013 growth stage – late booting) and Time point 2 (04/07/2013 and 05/07/2013 growth stage – grain filling). 2014 field-season samples were collected from the WISP donor trial, planted October 2013 and located at Redbourn Meadow field site, Rothamsted Research, Harpenden, UK. 2014 field-season sampling was conducted at one time point (21/05/2014 and 22/05/2014 growth stage – late booting). 2015 field-season samples were collected from the WISP donor trial, planted October 2014 and located at Summerdells field site, Rothamsted Research, Harpenden, UK. 2015 field-season sampling was conducted at one time point (21.05.2015 growth stage – late booting/ear emergence).

Samples of ten varieties that were identified in data mining of existing Rothamsted field data, that showed interesting Zn characteristics were taken. Plants were extracted from the soil carefully using a two-pronged garden fork. Soil was washed from the roots by a series of three soaks in deionised water, roots and shoots were separated and samples were frozen in liquid nitrogen. On return from the field-site, samples were stored at -80°C.

2.8.2 Paragon x WC239 mapping population

An F4 mapping population of the parent lines Paragon and WC239 (Watkins collection) developed within the WGIN (Wheat Genetic Improvement Network) project was sown at the Summerdells 2 field site, Rothamsted Research, Harpenden, UK in October 2014. Two nitrogen treatments were utilised (50 kg N/ha and 200 kg N/ ha). For each of the 91 lines (as well as the two parents), three replicate plots, 1 m x 1 m, were sown in a randomized block design. The field trial was harvested in September 2015. ICP-OES (see Section 2.9) was used to quantify Zn concentrations of straw and grain fractions from the 50 kg/ha N treatment field grown mapping

population lines, the results of which were used in a QTL analysis of the mapping population (see Section 2.8.3).

2.8.3 QTL analysis

The genetic map containing 268 mapped markers, available at http://wisplandracepillar.jic.ac.uk/results_resources.htm was utilised. The mean of the three plot replicates (93 in total) was used to detect Zn and yield QTLs using the software package QTL cartographer v2.5 available at <http://statgen.ncsu.edu/qtlcart/WQTLCart.htm>. Detection of QTLs was conducted using the composite interval mapping (CIM) method (Zeng, 1994). Parameters used were as follows: window size 10 cM, 2cM walk speed, five control markers and a QTL detection threshold determined with 1000 permutations at $\alpha = 0.05$.

2.9 ICP-OES analysis

Depending on the experiment, 0.02-3 g of freeze dried plant tissue samples were digested in 5 ml nitric acid/perchloric acid (85/15, v/v) (70% (v/v) concentration, trace analysis grade, Fisher Scientific, Loughborough, UK), for a minimum of 2 hr at room temperature followed by a 5 hr programmed thermoblock cycle. 5 ml of 25% (v/v) nitric acid was added to the solution and the tubes were reheated for 1 hr at 80°C. Ultra-pure water (>18 M Ω) was added to approximately 9 ml (for experiments with smaller samples) or 15 ml (for experiments with larger samples), mixed well and re-warmed for a further 30 min at 80°C. After cooling, the solutions were made up to final volumes of 10 ml (for experiments with smaller samples) or 25 ml (for experiments with larger samples) with deionized H₂O. ICP-OES analysis was carried out using an Optima Inductively Coupled Plasma – Optical Emission Spectrometer (Perkin Elmer Life and Analytical Sciences, Shelton, USA).

2.10 Statistical analysis

All data was statistically analysed using GenStat (2014, 17th edition, VSN International Ltd, Hemel Hempstead, UK). ANOVA was used for analysis of all data throughout this thesis, with the exception of Figure 3.8. If data were not normally distributed, they were transformed appropriately before testing. Following ANOVA, significant effects and interactions were investigated post-hoc using Fisher's least significant difference (LSD) test at 5%. LSDs were used to compare appropriate mean terms and significant comparisons were reported.

Chapter 3. Identification of *T. aestivum* ZIP and bZIP genes and their spatiotemporal expression responses to Zn-deficiency

3.1 Introduction

3.1.1 The ZIP transporter family

The journey of Zn from soil to seed is complex, involving many membrane transporters operating in a coordinated fashion to maintain Zn homeostasis within the plant. This process is not yet fully understood. The majority of work to date has been conducted in the model plant *A. thaliana*, however key Zn-transport proteins are now being elucidated in important crop species. One of the key membrane transporter families operating in Zn homeostasis is the ZIP (ZRT, IRT-related Protein) family of proteins.

Members of the ZIP family have been shown to be important in plant-wide Zn trafficking. ZIPs are involved in the initial transport of Zn²⁺ ions from the soil across the plasma membrane of the root (Grotz et al., 1998; Guerinot, 2000; Ramesh et al., 2004), in the processes of Zn xylem (Milner et al., 2013) and phloem loading (Ishimaru et al., 2005), and implicated in the controlled distribution of Zn throughout the grain (Tauris et al., 2009).

In *Arabidopsis* there are 18 members of the ZIP family. Although many have yet been characterised, a large proportion (*AtIRT3*, *AtZIP1*, 3, 4, 5, 7, 8, 9 and 12) have all been shown to be Zn responsive in expression, being upregulated under Zn-deficient conditions in either the root, the shoot or both (Grotz et al., 1998; Lin et al., 2009; Jain et al., 2013; Milner et al., 2013). Specific members of the ZIP family are now known to be involved in aspects of Zn-homeostasis in crop species including maize (*Zea mays*) (Li et al., 2013, 2015a), rice (*O. sativa*) (Ramesh et al., 2003; Bashir et al., 2012), soybean (*Glycine max*) (Moreau et al., 2002), barley (*H. vulgare*) (Tiong et al., 2013, 2015), grape (*V. vinifera*) (Gainza-Cortés et al., 2012), navel orange (*Citrus sinensis*) (Xing et al., 2016) as well as a relative of modern bread wheat; wild emmer wheat (*T. turgidum* ssp. *dicoccoides*) (Durmaz et al., 2011).

In rice, of the 16 ZIP family members, five have been shown to be induced by Zn-deficiency; *OsZIP1*, 3, 4, 5 and 8 (Ramesh et al., 2003; Lee et al., 2010b; Ishimaru et al., 2005). In barley, *HvZIP3*, 5, 7, 8, 10 and 13 have all been shown to be upregulated in response to Zn-deficient conditions (Pedas et al., 2009; Tiong et al., 2013, 2015). At present, there is only one study in which a ZIP transporter has been investigated in a wheat species (Durmaz et al., 2011); wild emmer wheat (*T. turgidum* ssp. *dicoccoides*) a tetraploid relative of modern bread wheat (*T. aestivum*). This emmer wheat ZIP transporter (*TdZIP1*) was shown to be upregulated in Zn-

deficient conditions and through complementation assays, the Zn-transporting capabilities of this transporter were confirmed (Durmaz et al., 2011).

The widespread responsiveness of *ZIPs* to Zn status, as well as their involvement in such a wide range of Zn transport processes makes members of the *ZIP* family especially interesting candidates for biofortification research. In this chapter the identification of *T. aestivum ZIP* genes is presented and their expression profiles in response to Zn-deficiency are determined.

3.1.2 The importance of bZIP transcription factors in Zn-homeostasis

An important aspect of Zn-homeostasis in plants is the regulation of the plant response to Zn deficiency. The tightly controlled expression of a suite of Zn membrane transporters is vital in bringing about an effective response to adverse Zn conditions. Research in *A. thaliana* has shown the importance of two bZIP transcription factors in the regulation of adaptation to Zn deficiency (Assunção et al., 2010). These two group F bZIPs (AtbZIP19 and AtbZIP23) are vital in bringing about the controlled, increased expression of *ZIP* genes in *Arabidopsis* under Zn-deficient conditions. However, to date the importance of crop *bZIP* homologs has not been determined, particularly with regard to Zn homeostasis. These response-regulating genes have potential interest in terms of biofortification as well as the breeding of Zn-efficient lines as they have the opportunity to control a suite of genes involved in the Zn homeostasis network of crop plants. Genome-wide analyses of *bZIPs* have been conducted in rice (Nijhawan et al., 2008), barley (Pourabed et al., 2015) and wheat (Li et al., 2015b). In this chapter a thorough bioinformatics analysis of group F bZIPs is conducted for *Arabidopsis*, *Brachypodium*, rice, barley and wheat. The wheat group F *bZIP* members present in the existing genome-wide analysis by Li et al. (2015b) are corrected and completed. The expression responses of these *TabZIPs* in response to Zn deficiency are determined.

3.1.3 The use of hydroponic culture methods to study micronutrient deficiency responses

In order to determine the importance of the identified *TaZIP* membrane transporters and *TabZIP* transcription factors in the Zn-regulatory framework of wheat, their relative expression levels will be examined under Zn-deficient conditions. The growth of plants in hydroponic culture systems gives direct control over the nutrient concentrations that plants are exposed to throughout the growth phase. This ability to accurately control nutrient concentrations is vital when examining plant responses to micronutrient deficiencies. Hydroponic culture systems vary in design, but all are systems that facilitate plant growth in a liquid medium that contains all required macro and micronutrients. Plants are suspended with their roots growing in the solution, this is most often aerated which also maintains a homogeneous mix. In this chapter, a hydroponic system

was set up and tested, with each individual wheat (*T. aestivum*) plant grown in a separate 1 L aerated, hydroponic-culture vessel. The efficacy of this system in providing Zn-deficient growth conditions on wheat was tested and the system was subsequently used to examine both the expression of *TaZIPs* and *TabZIPs* under Zn-deficient conditions and interactions of Zn deficiency with other plant nutrients.

3.2 Aims

- Identify and examine wheat *ZIP* and *bZIP* genes in the wheat genome using bioinformatics analyses
- Investigate the phylogenetic relationships of *TaZIPs* and *TabZIPs* identified
- Develop a hydroponic protocol that allows the induction of Zn deficiency in wheat
- Determine the transcriptional responses of wheat *ZIPs* and *bZIPs* in response to Zn deficiency

3.3 Results

3.3.1 ZIP transporter genes

Analysis of both the IWGSC and TGAC scaffold sequence assembly databases revealed a total of 13 wheat *TaZIP* genes. Full homeolog complements were found for all of these genes in each of the A, B and D genomes, except for *TaZIP3-7BL* of which only the 3' half of the sequence could be found. Additionally, the nucleotide sequence for *TaZIP7-1AS* produced a frameshift after 211 of the predicted 387 amino acids, which suggests this may be a non-functional homeolog. Tiong et al. (2015) previously published a phylogenetic analysis of *ZIPs* in *Arabidopsis thaliana*, *Oryza sativa*, *Brachypodium distachyon*, *Hordeum vulgare* and wheat (*T. aestivum*). Tiong et al. (2015) identified 11 wheat *ZIPs*, with only one homeolog of each being detailed. *TaZIP2* and *TaZIP8* were not identified. The wheat gene names given by Tiong et al. (2015) with respect to the *TaZIPs* identified and studied in this thesis are given in Table 3.1. A considerable number of inconsistencies in the *Brachypodium* and barley accession numbers were present in (Tiong et al., 2015); these were corrected and the phylogenetic analysis of cereal *ZIPs* (Figure 3.1) is presented with the corrected accession information.

The phylogenetic analysis of cereal and *Arabidopsis ZIP* genes (Figure 3.1) shows the homeologs of each wheat *ZIP* group closely to one another at the tips of clades. For 12 of the 13 *TaZIPs* identified the most closely related homolog was that from barley, followed by *Brachypodium* and then rice; this is in accordance with the evolutionary relatedness of these cereals. *TaZIP5* and *TaZIP8* grouped very close to one another, sharing a common barley homolog (*HvZIP13*). Upon further inspection, *TaZIP5* and *TaZIP8* shared very high sequence

similarity, *TaZIP5-2AL* and *TaZIP8-2AS* for example had 89% nucleotide sequence similarity. *TaZIP5* and *TaZIP8* are located on the long and short arms of chromosome 2 respectively. Their presence on the same chromosome and their high sequence similarity is indicative of gene duplication.

Nine of the 18 *Arabidopsis ZIPs* cluster together (*AtIRT1*, 2 and *AtZIP1*, 3, 5, 7, 8, 10 and 12) in a clade which contains only these dicotyledonous *ZIPs*. This suggests sequence divergence has occurred since the evolutionary split between monocotyledons and dicotyledons. *AtZIP 2, 4, 6, 9, 11, AtIRT3, AtPutZnT, AtIAR1* and *AtZTP29* are situated in clades containing monocot *ZIP* homologs which suggests functional conservation may exist within these clades. *AtPutZnT, AtIAR1* and *AtZTP29* and their cereal homologs are situated in a cluster of their own and are more distantly related to the other *ZIPs* included in the phylogenetic analysis. These proteins were omitted from the alignment shown in Figure 3.2 due to the low similarity in amino acid sequence and the lack of evidence characterising the suggested Zn-transporting capabilities of these proteins.

The multiple sequence alignment presented in Figure 3.2 shows the *ZIPs* investigated have highest sequence conservation within the predicted transmembrane (TM) spanning domains, and the wheat *TaZIPs* identified conform to the eight predicted TM domain locations proposed by Li et al. (2013). The variable region between TM III and IV is clear across all of the *ZIPs* included in the alignment and along with the variable N terminus accounts for the variation in length of 300-420 amino acids. Predicted topology diagrams of two *TaZIPs* (*TaZIP1-2AL* and *TaZIP5-2AL*) are shown in Figure 3.3. The residues underlying the predicted TM domains are shown. Additionally, histidine residues present between TM-III and TM-IV are indicated. Previously, (Guerinot, 2000; Eide, 2005) histidine residues within this region have been predicted to comprise part of an intramembranous heavy metal-binding site.

Table 3.1. Wheat ZIP gene identification details. Gene name indicates nomenclature used throughout this thesis, with the sequence identifiers for the IWGSC database and TGAC scaffolds given. The nomenclature used by Tiong et al. (2015) is shown, with (-) indicating a homeolog or gene not previously described. (N.C.) indicates a non-complete sequence (N.F.) indicates a likely non-functional translation caused by a frameshift in the coding sequence.

Gene name	IWGSC wheat survey sequence ID	TGAC scaffold ID	Tiong et al., 2015 name
<i>TaIRT1-4AL</i>	IWGSC_chr4AL_V2_ab_k71_contigs_7176064	TGACv1_scaffold_290140_4AL	-
<i>TaIRT1-4BS</i>	IWGSC_chr4BS_ab_k71_contigs_4892838	TGACv1_scaffold_328611_4BS	-
<i>TaIRT1-4DS</i>	IWGSC_chr4DS_ab_k71_contigs_2302189	TGACv1_scaffold_361462_4DS	TaIRT1
<i>TaZIP1-2AL</i>	IWGSC_chr2AL_ab_k71_contigs_6316275 IWGSC_chr2AL_ab_k71_contigs_1213723	TGACv1_scaffold_094530_2AL	TaZIP3
<i>TaZIP1-2BL</i>	IWGSC_chr2BL_ab_k71_contigs_8070141	TGACv1_scaffold_129658_2BL	-
<i>TaZIP1-2DL</i>	IWGSC_chr2DL_ab_k71_contigs_1693935	TGACv1_scaffold_160080_2DL	-
<i>TaZIP2-6AS</i>	IWGSC_chr6AS_ab_k71_contigs_4367735	TGACv1_scaffold_487184_6AS	-
<i>TaZIP2-6BS</i>	IWGSC_chr6BS_ab_k71_contigs_3004962	TGACv1_scaffold_513631_6BS	-
<i>TaZIP2-6DS</i>	IWGSC_chr6DS_ab_k71_contigs_907365	TGACv1_scaffold_544682_6DS	-
<i>TaZIP3-7AL</i>	IWGSC_chr7AL_ab_k71_contigs_4554120	TGACv1_scaffold_558847_7AL	TaZIP10
<i>TaZIP3-7BL</i> (N.C.)	IWGSC_chr7BL_ab_k71_contigs_6688105	TGACv1_scaffold_586691_7BL	-
<i>TaZIP3-7DL</i>	IWGSC_chr7DL_ab_k71_contigs_3374716	TGACv1_scaffold_603327_7DL	-
<i>TaZIP4-4AS</i>	IWGSC_chr4AS_V2_ab_k71_contigs_5977908	TGACv1_scaffold_306183_4AS	TaZIP5
<i>TaZIP4-4BL</i>	IWGSC_chr4BL_ab_k71_contigs_6973453	TGACv1_scaffold_321083_4BL	-
<i>TaZIP4-4DL</i>	IWGSC_chr4DL_V3_ab_k71_contigs_14352890	TGACv1_scaffold_342890_4DL	-
<i>TaZIP5-2AL</i>	IWGSC_chr2AL_ab_k71_contigs_6361092	TGACv1_scaffold_098072_2AL	-
<i>TaZIP5-2BL</i>	IWGSC_chr2BL_ab_k71_contigs_8072119	TGACv1_scaffold_129838_2BL	-
<i>TaZIP5-2DL</i>	IWGSC_chr2DL_ab_k71_contigs_9909609	TGACv1_scaffold_159221_2DL	TaZIP13
<i>TaZIP6-1AS</i>	IWGSC_chr1AS_ab_k71_contigs_3266067	TGACv1_scaffold_019973_1AS	-
<i>TaZIP6-1BS</i>	IWGSC_chr1BS_ab_k71_contigs_3300643	TGACv1_scaffold_050073_1BS	TaZIP6
<i>TaZIP6-1DS</i>	IWGSC_chr1DS_ab_k71_contigs_1891978	TGACv1_scaffold_082083_1DS	-

Table 3.1. continued.

Gene name	IWGSC wheat survey sequence ID	TGAC scaffold ID	Tiong et al., 2015 name
<i>TaZIP7-1AS</i> (N.F.)	IWGSC_chr1AS_ab_k71_contigs_3313103	TGACv1_scaffold_018996_1AS	-
	IWGSC_chr1AS_ab_k71_contigs_3258126		
<i>TaZIP7-1BS</i>	IWGSC_chr1BS_ab_k71_contigs_3424485	TGACv1_scaffold_049369_1BS	-
<i>TaZIP7-1DS</i>	IWGSC_chr1DS_ab_k71_contigs_1886991	TGACv1_scaffold_082535_1DS	TaZIP7
<i>TaZIP8-2AS</i>	IWGSC_chr2AS_ab_k71_contigs_5235569	TGACv1_scaffold_112113_2AS	-
<i>TaZIP8-2BS</i>	IWGSC_chr2BS_ab_k71_contigs_5173470	TGACv1_scaffold_146518_2BS	-
<i>TaZIP8-2DS</i>	IWGSC_chr2DS_ab_k71_contigs_5333023	TGACv1_scaffold_177487_2DS	-
	IWGSC_chr2DS_ab_k71_contigs_5328349		
<i>TaZIP11-3AL</i>	IWGSC_chr3AL_ab_k71_contigs_4363752	TGACv1_scaffold_195235_3AL	-
<i>TaZIP11-3BL</i>	IWGSC_chr3B_ab_k71_contigs_10599976	TGACv1_scaffold_221732_3B	TaZIP1
<i>TaZIP11-3DL</i>	IWGSC_chr3DL_ab_k71_contigs_4892864	TGACv1_scaffold_250330_3DL	-
<i>TaZIP12-1AS</i>	IWGSC_chr1AS_ab_k71_contigs_3311632	TGACv1_scaffold_019215_1AS	TaZIP11
<i>TaZIP12-1BS</i>	IWGSC_chr1BS_ab_k71_contigs_3412874	TGACv1_scaffold_049922_1BS	-
<i>TaZIP12-1DS</i>	IWGSC_chr1DS_ab_k71_contigs_1890292	TGACv1_scaffold_080155_1DS	-
<i>TaZIP14-3AS</i>	IWGSC_chr3AS_ab_k71_contigs_3337115	TGACv1_scaffold_212290_3AS	-
<i>TaZIP14-3BS</i>	IWGSC_chr3B_ab_k71_contigs_10529788	TGACv1_scaffold_224841_3B	-
<i>TaZIP14-3DS</i>	IWGSC_chr3DS_ab_k95_contigs_2572146	TGACv1_scaffold_273454_3DS	TaZIP14
<i>TaZIP16-6AS</i>	IWGSC_chr6AS_ab_k71_contigs_4347038	TGACv1_scaffold_485332_6AS	TaZIP16
<i>TaZIP16-6BS</i>	IWGSC_chr6BS_ab_k71_contigs_2962925	TGACv1_scaffold_513963_6BS	-
<i>TaZIP16-6DS</i>	IWGSC_chr6DS_ab_k71_contigs_1077896	TGACv1_scaffold_542944_6DS	-

Chapter 3. Identification and expression of *TaZIPs* and *TabZIPs*

I

```

At3g12750.1 (AtZIP1)  -MSEGCFSATTMLRIGVW---LITCQIHC---CS-----SDCT---SHD-DP--VSQD+AEKATR---LKGKSAALP
Os03g46470.1 (OsIRT1) ---MATPRTLVPITPPVAALLIITVAASSIPILAAQPA---DAGCGAPDQAAA-DG---LCHIVPPAIR---LKGKSAALP
Os03g46454.1 (OsIRT2) ---MMSSSQTPVRIAFV---FLVITIAATDAHSDHRTPP---PAGGG---AAV-GG---ECISVFAAIR---LKGKSAALP
TaIRT1-4AL          ---MPSSQALAVSIS---LALITCCTSPILLAHQTPATDPAADYCAA---LAT-DD---CINVPKAIR---LKGKSAALP
TaZIP1-2AL          ---MGATNHTQAII---PWLITFVHQAAAASCG---FEGCTT---AT---DGAIRKQGAIR---LKGKSAALP
Os04g52310.1 (OsZIP3) ---MGAKKHTLQVI---PWLITFAQ---HTAP---SAGD---CAN-TT---DGAIRKQGAIR---LKGKSAALP
Os08g10630.1 (OsZIP4) ---MDAMRQSTPRAMITICAVLITIAAPPGAATAAV---ACGE---CGN-AAAAAVGPTARGAIR---LKGKSAALP
TaZIP2-6AS          ---MATAASSRHHLLI---LWICAAASTAWAHGCG---GDDDADSGDADADGG---EKPDLRAPGLVAIKWCVLAV
Os01g74110.1 (OsZIP1) ---MARTMTMRSSITVAVVITIAALSF---QALSGHGGINDGQVDAPITPASSSVRSKGLIAIKWCVLAV
Os03g29850.1 (OsZIP2) MAGGRGARASLHLH---AMICAFATITAWAHGCG---CGGD---SDADAD---CGGKPKDLRARGLVAIKWCVLAV
TaZIP11-3AL        MARMARSTRRTSNLCTIITLLSLITITCFFQQAASGHC---VDHGDGDEEDEDGHH---DAGVIGHLRSGRLIAIKWCVLAV
TaZIP3-7AL         MAFRIPCLFETESYVYPYRAHLHQFAASV---SA---ASGEE---GAGD-DE---ECLDEPAAIR---LKGKSAALP
Os06g37010.1 (OsZIP10) ---MESSSSSYIP---FIRQAAS---VSA---ASCDVAVGGGGDKDE---ECLDEPAAIR---LKGKSAALP
TaZIP4-4AS         ---MAANLKAAAC---LITLSSLL---PLLRA---AEE---CEA-GE---EELHKACAIR---LKGKSAALP
Os05g39540.1 (OsZIP9) ---MAFDLKTAC---LITLAFSL---AAA---ADE---CQP-SD---EGHAKPKSRT---LKGKSAALP
TaZIP5-2AL         ---MKPSAGVIAAV---AIIIAAV---RD---DDCGSP---ES---ACDRRARNP---LKGKSAALP
Os05g39560.1 (OsZIP5) ---MATAAMTKVIV---LITVAACYLPAHAIA---AFD---CAT-DT---GHLKACAIR---LKGKSAALP
TaZIP8-2AS         ---MKRGAAVLIAAV---AIIISAV---RE---DECGSP---ES---ACDRRARNP---LKGKSAALP
Os07g12890.1 (OsZIP8) ---MRTNTTATVIAAAV---AIIATAA---RGDGD---GCG---KED-AA---GHLRARG---LKGKSAALP
TaZIP6-1AS        ---MMIGVAGFSRHIGQISKSNGLIAASL---SA---ASCADEAEKAE---GA---CHDDPAAIR---LKGKSAALP
Os05g10940.1 (OsZIP7) ---MERFVQFIRRGNTVAASL---AA---GSAEVEKAE---GA---CHDDPAAIR---LKGKSAALP
    
```

I

II

III

```

At3g12750.1 (AtZIP1)  LVAGVGVSLPI---GRIP-----ALCEPNDIFVKAFAAGVILITGVVHLPDAEIRLSPCLBDTTAG---FPFAGVAMSAAG
Os03g46470.1 (OsIRT1) LVSIVGVQLPI---SRSPV---ALREDGGRFAVKAFAAGVILITGVVHLPDAENNLSPCLPR-KEPSEFPFAGVAMSAAG
Os03g46454.1 (OsIRT2) LAIVYAGVQLPI---FARSVP---ALREDGGRFAVKAFAAGVILITGVVHLPDSENLSPCLPR-KEPSEFPFAGVAMSAAG
TaIRT1-4AL          LVSIVGVQLPI---FARSVP---ALCEPNDIFVKAFAAGVILITGVVHLPDSENLSPCLPE-KEPQFPFHTFVAMSAAG
TaZIP1-2AL          LITGAGVILPI---GRSMA---ALREDDIFVKAFAAGVILITGVVHLEAEADLSPCKRGGGDNFPFAGVAMSAAG
Os04g52310.1 (OsZIP3) LAIVGAGVILPI---GRSMA---ALREDDIFVKAFAAGVILITGVVHLEAEADLSPCKRGGGDNFPFAGVAMSAAG
Os08g10630.1 (OsZIP4) LAIVGAGVILPI---GRSFA---ALREDDIFVKAFAAGVILITGVVHLEAEADLSPCKRGGGDDGFPFAGVAMSAAG
TaZIP2-6AS         FAGLACGVSPY---FIRWNEAFLLGTCFAAGVILITGVVHLEADSNLTFGDL---VPSSEYPPFAGVAMSAAG
Os01g74110.1 (OsZIP1) LVSIVGVQLPI---GRSMA---FYRWNEAFLLGTCFAAGVILITGVVHLEADSNLTFGDL---VPSSEYPPFAGVAMSAAG
Os03g29850.1 (OsZIP2) FAGLACGVSPY---FIRWNEAFLLGTCFAAGVILITGVVHLEADSNLTFGDL---VPSSEYPPFAGVAMSAAG
TaZIP11-3AL        LVSIVGVQLPI---GRSMA---FYRWNEAFLLGTCFAAGVILITGVVHLEADSNLTFGDL---VPSSEYPPFAGVAMSAAG
TaZIP3-7AL         LITAGVGLPI---GRRRRGGGGGGGSSGGGRVAKAFAAGVILITGVVHLEADSNLTFGDL---VPSSEYPPFAGVAMSAAG
Os06g37010.1 (OsZIP10) LITAGVGLPI---GRRRRGGGGGGGSSGGGRVAKAFAAGVILITGVVHLEADSNLTFGDL---VPSSEYPPFAGVAMSAAG
TaZIP4-4AS         LVSACACAPSP---GRKFP---ALREDGGRFAVKAFAAGVILITGVVHLEADSNLTFGDL---VPSSEYPPFAGVAMSAAG
Os05g39540.1 (OsZIP9) LVSACACAPSP---GRKFP---ALREDGGRFAVKAFAAGVILITGVVHLEADSNLTFGDL---VPSSEYPPFAGVAMSAAG
TaZIP5-2AL         LVCGACVGLPI---GRVVP---ALREDDIFVKAFAAGVILITGVVHLEADSNLTFGDL---VPSSEYPPFAGVAMSAAG
Os05g39560.1 (OsZIP5) LVSIVGVQLPI---GRKFP---ALCEPNDIFVKAFAAGVILITGVVHLEADSNLTFGDL---VPSSEYPPFAGVAMSAAG
TaZIP8-2AS         LVSIVGVQLPI---GRHVP---ALREDDIFVKAFAAGVILITGVVHLEADSNLTFGDL---VPSSEYPPFAGVAMSAAG
Os07g12890.1 (OsZIP8) LVCGACVGLPI---GRHVP---ALREDDIFVKAFAAGVILITGVVHLEADSNLTFGDL---VPSSEYPPFAGVAMSAAG
TaZIP6-1AS        LVSIVGVQLPI---GRHVP---ALREDDIFVKAFAAGVILITGVVHLEADSNLTFGDL---VPSSEYPPFAGVAMSAAG
Os05g07210.1 (OsZIP6) LVSIVGVQLPI---GRHVP---ALREDDIFVKAFAAGVILITGVVHLEADSNLTFGDL---VPSSEYPPFAGVAMSAAG
TaZIP7-1BS        LVSIVGVQLPI---GRKRR---LVQTSVAEVAAKAFAAGVILITGVVHLEADSNLTFGDL---VPSSEYPPFAGVAMSAAG
Os05g10940.1 (OsZIP7) LVAGVGVQLPI---GRKRR---ALREDGGRFAVKAFAAGVILITGVVHLEADSNLTFGDL---VPSSEYPPFAGVAMSAAG
    
```

III

```

At3g12750.1 (AtZIP1)  TITLIDNFAAGYKQVFSNN-----HGSKQVNV-----VVDEEHAGHVHIEIT-----HASH
Os03g46470.1 (OsIRT1) TITLADNMLTNGS-PRP-----SSGCVVAA-----VADHCRSPDQGHREG-----H
Os03g46454.1 (OsIRT2) TITLIDNMLTHTRG-----SKRASSA-----VAHGD-----H
TaIRT1-4AL          TITLIDNMLTNRKVTGQD-----AGPSSAA-----VANLESPEEAHHT-----H
TaZIP1-2AL          TMVVDNFAAGYRFSFSKA-----RPDLNIDI-----PGDEGRADHPVIA-----H
Os04g52310.1 (OsZIP3) TMVVDNFAAGYRFSFRKA-----RPVDNINV-----HKHACDRAEAHCHIE-----NAHTHQGH
Os08g10630.1 (OsZIP4) TMVVDNFAAGYRFSFKKP-----RPVDDPAD-----AARAQVEEGGAEFA-----GHVHVHTHATH
TaZIP2-6AS         TMVACATISVVARGTAPAA---APTTAGE---LEEGKLGSTNGSGDQRAAQD-----AHGPS
Os01g74110.1 (OsZIP1) TMVSELIIVAVRGAAGVSDN---QVSEQQQR---QQACAVMSRKEEAA-----H
Os03g29850.1 (OsZIP2) TMVADCAIFVVAAGGGRT---EPVAAQA---GLEEGKLSSTNGNASDPPAADA-----A
TaZIP11-3AL        TMVSEVIVVANSQVNV-----RAPQOKE---AEEECSTSEGPA-----H
TaZIP3-7AL         TITLIDNFAAGYRFSRQEE---AAATAARDDTTALLEGSLSCMAAAMSGDDEKQDAMHIVGMRHAAAHQSHSHAHGHD
Os06g37010.1 (OsZIP10) TITLIDNFAAGYRFSRQEE---AAATAARDDTTALLEGSLSCMAAAMSGDDEKQDAMHIVGMRHAAAHQSHSHAHGHD
TaZIP4-4AS         TITLIDNFAAGYRFSRQEE---TSVAVGYV---EASDSEQAHG-----H
Os05g39540.1 (OsZIP9) TITLIDNFAAGYRFSRQEE---DSRGAVAA---VAACGDASSSHDE-----R
TaZIP5-2AL         TITLIDNFAAGYRFSRQEE---HGVSSAVVDEEKQAAAAAEEARRHEGGE-----VHVHTHATH
Os05g39560.1 (OsZIP5) TITLIDNFAAGYRFSRQEE---KAVAVADE---PADDLEASDEHS-----H
TaZIP8-2AS         TITLIDNFAAGYRFSRQEE---SSVAVVDE---EKQAAAAAASELARHED-----DGEHGHVHLHTHATH
Os07g12890.1 (OsZIP8) TITLIDNFAAGYRFSRQEE---TAVAVADE---EKQAAAAAASELARHED-----DGEHGHVHLHTHATH
TaZIP6-1AS        ALVADLSSSHLEAHGHQHP---QQQEQPYAPIPTTKKAPAFELTCMRPKRFAFLDESRRDDPAPRADENGDDPRDDVALF
Os05g07210.1 (OsZIP6) ALVADLSSSHLEAHGHQHP---QQQEQPYAPIPTTKKAPAFELTCMRPKRFAFLDESRRDDPAPRADENGDDPRDDVALF
TaZIP7-1BS        TITLIDNFAAGYRFSRQEE---ARVADAA---AALAASTASDEDI-----TVTVVEGHEKVPPLLQASHH
Os05g10940.1 (OsZIP7) TITLIDNFAAGYRFSRQEE---ETERVKAA-----AAAALASSASDDDIITVTVTEDDNDNKAPLLQPHSHSHS-H
    
```

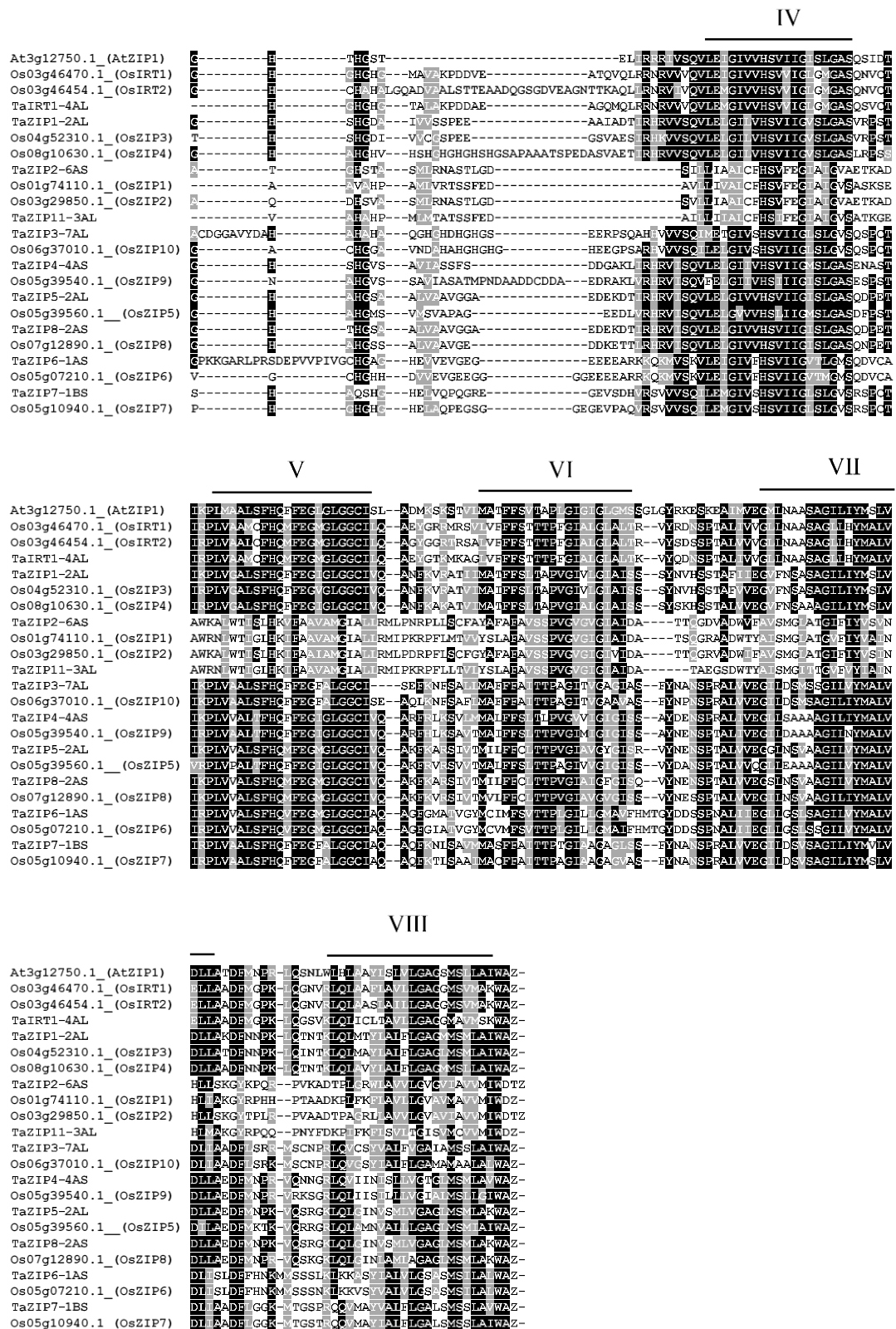


Figure 3.2. Multiple sequence alignment of *Arabidopsis*, rice and wheat ZIPs. The Muscle algorithm (Edgar, 2004) was used for the alignment of sequences and BoxShade software was used to generate this figure. The transmembrane domains predicted using HMMTOP (Tusnady and Simon, 2001) are indicated as lines above the sequence and numbered I-VIII respectively.

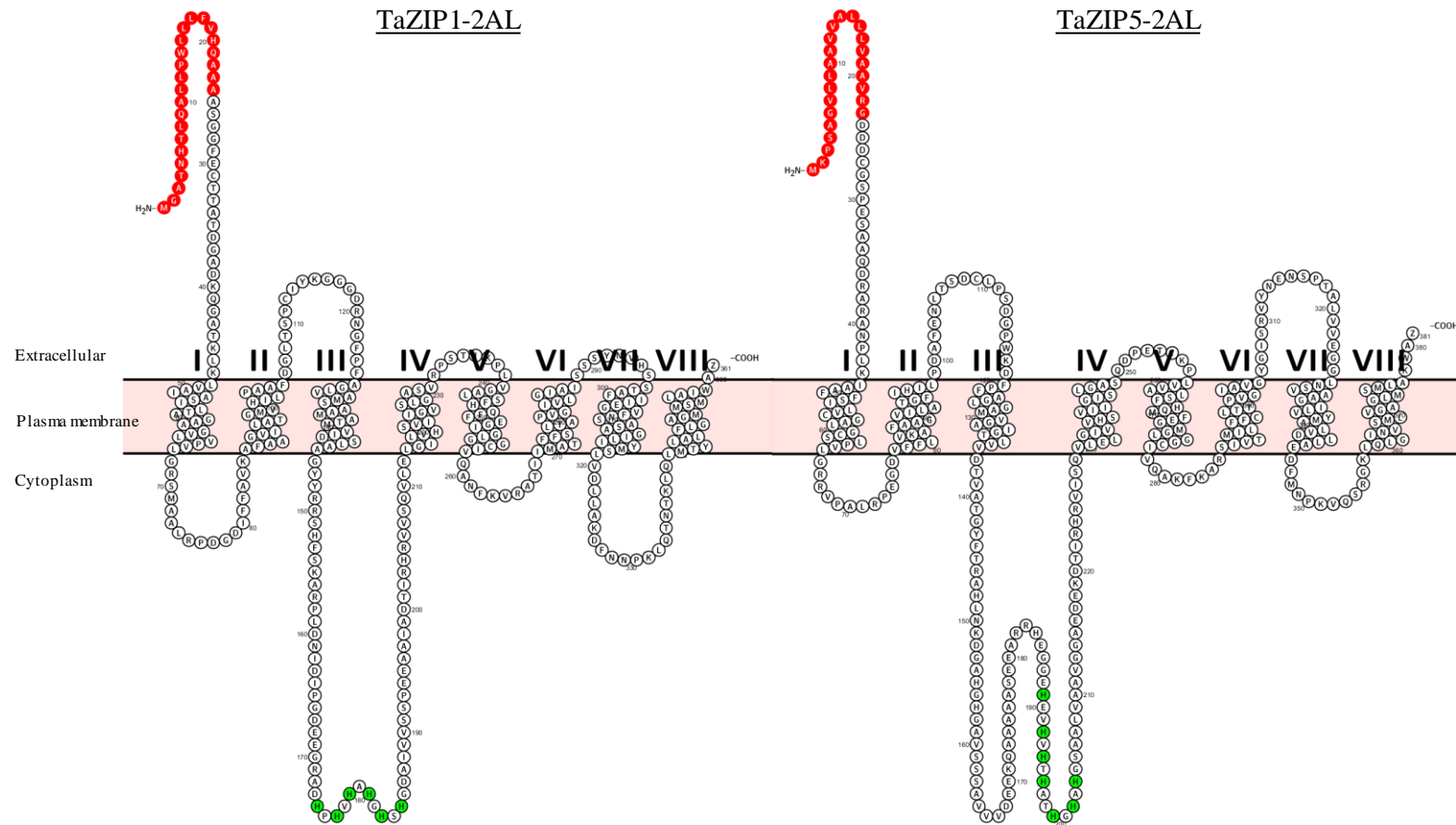


Figure 3.3. Topology predictions of TaZIP1-2AL and TaZIP5-2AL. Topology diagrams generated with Protter (V1.0) based on topology predictions using HMMTOP (Tusnády and Simon, 2001). Transmembrane domains are numbered, residues shaded in red are predicted to be plasma membrane localisation signals (localisation predictions made using Plant-mPLoc (Chou and Shen, 2010)). The variable region between TMs III and IV is clearly seen, histidine residues shaded green within may comprise part of the heavy metal-binding site (Guerinot, 2000).

3.3.2 bZIP transcription factor genes

Analysis of the IWGSC and TGAC scaffold sequence assembly databases resulted in the identification of seven group F *TabZIP* genes. For each of these genes a full homeolog set was identified with a homeologous gene present in each of the A, B and D genomes. Li et al. (2015b) carried out a genome wide identification of bZIP transcription factors in wheat using sequence data for *T. aestivum* from Gramene (Release note 41, www.gramene.org). They identified 11 group F *TabZIPs*. However, upon closer examination a considerable proportion of these were homeologs of the same gene. Table 3.2 details the group F *TabZIPs* Li et al. (2015b) identified and how their nomenclature compares to the group F *TabZIPs* identified in this thesis. Li et al. (2015b) identified at least one homeolog from six of the seven group F *TabZIPs* identified in this thesis, although no *TabZIP3b* genes have been previously identified.

The phylogenetic analysis presented in Figure 3.4 shows that six of the seven group F *TabZIPs* had a related barley homolog, with *TabZIP4* being the only *TabZIP* identified without a barley counterpart. Four of the seven *TabZIPs* (*TabZIP1*, *3a*, *3b* and *4*) are present on chromosome 7. *TabZIP3a* and *TabZIP3b* are closely related, for example *TabZIP3a-7AL* and *TabZIP3b-7AL* share 88.4% nucleotide sequence similarity. They each have a barley homolog and cluster together in the phylogenetic analysis presented in Figure 3.4. Their sequence similarity and location on the same chromosome suggests they have evolved through gene duplication and that this gene duplication also likely exists in barley. *TabZIP1* and *TabZIP4*, which are also both located on chromosome 7, are less closely related to one another than *TabZIP3a* and *TabZIP3b* are to each other. The phylogeny suggests that *TabZIP1*, *2*, *3a*, *3b* and *4* likely all share a common ancestor with *OsZIP48* and *BdbZIP11*. It is interesting that in this large cluster, there is only one rice and one *Brachypodium* bZIP, yet four barley bZIPs and five *TabZIPs*.

TabZIP5 and *TabZIP6* are positioned in a cluster, distanced from the other five *TabZIPs*. They each have a closely related barley and *Brachypodium* homolog. Compared to the other main cluster on the tree which contains the five other *TabZIPs* it seems these genes have not duplicated in number to the same extent, as there are the same number of barley, *Brachypodium* and rice bZIPs in this cluster. The two *Arabidopsis* bZIPs shown to be involved in the Zn deficiency response (*AtZIP19* and *AtZIP23*) cluster together away from *AtZIP24*. This is in agreement with their different functions; Zn deficiency response for *AtZIP19* and *AtZIP23* (Assunção et al., 2010) and salt tolerance for *AtZIP24* (Yang et al., 2009a).

The phylogenetic analysis presented in Figure 3.5 shows all of the group F *TabZIPs* identified by Li et al. (2015b), the group F *TabZIPs* identified in this thesis and a selection from each of the other nine *TabZIP* groups identified by Li et al. (2015b). The different *TabZIP* groups cluster together to form distinct clades based on amino acid sequence similarity. This is as

expected due to their common group-defining motifs. The group F *TabZIPs* identified in this thesis, depicted with black boxes in Figure 3.5, are all positioned within the group F clade. The matter of homeologs being numbered as different genes by Li et al. (2015b) is clearly shown in this phylogeny. For instance *TabZIP97*, *150* and *33* (Li et al. (2015b) numbering) are actually homeologs of the same gene; *TabZIP2*. Additionally for the majority of group F *bZIPs* Li et al. (2015b) did not identify full homeolog sets, with only one homeologous member in three of the six group F *bZIPs* identified by them being found. This analysis has addressed this shortcoming and gives a complete analysis of group F *TabZIP* genes present in the wheat genome.

In addition to the group F *bZIPs* that were identified in this analysis, a wheat gene from another *bZIP* group was identified. Zhang et al. (2008) reported the cloning and characterisation of a gene entitled '*TabZIP1*'. This is in fact a member of the group G *bZIP* transcription factors. It does not contain the characteristic cysteine-histidine-rich motifs of the group F members. In their study Zhang et al. (2008) characterised this *bZIP* as being important in the response of wheat to the rust pathogen *Puccinia striiformis* f. sp. *tritici*. In this thesis, this *TabZIP* is referred to as *TabZIPG*. The three homeologs of this gene were identified and the position of *TabZIPG-5AS* position in the group G clade of Figure 3.5 is shown. This will be used as a control in subsequent expression analyses.

The multiple sequence alignment shown in Figure 3.6 reveals that there is a very strong conservation in the general *bZIP* domain across the group F *bZIPs* examined. This *bZIP* (basic region/leucine zipper) domain consists of a basic region of 15 residues rich in lysine (K) and arginine (R) which is positively charged and a leucine zipper region which is 16 amino acids long, with leucine (L) residues every 7th amino acid (Jakoby et al., 2002). The two group F *bZIP* motifs predicted by Jakoby et al. (2002) are shown in Figure 3.6, the predicted consensus of these regions is C[ST]HTH[ST]CNP[PT]GPE and H[ST]STC[FL]H[AV]HT. The alignment reveals that the group F motifs are highly conserved across the group F *bZIPs* identified. The first motif is slightly more variable, especially toward the 3' end. High conservation is observed in the cysteine (C), histidine (H) and threonine (T) residues at the 5' end of this first group F motif.

Table 3.2. Wheat bZIP gene identification details. Gene name indicates nomenclature used throughout this thesis, with the sequence identifiers for the IWGSC database and TGAC scaffolds given. The nomenclature used by Li et al. (2015b) is given for reference, with (-) indicating a homeolog or gene not previously described.

Gene name	IWGSC wheat survey sequence ID	TGAC scaffold ID	Li et al. 2015b name
<i>TabZIP1-7AL</i>	IWGSC_chr7AL_ab_k71_contigs_4556556	TGACv1_scaffold_641258_U	TabZIP 56
<i>TabZIP1-7BL</i>	IWGSC_chr7BL_ab_k71_contigs_6718204	TGACv1_scaffold_577539_7BL	-
<i>TabZIP1-7DL</i>	IWGSC_chr7DL_ab_k71_contigs_3330672 IWGSC_chr7DL_ab_k71_contigs_547885	TGACv1_scaffold_604895_7DL	TabZIP 180
<i>TabZIP2-5AS</i>	IWGSC_chr5AS_ab_k95_contigs_1552249 IWGSC_chr5AS_ab_k95_contigs_856976	TGACv1_scaffold_393100_5AS	TabZIP 33
<i>TabZIP2-5BS</i>	IWGSC_chr5BS_ab_k71_contigs_933044	TGACv1_scaffold_423566_5BS	TabZIP 97
<i>TabZIP2-5DS</i>	IWGSC_chr5DS_ab_k71_contigs_2752495	TGACv1_scaffold_456500_5DS	TabZIP 150
<i>TabZIP3a-7AL</i>	IWGSC_chr7AL_ab_k71_contigs_4498861 ¹	TGACv1_scaffold_557389_7AL	-
<i>TabZIP3a-7BL</i>	IWGSC_chr7BL_ab_k71_contigs_6739371	TGACv1_scaffold_577387_7BL	-
<i>TabZIP3a-7DL</i>	IWGSC_chr7DL_ab_k71_contigs_3330556	TGACv1_scaffold_602722_7DL	TabZIP 179
<i>TabZIP3b-7AL</i>	IWGSC_chr7AL_ab_k71_contigs_4539775	TGACv1_scaffold_556472_7AL	-
<i>TabZIP3b-7BL</i>	IWGSC_chr7BL_ab_k71_contigs_6751348	TGACv1_scaffold_577539_7BL	-
<i>TabZIP3b-7DL</i>	IWGSC_chr7DL_ab_k71_contigs_3393460	TGACv1_scaffold_604895_7DL	-
<i>TabZIP4-7AL</i>	IWGSC_chr7AL_ab_k71_contigs_45254407	TGACv1_scaffold_558616_7AL	TabZIP 55
<i>TabZIP4-7BL</i>	IWGSC_chr7BL_ab_k71_contigs_6707253	TGACv1_scaffold_577103_7BL	-
<i>TabZIP4-7DL</i>	IWGSC_chr7DL_ab_k71_contigs_3338623	TGACv1_scaffold_603100_7DL	-
<i>TabZIP5-1AL</i>	IWGSC_chr1AL_v2_ab_k71_contigs_3930938	TGACv1_scaffold_001373_1AL	TabZIP 4
<i>TabZIP5-1BL</i>	IWGSC_chr1BL_ab_k71_contigs_3875125	TGACv1_scaffold_032488_1BL	TabZIP 62
<i>TabZIP5-1DL</i>	IWGSC_chr1DL_ab_k71_contigs_1011346	TGACv1_scaffold_061505_1DL	-
<i>TabZIP6-3AL</i>	IWGSC_chr3AL_ab_k71_contigs_3773819	TGACv1_scaffold_196209_3AL	-
<i>TabZIP6-3BL</i>	IWGSC_chr3B_ab_k71_contigs_10399178	TGACv1_scaffold_221777_3B	TabZIP 79
<i>TabZIP6-3DL</i>	IWGSC_chr3DL_ab_k71_contigs_6891609	TGACv1_scaffold_251113_3DL	-
<i>TabZIPG-5AS</i>	IWGSC_chr5AS_ab_k71_contigs_1543784	TGACv1_scaffold_392564_5AS	TabZIP165
<i>TabZIPG-5BL</i>	IWGSC_chr5BL_ab_k71_contigs_10925110	TGACv1_scaffold_640756_U	TabZIP 106
<i>TabZIPG-5DL</i>	IWGSC_chr5DL_ab_k71_contigs_4513163	TGACv1_scaffold_434504_5DL	-

¹Chimeric contig is present in the IWGSC wheat survey sequence database

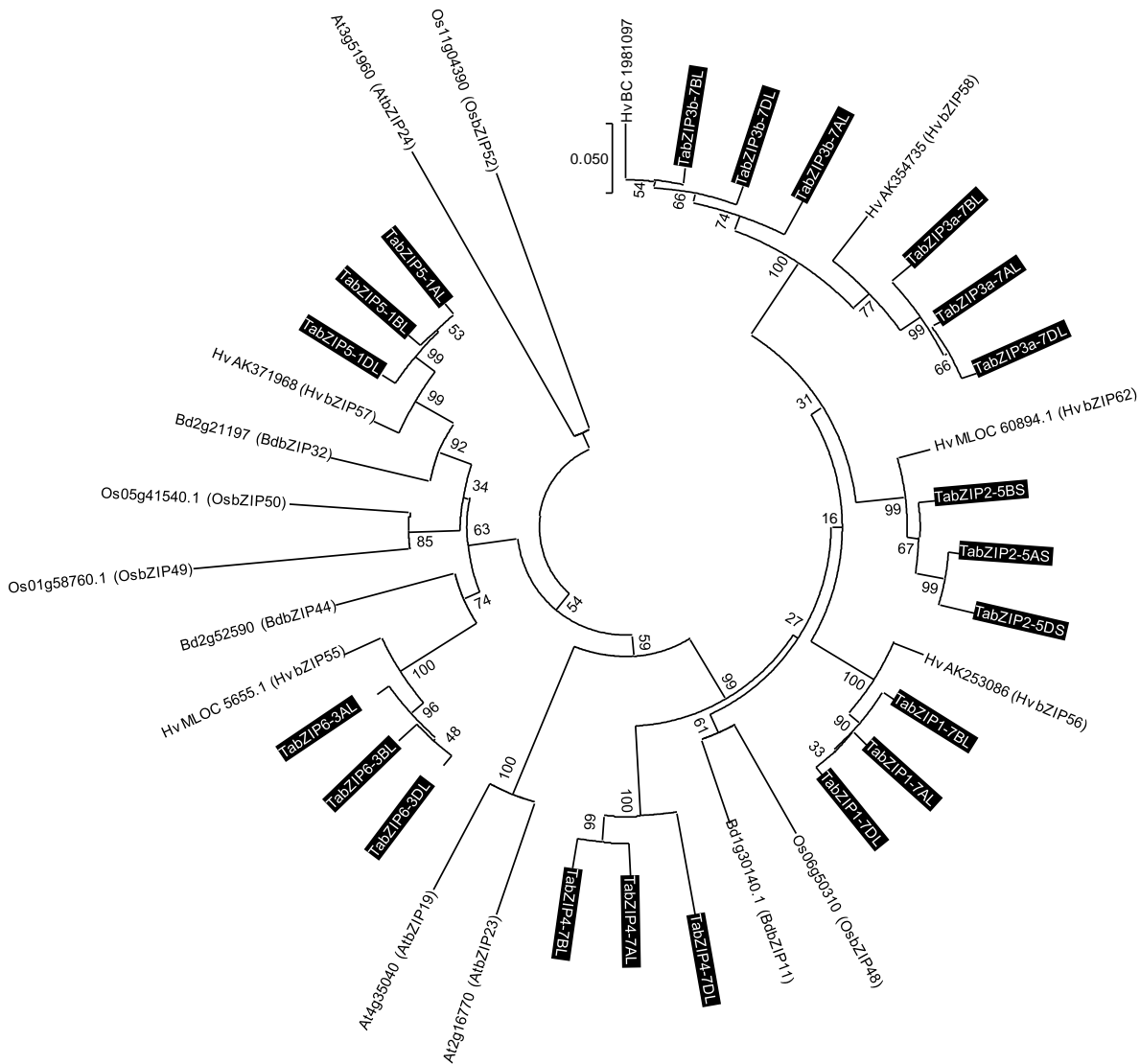


Figure 3.4. Phylogenetic analysis of group F bZIP genes in cereals and *Arabidopsis*. A neighbour joining tree was generated for *Arabidopsis* (At), rice *Oryza sativa* (Os), *Brachypodium distachyon* (Bd), barley *Hordeum vulgare* (Hv) and wheat *T. aestivum* (Ta) group F bZIP coding nucleotide sequences. The Muscle algorithm (Edgar, 2004) was used for the alignment of sequences and the phylogenetic tree was created using MEGA (v5.2) software. Evolutionary distances were computed using the p-distance method and are in the units of the number of base differences per site. 1000 bootstrap replicates were used and bootstrap values are shown as percentages. Wheat genes are shown with text boxes shaded in black, gene information is provided in Table 3.2. Gene nomenclature for *Arabidopsis* is from Jakoby et al. (2002), *Brachypodium* is from Liu and Chu (2015), rice is from Corrêa et al. (2008) and barley is from Pourabed et al. (2015).

3.3.3 Development of a hydroponic growth system to subject wheat (*T. aestivum*) to Zn-deficient conditions

The aim of this initial experiment was to test an existing hydroponic protocol to establish whether Zn deficiency in wheat plants could be imposed. Plants were grown in the modified Letcombe solution detailed in Section 2.1.1 for 14 days under two conditions, containing either 8 μM or 0 μM Zn (subsequently referred to as +Zn and -Zn respectively). Reduction in shoot growth was evident from day 7 (D7) in the -Zn grown plants and by day 14 (D14) these -Zn grown plants showed moderate chlorosis see Figure 3.7. This phenotype is in accordance with known Zn deficiency symptoms, as described by Cakmak et al. (1996), with plants showing whitish-brown lesions on leaves spreading from the mid vein and a reduction in plant height.

Plants grown under -Zn conditions showed a significant reduction in root fresh weight when compared to those grown in +Zn control conditions (-Zn = 0.64 g, +Zn = 2.24 g) (see Figure 3.8). Although root lengths were not measured, they varied little between treatments (see Figure 3.7A). The shoot fresh weight of -Zn grown plants was also significantly lower compared to the +Zn control grown plants (-Zn = 0.34 g, +Zn = 2.04 g). Using root and shoot fresh weights, the root to shoot ratio was calculated. The larger the root to shoot ratio, the larger the proportion of total plant biomass that is found in the root system. Interestingly, the root to shoot ratio of -Zn plants was significantly higher than the +Zn control plants (-Zn = 2.03, +Zn = 1.09). This result suggests that either the plants invest a greater proportion of total biomass growth into root development when subjected to the -Zn treatment or that the plant Zn requirement is higher in the shoot.

It is clear from the fresh weight results and the phenotypes observed that the hydroponic growth protocol used gives the opportunity to study the effect of Zn-deficient conditions on wheat growth. This protocol was used in subsequent hydroponic experiments.

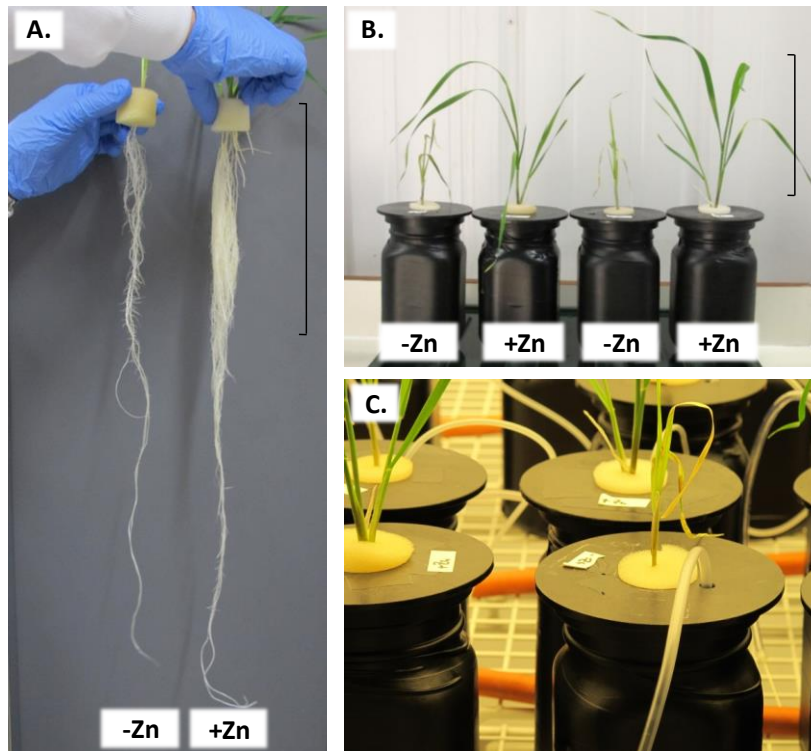


Figure 3.7. Visible phenotypic differences between Zn treatments observed in hydroponically grown wheat (*T. aestivum* cv. Paragon). Zn-deficient conditions reduce root growth (A.) and shoot growth (B.). C. shows the hydroponic culture system with aeration tubes visible. All images were taken 14 days after the initiation of Zn-deficient treatment. +Zn = 8 μ M Zn, -Zn = 0 μ M Zn. Scale bars shown represent 20 cm.

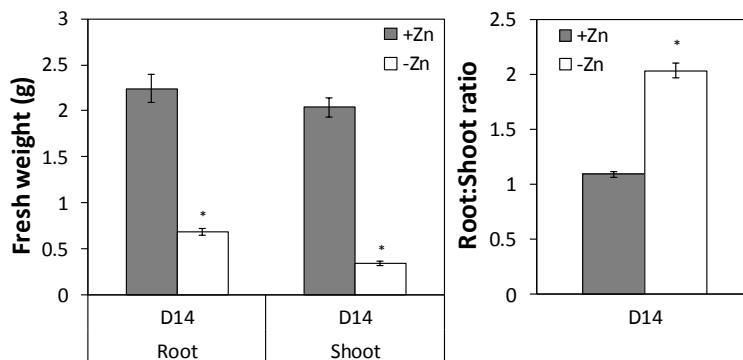


Figure 3.8. Hydroponic-induced Zn deficiency significantly reduces wheat (*T. aestivum* cv. Paragon) root and shoot fresh weights and increases the root to shoot ratio. Results shown are from samples taken at 14 days after initiation of Zn-deficient treatment. Bars represent means \pm S.E.M. (n=9). * indicates $P < 0.05$ (1-tailed T-Test, 8 d.f.). +Zn = 8 μ M Zn, -Zn = 0 μ M Zn.

3.3.4 Three-week Zn starvation experiment

3.3.4.1 Phenotypic data

Following the initial development and testing of the hydroponic protocol (Section 3.3.3), a time-course experiment was carried out in order to investigate the expression of previously identified *ZIP* transporter genes and *bZIP* transcription factors in Zn-deficient grown wheat plants. As in the protocol test experiment (Section 3.3.3), plants showed signs of Zn deficiency after 7 days of growth in $-Zn$ conditions. After 7 days, biomass reduction and chlorosis was observed and after 21 days of Zn-deficient conditions the exposed plants appeared very sickly with an extreme chlorotic phenotype and substantial necrosis being observed (Figure 3.9). Significant reductions in root fresh weight and shoot fresh weight were observed across all three sampling points in the $-Zn$ treatment (Figure 3.10). Root to shoot ratios were significantly higher at D14 and D21, with the $-Zn$ treated plants again having a greater proportion of total biomass in their roots than the $+Zn$ treated plants. Throughout the course of the experiment, the root to shoot ratio of the $+Zn$ treated plants showed the opposite trend, with mean ratios reducing over time, although this was not significant.

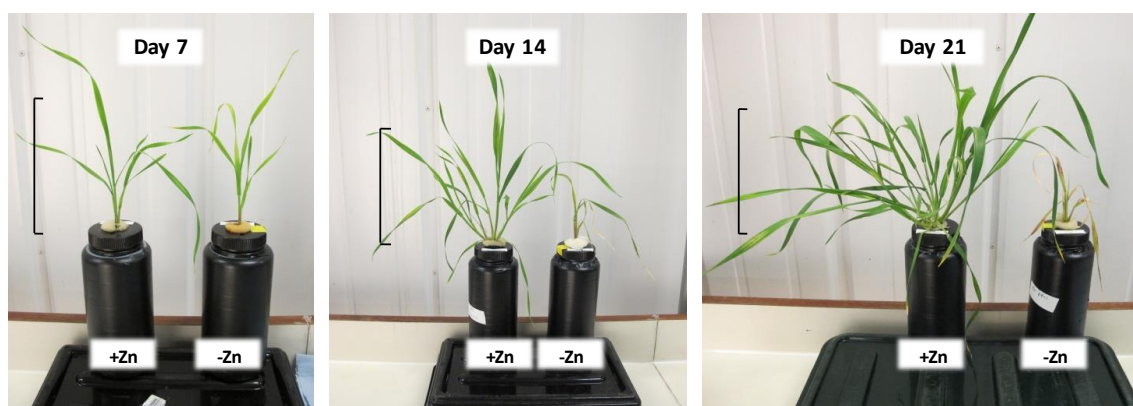


Figure 3.9. Visible phenotypic effects of Zn starvation throughout a three-week period. Zn deficiency causes observable effects from 7 days after treatment initiation, chlorosis is observable after 14 days. $+Zn = 8 \mu M Zn$, $-Zn = 0 \mu M Zn$. Scale bars shown represent 20 cm.

The mineral concentration of freeze dried root and shoot samples throughout the three-week Zn starvation period was analysed using ICP-OES. Results are shown in Figure 3.11. The mineral concentrations from this experiment reveal interesting patterns across the elements analysed. As would be expected, Zn concentration was reduced in both the root and shoot material of $-Zn$ treated plants. This reduction in Zn concentration was significant from D7 (the first time point sampled following the initiation of the $-Zn$ treatment condition). Interestingly the concentration of Zn in the $+Zn$ grown material increased through the time-course despite an increase in fresh weight.

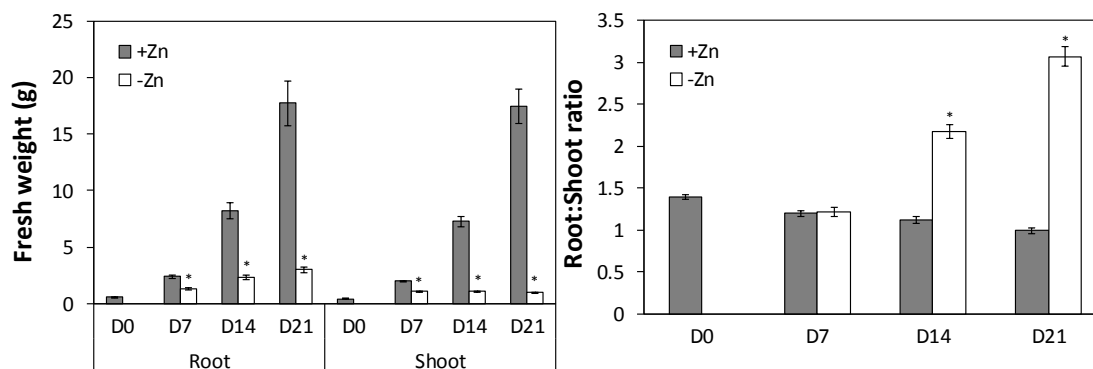


Figure 3.10. The effect of Zn starvation on wheat fresh weight throughout a three-week period. Results shown are means \pm S.E.M. ($n=12$). * indicates $P<0.05$, tested using Fisher's LSD on log-transformed data. +Zn = 8 μ M Zn, -Zn = 0 μ M Zn.

Trends were observed in three other micronutrients; manganese (Mn), copper (Cu) and molybdenum (Mo). Mn showed significant increases in both root and shoot concentrations under the -Zn treatment. Cu concentrations were reduced significantly in the root by the -Zn treatment, but at D21 in the shoot were significantly higher in the -Zn treatment plants. Mo concentrations in the shoot were significantly higher in the -Zn treatment plants from D14 onwards. The final micronutrient examined was Fe, this showed no trend between the two treatments, however it is interesting to note the large range in concentrations observed in the +Zn root samples at D21. The three Fe concentrations at this time point were 89, 116 and 642 mg/kg Fe (DW). The beneficial element sodium (Na) showed no trend in root concentrations, however shoot concentrations were significantly higher in the -Zn treatment from D14 onwards.

Four macronutrients were examined in the analysis, phosphorus (P), potassium (K), calcium (Ca) and magnesium (Mg). K showed no clear trends across the three-week period. P concentrations showed a strong trend of higher concentrations in the -Zn treatment from D14 in the root and from the earliest sampling point, D7, in the shoot. Ca concentrations were significantly higher in the shoots of plants grown under the -Zn treatment from D7, but there was no trend in Ca concentration in the root. Interestingly Mg showed opposing trends in concentrations between the root and shoot portions of the plants. In the root, -Zn treatment resulted in a significant reduction in Mg concentrations at all time points, whereas in the shoot -Zn grown plants had significantly higher Mg concentrations.

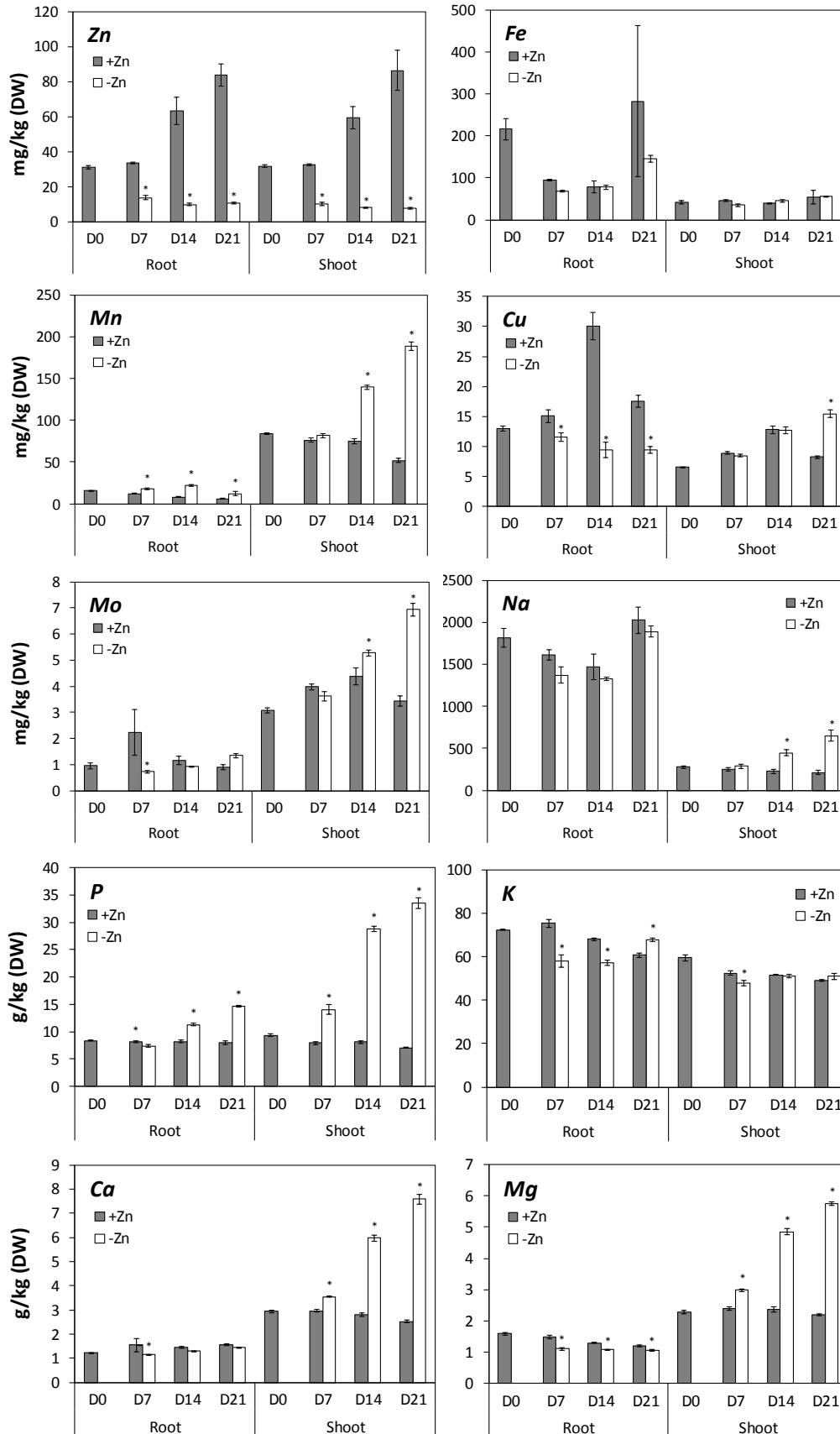


Figure 3.11. Mineral concentration analysis of wheat root and shoot samples throughout a three-week Zn starvation period. Results shown are means \pm S.E.M. (n=3). * indicates $P < 0.05$, tested using Fisher's LSD on log-transformed data. (DW) is dry weight. +Zn = 8 μ M Zn, -Zn = 0 μ M Zn.

3.3.4.1 Gene expression

The relative gene expression levels of five *TaZIP* transporters and five *TabZIP* transcription factors (identification discussed in Section 3.3.1 and 3.3.2) were analysed in the root and shoot tissue obtained throughout the three-week Zn-starvation period. Real-time PCR analysis was used to give relative gene quantification throughout the Zn-starvation period. All expression levels were normalised to the *TaActin3* reference gene, which showed stable expression across samples (Figure 3.12). Figure 3.12 shows the variability in cycle threshold value (Ct) throughout the three-week period for the reference gene *TaActin3* is low (Ct averages had a range of 0.7 in the root samples and 1.1 in the shoot samples) and the Ct values show no observable trend throughout the time-course. Ct values for *TaZIP1* are also shown in Figure 3.12 to allow comparison. *TaZIP1* Ct values were far less stable (Ct averages had a range of 6.4 in the root samples and 4.8 in the shoot samples), additionally clear trends were observable throughout the time-course, notably between treatments. The stability and absence of trends in Ct values of *TaActin3* made this a reliable reference gene for normalisation in the following gene expression data.

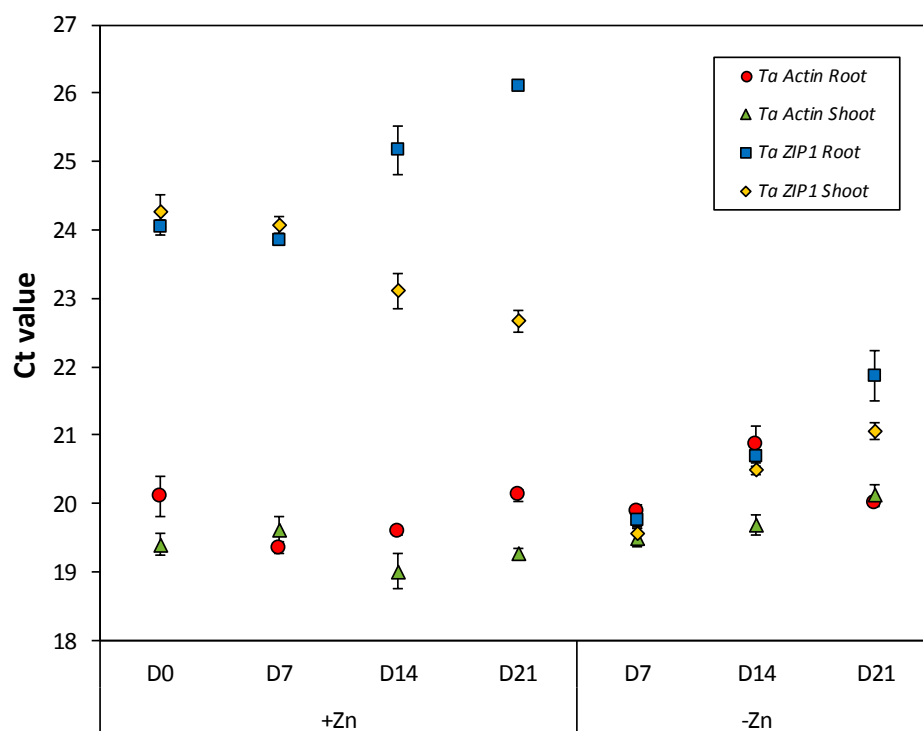


Figure 3.12. Stability of the *TaActin3* reference gene throughout a three-week Zn starvation period in root and shoot material. Cycle threshold values (Ct) are shown for *TaActin3* the housekeeping gene used for normalisation in this experiment and a representative *TaZIP* gene (*TaZIP1*) throughout the three-week starvation period in both root and shoot. Data points represent averages from three biological replicates \pm S.E.M. +Zn = 8 μ M Zn, -Zn = 0 μ M Zn.

Gene expression analyses for five *TaZIPs* and five *TabZIPs* are presented in Figures 3.13 to 3.16. All five of the *TaZIPs* examined showed significant upregulation under $-Zn$ conditions at all sampling points throughout the three-week Zn starvation period in both the root and shoot (Figures 3.13 and 3.14). When comparing the expression levels of individual *TaZIPs* it is interesting that the magnitude of upregulation in response to the $-Zn$ treatment varies between root and shoot in some genes. Notably *TaZIP4* is induced to a much greater extent in response to the $-Zn$ treatment in the shoot when compared to the same gene in the root. Conversely *TaZIP5* shows a higher degree of upregulation in response to the $-Zn$ treatment in the root when compared to the same gene in the shoot. The upregulation response of *TaZIP1* and *TaZIP7* is comparable for each gene between both the root and shoot.

The majority of *TaZIPs* exhibit a slight decrease in expression levels of the $-Zn$ treatment material at the last sampling point of D21. This could be explained by the critical Zn deficiency levels being experienced by the plant, at the last sampling point (D21) the plants were visibly very sickly (see Figure 3.9) and likely severely stressed. A final observation from the *TaZIP* gene expression dataset is the differential regulation of *TaZIPs* under Zn-replete conditions. In the root *TaZIP1*, 4 and 7 show negative trends in expression throughout the three-week period under $+Zn$ conditions, however *TaZIP6* has a positive trend in expression across the time-course in Zn-replete material. In the shoot, this expression pattern varies; *TaZIP1* has a slight positive trend in expression in $+Zn$ grown shoot material, as does *TaZIP5*. The varying magnitude of *TaZIP* upregulation under $-Zn$ conditions between root and shoot portions of the plant as well as the differential trends observed in expression under $+Zn$ conditions suggest individual *TaZIPs* may have distinct roles spatially and temporally within the plant.

The expression of four group F *TabZIPs* and one group G *TabZIP*, (*TabZIPG*) was examined in response to the $-Zn$ treatment. Significant upregulation of the four group F *TabZIPs* was observed across the three-week period. The magnitude of upregulation for *TabZIP3a*, *3b* and *4* were much higher in the shoot than in the root. *TabZIP1* was consistently upregulated across both the root and the shoot in response to the $-Zn$ treatment. As observed across the *TaZIPs*, there was a tailing off in expression level at the latter time point (D21) in the group F *TabZIPs*. As discussed in Section 3.3.2, a non-group F *TabZIP* was examined; *TabZIPG* showed no expression response to the different Zn treatments in the root, but was significantly upregulated in the shoot from D7 under the $-Zn$ treatment.

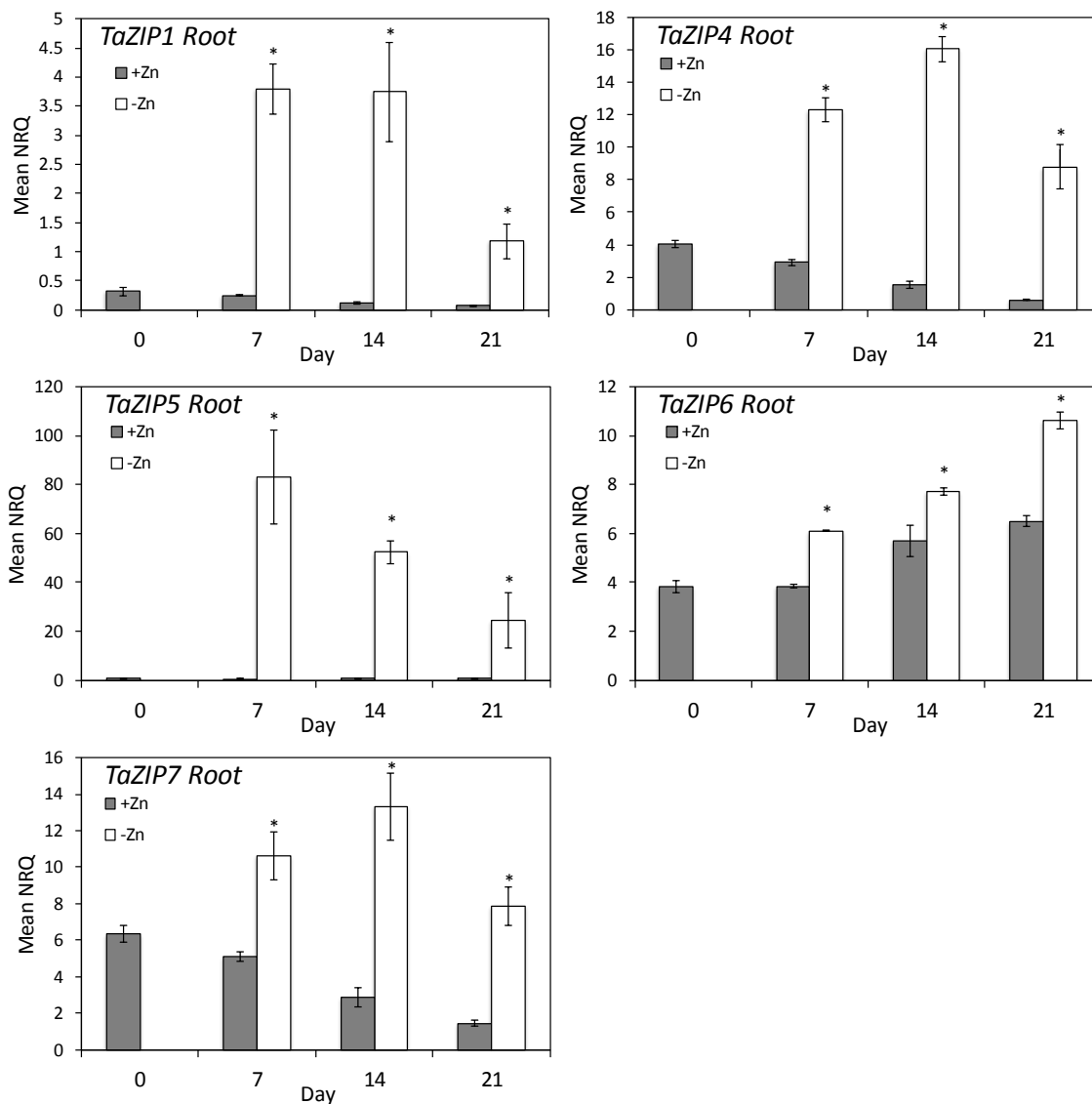


Figure 3.13. Gene expression analysis of *TaZIPs* in wheat root material throughout a three-week Zn starvation period. Normalised relative quantification (NRQ) of five wheat *ZIP* transporter gene transcripts in root material throughout three weeks of Zn starvation. All NRQ values given are normalised to *TaActin3* expression and means of three biological replicates are given (\pm S.E.M). Bars within individual graphs displaying an asterisk show significant difference between treatment means at a given time point. Significance ($P < 0.05$) was tested post-hoc, using Fisher's LSD test on $\text{Log}_2(1/\text{NRQ})$ transformed data. +Zn = 8 μM Zn, -Zn = 0 μM Zn.

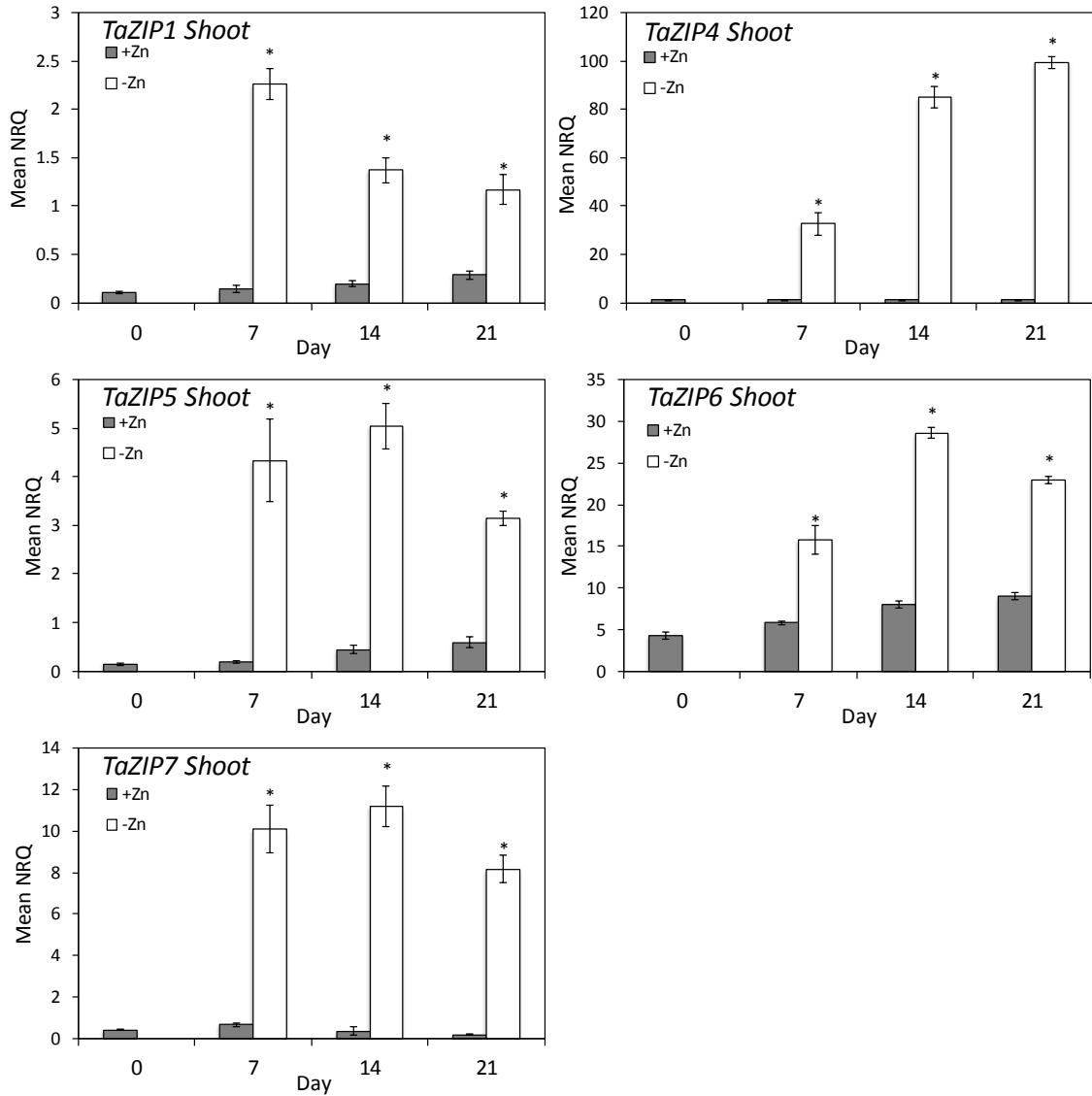


Figure 3.14. Gene expression analysis of *TaZIPs* in wheat shoot material throughout a three-week Zn starvation period. Normalised relative quantification (NRQ) of five wheat *ZIP* transporter gene transcripts in shoot material throughout three weeks of Zn starvation. All NRQ values given are normalised to *TaActin3* expression and means of three biological replicates are given (\pm S.E.M). Bars within individual graphs displaying an asterisk show significant difference between treatment means at a given time point. Significance ($P < 0.05$) was tested post-hoc, using Fisher's LSD test on $\text{Log}_2(1/\text{NRQ})$ transformed data. +Zn = 8 μM Zn, -Zn = 0 μM Zn.

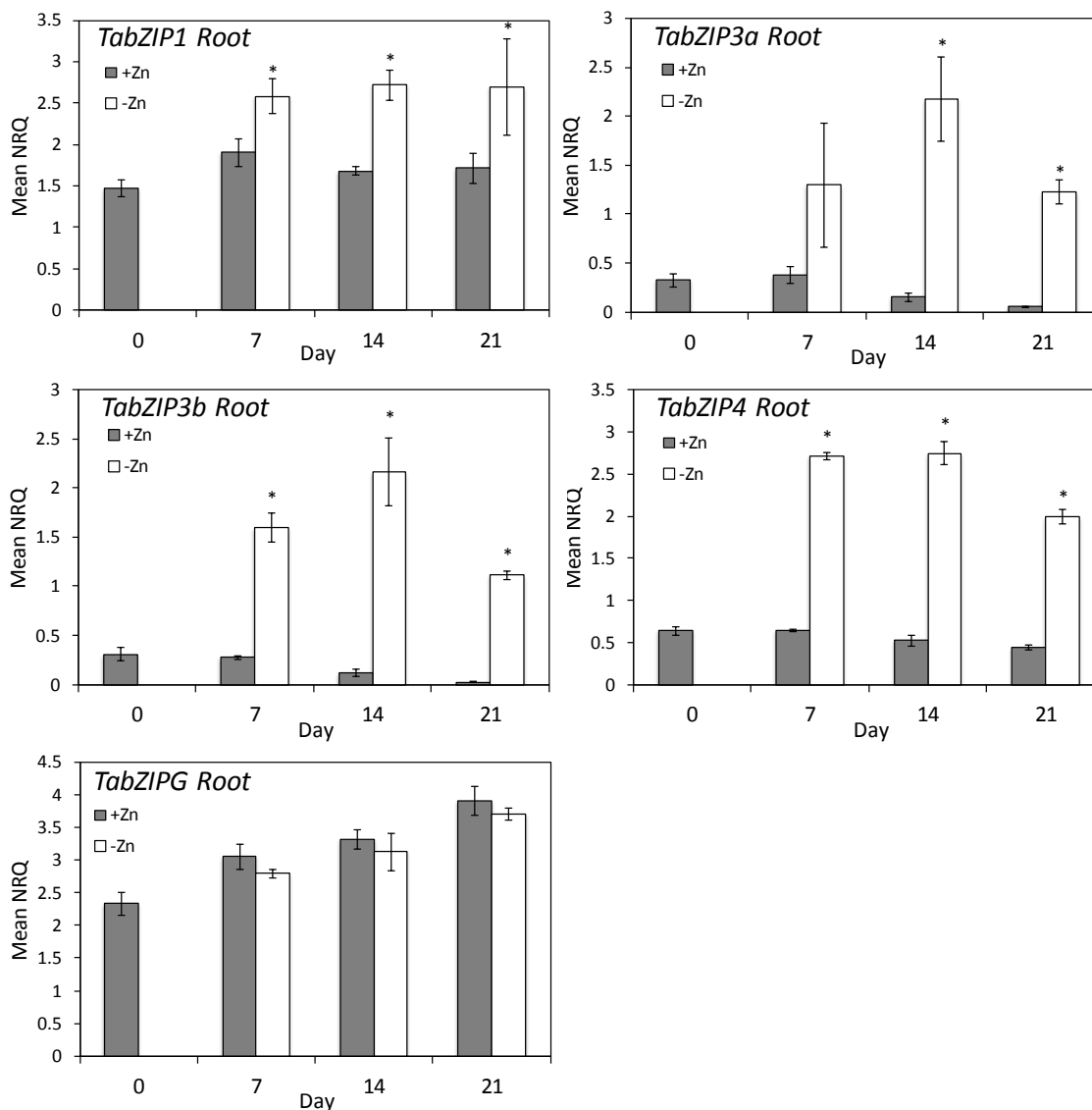


Figure 3.15. Gene expression analysis of *TabZIPs* in wheat root material throughout a three-week Zn starvation period. Normalised relative quantification (NRQ) of five wheat *bZIP* transcription factor gene transcripts in root material throughout three weeks of Zn starvation. All NRQ values given are normalised to *TaActin3* expression and means of three biological replicates are given (\pm S.E.M). Bars within individual graphs displaying an asterisk show significant difference between treatment means at a given time point. Significance ($P < 0.05$) was tested post-hoc, using Fisher's LSD test on $\text{Log}_2(1/\text{NRQ})$ transformed data. +Zn = 8 μM Zn, -Zn = 0 μM Zn.

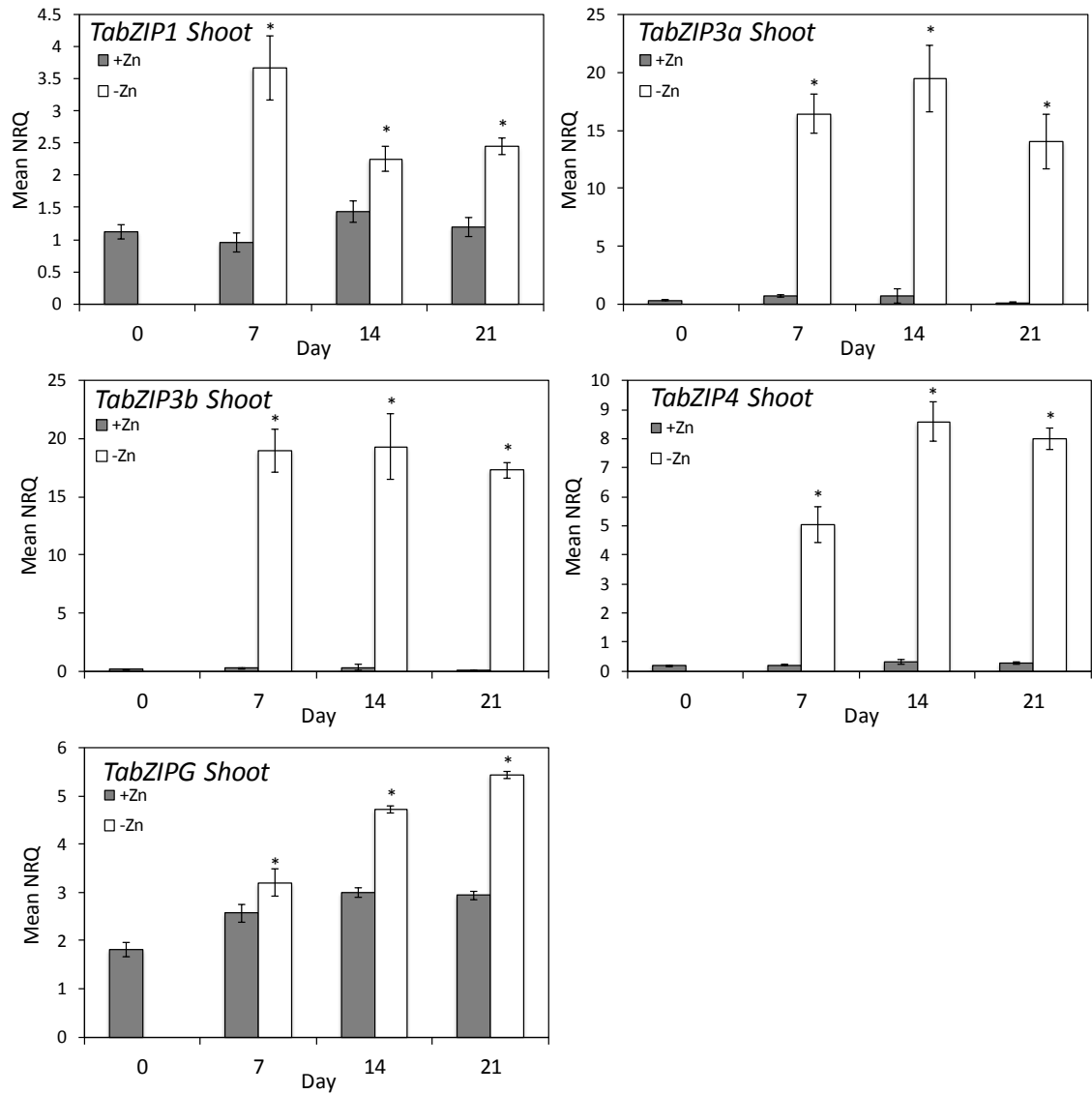


Figure 3.16. Gene expression analysis of *TabZIPs* in wheat shoot material throughout a three-week Zn starvation period. Normalised relative quantification (NRQ) of five wheat *bZIP* transcription factor gene transcripts in shoot material throughout three weeks of Zn starvation. All NRQ values given are normalised to *TaActin3* expression and means of three biological replicates are given (\pm S.E.M). Bars within individual graphs displaying an asterisk show significant difference between treatment means at a given time point. Significance ($P < 0.05$) was tested post-hoc, using Fisher's LSD test on $\text{Log}_2(1/\text{NRQ})$ transformed data. +Zn = 8 μM Zn, -Zn = 0 μM Zn.

3.3.5 One-week Zn starvation experiment

3.3.5.1 Phenotypic data

To allow gene expression analysis to be determined over a shorter time scale the response of wheat to a one-week Zn starvation period was examined. This shorter time-course allowed the examination of gene expression differences identified over the three-week deficiency time-course (Section 3.3.4) to be analysed in more depth, at time points closer together and in plants with reduced Zn-deficiency symptoms.

Figure 3.17 shows that there were no observable differences in wheat plants throughout a one-week period of $-Zn$ treatment. There were no clear, consistent effects on root or shoot fresh weight (Figure 3.18). This is unsurprising as the deficiency was only inflicted for 7 days and at the initiation of the $-Zn$ treatment the plants were aged 14 days rather than 7 days as in the previous three-week Zn starvation time-course. A higher level of within group variation was observed compared to fresh weight data from previous experiments; this is likely due to there being fewer biological replicates than in previous experiments. The root to shoot ratio was significantly increased under the $-Zn$ treatment at D5 and D7 which is in agreement with previous longer-term hydroponic experiments.

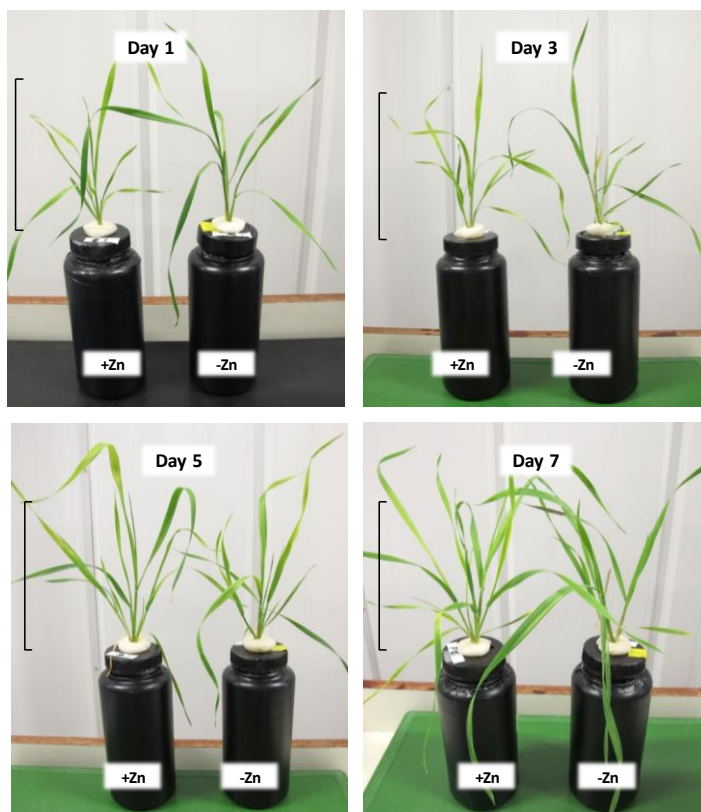


Figure 3.17. Visible phenotypic effects of Zn starvation throughout a one-week period. The $-Zn$ treatment caused no visible phenotype after 7 days of treatment. $+Zn = 8 \mu M Zn$, $-Zn = 0 \mu M Zn$. Scale bars shown represent 20 cm.

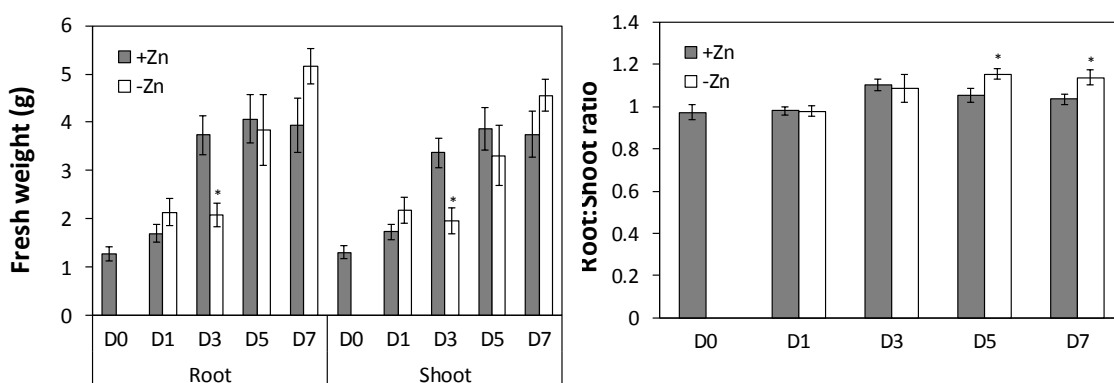


Figure 3.18. The effect of Zn starvation on wheat fresh weight throughout a one-week period. Results shown are means \pm S.E.M. (n=6). * indicates $P < 0.05$, tested using Fisher's LSD on log-transformed data. +Zn = 8 μ M Zn, -Zn = 0 μ M Zn.

The mineral concentration of freeze dried root and shoot samples taken throughout the one-week Zn starvation period was determined using ICP-OES. Results are shown in Figure 3.19. The results show that although a visible phenotype was not observed across the -Zn treatment, the roots and shoots had significantly lower Zn concentrations from D3. The Zn concentrations reduced further at D5 and D7 in both the root and shoot of -Zn grown plants. Zn concentrations of +Zn grown material remained stable throughout the 7 days. These results are in accordance with the trends in Zn concentration observed throughout the previously described three-week starvation experiment, in which Zn concentrations remained stable in +Zn grown plants, and reduced in -Zn grown material over the first 7 days.

Few trends were observed in the other micronutrients studied. Mn concentration showed the same trend as in the previous time-course experiment with lower overall root concentrations compared to shoot, and again after 7 days of growth in -Zn conditions root concentrations were significantly increased compared to +Zn grown roots. Although not significant, Cu levels in the roots of -Zn grown plants were lower than +Zn grown roots, as supported by previous findings. Fe concentrations were again variable throughout the dataset.

Across the macronutrients analysed P concentrations are in keeping with those previously found, with increased shoot concentrations in -Zn grown material at D7. Interestingly in the three-week long Zn deficiency experiment, root P concentration at D7 was reduced in -Zn plants, before this trend was reversed at D14 and D21. In this one-week experiment again at D7 the P concentration of the root was significantly reduced in Zn-deficient material. K root and shoot concentrations at D7 were again reduced under -Zn conditions which is supported by previous results. Ca showed no trend between treatments, but Ca concentration was lower overall in the root than the shoot. Mg concentration was reduced in the root of -Zn grown material at D7, as observed previously.

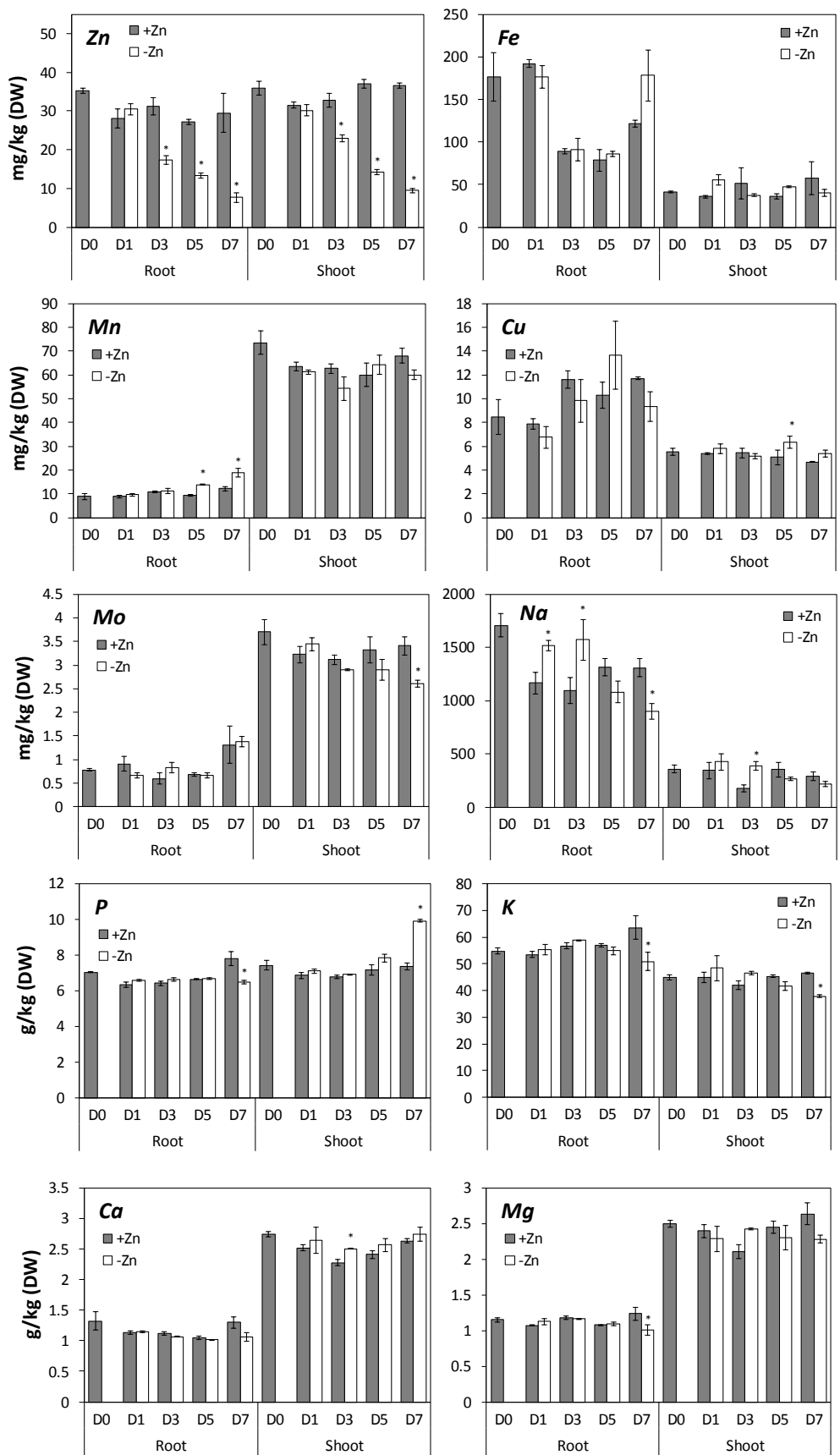


Figure 3.19. Mineral concentration analysis of wheat root and shoot samples throughout a one-week Zn starvation period. Results shown are means \pm S.E.M. (n=3). * indicates $P < 0.05$, tested using Fisher's LSD on log-transformed data. (DW) is dry weight. +Zn = 8 μ M Zn, -Zn = 0 μ M Zn.

3.3.5.2 Gene expression

The relative gene expression levels of five *TaZIP* transporters and five *TabZIP* transcription factors (identification discussed in Section 3.3.1 and 3.3.2) were analysed in the root and shoot tissue obtained throughout the one-week Zn starvation period. Real-time PCR analysis was used to give relative gene quantification throughout the Zn starvation period. All expression levels were normalised to the known reference genes: *TaActin3* and *TaSuccDH*, which showed stable expression across samples (Figure 3.20). The variation in Ct value for *TaActin* was 0.5 across all root samples and 0.8 across shoot samples, *TaSuccDH* Ct values had a range of 0.7 across root samples and 0.4 across shoot samples. When compared to the Ct ranges of *TaZIP1* which were 4.9 for root samples and 4.1 for shoot samples it is clear that these housekeeping genes are stable and reliable reference genes for the normalisation of gene expression data in this dataset.

The gene expression analyses for five *TaZIPs* and five *TabZIPs* are presented in Figures 3.21 to 3.24. In the root material, four of the five *TaZIPs* examined showed upregulation under –Zn treatments, with only *TaZIP6* showing no upregulation under the –Zn treatment. In the shoot material, all five *TaZIPs* showed upregulation under –Zn conditions, the duration of time before significant upregulation occurred varied between individual genes, with *TaZIP6* expression remaining constant until D5. As in the previous gene expression analysis the magnitude of upregulation varied between *TaZIPs*. *TaZIP4* was upregulated to a much greater extent in the shoot compared to the root.

All four of the group F *TabZIPs* examined showed upregulation under the –Zn treatment as observed in the previous gene expression dataset. *TabZIP1* exhibited less Zn-regulation compared to the other group F *TabZIPs*. Upregulation of *TabZIP1* was slower, taking until D5 to become significantly upregulated in the root and until D3 in the shoot. *TabZIPG* showed no response to Zn treatment in the root, and only a moderate response from D5 onwards in the shoot.

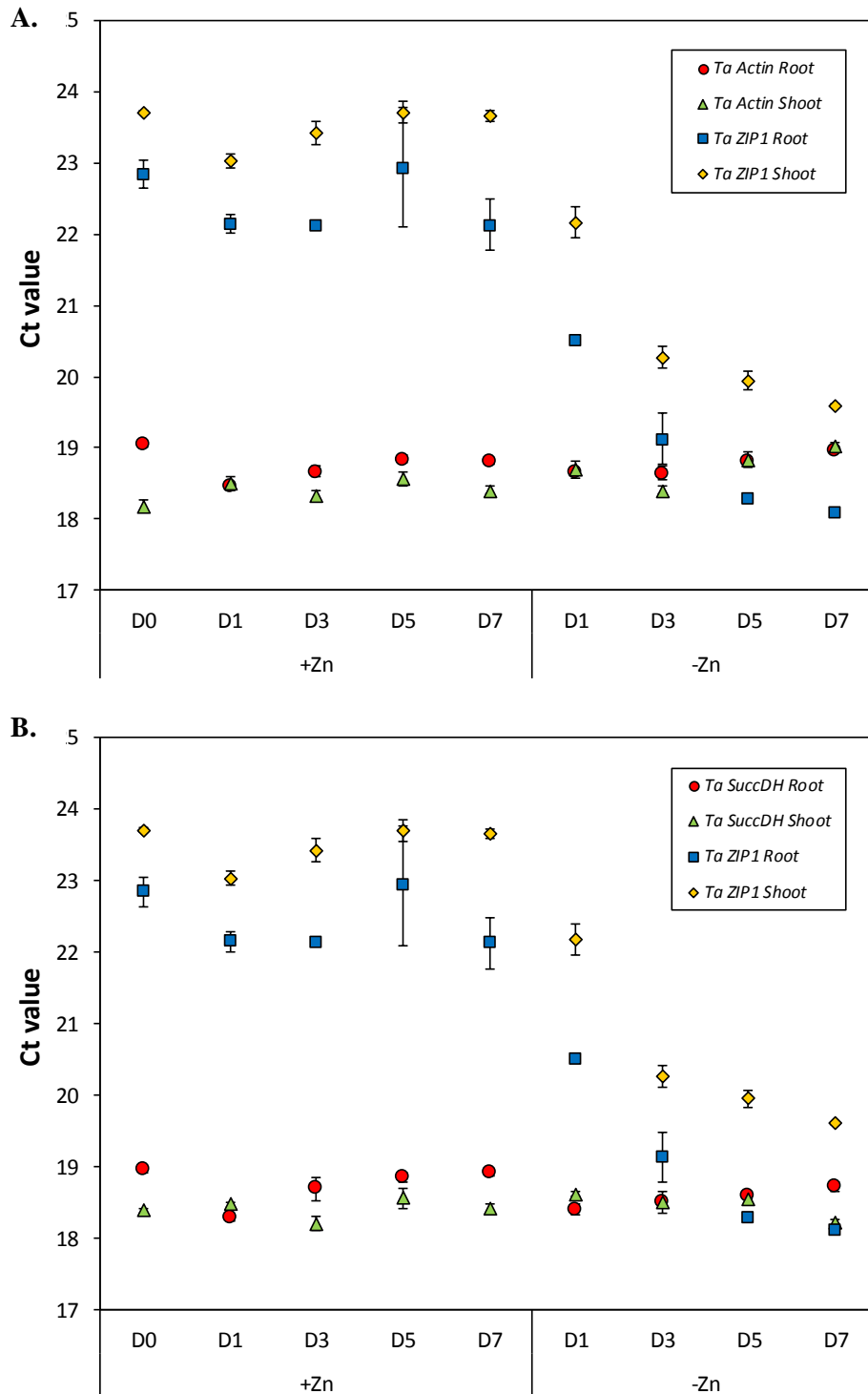


Figure 3.20. Stability of the *TaActin3* and *TaSuccDH* reference genes throughout a one-week Zn starvation period in root and shoot material. Cycle threshold values (Ct) are shown for **A. *TaActin3*** and **B. *TaSuccDH*** the housekeeping genes used for normalisation in this experiment as well as a representative *TaZIP* gene (*TaZIP1*) throughout the one-week starvation period in both root and shoot. Data points represent averages from three biological replicates \pm S.E.M. +Zn = 8 μ M Zn, -Zn = 0 μ M Zn.

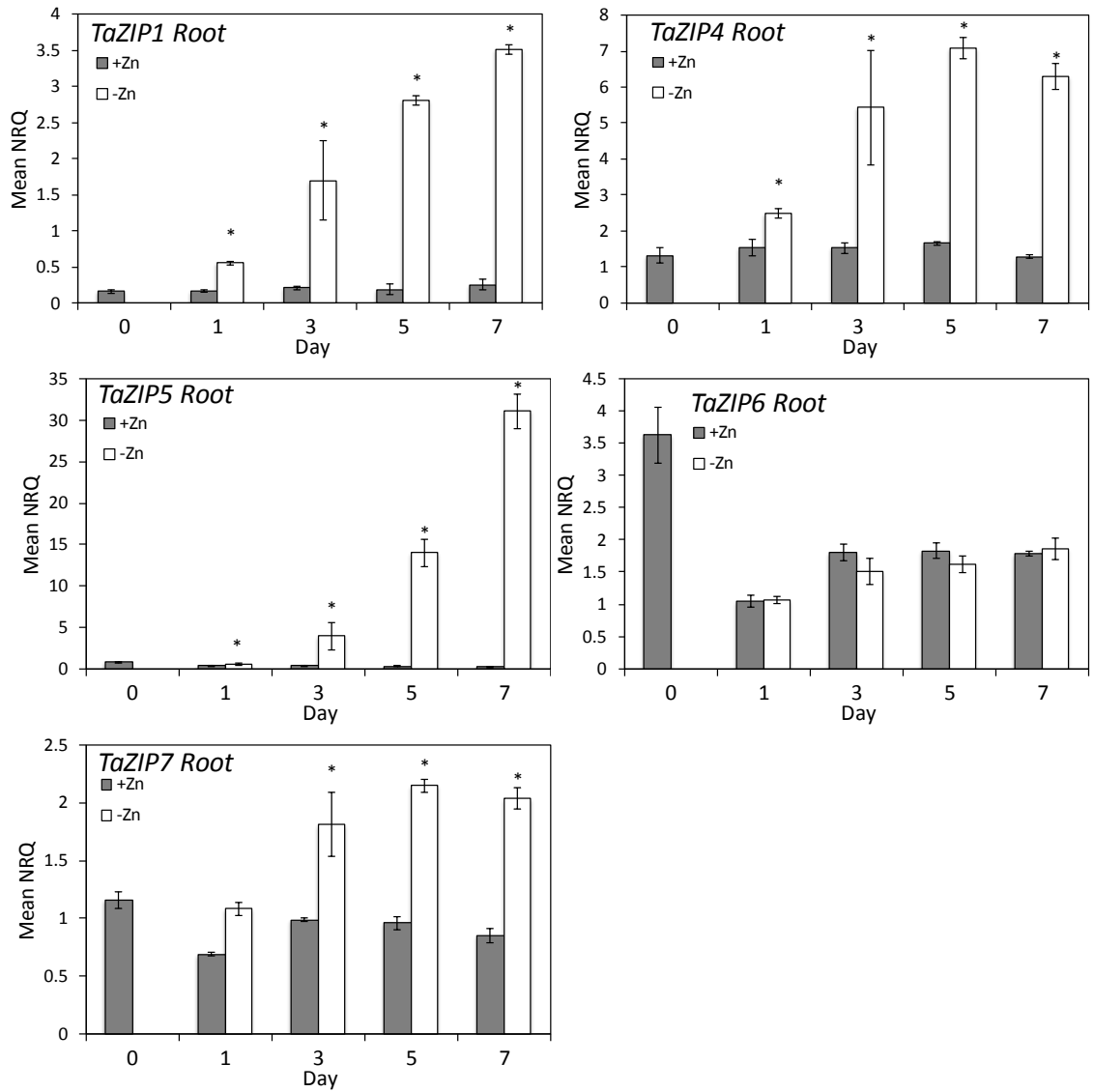


Figure 3.21. Gene expression analysis of *TaZIPs* in wheat root material throughout a one-week Zn starvation period. Normalised relative quantification (NRQ) of five wheat *ZIP* transporter gene transcripts in root material throughout one week of Zn starvation. All NRQ values given are normalised to *TaActin3* and *TaSuccDH* expression, means of three biological replicates are given (\pm S.E.M). Bars within individual graphs displaying an asterisk show significant difference between treatment means at a given time point. Significance ($P < 0.05$) was tested post-hoc, using Fisher's LSD test on $\text{Log}_2(1/\text{NRQ})$ transformed data. +Zn = 8 μM Zn, -Zn = 0 μM Zn.

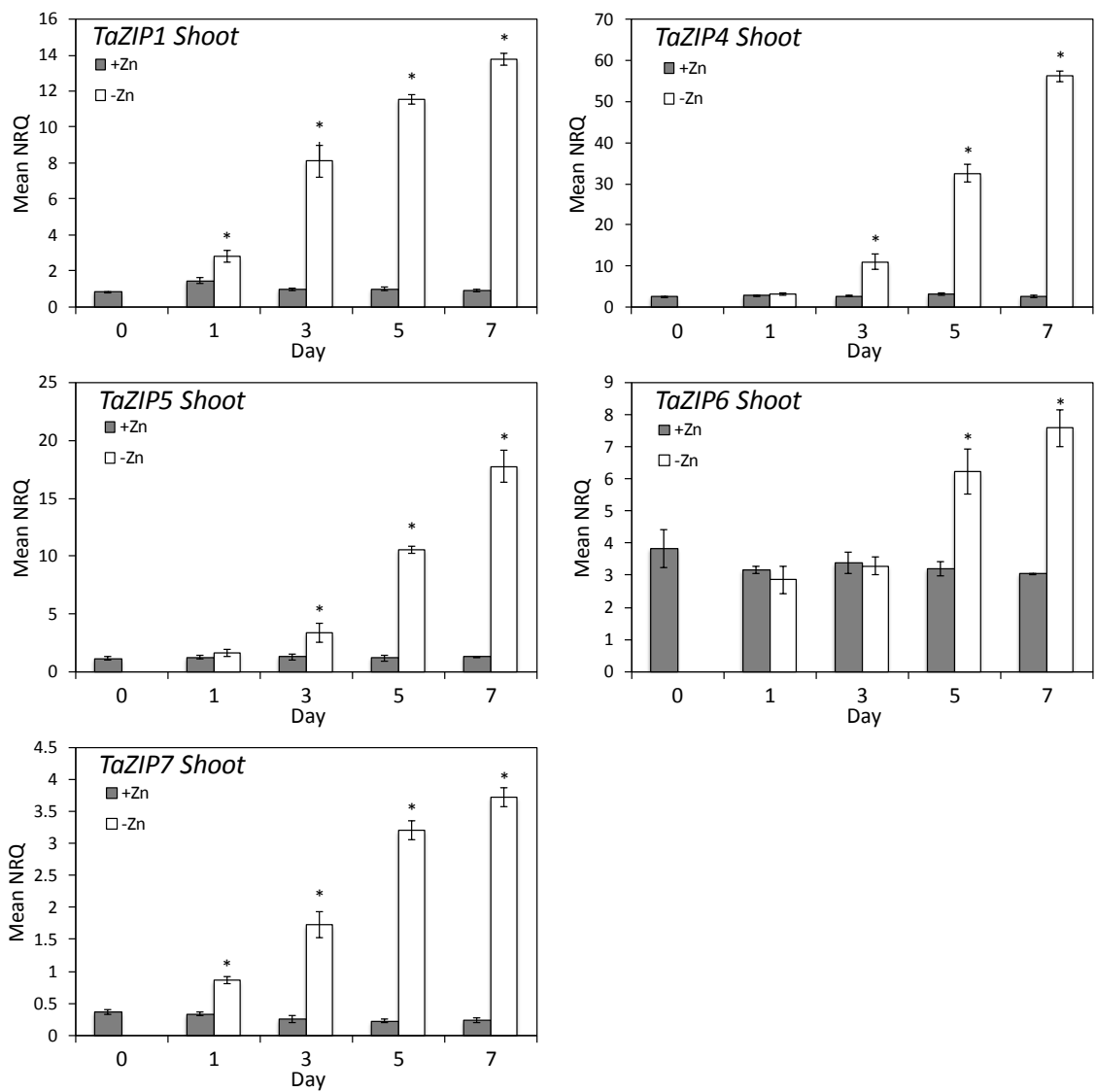


Figure 3.22. Gene expression analysis of *TaZIPs* in wheat shoot material throughout a one-week Zn starvation period. Normalised relative quantification (NRQ) of five wheat *ZIP* transporter gene transcripts in shoot material throughout one week of Zn starvation. All NRQ values given are normalised to *TaActin3* and *TaSuccDH* expression, means of three biological replicates are given (\pm S.E.M). Bars within individual graphs displaying an asterisk show significant difference between treatment means at a given time point. Significance ($P < 0.05$) was tested post-hoc, using Fisher's LSD test on $\text{Log}_2(1/\text{NRQ})$ transformed data. +Zn = 8 μM Zn, -Zn = 0 μM Zn.

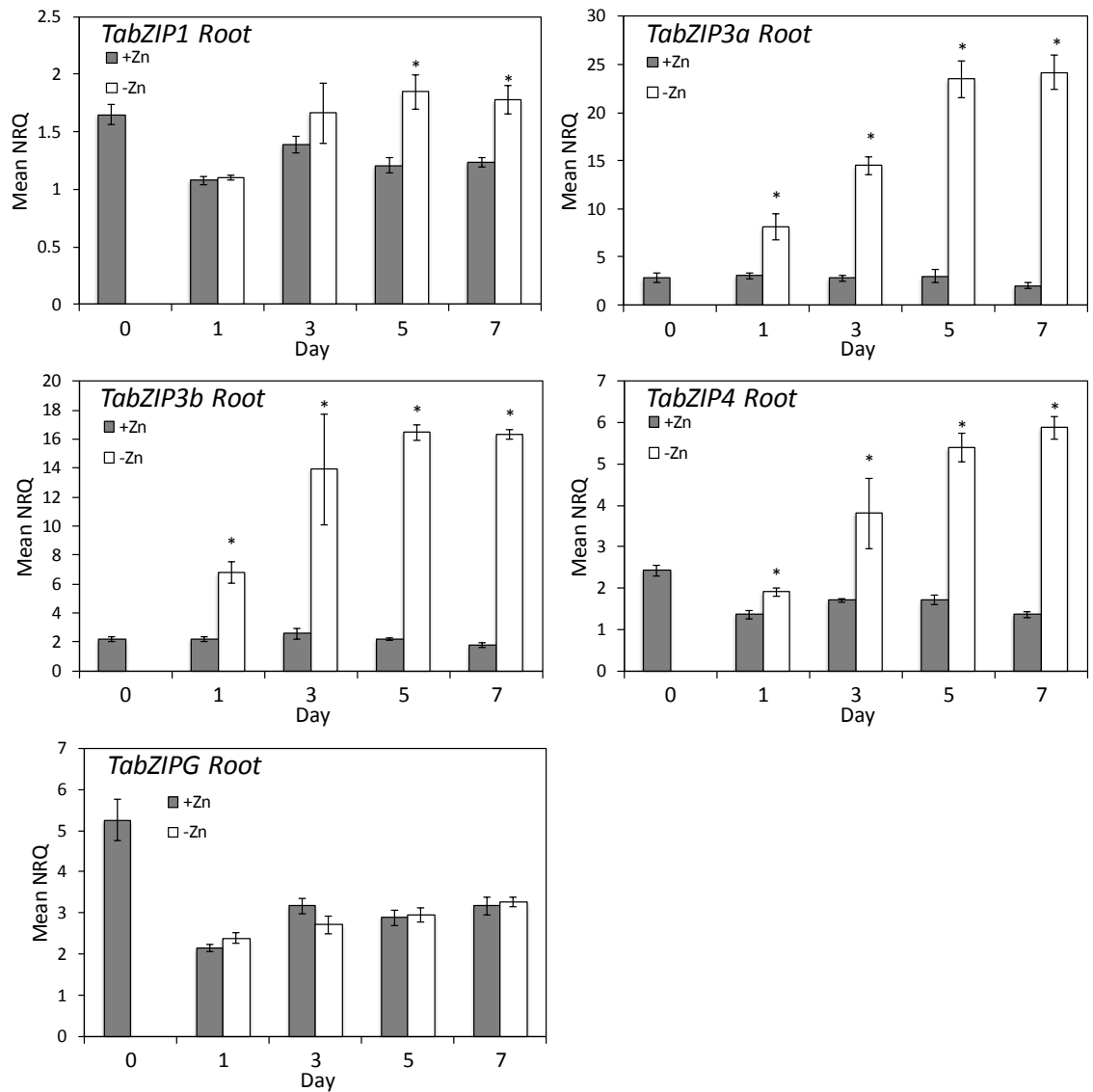


Figure 3.23. Gene expression analysis of *TabZIPs* in wheat root material throughout a one-week Zn starvation period. Normalised relative quantification (NRQ) of five wheat *bZIP* transcription factor gene transcripts in root material throughout one week of Zn starvation. All NRQ values given are normalised to *TaActin3* and *TaSuccDH* expression, means of three biological replicates are given (\pm S.E.M). Bars within individual graphs displaying an asterisk show significant difference between treatment means at a given time point. Significance ($P < 0.05$) was tested post-hoc, using Fisher's LSD test on $\text{Log}_2(1/\text{NRQ})$ transformed data. +Zn = 8 μ M Zn, -Zn = 0 μ M Zn.

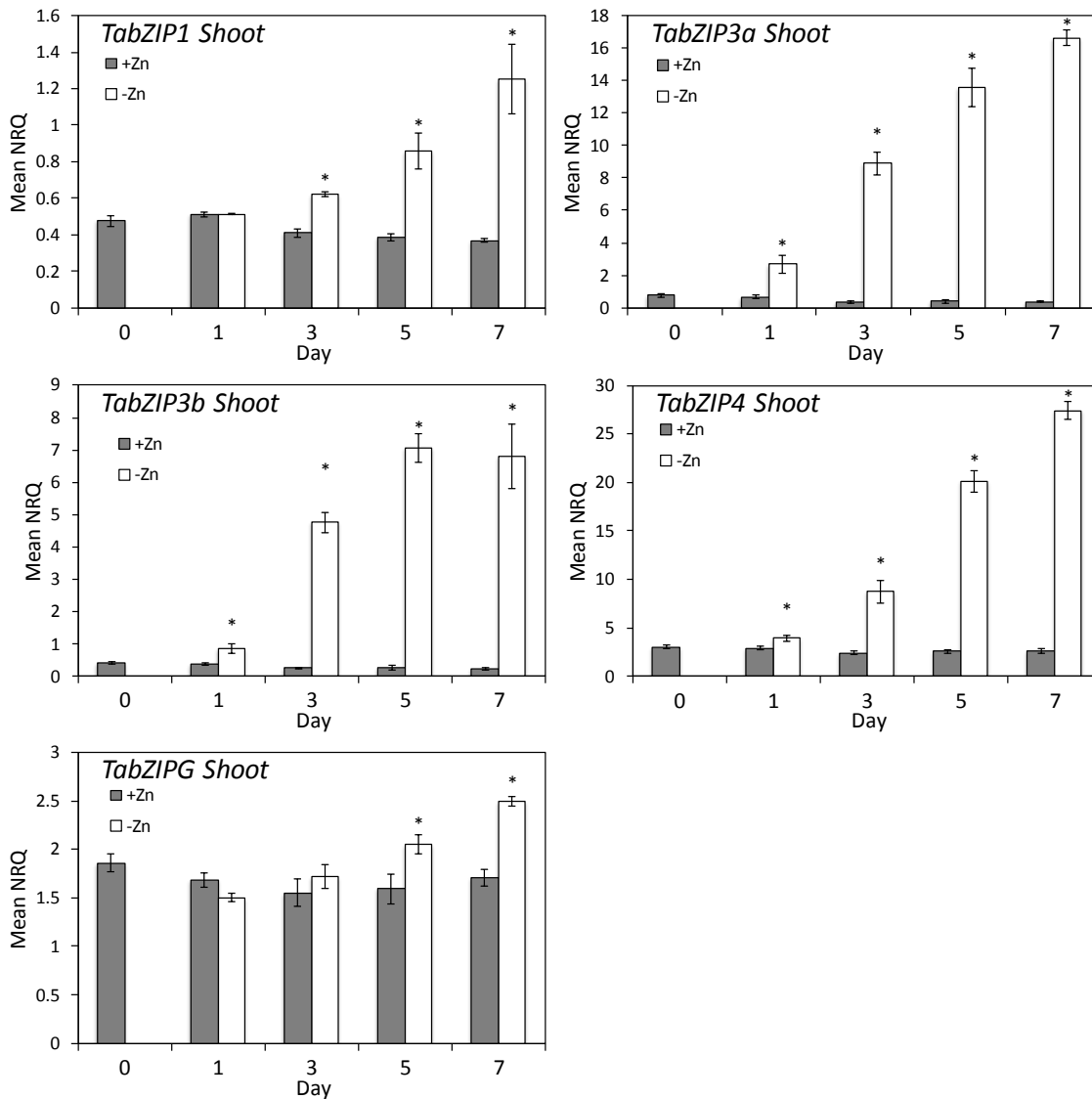


Figure 3.24. Gene expression analysis of *TabZIPs* in wheat shoot material throughout a one-week Zn starvation period. Normalised relative quantification (NRQ) of five wheat *bZIP* transcription factor gene transcripts in shoot material throughout one week of Zn starvation. All NRQ values given are normalised to *TaActin3* and *TaSuccDH* expression, means of three biological replicates are given (\pm S.E.M). Bars within individual graphs displaying an asterisk show significant difference between treatment means at a given time point. Significance ($P < 0.05$) was tested post-hoc, using Fisher's LSD test on $\text{Log}_2(1/\text{NRQ})$ transformed data. +Zn = 8 μ M Zn, -Zn = 0 μ M Zn.

3.4 Discussion

3.4.1 Identification of *T. aestivum* ZIP transporters and *bZIP* transcription factors

Wheat contains a multigene ZIP family

The bioinformatics analysis of the wheat genome led to the identification of 13 putative *TaZIP* transporter genes. The length of *Ta ZIP* translation predictions ranged from 277-578 residues, which is in agreement with the ~300 to 600 amino acid length of other ZIP family members reported by Eide, (2005). However, much of this variability in length came from the homologs of the newest categorised ZIP family members; *AtIAR*, *AtZTP29* and *AtPutZnT* (wheat homologs are *TaZIP14*, *16* and *12* respectively). These genes and their homologs clustered in a separate clade from all other ZIPs examined. Previously, root expression responses of the barley homologs (*HvZIP11*, *14* and *16*) were shown to be less Zn responsive than other *HvZIPs* from the main clade (*HvZIP3*, *5*, *7*, *8*, *10* and *13*), with only *HvZIP16* showing a weakly enhanced expression following Zn-deficient growth (Tiong et al., 2015).

Due to a lack of characterisation it remains unclear whether *AtIAR*, *AtZTP29* and *AtPutZnT* are functional Zn transporters, but from sequence similarity they have been assigned into the ZIP family. *AtIAR* is thought to be involved in regulating the concentration of unconjugated indole-3-acetic acid (IAA) possibly by transporting inhibitory metals out of the endoplasmic reticulum (ER), although it cannot rescue the *zrt1/zrt2* mutant yeast strain (Lasswell et al., 2000). The Zn-transporting capability of *AtZTP29* is as yet functionally unconfirmed, however it is proposed to play a role in the response to salt stress through regulation of Zn levels required for the induction of the unfolded protein response pathway in the ER (Wang et al., 2010). *AtPutZnT* is entirely uncharacterised but is predicted to be a putative Zn transporter due to sequence similarity with other *AtZIP* family members. The phylogenetic positioning of *AtPutZnT* close to *AtZTP29* and *AtIAR1* suggests they may have similar roles and given that evidence suggests *AtZTP29* and *AtIAR1* are both involved in transporting Zn out of the ER, this may be a possible function for *AtPutZnT*. The wheat homologs of these genes are identified and detailed in Table 3.1. and although not studied in this thesis, could be interesting candidates to investigate further, particularly with regard to salt stress tolerance due to the adverse effects of soil salinity on agricultural productivity. It is interesting that of the three group F *bZIPs* in *Arabidopsis* *AtbZIP19* and *AtbZIP23* are both involved in the Zn-regulatory framework, yet *AtbZIP24* has been shown to be involved in salt tolerance (Yang et al., 2009a). Perhaps *AtbZIP24* also interacts with Zn, yet targets the transcription of these more distant ZIP family members during abiotic stresses such as salt stress, bringing about responses based on Zn levels associated with these fluctuating abiotic stresses.

The ZIP phylogenetic analysis presented in this chapter shows that all other ZIP members aside from the three discussed above form one large clade (Figure 3.1). Alignments showed that the TM domains predicted by (Grotz et al., 1998; Gainza-Cortés et al., 2012; Li et al., 2013) were highly conserved in these *TaZIPs* (Figure 3.2). A variable region was present between TM-III and TM-IV. Within this variable region, histidine residues were present that showed widespread consensus across the ZIPs examined. Previously, Guerinot (2000) suggested this region may comprise part of an intramembranous heavy metal binding site. Both *TaZIP6* and the homolog *OsZIP6* have quite pronounced sequence disparities in this variable region. It could be that variation in this region possibly regulates the specificity of substrate transport and perhaps even the specificity of substrate speciation which could be important in the transport of the often chelated Zn^{2+} cation.

There are seven distinct F group bZIPs in wheat

Seven distinct sets of group F *bZIP* homeologs were identified within the wheat genome. In *Arabidopsis* and *Brachypodium* there are only three members of this bZIP group, this indicates that the roles of the seven group F *TabZIPs* may be more complex. The alignments of these *TabZIPs*, as well as the other cereal *bZIPs* identified in the bioinformatics analysis (shown in Figure 3.6) shows how well conserved the general basic-leucine zipper (bZIP) domains are across the *bZIPs* investigated. These bZIP domains contain a basic region of 15 residues which is rich in lysine and arginine that results in positive charge which allows the bZIP to bind to the double stranded DNA. Downstream of this basic region is the leucine zipper domain; through van der Waals forces, these leucine residues bind to other leucine zipper regions of other bZIP proteins and produce functional dimers (Jakoby et al., 2002). *AtbZIP19* and *AtbZIP23* are categorised as group F bZIP transcription factors. This grouping is based on members containing two domains that are both rich in histidine and cysteine residues. These domains have been proposed to be the binding site of Zn in the deficiency response mechanisms of *A. thaliana* (Assunção et al., 2013). Zn^{2+} is a small, efficient electron acceptor and therefore forms strong covalent bonds with sulphur and nitrogen atoms, as found in the amino acid side chains of cysteine and histidine residues (Tauris et al., 2009). The alignment shown in Figure 3.6 shows the residue conservation found in the group F motif 2 is high. The 3' end of the group F motif 1 is however less conserved between sequences and shows less consensus to the domain prediction based on the Jakoby et al. (2002) bZIP classifications.

In addition to the seven sets of group F *TabZIPs* identified, another *TabZIP* was analysed. Referred to in this thesis as *TabZIPG*, this gene has been published under the name of '*TabZIP1*' (Zhang et al., 2008) and (GenBank accession no. FJ194457). This GenBank accession contains only the coding sequence for one homeolog of this gene. Using this information the wheat genomic sequences for all three homeologs of this gene were identified. Introns were predicted

and the subsequent coding sequences and their translations show this *bZIP* is a group G *bZIP* according to the classification presented in (Jakoby et al., 2002). Zhang et al. (2008) report the upregulation of this gene in wheat leaves infected with stripe rust pathogen *Puccinia striiformis* f. sp. *tritici* as well as wounded leaves and leaves treated with methyl jasmonate or abscisic acid. This *TabZIP* was used as a control to examine how the domain differences between the *bZIP* groups affect their behaviour with regards to Zn-deficiency.

3.4.2 Zn starvation impacts wheat growth and mineral concentration

The root and shoot fresh weights measured and the phenotypes observed in both the hydroponics protocol test experiment (Section 3.3.3) and the three-week Zn starvation experiment (Section 3.3.4) validated the hydroponic method and showed that a consistent Zn-deficiency could be inflicted upon hydroponically grown wheat (*T. aestivum*). Further analysis of root and shoot fresh weights allowed the root to shoot ratios of the plants to be explored under the different treatment conditions. The root to shoot ratios of plants grown in $-Zn$ conditions were higher; this indicates that a higher proportion of present biomass is allocated for root growth. These results are supported by Lombnaes & Singh (2003) and Rengel & Graham (1995). There are two hypotheses to explain the increase in root to shoot ratio observed in the Zn-deficient plants. Firstly, as Rengel & Graham (1995) proposed, this phenomenon may be a compensatory mechanism to acquire greater amounts of Zn. In terms of plant survival this seems logical; in order for a plant to successfully mature and produce seed it needs an adequate supply of essential micronutrients (this includes Zn). At an early growth stage, where nutrient stores are limited to the endosperm of the grain from which the plant is growing, uptake of essential nutrients from the growth media is very important. However, if any of these essential micronutrients are in short supply it is necessary for the plant to attempt to increase uptake. By increasing the allocation of finite growth resources to root growth, the plant increases its chances of uptaking enough of the lacking micronutrient by promoting growth and development of the roots. This could explain the increase in root to shoot ratio observed in the Zn-deficient plants. Alternatively, this could be due to an increased Zn requirement in the shoot compared to the root leading to more limited growth in the shoot portion of the plant. This hypothesis is not supported by the concentration ranges observed in $+Zn$ grown plants where across the hydroponic experiments, Zn concentrations were comparable at any given time point between both root and shoot portions of the plants.

The root and shoot fresh weights from the one-week Zn starvation experiment showed no clear effect of the $-Zn$ treatment. No significant trends were observed in terms of weight differences between treatments and, unlike the two previous experiments, there were no observable Zn-deficiency symptoms in this experiment. This was likely due to the exposure time of $-Zn$ conditions being reduced, but may also be due in some part to the increased duration of

+Zn growth conditions before the initiation of the -Zn treatment in this experiment (14 days, see Table 2.2). This extended +Zn growth stage before the treatment split was implemented to allow for more sample material in the given cabinet space, thus allowing more time points to be examined in this shorter time-course experiment. It could be that plants one week further on in development are slightly more robust in terms of coping with Zn-deficient growth conditions due to their larger size at the point of subjecting them to -Zn conditions.

The results from the mineral analysis showed clearly that in both the three-week and the one-week Zn starvation experiments, Zn concentrations were reduced in both the root and the shoot of -Zn grown plants. Results from similar experiments using hydroponic techniques are reported by Rengel (1999) in wheat, Lombnaes & Singh (2003) in both wheat and barley, as well as Jain et al. (2013) in *A. thaliana* which show this reduction in Zn concentration with Zn-deficient conditions. Throughout the three-week Zn starvation experiment the Zn concentration of +Zn roots and shoots increased steadily from D7 onwards. Previously Rengel (1999b), observed that both roots and shoots of hydroponically grown wheat (*T. aestivum* cv. Durati and Aroona) increased in Zn concentration from 13 days to 22 days post germination. The increasing Zn root and shoot concentrations between D7 and D21 observed are even more pronounced when the increased fresh weight of both the root and shoot portions of the plants between these time points are considered. Despite the plant biomass increasing significantly, the Zn concentrations also increased. This suggests that during this developmental period Zn uptake is high; this is likely a key time-period in terms of Zn uptake for the plant.

After the Zn concentrations reported, the second most striking mineral concentration trends are shown by phosphorus; a macronutrient. In both the three-week and one-week Zn starvation experiments phosphorus concentrations consistently increased in both root and shoot samples when grown under -Zn conditions. Similar trends were reported by Lombnaes & Singh (2003) in both wheat and barley, who observed increased phosphorus concentrations in Zn-deficient plants. In their study the increase in concentration was so severe that at the time points sampled the levels were within the toxicity range (8-12 g/kg for wheat and barley shoots (Loneragan et al., 1982)). Their phosphorus measurements were likely exacerbated by the increased phosphorus added to both +Zn and -Zn treatments a week before sampling to meet the requirement of the fast-growing biomass. They concluded that the extreme phenotypes they observed in the -Zn treatment were in part due to phosphorus toxicity in addition to Zn deficiency. The highest shoot phosphorus concentrations that were recorded in this study did enter the toxic threshold for the three-week starvation experiment at D14 and D21 (highest recorded was 35 g/kg in the three-week starvation, shoot samples, D21). These results demonstrate the strong link between Zn and phosphorus. An investigation into the expression of high-affinity phosphate transporter genes under Zn deficiency goes some way to explaining this relationship (Huang et

al., 2000). Huang et al. (2000) report that under Zn-deficient conditions, barley (*H. vulgare* cv. Weeah) high-affinity phosphate transporter genes are upregulated. Huang et al. (2000) hypothesised this is due to a role of Zn in the complex signal induction cascade that brings about phosphate transporter regulation. This effect shows just how vital Zn levels are in the functioning of basic plant processes and the phosphorus concentration results shown in this thesis support this hypothesis.

In both hydroponic experiments that had mineral analysis, the Fe concentrations of both root and shoot were variable. Jain et al. (2013), showed that in a Zn-starvation hydroponic experiment with *A. thaliana* the levels of Fe remained constant between treatments. In contrast, Lombnaes & Singh (2003) reported an increase in wheat shoot concentration of Fe under Zn-deficient treatment and little change in root concentration. The lack of agreement in the literature (as noted by Jain et al., 2013) is evident. Perhaps Fe is more reliant than other minerals on the binding of phytosiderophore complexes in the rhizosphere before uptake into root tissue. Phytosiderophore release into the 'hydroponic rhizosphere' would likely have little efficacy due to continued aeration and regular solution changes, thus the varied Fe concentrations of hydroponically grown plants in the Zn-starvation literature could be due to this.

The variation observed in both fresh weight and mineral concentrations examined highlights the importance of Zn not only in the essential cellular functions that maintain growth and development, but also in the homeostasis of other essential macro- and micronutrients.

3.4.3 *TaZIPs* are regulated by Zn status in wheat

Grotz et al. (1998) first characterised the function of the *ZIP1* gene in *A. thaliana*, using a complementation assay in yeast. Since then, further ZIP transporters have been identified in *A. thaliana* (Milner et al., 2013) as well as other crop species. Presently, there is only one study in which a ZIP transporter has been investigated in a wheat species (Durmaz et al., 2011); wild emmer wheat (*Triticum turgidum* ssp. *dicoccoides*) a tetraploid relative of modern bread wheat (*Triticum aestivum*). This emmer wheat ZIP transporter was shown to be upregulated in -Zn conditions (Durmaz et al., 2011). The results from the ZIP gene expression analyses carried out in this study, using the hexaploid spring wheat (*Triticum aestivum* cv. Paragon) are the first in a hexaploid wheat variety. Results across Zn starvation experiments showed that the five *TaZIPs* examined (*TaZIP1*, 4, 5, 6 and 7) were Zn regulated. Zn-deficient conditions resulted in an upregulation of these putative Zn transporters. However, the induction of *TaZIP* expression may also be caused or enhanced by the fluctuations observed in other nutrients in the -Zn grown plants. If the functional analysis of these *TaZIP* genes confirms they are able to transport Zn, we can conclude that this up-regulation of expression is either to take up more Zn into the roots and/or to redistribute this limited micronutrient resource throughout the plant.

The upregulation of *ZIP* genes occurred in both root and shoot portions of the wheat plants. By D7, the first time point in the three-week Zn starvation, all *ZIP* transporters were upregulated in both the root and the shoot of -Zn plants. Three of the *TaZIPs* investigated have a barley homolog that has also been shown to be Zn responsive (*TaZIP1/HvZIP3*, *TaZIP4/HvZIP5* and *TaZIP7/HvZIP7*) (Tiong et al., 2015; Pedas et al., 2009). For the other two *TaZIPs* investigated in this thesis, the barley *TaZIP5* homolog (*HvZIP13*) has not been previously investigated whilst the barley *TaZIP6* homolog (*HvZIP6*) was shown to be unresponsive to Zn status in the shoot, but upregulated in the root (Tiong et al., 2015). Interestingly however, the rice *TaZIP6* homolog (*OsZIP6*) is induced in both the roots and shoots of Zn-deficient rice plants (Kavitha et al., 2015). *OsZIP6* expression in response to Zn-deficiency is in agreement with the expression results of *TaZIP6* presented in this chapter.

Upon closer inspection of the seven-day period from treatment initiation, results showed *TaZIP* response upregulation times varied both between genes and also within genes between root and shoot material. For instance, *TaZIP4* transcripts were significantly higher in Zn-deficient root material at D1, whereas in the shoot this gene was upregulated only from D3 of Zn starvation. Zn concentrations were significantly reduced in the -Zn grown root and shoot samples from D3 onwards; *TaZIP4* upregulation preceded the root Zn-deficiency observed. *TaZIP6* expression levels were not Zn-responsive in the root for the first 7 days of -Zn treatment, yet in the shoot were strongly upregulated from D5. These results indicate that response times between *ZIP* genes vary in reaction to the exposure of the plants to Zn-deficient conditions.

The levels of upregulation were not consistent across the *ZIP* transporters studied. For example, the magnitude of *TaZIP4* upregulation was far greater in the shoot than in the root. Conversely, *TaZIP5* was upregulated to a higher extent in the root than in the shoot. Taken together, the variable response times of *TaZIPs* in response to -Zn conditions, as well as their tissue specific levels of upregulation suggests individual *TaZIPs* have distinct roles in the Zn-homeostasis network. This may be due to the specific locations within the plant that these transporters occupy. If a particular *ZIP* is involved in uptake directly from the rhizosphere it is plausible that it would be upregulated in the plant earlier in response to -Zn conditions than perhaps *ZIPs* involved in the loading of Zn into the xylem for example. *TaZIP* upregulation may relate to Zn-concentration parameters of specific tissues or cells.

3.4.4 Group F *TabZIPs* are upregulated in response to Zn deficiency

The group F *TabZIPs* identified in this study show clear upregulation under Zn-deficient conditions. However, as noted with the *TaZIPs* this induction of *TabZIP* expression may have been enhanced or even caused by fluctuations in other nutrients observed in the -Zn grown material. *TabZIP* upregulation levels varied between *TabZIPs*, with *TabZIP3a* and *TabZIP3b*

displaying very strong upregulation in response to Zn deficiency, whilst the upregulation of *TabZIP1* was less drastic. This upregulation is supported by data published by Assunção et al. (2010), which showed *AtbZIP19* and *AtbZIP23* were upregulated in $-Zn$ grown *Arabidopsis*. In the present study, across both the three-week starvation and the one-week starvation experiments upregulation of *TabZIPs* was greater in the shoot material than in the root material. Recently Assunção et al. (2013) have developed a model of how Zn-deficiency may be sensed by plants. They predict that the binding of Zn to *AtbZIP19* and *AtbZIP23* renders their conformation non-functional. When intracellular Zn levels drop below a threshold, Zn ‘releases’ from the *bZIP* and the conformation becomes active. Assunção et al. (2013) also predict that *bZIP* levels are constant in the response to Zn deficiency. The constant expression level of *bZIPs* contradicts their previous findings where *AtbZIP19* and *AtbZIP23* were upregulated approximately two times higher under the $-Zn$ treatment compared to control conditions (Assunção et al., 2010). Furthermore, in a separate study *AtbZIP19* was also shown to be upregulated by Zn-deficiency (Inaba et al., 2015). The group F *TabZIP* upregulation levels under Zn-deficiency found in this thesis also contradict this aspect of the model. Perhaps, an improvement to their model could be the addition of a feedback loop that causes the up-regulation of *bZIPs* after Zn-deficiency is sensed, thus the up-regulation of *ZIPs* may be faster in order to maintain plant Zn concentrations more effectively. It could also be the case that there is an upstream signalling pathway a level higher than the *bZIPs* that is sensing Zn-deficiency and bringing about a transcriptional response of both the *bZIPs* and *ZIPs*. Finally, because of the differential upregulation levels across the *TabZIPs* examined it seems possible that certain *bZIPs* (notably the less Zn-deficiency induced members, such as *TabZIP1*) are ‘master regulators’ of other *bZIPs*.

The results from the one-week starvation experiment showed the upregulation of *TaZIPs* and *TabZIPs* initiating at the same time. The timing of upregulation could be the same; this would support the idea of some form of feedback loop or upstream signalling pathway in the homeostatic mechanism. However, it could be that the length of time between infliction of Zn-deficient conditions and the first sampling point was too long (24 hours) and subtleties of this response were overlooked.

An interesting observation from the results of the one-week Zn starvation experiment is that significant upregulation of both *TaZIPs* and *TabZIPs* occurred after only one day of Zn-starvation and was present before any reduction in Zn concentration could be seen in the root and shoot portions of the plants examined. It is conceivable that whilst the measured root or shoot total Zn concentration is not reducing, perhaps at a smaller scale specific zones are becoming depleted of Zn. It is plausible for instance that the root epidermis could be the first region of the root to become Zn-deficient and an upregulation of key transcription factors and Zn membrane transporters occurs here while the total Zn concentration of the root is still unchanged.

The non-group F *TabZIP* examined in this study (*TabZIPG*) exhibited interesting transcript expression profiles. In roots, relative expression of *TabZIPG* did not change throughout the one-week, or three-week starvation period, yet there was a modest, albeit significant, upregulation in the Zn-deficient shoot material at D5 and D7 in the one-week period and from D7 onwards in the three-week Zn-starvation experiment. When compared to the very clear upregulation of the group F *TabZIPs* investigated however, this Zn-response is less pronounced. *TabZIPG* has been shown to be upregulated by exposure to stripe rust fungus and wounding (Zhang et al., 2008), feasibly the shoot upregulation of *TabZIPG* observed at latter time points could be an adaptive response to a potentially increased susceptibility to stripe rust caused by Zn-deficiency, which infects the plant by penetration through the stomata. Alternatively, the moderate upregulation of *TabZIPG* in Zn-deficient shoots could be a result of Zn absence, altering the regulatory network of this pathogen-defence response. A Zn containing Zn finger protein, TaLSD1, has been shown to negatively regulate the response of wheat to stripe rust pathogen (Guo et al., 2013); perhaps Zn deficiency disrupts the regulation by TaLSD1 and causes pathogen-defence response genes such as *TabZIPG* to become unregulated.

In conclusion, the clear Zn-responsiveness of the group F *TabZIPs* identified suggests this bZIP group is of particular importance in the Zn-homeostasis network of wheat. The presence of the cysteine-histidine-rich motifs in these bZIPs is consistent with their proposed binding site of Zn in the deficiency-response model developed by Assunção et al. (2013) and conveys agreement of this model in wheat, although this requires more detailed analysis.

Having identified wheat *TaZIPs* and *TabZIPs* that are Zn-responsive in expression, their functional roles in the Zn-regulatory network of wheat will be further investigated in subsequent Chapters. The Zn transport ability of five *TaZIPs* are examined and their substrate specificities are investigated in Chapter 4. Additionally, the ability of four Zn-responsive *TabZIPs* to rescue a mutant *Arabidopsis bzip19bzip23* line are tested, to ascertain if these *TabZIPs* play a similar role in the Zn-regulatory mechanism of wheat to those previously discovered to be vital in the Zn-response of *Arabidopsis* (Chapter 5). The binding ability of the *TabZIPs* identified to predicted ZDRE motifs found in the promoter regions of *TaZIPs* are also explored in Chapter 5 in order to further characterise the Zn-regulatory network of wheat.

Chapter 4. Cloning and functional characterisation of *T. aestivum* ZIPs

4.1 Introduction

Membrane transporters from the ZIP family have been shown to transport a range of cations. Heterologous expression studies in *Saccharomyces cerevisiae* (yeast) have demonstrated the ability of ZIPs from a range of plant species to transport Zn, Fe, Mn, Cu and cadmium (Cd) (Grotz et al., 1998; Milner et al., 2013; Lee et al., 2010a; Yang et al., 2009b; Li et al., 2013; Pedas et al., 2008, 2009; Tiong et al., 2015). The most studied ZIP family members are those from the model plant species *A. thaliana*.

The first plant member of the ZIP family to be characterised was AtIRT1 (Eide et al., 1996). The ability of AtIRT to transport Fe was demonstrated by expression in the yeast Fe uptake mutant *fet3/fet4*. Subsequently the substrate range of AtIRT1 was proven to be broader than first thought, and was shown to complement the Mn *smf1* mutant yeast strain and the Zn uptake-deficient mutant strain *zrt1/zrt2* (Korshunova et al., 1999). AtIRT2 and AtIRT3 also transport Fe and Zn (Vert et al., 2001; Lin et al., 2009).

The ability to alter the substrate selectivity of AtIRT1 through the substitution of conserved amino acids has been investigated (Rogers et al., 2000). It was shown that the substitution of five out of 11 of the conserved residues in or near transmembrane domains that were tested were vital in maintaining any cation transport function of AtIRT1. Furthermore, three mutations altered the specificity of AtIRT1 from Fe, Mn and Zn transport ability to just Zn, or just Fe and Mn. These substitutions were all of either glutamic acid (E) or aspartic acid (D), which both contain negatively charged side chains, substituted with the hydrophobic amino acid alanine (A). Most interestingly was the location of the residues that affected selectivity, two were between the TM domain II and III with the final one being just after the predicted TM III. These results indicate this region may be important in determining the substrate specificity of the ZIPs.

Of the remaining *Arabidopsis* ZIP members *AtZIP1*, *AtZIP2* and *AtZIP3* were initially identified through a library screening approach using the Zn-uptake defective mutant yeast strain *zrt1/zrt2* (Grotz et al., 1998). Until recently the remaining *Arabidopsis* ZIP transporters had remained largely unstudied. Milner et al. (2013) have now characterised 11 of the *Arabidopsis* ZIPs, including *AtZIP1*, *AtZIP2* and *AtZIP3*, as well as eight previously unstudied ZIP members (*AtZIPs* 5 to 12). Heterologous expression in yeast showed six of these were able to transport Zn (*AtZIP1*, 2, 3, 7, 11 and 12) and additionally six transported Mn (*AtZIP1*, 2, 5, 6, 7 and 9). Only one however transported Fe (*AtZIP7*) and none were shown to transport Cu. Whilst yeast

expression studies are a valuable technique in characterising the substrate specificities of the *Arabidopsis* ZIPs, it should be noted that contradictory evidence exists between the reported transport ability of ZIPs using yeast mutant assays and studies in whole plant systems. AtZIP9 was unable to rescue the *zrt1/zrt2* yeast Zn-uptake mutant phenotype (Milner et al., 2013). However, in a more recent study AtZIP9 was reported to be involved in Zn uptake by the roots (Inaba et al., 2015). Results from two independent *Arabidopsis zip9* T-DNA insertion mutants showed reduced Zn concentrations of mutants grown at higher Zn levels indicating a role of AtZIP9 in Zn uptake.

ZIP transporters have been identified and functionally characterised in the crop species *Glycine max* (soybean) (Moreau et al., 2002) and *Zea mays* (maize) (Li et al., 2013) however rice ZIPs are the most widely characterised of all the crop species. OsIRT1 and OsIRT2 have been shown to transport Fe but not Zn (Bugchio et al., 2002; Ishimaru et al., 2006). OsZIP3, OsZIP4, OsZIP5 and OsZIP8 have all been shown to be functional Zn transporters (Ishimaru et al., 2005; Lee et al., 2010a; Yang et al., 2009b), while OsZIP6 and OsZIP7 have been shown to transport Fe but not Zn (Yang et al., 2009b; Kavitha et al., 2015). In barley, members of the ZIP family have also been functionally characterised. HvIRT1 can transport Zn, Mn, Fe and Cd (Pedas et al., 2008). HvZIP3, HvZIP5 and HvZIP8 (which are homologous to TaZIP1 and TaZIP4 in this thesis) have all been shown to rescue the *zrt1/zrt2* Zn mutant yeast strain to a varying degree, indicating Zn transport ability (Pedas et al., 2009). Additionally, expression levels of *HvZIP3*, 5 and 8 (as well as *HvZIP7*, 10 and 13) increased in both the root and shoot, upon Zn-resupply following a period of Zn-deficiency (Tiong et al., 2015). In particular *HvZIP5* and *HvZIP8* showed strong upregulation in the root (particularly the epidermis) in plants previously grown in Zn-deficient conditions, indicating a role in Zn uptake (Tiong et al., 2015). Evidence suggests the substrate range of *HvZIP3*, *HvZIP5* and *HvZIP8* is narrow, as they are all unable to complement the *smf* Mn mutant or the *fet3/fet4* Fe mutant yeast strains. The rescue of the *zrt1/zrt2* strain was noticeably more complete with *HvZIP5* than both *HvZIP3* and *HvZIP8*. Pedas et al. (2009) also hypothesised that the differential extent to which the *zrt1/zrt2* mutant yeast strain was complemented could be due to *HvZIP3* and *HvZIP8* being low affinity Zn transporters, whereas *HvZIP5* may be a high affinity Zn transporter able to transport Zn at relatively lower Zn concentrations. *HvZIP5* showed a higher degree of *zrt1/zrt2* complementation than *HvIRT1* which was used as a positive control, suggesting it plays a more important role in Zn uptake within the barley plants.

To date, only one study that has characterised a wheat ZIP: Durmaz et al. (2011) identified and cloned homologs of *TaZIP1* from wild emmer wheat *Triticum turgidum* ssp. *dicoccoides*, accessions, *TdZIP1*. The translated products of *TdZIP1* across the accessions studied gave approximately 100% sequence similarity to *TaZIP1*. Expression under the inducible promoter GAL1 showed the ability of *TdZIP1* from two emmer wheat accessions to rescue the Zn-

deficiency phenotype of *zrt1/zrt2* on Zn limited media indicating a role in Zn transport. Interestingly when the transformed *TdZIP1 zrt1/zrt2* strain was grown on normal media, growth was reduced in the *TdZIP1* transformed strain compared to the empty pYES2 control, suggesting *TdZIP1* Zn uptake caused toxicity to the cells under normal Zn supply.

There is a distinct lack of information on the ZIP members of the globally important cereal species wheat. In this chapter *TaZIPs* are cloned from hydroponically grown wheat material (*T. aestivum* cv. Paragon). The sequences of the *TaZIPs* cloned are compared to those obtained from the wheat genome survey databases (*T. aestivum* cv. Chinese spring) as discussed in Chapter 3. *TaZIPs* are also functionally characterised through heterologous expression in three yeast strains: *zrt1/zrt2* a Zn uptake mutant, *zrc1/cot1* a Zn sequestration mutant and *fet3/fet4* an Fe uptake mutant.

4.2 Aims

- Clone *TaZIPs* from *T. aestivum* cv. Paragon.
- Examine the sequence similarity of the Paragon *TaZIPs* to the predicted sequences from the wheat genome databases (*T. aestivum* cv. Chinese Spring).
- Determine the substrate specificity of *TaZIPs* through heterologous expression of the *TaZIPs* in the *Saccharomyces cerevisiae* mutant yeast strains defective in Zn uptake *zrt1/zrt2*, Zn sequestration *zrc1/cot1* and Fe uptake *fet3/fet4*.

4.3 Results

4.3.1 Cloning of TaZIPs

Members of the *TaZIP* family identified and discussed in Chapter 3 were cloned from hydroponically grown *T. aestivum* cv. Paragon material using the cloning methods described in Section 2.4. Full-length *TaZIPs* were cloned into the yeast expression vector pYES2, which contains the strong inducible promoter GAL1 (galactose induced) as presented in the following section.

4.3.1.1 TaZIP1-2AL

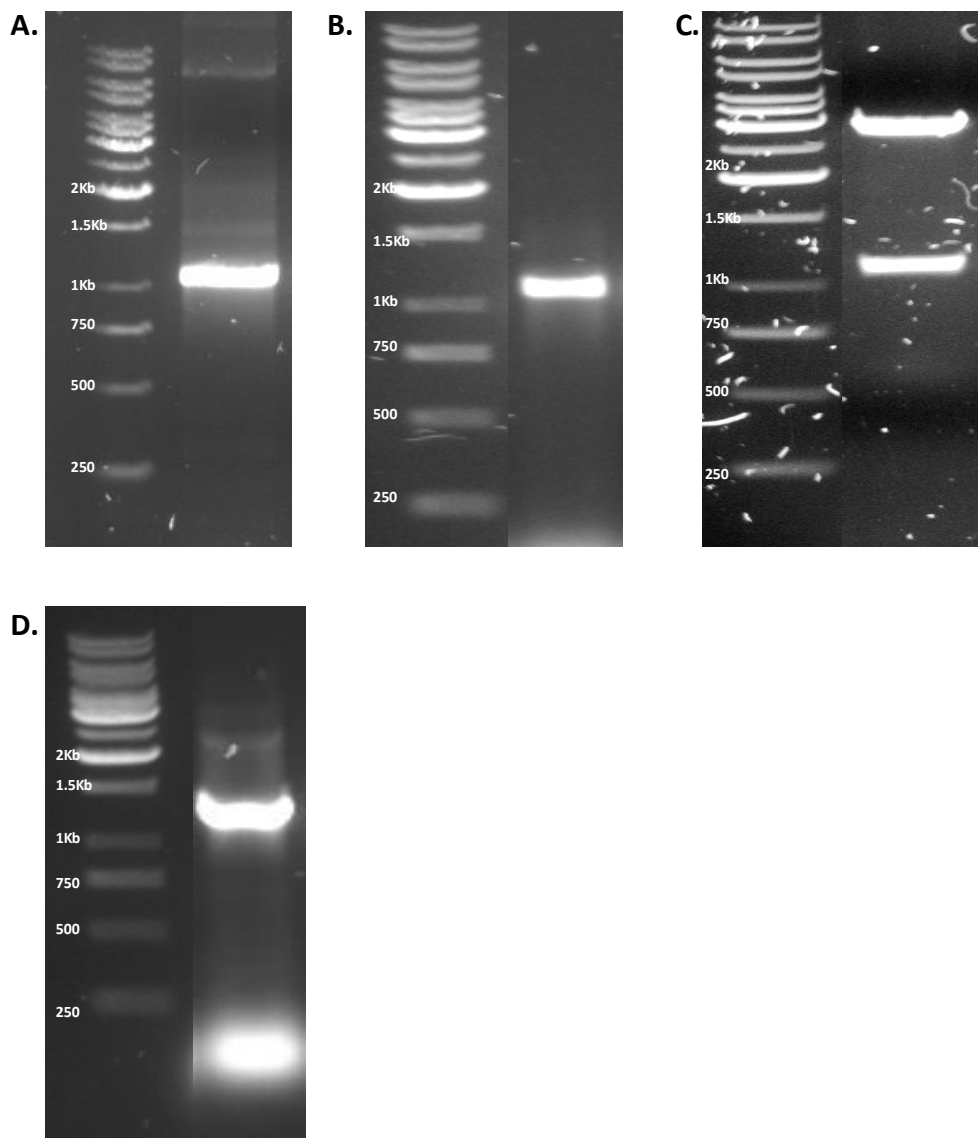


Figure 4.1. Cloning of TaZIP1-2AL into pYES2 yeast expression vector. **A.** Initial amplification of a blunt ended fragment from shoot cDNA using TaZIP1TOPO primers (expected size 1083 bp). **B.** Colony PCR of a positive DH5 α colony containing pGEMTaZIP1 screened using TaZIP1TOPO primers. **C.** EcoRI digestion of pGEMTaZIP1 with expected fragment size 1093 bp shown. **D.** Colony PCR of a positive DH5 α colony containing pYES2TaZIP1 screened using Gal1P Forward and TaZIP1TOPOS (expected size 1276 bp). DNA ladder used in all gels is Thermo Scientific GeneRuler 1Kb.

```

Prediction  MGATNHTLQALLPWLLLFVHQAAAASGGFECTTATDGADKQGATKCLKLVAIASILTAGAA
Cloned      MGATNHTLQALLPWLLLFVHQAAAASGGFECTTATDGADKQGATKCLKLVAIASILTAGAA
*****

Prediction  GVLVPVLGRSMAALRPDGDIFFAVKAFAGVILATGMVHILPAAFDGLTSPCIYKGGGDR
Cloned      GVLVPVLGRSMAALRPDGDIFFAVKAFAGVILATGMVHILPAAFDGLTSPCIYKGGGDR
*****

Prediction  NGFPFAGLVAMSAAMATMVIDSLAAGYYRRSHFSKARPLDNIDIPGDEEGRADHPHVHAH
Cloned      NGFPFAGLVAMSAAMATMVIDSLAAGYYRRSHFSKARPLDNIDIPGDEEGRADHPHVHAH
*****

Prediction  GSHGDAIVVSSPEEAAIADTIRHRVVSQVLELGILVHSVIIIGVSLGASVRPSTIKPLVG
Cloned      GSHGDAIVVSSPEEAAIADTIRHRVVSQVLELGILVHSVIIIGVSLGASVRPSTIKPLVG
*****

Prediction  ALSFHQFFEGIGLGGCIVQANFKVRATIIMATFFSLTAPVGIVLGLIAISSYNVHSSTAF
Cloned      ALSFHQFFEGIGLGGCIVQANFKVRATIIMATFFSLTAPVGIVLGLIAISSYNVHSSTAF
*****

Prediction  IIEGVFNSASAGILIYMSLVDLLAKDFNNPKLQTNKTLQMLTYLALFLGAGMMSMLAIWA
Cloned      IIEGVFNSASAGILIYMSLVDLLAKDFNNPKLQTNKTLQMLTYLALFLGAGMMSMLAIWA
*****

Prediction  Z
Cloned      Z
            *

```

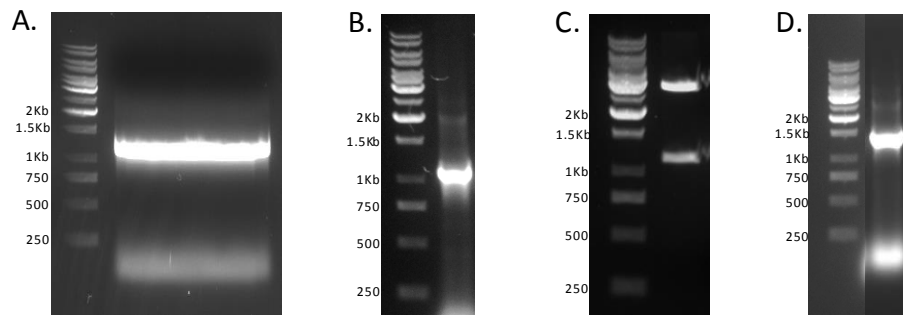
Figure 4.2. Amino acid alignment of cloned TaZIP1-2AL with the predicted sequence. Alignment created using Clustal omega, showing the predicted amino acid sequence of TaZIP1-2AL from the wheat genome database (Prediction, top of pairing) against the amino acid translation of the sequence cloned from the workflow presented in Figure 4.1 (Cloned, lower of pairing).

Figure 4.1 shows the cloning procedures used in the cloning of TaZIP1-2AL. Figure 4.2 shows that the amino acid translations of the cloned TaZIP1-2AL (cv. Paragon) and the prediction from the genome sequence database (cv. Chinese Spring) are identical. This plasmid was used in subsequent yeast transformation and heterologous expression studies.

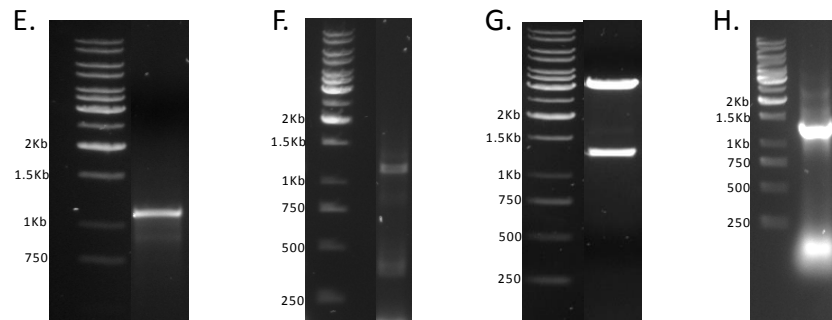
4.3.1.2 TaZIP5-2BL, TaZIP6-1BS, TaZIP7-1DS and TaZIP8-2BS

Figure 4.3 shows the cloning procedures used in the cloning of TaZIP5-2BL, TaZIP6-1BS, TaZIP7-1DS and TaZIP8-2BS. These TaZIPs were cloned from cv. Paragon cDNA. Amino acid alignments of the genes cloned are presented in Figure 4.4 and allow sequence comparisons with genomic predictions (cv. Chinese Spring). The plasmids generated were used in subsequent yeast transformation and heterologous expression studies.

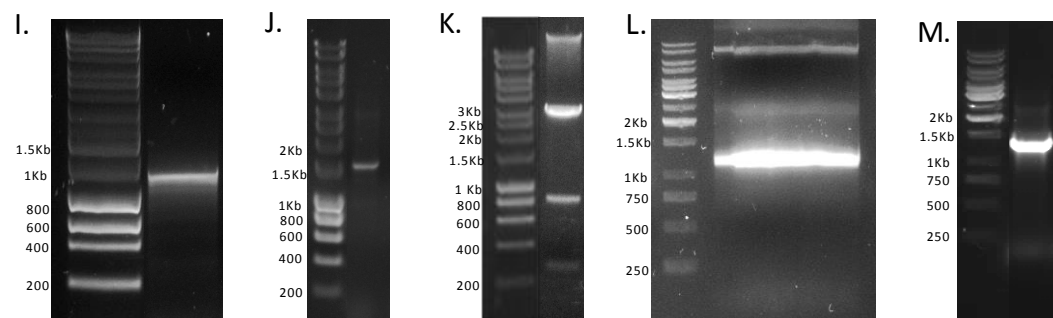
TaZIP5-2BL



TaZIP6-1BS



TaZIP7-1DS



TaZIP8-2BS

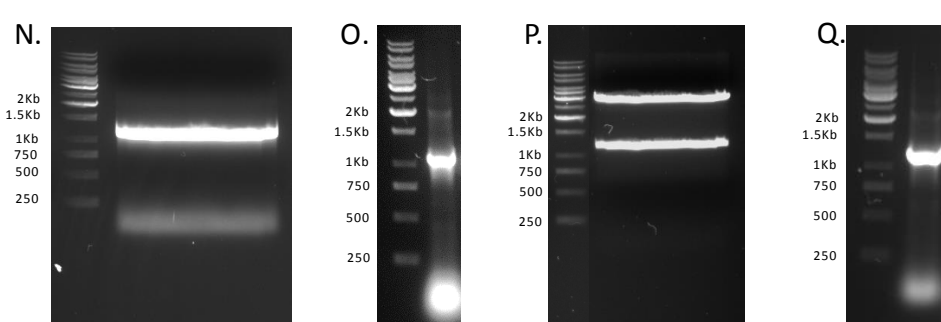


Figure 4.3. Cloning of TaZIP5-2BL, TaZIP6-1BS, TaZIP7-1DS and TaZIP8-2BS into pYES2 yeast expression vector. Composite figure showing the cloning workflow of the following TaZIPs:

TaZIP5-2BL (A.-D.). **A.** Initial amplification of a blunt ended fragment from root cDNA using TaZIP5TOPO primers (expected size 1143 bp). **B.** Colony PCR of a positive DH5α colony containing pGEMTaZIP5 screened using TaZIP5TOPO primers. **C.** EcoRI digestion of pGEMTaZIP5 with expected fragment size 1153 bp shown. **D.** Colony PCR of a positive DH5α

colony containing pYES2TaZIP5 screened using Gal1P Forward and TaZIP5TOPOS (expected size 1336 bp).

TaZIP6-1BS (E.-H.). **E.** Initial amplification of a blunt ended fragment from shoot cDNA using TaZIP6TOPO primers (expected size 1192 bp). **F.** Colony PCR of a positive DH5 α colony containing pGEMTaZIP6 screened using TaZIP6TOPO primers. **G.** EcoRI digestion of pGEMTaZIP6 with expected fragment size 1202 bp shown. **H.** Colony PCR of a positive DH5 α colony containing pYES2TaZIP1 screened using Gal1P Forward and TaZIP6TOPOS (expected size 1381 bp).

TaZIP7-1BS (I.-M.). **I.** Initial amplification of a blunt ended fragment from shoot cDNA using TaZIP7TOPO primers (expected size 1161 bp). **J.** Colony PCR of a positive One Shot $\text{\textcircled{R}}$ TOP10 colony containing pENTRTaZIP7 screened using M13F and M13R primers (expected size 1461 bp). **K.** NaeI digestion of pENTRTaZIP7 with expected fragment sizes of 2758, 723 and 260 bp shown. **L.** Reamplification of TaZIP7 from pENTRTaZIP7 using TaZIP7EcoRIF and TaZIP7XhoIR (detailed in Table 2.5) Expected size (1171 bp). **M.** Colony PCR of a positive DH5 α colony containing pYES2TaZIP7 screened using Gal1P Forward and TaZIP7TOPOS (expected size 1354 bp).

TaZIP8-2BS (N.-Q.). **N.** Initial amplification of a blunt ended fragment from root cDNA using TaZIP5TOPO primers (expected size 1140 bp). **O.** Colony PCR of a positive DH5 α colony containing pGEMTaZIP8 screened using TaZIP5TOPO primers. **P.** EcoRI digestion of pGEMTaZIP8 with expected fragment size 1150 bp shown. **Q.** Colony PCR of a positive DH5 α colony containing pYES2TaZIP8 screened using Gal1P Forward and TaZIP5TOPOS (expected size 1333 bp).

DNA ladder used in all gels is Thermo Scientific GeneRuler 1 kb except **I.**, **J.** and **K.**, where Bioline Hyperladder 1 kb was used.

Figure 4.4 shows that the amino acid translations of the TaZIP5-2BL gene cloned and the prediction from the genome sequence database contain three residue differences. The substitutions are: a leucine (L) for a methionine (M) (hydrophobic side chain residue substituted with neutral side chain residue), an alanine (A) for a serine (S) (hydrophobic side chain residue substituted with neutral side chain residue) and an aspartic acid (D) for a glutamic acid (E) (both acidic residues). The substitutions seen in the gene cloned do not result in amino acid changes with significantly different characteristics to those predicted from the genome prediction. The amino acid translations of the TaZIP6-1BS gene cloned and the prediction from the genome sequence database varied in only one residue. This residue substitution is a histidine (H) for an aspartic acid (D). This substitution may be significant as histidine is a basic residue and aspartic acid is acidic. The amino acid translations of TaZIP7-1DS and TaZIP8-2BS genes cloned showed no differences with the sequence predictions from the genome sequence database.

Chapter 4. Cloning and functional characterisation of TaZIPs

TaZIP5-2BL

```
Prediction MKPSAAVLLAAVVALLLVAAVRGDDDCGSPESAAQDRARANPLKIAAFFSILVCGALGCS
Cloned MKPSAAVMLAAVVALLLVSAVRGEDDCGSPESAAQDRARANPLKIAAFFSILVCGALGCS
*****:*****:*****:*****

Prediction LPVLGRRVPALRPEGDVFFLVKAFAGVILATGFIHILPDAFENLTSDCCLPSDGPWKDFP
Cloned LPVLGRRVPALRPEGDVFFLVKAFAGVILATGFIHILPDAFENLTSDCCLPSDGPWKDFP
*****

Prediction FAGLGAMAGAIGTLVVDTVATGYFTRAHLNKDGAHGHGAISSSAAVVDEEKQAAAAAASEE
Cloned FAGLGAMAGAIGTLVVDTVATGYFTRAHLNKDGAHGHGAISSSAAVVDEEKQAAAAAASEE
*****

Prediction ARRHGGEHEVHVHATHATHGHAHGSAAALVAAVGGAEDEKDTVHRHVISQVLELGI VVHVS
Cloned ARRHGGEHEVHVHATHATHGHAHGSAAALVAAVGGAEDEKDTVHRHVISQVLELGI VVHVS
*****

Prediction IIGISLGASQDPETIKPLVVALSFHQMFEGMGLGGCIVQAKFKARSIVTMILFFCLTTPV
Cloned IIGISLGASQDPETIKPLVVALSFHQMFEGMGLGGCIVQAKFKARSIVTMILFFCLTTPV
*****

Prediction GIAVFGFISRVYNENSPTALVVEGGLNSVAAGILVYMALVDLLAEDFMNPKVQSRGKLQL
Cloned GIAVFGFISRVYNENSPTALVVEGGLNSVAAGILVYMALVDLLAEDFMNPKVQSRGKLQL
*****

Prediction GINVSMLVGAGLMSMLAKWAZ
Cloned GINVSMLVGAGLMSMLAKWAZ
*****
```

TaZIP6-1BS

```
Prediction MSGKGCLPEGELAALSRVCRDGA AAAARLKTGSLLAAILIASAVGVCLPVALTRAFRGRDGY
Cloned MSGKGCLPEGELAALSRVCRDGA AAAARLKTGSLLAAILIASAVGVCLPVALTRAFRGRDGY
*****

Prediction ARGLLLVKCYAAGVILSTSLVHVLPDAYAALADCAVASRRPWKDFPFAGLLCLVGALLAL
Cloned ARGLLLVKCYAAGVILSTSLVHVLPDAYAALADCAVASRRPWKDFPFAGLLCLVGALLAL
*****

Prediction LVDLSASSHLEAHGHQPPQEEGQPYAPIPTTKKAPAFELTGEMSPRKRAFLDES DRDDK
Cloned LVDLSASSHLEAHGHQPPQEEGQPYAPIPTTKKAPAFELTGEMSPRKRAFLDES DRDDK
*****

Prediction NGGDPDRDDVALFGPKKGARLPRSDEPVVPVVGCHGAGHEVVEVGE GEEEEEARKKQKMVS
Cloned NGGDPDRDDVALFGPKKGARLPRSDEPVVPVVGCHGAGHEVVEVGE GEEEEEARKKQKMVS
*****

Prediction KVLEIGIVFHSVIIGVTLGMSQDVCAIRPLVVALSFHQVFEGMGLGGCIAQAGFGMATVG
Cloned KVLEIGIVFHSVIIGVTLGMSQDVCAIRPLVVALSFHQVFEGMGLGGCIAQAGFGMATVG
*****

Prediction YMCIMFSVTTPLGILLGMAVFHMTGYDDSSPNALIEGLLGSLSAGILVYMALVDLISLD
Cloned YMCIMFSVTTPLGILLGMAVFHMTGYDDSSPNALIEGLLGSLSAGILVYMALVDLISLD
*****

Prediction FFHNKMMSSSLK LKKASYIALVLGSASMSILALWAZ
Cloned FFHNKMMSSSLK LKKASYIALVLGSASMSILALWAZ
*****
```

Figure 4.4. figure legend overleaf

TaZIP7-1DS

```

Prediction  MMIGVAGFSRHIGQLLSKSNGFIAASLSAASCADAEAEKAEGAGCRDDAAALRLKWIAMAA
Cloned      MMIGVAGFSRHIGQLLSKSNGFIAASLSAASCADAEAEKAEGAGCRDDAAALRLKWIAMAA
*****

Prediction  ILVSGVMGVGLPLAGRKRRTVQTGS AVFVAAKAFAAGVILATGFVHMLHDAEHALSNPCL
Cloned      ILVSGVMGVGLPLAGRKRRTVQTGS AVFVAAKAFAAGVILATGFVHMLHDAEHALSNPCL
*****

Prediction  PAGPWRRFPFPGFVAMLALATLVLDVLTFRFYETKHRAEVARVKADAAAALAAASTSAS
Cloned      PAGPWRRFPFPGFVAMLALATLVLDVLTFRFYETKHRAEVARVKADAAAALAAASTSAS
*****

Prediction  DEDITVVTVVESEHKVPLLQAHSHSHAQSHGHELMQPQGREGEVSDHVR SVVVSQIILEMG
Cloned      DEDITVVTVVESEHKVPLLQAHSHSHAQSHGHELMQPQGREGEVSDHVR SVVVSQIILEMG
*****

Prediction  IVSHSVIIIGLSLGVSRSPCTIRPLVAALSFHQFFEGFALGGCIAQAQFKNLSAVMMASFF
Cloned      IVSHSVIIIGLSLGVSRSPCTIRPLVAALSFHQFFEGFALGGCIAQAQFKNLSAVMMASFF
*****

Prediction  AITPTPTGIAAGAGLSSFY NANS PRALVVEGILDSVSAGIL IYMALVDLIAADFLGGKMTG
Cloned      AITPTPTGIAAGAGLSSFY NANS PRALVVEGILDSVSAGIL IYMALVDLIAADFLGGKMTG
*****

Prediction  SPRQQVMAYVALFLGALSMSSLAVWAZ
Cloned      SPRQQVMAYVALFLGALSMSSLAVWAZ
*****

```

TaZIP8-2BS

```

Prediction  MKPSAAVLLAAVVALLLVSAVRGEDDCGSPESAARDRARAKPLKIAAFFSILICGALGCS
Cloned      MKPSAAVLLAAVVALLLVSAVRGEDDCGSPESAARDRARAKPLKIAAFFSILICGALGCS
*****

Prediction  LPVLGRHVPVLRPDGDIFFLVKAFAAGVILATGFIHILPDAFENLTS DCLPAAGPWKDFP
Cloned      LPVLGRHVPVLRPDGDIFFLVKAFAAGVILATGFIHILPDAFENLTS DCLPAAGPWKDFP
*****

Prediction  FAGLGAMVGAIGTLVVDTVATGYFTRAHLNKDRAHGSSAAVVDEEKQAAAAAAASELARH
Cloned      FAGLGAMVGAIGTLVVDTVATGYFTRAHLNKDRAHGSSAAVVDEEKQAAAAAAASELARH
*****

Prediction  HDGGEHDGHVHMHTHATHGHAGHSAAALVAAVGGAEDEKDTIRHRVISQVLELGIVVHSV I
Cloned      HDGGEHDGHVHMHTHATHGHAGHSAAALVAAVGGAEDEKDTIRHRVISQVLELGIVVHSV I
*****

Prediction  IGISLGASQDPETIKPLVVALSFHQMFEGMGLGGCIVQAKFKARSIVTMILFFCLTTPVG
Cloned      IGISLGASQDPETIKPLVVALSFHQMFEGMGLGGCIVQAKFKARSIVTMILFFCLTTPVG
*****

Prediction  IAIGLGISRVYNENSPTALVVEGSLNSVAAGILVYMALVDLLAEDFMNPKVQSRGKLQLG
Cloned      IAIGLGISRVYNENSPTALVVEGSLNSVAAGILVYMALVDLLAEDFMNPKVQSRGKLQLG
*****

Prediction  INVSMLVGAGLMSMLAKWAZ
Cloned      INVSMLVGAGLMSMLAKWAZ
*****

```

Figure 4.4. Amino acid alignments of cloned TaZIP5-2BL, TaZIP6-1BS, TaZIP7-1DS and TaZIP8-2BS with the predicted sequences. Alignments created using Clustal omega, showing the predicted amino acid sequence of TaZIPs from the genome sequence database (cv. Chinese Spring) (Prediction, top of pairings) against the amino acid translations of the sequences cloned (cv. Paragon) from the corresponding workflows presented in Figure 4.3 (Cloned, lower of pairings). Red boxes indicate amino acid changes between cloned TaZIPs, with genome sequence predictions.

4.3.2 *zrt1/zrt2* yeast complementation

To determine the Zn transport ability of the five *TaZIPs* cloned in Section 4.3.1 each gene was tested for its ability to complement the *zrt1/zrt2* mutant yeast strain. Following the cloning of the *TaZIPs* into the yeast expression vector pYES2 as described in the previous section, the *zrt1/zrt2* mutant yeast strain and the wild type of this strain (DY1457) were transformed with the pYES2*TaZIP* vectors and an empty pYES2 vector as a control, as described in Section 2.5.2.1. Transformations were confirmed using colony PCR with pYES2 backbone primers as described in Section 2.3.4. Figure 4.5 shows amplifications for five colonies of each transformation. Positive colonies were chosen from these and used in the subsequent complementation assay.

TaZIP expression was induced prior to the plating of the drop spot assay through growth of the transformed yeast in galactose-containing media as described in Section 2.5.2.1. pYES2 contains a *GALI* promoter upstream of the multiple cloning site. Following *TaZIP* induction, drops of culture serial dilutions were plated on selective media containing sufficient Zn for growth of the mutant yeast strain (200 μ M Zn) and media with Zn absent containing increasing levels of the Zn chelator EGTA (0 mM to 7.5 mM EGTA). The *zrt1/zrt2* mutant yeast strain is defective in both the *ZRT1* high affinity Zn uptake transporter (Zhao and Eide, 1996a) and the *ZRT2* low affinity Zn uptake transporter (Zhao and Eide, 1996b). As shown in Figure 4.6, the *zrt1/zrt2* strain transformed with the empty pYES2 vector was able to grow at Zn levels of 200 μ M to a similar extent of that shown by the wild type strain DY1457. However, the addition of EGTA chelator reduced growth of this mutant yeast strain. This was evident at concentrations of 5 mM and 7.5 mM, where the Zn-deficient phenotype of this strain could be clearly seen.

Heterologous expression of the five *TaZIPs* partially rescued the Zn-deficient phenotype exhibited by the *zrt1/zrt2* mutant yeast strain (Figure 4.6). Growth levels in the Zn-deficient media (notably 5 mM EGTA and 7.5 mM EGTA) were higher in the *zrt1/zrt2* strain expressing the *TaZIP* containing pYES2 vectors compared to the empty pYES2 vector. Although all *TaZIPs* investigated showed good ability to rescue the mutant *TaZIP5* showed strong rescue ability when compared to the other *TaZIPs* at the 7.5 mM EGTA concentration. Growth levels were not fully restored through the expression of any of the *TaZIPs*, as growth of the empty pYES2 containing wild type were still greater at all EGTA concentrations.

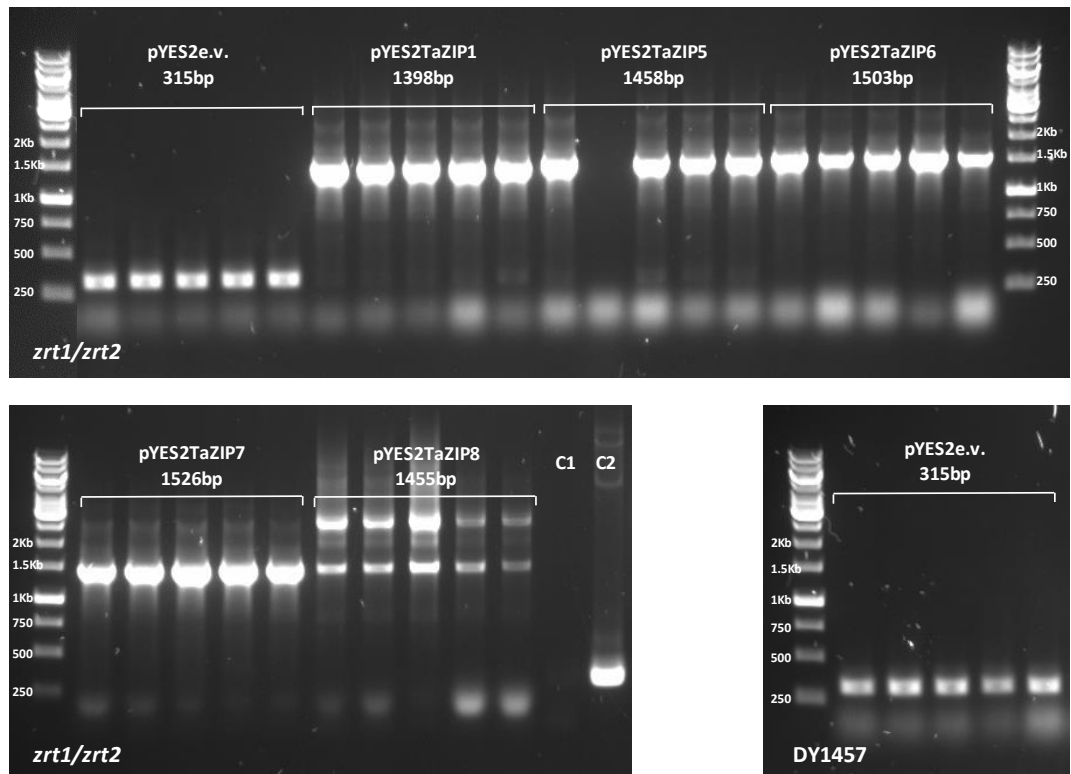


Figure 4.5. Colony PCR confirmation of pYES2TaZIP transformation into the *zrt1/zrt2* mutant yeast strain. Transformed *zrt1/zrt2* and wild type DY1457 yeast colonies showing the amplification of the pYES2TaZIPs and empty vector (pYES2e.v.), confirming successful transformation. Backbone primers used across all amplifications are Gal1p Forward and CycTerm Reverse as detailed in Section 2.3.4. Expected sizes of individual amplicons are given below vector names. C1 is a negative PCR control lane containing no yeast colony. C2 is an empty vector control lane from a known stock of untransformed empty pYES2 vector. DNA ladder used in all gels is Thermo Scientific GeneRuler 1 kb.

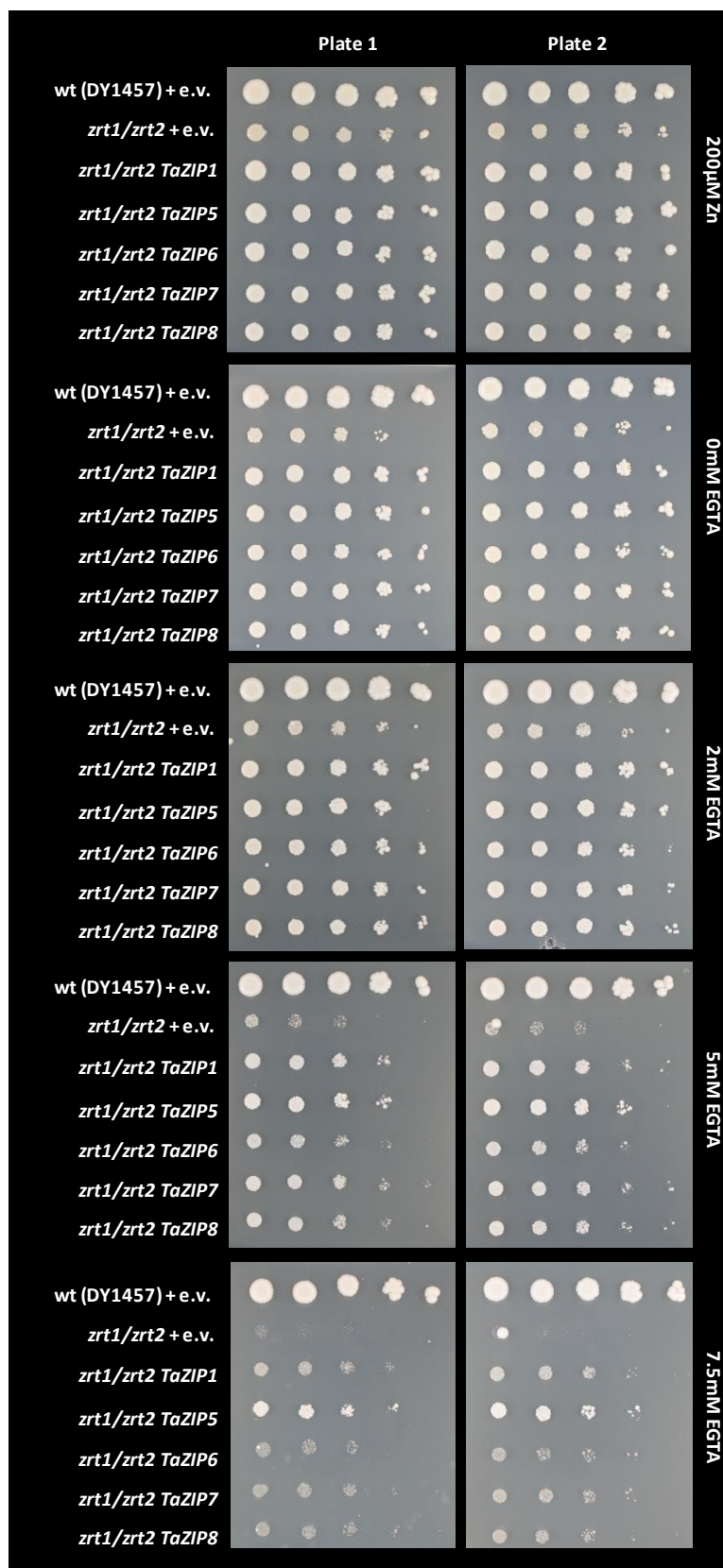


Figure 4.6. Complementation of the yeast Zn uptake mutant *zrt1/zrt2* with *TaZIP* genes. The yeast mutant *zrt1/zrt2* was transformed with five wheat *TaZIP* genes, shown here with empty vector controls (e.v.) in both the mutant and wild type. Two plate replicates are shown, with each spot being a dilution of the culture starting on the left of each plate (undiluted, 1/2, 1/10, 1/100, 1/1000). Complementation is shown following 8 days of growth, with the contents of selective media described to the right of each plate pair.

4.3.3 *zrc1/cot1* yeast complementation

To further investigate the possible role in Zn-homeostasis of the *TaZIPs* cloned in Section 4.3.1 each gene was tested for its ability to complement the *zrc1/cot1* mutant yeast strain. As previously described (Section 2.5.2.1), the *zrc1/cot1* mutant yeast strain and the wild type of this strain (BY4741) were transformed with the pYES2TaZIP vectors and an empty pYES2 vector as a control. Transformations were confirmed using colony PCR with pYES2 backbone primers (see Section 2.3.4). Figure 4.7 shows amplifications for five colonies of each transformation. Positive colonies were chosen from these and used in the subsequent complementation assay.

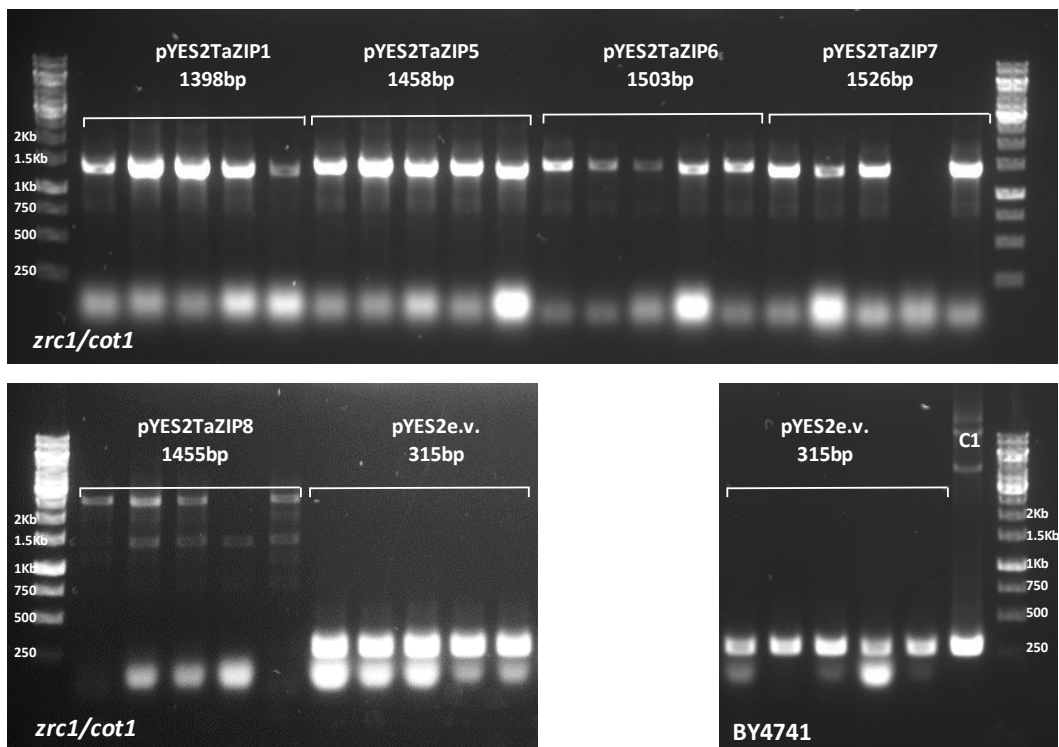


Figure 4.7. Colony PCR confirmation of pYES2TaZIP transformation into the *zrc1/cot1* mutant yeast strain. Transformed *zrc1/cot1* and wild type BY14741 yeast colonies showing the amplification of the pYES2TaZIPs and empty vector (pYES2e.v.), confirming successful transformation. Backbone primers used across all amplifications are Gal1p Forward and CycTerm Reverse as detailed in Section 2.3.4. Expected sizes of individual amplicons are given below vector names. C1 is an empty vector control lane from a known stock of untransformed empty pYES2 vector. DNA ladder used in all gels is Thermo Scientific GeneRuler 1 kb.

TaZIP expression was induced with galactose growth prior to plating of the drop spot assay. Serial dilutions were plated on selective media comprising of three Zn concentrations ranging from 0 mM Zn to 1 mM Zn (see Section 2.5.2.1 for full media details). The *zrc1/cot1* mutant yeast strain displays both Zn and cobalt (Co) sensitivity as it is defective in both the *ZRC1* vacuolar membrane Zn transporter and the *COT1* paralog that mediates both Zn and Co transport

into the vacuole (Conklin et al., 1992). This strain is unable to effectively sequester Zn into the vacuole, so at media Zn concentrations of 0.25 mM and above shows a Zn sensitive phenotype compared to the wild type strain. Figure 4.8 shows that growth of the *zrc1/cot1* strain is reduced at 0.25 mM Zn and at 1 mM Zn is completely unable to grow, whereas wild type growth continues unaffected.

Heterologous expression of the five *TaZIPs* in the *zrc1/cot1* mutant strain did not rescue the Zn-sensitivity exhibited by this mutant (Figure 4.8). In fact, *TaZIP1* and *TaZIP7* actually seemed to increase the Zn-sensitivity. At 0.25 mM there was barely discernible growth of the *TaZIP1* expressing *zrc1/cot1* yeast, and a slight reduction in growth of *TaZIP7* expressing *zrc1/cot1* yeast.

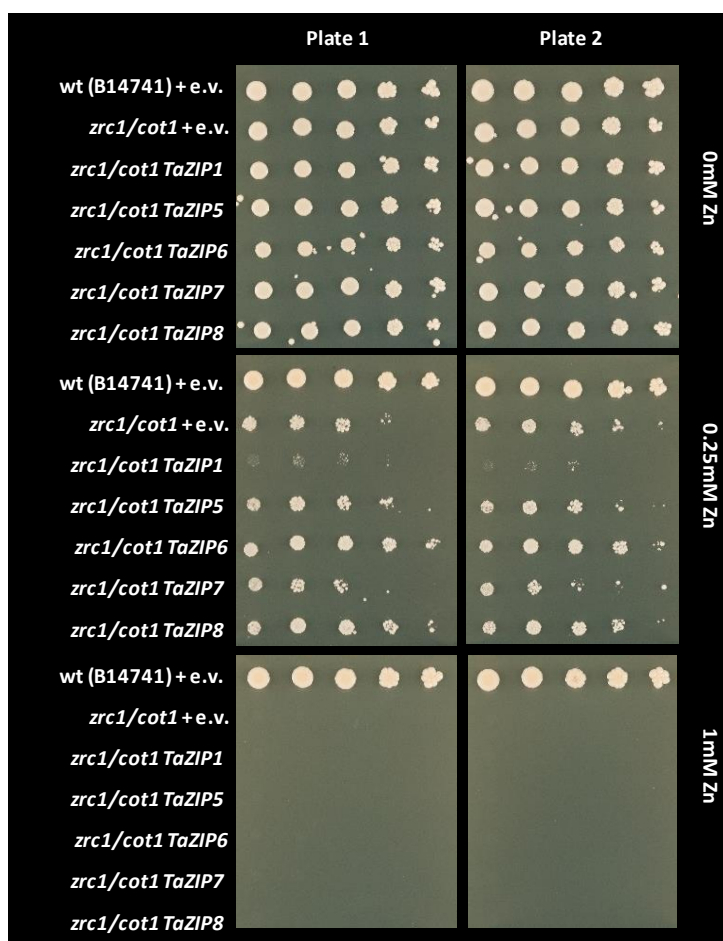


Figure 4.8. Complementation of the yeast Zn-sensitive mutant *zrc1/cot1* with *TaZIP* genes. The yeast mutant *zrc1/cot1* was transformed with five wheat *TaZIP* genes, shown here with empty vector controls (e.v.) in both the mutant and wild type. Two plate replicates are shown, with each spot being a dilution of the culture starting on the left of each plate (undiluted, 1/2, 1/10, 1/100, 1/1000). Complementation is shown following 5 days of growth, with the contents of selective media described to the right of each plate pair.

4.3.4 *fet3/fet4* yeast complementation

The *fet3/fet4* mutant yeast strain was transformed and tested to determine the Fe transport ability of the cloned *TaZIPs*. As previously discussed in Section 2.5.2.2 the pYES2*TaZIP* vectors and empty pYES2 controls were transformed into the *fet3/fet4* and the wild type DY1457 strains. Transformations were confirmed using colony PCR with pYES2 backbone primers (see Section 2.3.4). Figure 4.9 shows amplifications for five colonies of each transformation. Positive colonies were chosen from these and used in the subsequent complementation assay.

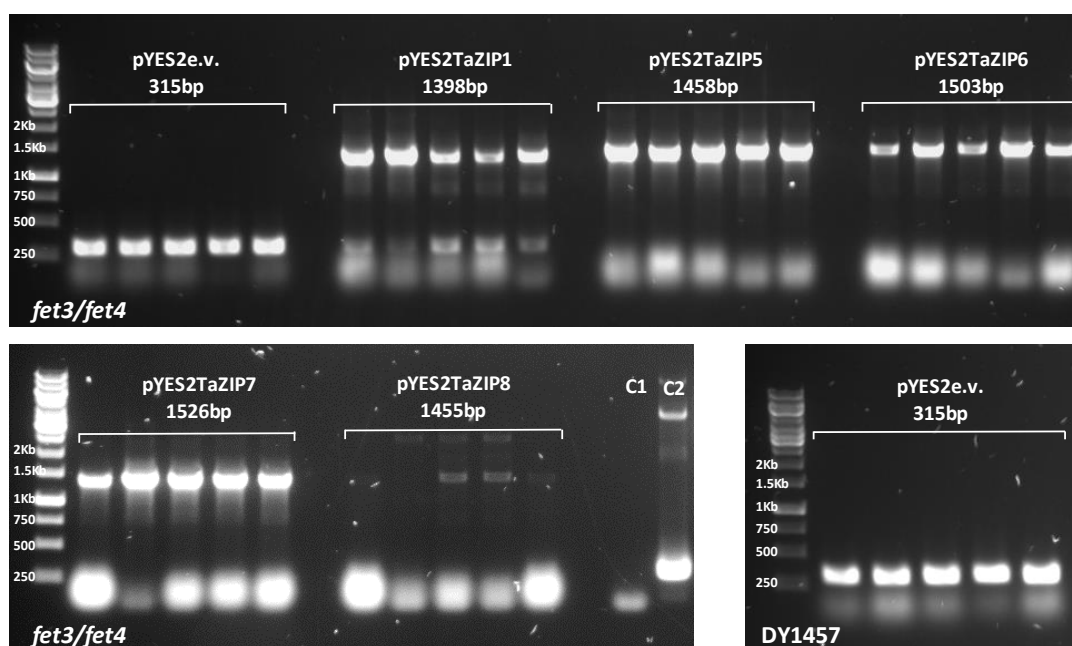


Figure 4.9. Colony PCR confirmation of pYES2*TaZIP* transformation into the *fet3/fet4* mutant yeast strain. Transformed *fet3/fet4* and wild type DY1457 yeast colonies showing the amplification of the pYES2*TaZIPs* and empty vector (pYES2e.v.), confirming successful transformation. Backbone primers used across all amplifications are Gal1p Forward and CycTerm Reverse as detailed in Section 2.3.4. Expected sizes of individual amplicons are given below vector names. C1 is a negative PCR control lane containing no yeast colony. C2 is an empty vector control lane from a known stock of untransformed empty pYES2 vector. DNA ladder used in all gels is Thermo Scientific GeneRuler 1 kb.

TaZIP expression was induced prior to the plating of the drop spot assay through growth of the transformed yeast in galactose containing culture. Following *TaZIP* induction serial dilutions drops were plated onto selective media with varying Fe concentrations. Fe concentrations were 10 μM for the highest concentration, 0.74 μM (the concentration commonly found in yeast growth media) and Fe completely absent (-Fe) (see Section 2.5.2.2 for full media concentrations). The *fet3/fet4* mutant yeast strain is defective in both the *FET3* high affinity Fe uptake transporter and the *FET4* low affinity Zn uptake transporter (Dix et al., 1994) and exhibits an Fe-deficient phenotype at higher Fe concentrations than the wild type strain. For the Fe-

deficient phenotype to be observed the strain was grown on plate media at a pH of 4. At 10 μ M Fe, *fet3/fet4* growth was similar to the wild type (DY1457) however at the basal 0.74 μ M and – Fe concentrations, growth was severely reduced compared to the wild type (Figure 4.10).

None of the five *TaZIPs* heterologously expressed rescued the Fe-deficient phenotype displayed by the *fet3/fet4* strain. This suggests that none of the *TaZIPs* investigated are functional Fe transporters.

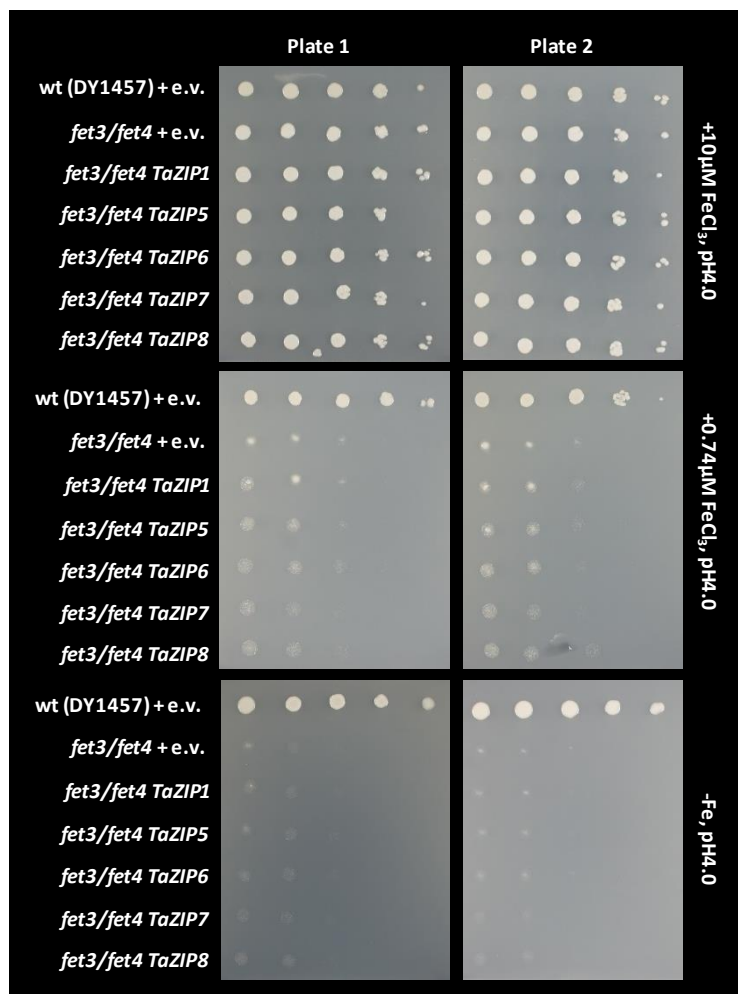


Figure 4.10. Complementation of the yeast Fe uptake mutant *fet3/fet4* with *TaZIP* genes. The yeast mutant *fet3/fet4* was transformed with five wheat *TaZIP* genes, shown here with empty vector controls (e.v.) in both the mutant and wild type. Two plate replicates are shown, with each spot being a dilution of the culture starting on the left of each plate (undiluted, 1/2, 1/10, 1/100, 1/1000). Complementation is shown following 3 days of growth, with the contents of selective media described to the right of each plate pair.

Taken together the results from the yeast complementation studies of the five TaZIPs presented in this Chapter, across the different yeast mutant strains used, suggests they have the ability to transport Zn, but not Fe (see Table 4.1 for complementation overview). Rogers et al. (2000) examined the altered metal selectivity in the *Arabidopsis* ZIP family member *AtIRT1*. The point mutations of particularly conserved residues of aspartic acid (D) at positions 100 or 136 with Ala (A) altered the substrate specificity of *AtIRT1*, eliminating the Fe and Mn transport ability whilst maintaining Zn transport ability. Figure 4.11 shows an alignment of the exact amino acid translations from the *TaZIPs* cloned and used in the heterologous studies in this chapter. The positions of the residues examined by Rogers et al. (2000) are shown in red and are also numbered. The presence of an alanine residue at position 100 compared to the consensus aspartic acid may explain the lack of Fe transport observed by TaZIP1-2AL, however no other differences are observed at the residues 100 or 136 that explain the lack of Fe transport. It was also observed in *AtIRT1* that substituting a glutamic acid at residue 103 to alanine stopped Zn transport, whilst maintaining Fe and Mn transport. Interestingly, TaZIP6-1BS in this study defied this consensus by being able to transport Zn and not Fe with an alanine residue at this position.

Table 4.1. Overview of TaZIP complementation ability across three mutant yeast strains. + and ++ indicate the level at which the yeast mutant phenotype was rescued by the *TaZIP* in question. - and -- indicate the level at which the mutant phenotype was exacerbated by the gene in question. No effect indicates the gene did not alter the yeast mutant phenotype.

Gene	Rescue ability		
	<i>zrt1/zrt2</i>	<i>zrc1/cot1</i>	<i>fet3/fet4</i>
<i>TaZIP1-2AL</i>	+	--	no effect
<i>TaZIP5-2BL</i>	++	no effect	no effect
<i>TaZIP6-1BS</i>	+	no effect	no effect
<i>TaZIP7-1DS</i>	+	-	no effect
<i>TaZIP8-2BS</i>	+	no effect	no effect

Chapter 4. Cloning and functional characterisation of TaZIPs

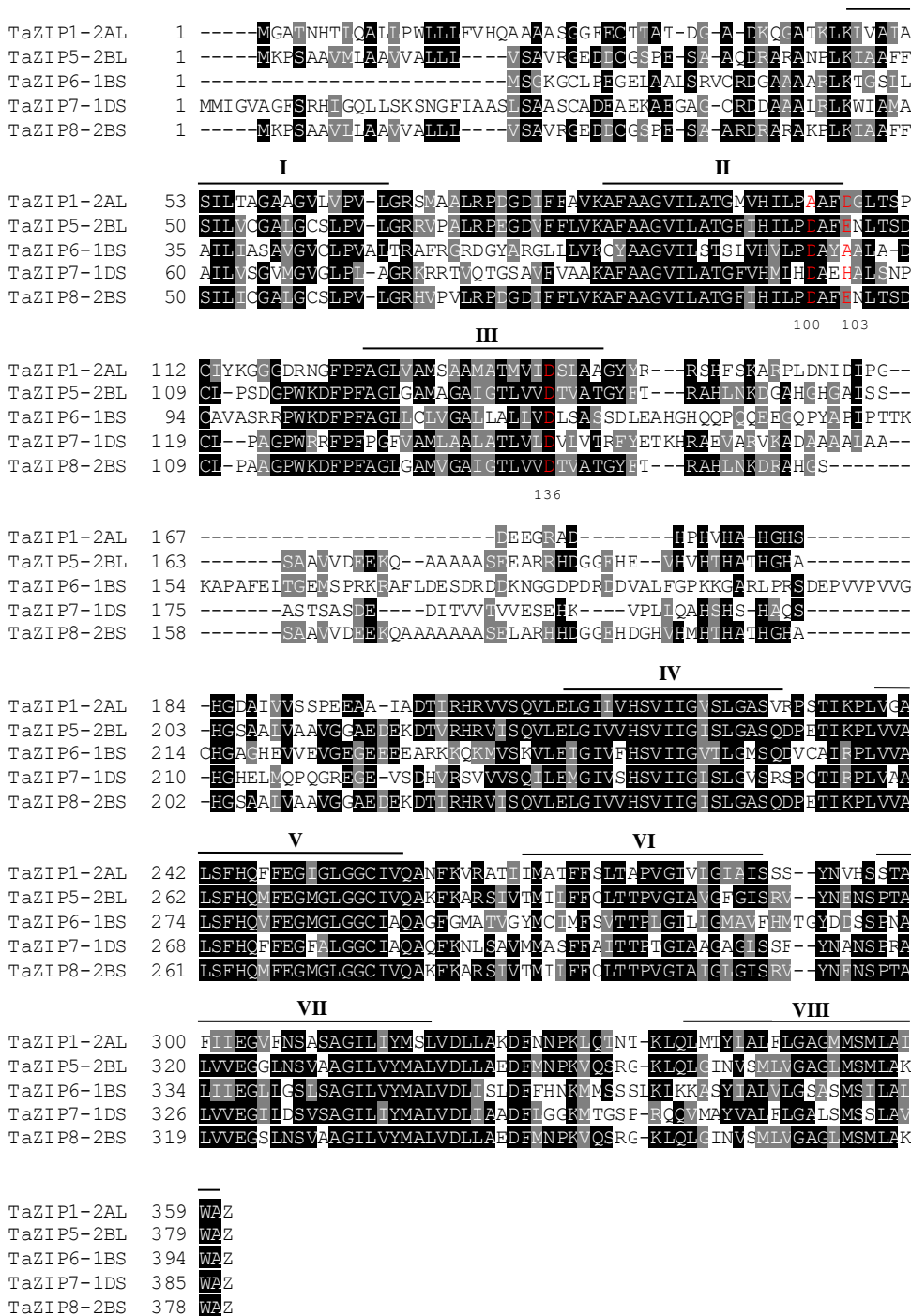


Figure 4.11. Multiple sequence alignment of TaZIPs cloned from cv. Paragon used in yeast heterologous expression studies. The muscle algorithm (Edgar, 2004) was used for this alignment of sequences and the Boxshade software was used to generate this figure. Shown in red, with amino acid number positions given are the three residue positions at which Rogers et al. (2000) showed a change from Glu (E) or Asp (D) to Ala (A) altered the substrate specificity of AtIRT1. The predicted TM domains of TaZIP1-2AL are shown. TM predictions made using HMMTOP (Tusnády and Simon, 2001).

4.4 Discussion

4.4.1 The role of TaZIPs in the transport of Zn

The predicted sequences of five *TaZIPs* identified from the wheat genome database were confirmed through cloning. SNPs that lead to amino acid changes were present in both *TaZIP5-2BL* and *TaZIP6-1BS*. *TaZIP5-2BL* contained three SNPs that resulted in amino acid substitutions. These were located toward the N terminus, before any predicted TM domains. The methionine present in the place of the predicted leucine at amino acid position 8 is a leucine in the closest homologs of *TaZIP5-2BL* (*HvZIP13*, *BdZIP13* and *OsZIP8*) as well as the cv. Chinese Spring *TaZIP5* homeologs on the A and D genomes. The other amino acid changes present at positions 19 and 24 of *TaZIP5-2BL* also contradict the translations of *HvZIP13* and *OsZIP8*, however these residue changes are the same as those present in *BdZIP13*. The single amino acid change in *TaZIP6-1BS* was located at the end of the predicted third TM domain at amino acid position 129, this residue change was a histidine residue substituted with an aspartic acid residue both of which have quite different characteristics; histidine being basic and aspartic acid being acidic. In the homologs of *TaZIP6* (*HvZIP6*, *BdZIP6* and *OsZIP6*), as well as the cv. Chinese Spring homeologs on the A and D genome, there is a histidine residue at this position. The SNPs are likely due to the varietal variation that exists between the cultivar used for the cloning of the *TaZIPs* (cv. Paragon) and the wheat genome database used in the bioinformatics prediction of *TaZIPs* being based on reads from the Chinese Spring cultivar. SNP rates were in keeping with those previously found across 21 hexaploid wheat varieties, where an average of five varietal SNPs per kilobase were present (Allen et al., 2011). However, although polymerase with 3' to 5' exonuclease (proofreading) activity was used in amplifications, the SNP that results in the amino acid change at position 129 of *TaZIP6-1BS* should be investigated further in other wheat cultivars due to its location in an otherwise strongly conserved TM domain and the different characteristics of residues concerned. The cloning of the *TaZIPs* presented in this chapter confirms their expression *in-planta* and validates the coding sequence predictions made during the identification and bioinformatics analysis of ZIP family members in wheat.

The Zn transport ability of the five cloned *TaZIPs* was examined through heterologous expression in two mutant yeast strains; *zrt1/zrt2* and *zrc1/cot1*. The Zn-deficiency phenotype of *zrt1/zrt2* observed under low Zn media concentrations was partially rescued by all five of the *TaZIPs* tested. The *zrt1/zrt2* rescue ability varied across the five *TaZIPs* examined, with *TaZIP5* complementing the mutant to a notably greater extent than *TaZIP1*, *TaZIP6*, *TaZIP7* and *TaZIP8* at the highest chelator concentration (7.5 mM EGTA). Interestingly, Pedas et al. (2009) tested the same Zn-uptake mutant yeast strain with four *HvZIPs*: *HvIRT1*, *HvZIP3* (close homolog of *TaZIP1*), *HvZIP5* (close homolog of *TaZIP4*) and *HvZIP8* (closest wheat homolog is *TaZIP4*). A

similar trend was observed with a differential rescue ability being observed across the HvZIPs. The only homolog to these in the selection of TaZIPs investigated in this chapter is TaZIP1 which is the homolog of HvZIP3. Of the four HvZIPs studied by Pedas et al. (2009) HvZIP3 was least effective at rescuing the mutant. This is supported by results shown in this study, where TaZIP1 showed a lesser rescue ability of *zrt1/zrt2* compared to TaZIP5 at the highest chelator concentration (7.5 mM EGTA).

The differential degree of *zrt1/zrt2* complementation ability could be due to the TaZIPs being either high- or low-affinity Zn transporters. TaZIP5 could be a high-affinity transporter more adept at transporting Zn when present in lower concentrations, whereas the other TaZIPs tested could be low-affinity transporters less capable of transporting Zn when it is present in only low concentrations. Indeed, Grotz et al. (1998) showed that the K_m values across three AtZIPs: AtZIP1, AtZIP2 and AtZIP3 varied significantly, suggesting differential affinities of the transporters. In order to validate this hypothesis with regard to the TaZIPs studied in this thesis, additional protein analysis and kinetic assays would have to be performed. Isolation and purification for further direct transport studies of these ZIPs would be useful.

Differential ability of the closely related TaZIP5-2BL and TaZIP8-2BS to rescue the *zrt1/zrt2* mutant strain was observed. The alignment of these two genes in Figure 4.11 shows they are closely related; they share 93.4% sequence identity at the amino acid level yet they have very different functional abilities in the rescue of the *zrt1/zrt2* strain. Differences exist between these two genes between TM III and IV. Previously this region has been proposed to be involved in metal binding of the ZIP transporters and contributing to Zn transport and regulation (Guerinot, 2000). A suggestion is that the presence of the residue sequence, HGAISS between TMs III and IV present in TaZIP5-2BL and TaZIP8-2BS may play a role in altering the affinity and functioning of this protein. If these two closely related genes have different localisations in the plant and roles in the Zn regulatory network, these slight changes in Zn transport characteristics may be favourable. For example, the optimal transport rate required for a ZIP functioning in Zn uptake from the rhizosphere may be different to that of a ZIP functioning in phloem loading during nutrient remobilisation at senescence. In order to investigate these proteins further it would be logical to delete the HGAISS region from TaZIP8-2BS and compare the *zrt1/zrt2* rescue ability and enzyme kinetic values with that of TaZIP5-2BL. Additionally, discovering the exact *in-planta* expression pattern of individual TaZIPs such as the closely related TaZIP5 and TaZIP8 genes will provide information that will advance the potential use of these genes for biofortification purposes.

The ability of the five TaZIPs to rescue the *zrc1/cot1* Zn-sensitive mutant was also tested. The *zrc1/cot1* mutant yeast strain displays Zn sensitivity as it is defective in the ZRC1 vacuolar membrane transporter which is vital in the sequestration of Zn to the vacuole when Zn in the growth media is present at high concentrations. None of the TaZIPs tested rescued the *zrc1/cot1*

mutant strain under high Zn conditions suggesting they do not have a role in the transport of Zn into the vacuole. Furthermore, the expression of TaZIP1 and to a lesser extent TaZIP7 actually increased the Zn-sensitivity of *zrc1/cot1*. This could be further examined using additional Zn media concentrations between the 0.25 and 1 mM Zn range used in this study to assess if other TaZIPs confer a sensitive phenotype. There are two potential hypotheses for the increased Zn sensitivity displayed by *zrc1/cot1* when expressing TaZIP1 and TaZIP7. Firstly, it could be that TaZIP1 has a role in the efflux of Zn out of the vacuole. If this is the case, under high Zn conditions the Zn-sensitive phenotype of *zrc1/cot1* would be exacerbated as more Zn is being pumped out of the vacuole and other, more Zn-sensitive areas of the cell are being exposed to a detrimentally high Zn concentration. Yeast does have a Zn efflux protein that functions in the transport of Zn from the vacuole *ZRC3* (MacDiarmid et al., 2003). It seems unlikely that under high Zn conditions the native *ZRC3* would be expressed, but due to the galactose inducible promoter present in the pYES2TaZIP1-2AL vector this may be working in concert with *ZRC3* or alone in this function. If the function of TaZIP1 is in the efflux of Zn from the vacuole this could be another alternative explanation to the rescue of the Zn uptake mutant strain *zrt1/zrt2*. Under low concentrations TaZIP1 may pump Zn that has been accumulated in the vacuole during previous growth stages prior to plating, in conjunction with *ZRC3* and partially rescue the phenotype as observed.

The second hypothesis for the increased Zn-sensitivity shown by the TaZIP1 expressing *zrc1/cot1* strain is that TaZIP1 may be localised to the plasma membrane and transports Zn into the cell, as the partial rescue ability of *zrt1/zrt2* suggests, thus increasing the Zn-sensitivity of the *zrc1/cot1* phenotype. However why this is observed in only TaZIP1 (and to a lesser extent TaZIP5), but not the other TaZIPs examined is unclear. There may be post-transcriptional mechanisms able to downregulate the protein expression of TaZIPs in the *zrc1/cot1* strain however for some reason this is less effective at downregulating TaZIP1 than the other TaZIPs examined. In order to fully understand the cellular location and function of the TaZIPs, localisation studies using green fluorescent protein (GFP) tags downstream of the full length TaZIPs (without stop codons) in a yeast expression vector would be useful.

4.4.2 TaZIP1, 5, 6, 7 and 8 seem unable to transport Fe

None of the TaZIPs tested in this study were able to rescue the *fet3/fet4* Fe-uptake mutant yeast strain. This suggests that none are able to transport Fe and may have quite a selective substrate range. Pedas et al. (2009) showed that HvZIP3, HvZIP5 and HvZIP8 were also unable to complement the Fe uptake mutant *fet3/fet4*. Additionally, it was shown that these HvZIPs were unable to complement the Mn mutant strain *smf1* and the Cu mutant strain *ctr1*. The fact that the TaZIPs were shown to transport Zn, but not Fe in this study suggests the TaZIPs examined may have a similar narrow substrate range. The mechanistic determination of this substrate specificity

is unknown. Rogers et al. (2000) showed through the use of point mutations that the substrate specificity of AtIRT1 could be altered from Mn, Fe and Zn to just Zn through the change of amino acids at positions 100 (D, aspartic acid), 136 (D, aspartic acid) or 100 and 103 combined (D, aspartic acid and E, glutamic acid respectively) to alanine (A) residues. These positional changes likely explain the Zn specificity and lack of Fe transport seen in TaZIP1, TaZIP6 and possibly TaZIP7 as substitutions of residues in positions 100 or 103 are in keeping with the alterations in specificity seen by Rogers et al. (2000). More specifically TaZIP1 has an alanine (A) at position 100, not an aspartic acid (D). TaZIP6 has an alanine (A) at position 103, not an aspartic acid (D). TaZIP7 has a histidine (H) residue at position 103 rather than an aspartic acid (D) or glutamic acid (E), which is untested, but due to the quite different residue characteristics (positively charged side chain rather than negatively in a previously shown critical position) may affect the substrate specificity. However, the underlying cause of TaZIP5 and TaZIP8 being able to transport Zn but not Fe remains unanswered. Further Fe-dependent yeast strains such as *aft1/aft2* (Rutherford et al., 2001) could be tested to further examine the lack of rescue observed in TaZIP transformed *fet3/fet4* as observed in this study.

4.4.3 Conclusions

Five predicted *TaZIP* sequences have been confirmed by cloning and sequencing directly from *T. aestivum* (cv. Paragon) material. The ability of the encoded proteins to transport Zn differentially has also been proven. The combination of this data with the gene expression data (presented in Chapter 3), which showed upregulation under Zn-deficiency for four of the five *TaZIPs* investigated in this Chapter, provides a good starting point in unravelling the molecular basis of Zn uptake and transport throughout wheat. Confirming the exact location at both a cellular and plant level of *TaZIP* expression is a logical next step in order to further understand the role of this important membrane transporter family in wheat.

The exact location at which *TaZIPs* function in the plant remains unknown, however their confirmed ability to transport Zn and their expression profiles in response to Zn-deficiency indicates they are promising candidates for biofortification strategies. For example, the overexpression of any of the *TaZIPs* tested in this Chapter may increase Zn content in wheat by increasing Zn uptake from the soil. Alternatively directing this overexpression to the endosperm (through endosperm-specific promoters) may increase the Zn content of wheat grains. Similarly, overexpression of *TaZIPs* may increase the Zn translocation ratio, moving more Zn from the roots to the above ground portion of the plant; this increased Zn may be remobilised at senescence to the grain, improving the Zn content of the edible components. Testing these suggestions would be a logical next step in utilising this transporter family to achieve the goal of Zn-enriched wheat grains. Moreover, if the regulators of these TaZIPs can be identified and their mechanisms understood, this may provide an alternative and more effective route in using the TaZIPs to

increase Zn uptake as well as control partitioning through the plant. The group F TabZIPs identified in Chapter 3 may be promising candidates for this exact requirement. Further study of these TabZIPs and their role in the regulation of TaZIPs is however imperative, this is addressed in the next chapter.

Chapter 5. Cloning and functional characterisation of *T. aestivum* bZIPs

5.1 Introduction

Transcription factors are fundamental to much of the complexity observed across eukarya. The adaptable gene expression patterns exhibited through the life cycle of complex organisms is largely due to the binding of these small proteins to *cis*- regulatory DNA sequences present in the genome (Franco-Zorrilla et al., 2014). This binding often results in a change in the conformation of the transcription factor which alters the ability to interact and complex with other transcription factors and recruit RNA polymerase II (Levine and Tijan, 2003). Transcription factors are essential in orchestrating the controlled responses required for transition metal homeostasis in plants (Pilon et al., 2009).

Zn regulation has been shown to be dependent on two group F bZIP transcription factors in *Arabidopsis*; AtbZIP19 and AtbZIP23 (Assunção et al., 2010; Inaba et al., 2015). These bZIPs were initially identified using a yeast-one-hybrid assay with fragments of the *AtZIP4* promoter as bait. EMSA assays were then used to identify and confirm the specific binding regions within this promoter, subsequently termed the Zn-Deficiency Response Element (ZDREs). Assunção et al. (2010) demonstrated the ability of both bZIP19 and bZIP23 to bind to two and three tandem repeats of the ZDREs found in the promoter of *AtZIP4* using the EMSA technique. Moreover, when the TCGA core of the ZDRE was mutated to TAGA this binding was prevented.

In mutant *Arabidopsis* plants containing T-DNA insertions for *bzip19* and *bzip23* (*bzip19-1*, *bzip23-1*), reductions in root Zn concentration and overall root growth were observed when grown under Zn-deficient conditions (Assunção et al., 2010; Inaba et al., 2015). *Arabidopsis bzip19* mutants also showed a reduction in shoot Zn concentration and shoot growth (Assunção et al., 2010). When mutations are combined in the double mutant *bzip19-1bzip23-1* the phenotype is more severe (Assunção et al., 2010). The *Arabidopsis* mutant, *bzip19-1bzip23-1* loses the ability to regulate key Zn-responsive genes, including *AtZIP1*, 3, 4, 5, 9 and 10, as well as the nicotianamine synthase genes *AtNAS2* and *AtNAS4*, which all contain one or more copies of the ZDRE in their promoter (Assunção et al., 2010). Furthermore, non ZDRE containing genes were also differentially expressed, including the previously discussed (Section 1.4.2) *AtFRD3* (Assunção et al., 2010) suggesting another binding site may be recognised by bZIP19 and bZIP23, or alternatively the effect of their absence on the plant results in widespread disorder by disrupting the complex interplay of cellular processes reliant upon accurate Zn homeostasis.

Further analysis of the transcript levels of *AtZIP* membrane transporters in the single mutants *bzip19-1* and *bzip23-1*, has revealed information on regulatory interactions. *bzip23-1* mutants but not *bzip19-1* mutants are able to upregulate *AtZIP9* under Zn-deficient conditions. Conversely, *bzip19-1* mutants but not *bzip23-1* mutants are able to upregulate *AtZIP12* under Zn-deficient conditions (Inaba et al., 2015). *AtZIP7* and *AtZIP10* are also differentially affected in the two single mutant *bzip* lines. These gene specific effects of the two closely related bZIPs suggests that as well as operating in combination for certain genes, they also operate in isolation to control the regulation of specific ZIPs.

Currently the only reported functional work on a group F bZIP transcription factor in a monocotyledonous species is in the model organism *Brachypodium distachyon*; BdbZIP10, Bd1g30140.1 (termed BdbZIP11 in Chapter 3) (Glover-Cutter et al., 2014). When overexpressed, this *BdbZIP* led to an upregulation of key oxidative stress response genes, as well as the putative Zn-responsive ZIP gene, *BdZIP3*. Interestingly of the three Zn-responsive genes analysed, overexpression of *BdbZIP10* only induced the expression of *BdZIP3* and not of *BdZIP5* or *BdNAS4*. This may suggest that heterodimer formation is important in the control of a suite of Zn-responsive genes by group F bZIPs, or that the targets of individual bZIPs are quite specific.

At present there is little published information on the functional importance of group F bZIPs in the Zn-deficiency response of crop species. Previously in Chapter 3, seven group F *bZIPs* were identified in the wheat genome. Expression analysis of four of these bZIPs showed upregulation under Zn-deficient conditions, indicating a role in the Zn-homeostasis network of wheat. In this Chapter, the ability of four wheat bZIPs to complement an independently created *Arabidopsis bzip19-4bzip23-2* mutant (Nazri, Z and Williams, L. E., unpublished) is investigated to establish if the role of these TabZIPs is analogous to *AtbZIP19* and *AtbZIP23* previously confirmed to be essential in the Zn-regulatory mechanism of *Arabidopsis*. Additionally, the promoter regions of the *TaZIP* transporters, identified in Chapter 3, are analysed for the presence of putative ZDRE sequences. The binding of representative wheat bZIPs to these identified wheat ZDREs is also tested in order to explore links between the functionally characterised TaZIPs (Chapter 4) and the group F TabZIPs within the Zn-homeostasis network of wheat.

5.2 Aims

- Clone identified *TabZIPs* from hydroponically grown *T. aestivum* cv. Paragon.
- Examine sequence similarities of cloned *TabZIPs* to wheat genome database sequence predictions.
- Use the cloned *TabZIPs* to transform the *Arabidopsis* double mutant *bzip19-4bzip23-2* line to test functional complementation. By testing functional complementation, we aim to determine the importance of the group F *TabZIPs* identified in the Zn-regulatory framework of wheat.
- Determine if ZDRE motifs exist in the promoter regions of the *TaZIPs* identified in Chapter 3. Determine if the *TabZIPs* are able to bind to these putative ZDRE motifs. This will provide further insight into the mechanistic basis of the Zn-regulatory response in wheat.

5.3 Results

5.3.1 Cloning of TabZIPs

Four of the group F *TabZIPs* identified in Chapter 3 were cloned using the directional TOPO® cloning system (Invitrogen, CA, USA). *TabZIPs* were cloned into the destination vector pMDC32 (Curtis and Grossniklaus, 2003), which contains the strong constitutive promoter, dual 35S CaMV (cauliflower mosaic virus 35S promoter). Initially, cDNA synthesised from plant RNA obtained in the Zn-starvation hydroponic experiments was used to amplify *TabZIPs* identified previously, using the TOPO primers detailed in Table 2.4. Following successful amplification of promising blunt end products, gel extractions were carried out and resulting products were cloned into the TOPO® pENTR/D entry vector as detailed in Section 2.4.1 and subsequently transformed to One Shot® TOP10 cells. Resulting colonies were screened as outlined in Section 2.3.4 and the plasmid contained in any promising colonies was subjected to restriction enzyme digest to confirm the gene of interest (see Section 2.3.5). Subsequently, genes were shuttled from the pENTR vector to the pMDC32 destination vector using the LR clonase™ kit as outlined in Section 2.4.2. Again, colonies were screened and diagnostic restriction enzyme digests were conducted before plasmids were sent for sequencing (see Section 2.3.6 for further details). In this section, the cloning of four group F wheat *bZIPs* as well as *TabZIPG-5DL* are outlined and their sequences are compared to the genomic predictions.

5.3.1.1 TabZIP1-7DL

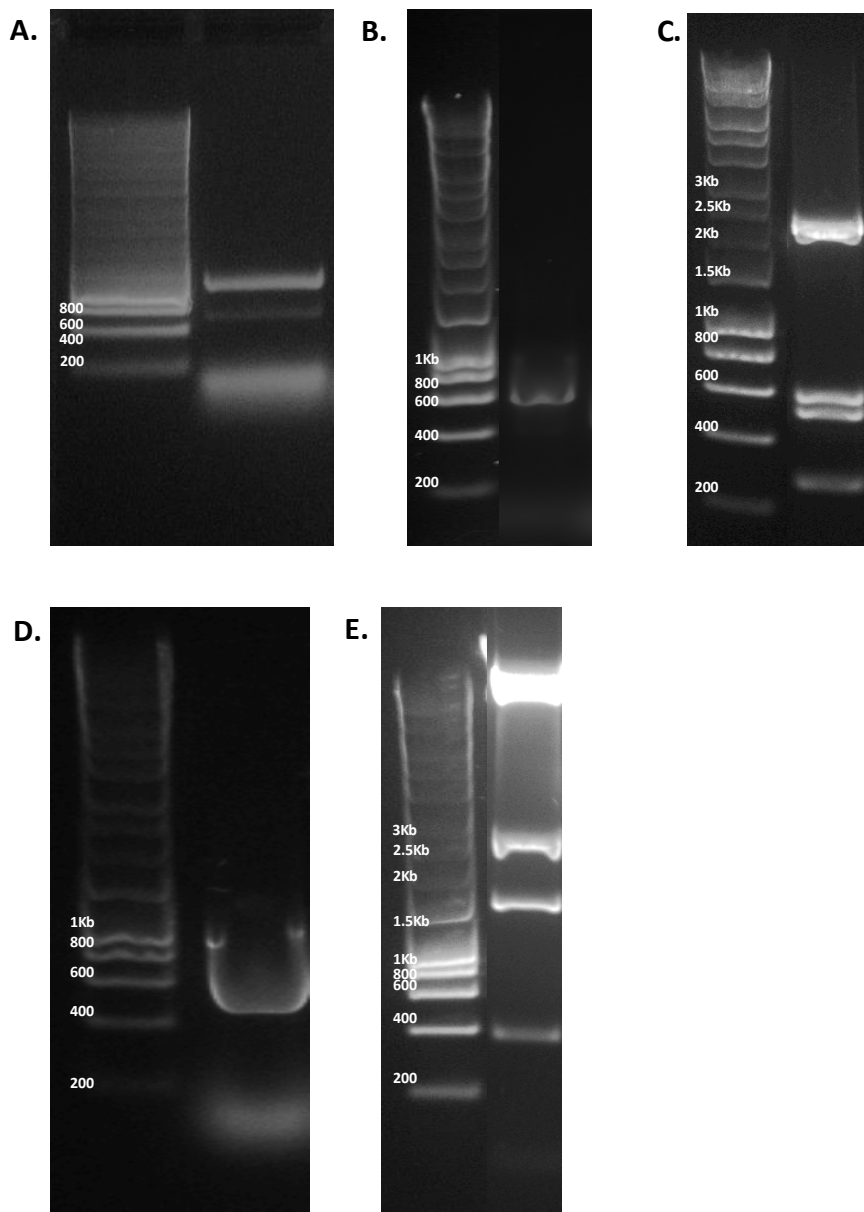


Figure 5.1. Cloning of TabZIP1-7DL into pMDC32 *Arabidopsis* expression vector. **A.** Initial amplification of a blunt ended fragment from shoot cDNA using TabZIP1TOPO primers (expected size 757 bp). **B.** Colony PCR of a positive One Shot® TOP10 colony containing pENTRTabZIP1 screened using TabZIP1TOPO primers. **C.** PvuII digestion of pENTRTabZIP1 with the expected fragments of 1942, 591, 520 and 280 bp present. **D.** Colony PCR of a positive DH5α colony containing pMDC32TabZIP1 screened using TabZIP1TOPO primers. **E.** XhoI digestion of pMDC32TabZIP1 with the expected fragments of 7587, 1720, 1094 and 413 bp present. DNA ladder used in all gels is Bioline Hyperladder 1 kb.

Figure 5.1 shows a detailed workflow following the cloning procedure of *TabZIP1-7DL* into the pMDC32 *Arabidopsis* expression vector. The alignment of the amino acid translation of the cloned *TabZIP1-7DL* homeolog with the amino acid translation of the predicted coding sequence shown in Figure 5.2 shows there are no amino acid differences between the protein translations. The two group F motifs described by Jakoby et al. (2002) are shown underlined in

this alignment, as is the general bZIP domain. As previously discussed in Chapter 3, the 3' end of the first group F motif does not fit the predicted consensus perfectly, with the final three amino acids deviating from the expected motif 1 sequence.

```

Prediction      MDDGDIDFSNPETFLCEAMGNDPPASCMSMGTYFDDILNGDTHLACTHTHTCNPPVHDLA
Cloned          MDDGDIDFSNPETFLCEAMGNDPPASCMSMGTYFDDILNGDTHLACTHTHTCNPPVHDLA
                *****

Prediction      HHTHTCVHVHTKILSASDDAAETSESLPESKKQRPSGNRAAVRKYREKKAHTALLEEV
Cloned          HHTHTCVHVHTKILSASDDAAETSESLPESKKQRPSGNRAAVRKYREKKAHTALLEEV
                *****

Prediction      AHLKAVNQQLVKKLQSHSALEAEVARLRCLLVDIRGRIEIGEIGTFPYQRTVKSNDFVDQG
Cloned          AHLKAVNQQLVKKLQSHSALEAEVARLRCLLVDIRGRIEIGEIGTFPYQRTVKSNDFVDQG
                *****

Prediction      SFLGGAQVMNSCGFRCNDQLYCNPGMQQARTMDDDGVMMSGQVLGQAGDSMGCVKPGSLN
Cloned          SFLGGAQVMNSCGFRCNDQLYCNPGMQQARTMDDDGVMMSGQVLGQAGDSMGCVKPGSLN
                *****

Prediction      PPGCRGGQMLZ
Cloned          PPGCRGGQMLZ
                *****
    
```

Figure 5.2. Amino acid alignment of cloned TabZIP1-7DL with the predicted sequence. Alignment created using Clustal omega, showing the predicted amino acid sequence of TabZIP1-7DL from the wheat genome database (Prediction, top of pairing) against the amino acid translation of the sequence cloned from the workflow presented in Figure 5.1 (Cloned, lower of pairing). The two group F motifs are underlined in consensus with the sequence prediction by Jakoby et al. (2002); motif 1 C[ST]HTH[ST]CNP[PT]GPE, motif 2 H[ST]HTC[FL]H[AV]HT. The bZIP domain common to all bZIP groups is also underlined, the consensus of which is N-x₇-R/K-x₉-L-x₆-L-x₆-L.

5.3.1.2 TabZIP3b-7BL, TabZIP4-7AL, TabZIP4-7DL and TabZIPG-5DL

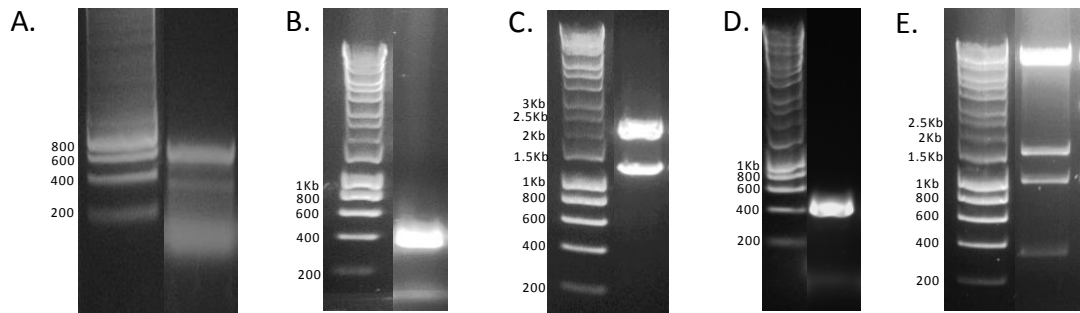
Figure 5.3 shows the cloning workflow for three further group F motifs: TabZIP3b-7BL, TabZIP4-7AL and TabZIP4-7DL as well as TabZIPG-5DL. The amino acid alignments with the genes cloned and their respective predictions from the wheat genome databases are shown in Figure 5.4. The amino acid alignment of the cloned *TabZIP3b-7BL* homeolog with that predicted from the genome databases shows the cloned homeolog is exactly as expected (Figure 5.4A). The first group F motif in this homeolog is completely truncated and not present in this homeolog. This truncation has also been confirmed through amplification and subsequent sequencing of this gene from a field grown cv. Paragon genomic DNA preparation. The truncation of the first group F motif in TabZIP3b-7BL can be seen clearly in Figure 5.4B, where an amino acid alignment of TabZIP3b-7DL with the homeolog TabZIP3b-7BL is shown with the group F motif 1 highlighted in yellow.

The amino acid alignments of the TabZIP4-7AL gene cloned, aligned with the predicted amino acid sequence based on information in genome sequence databases is provided in Figure 5.4. Two amino acid substitutions are present between the predicted sequence and that cloned. These substitutions are likely the result of varietal SNPs between the cultivar used in the genomic sequence database construction (cv. Chinese Spring) and that of the material used to clone this gene (cv. Paragon).

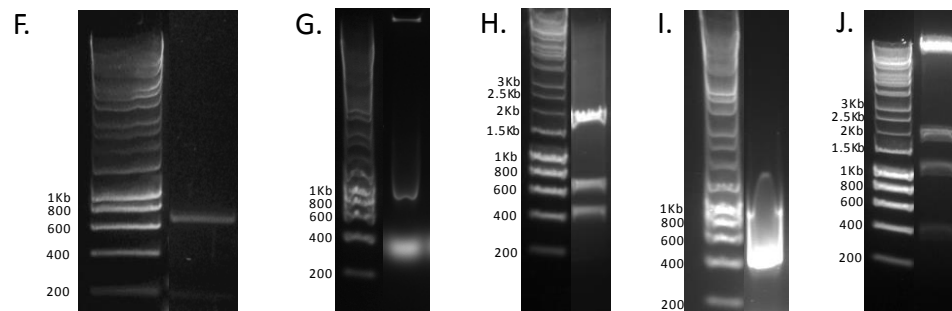
Figure 5.4 shows an amino acid alignment of the TabZIP4-7DL gene, aligned with the predicted amino acid sequence based on information from genome sequence databases. An amino acid substitution is present near the N terminus of this protein which again is most likely due to a varietal SNP. Unlike in TabZIP4-AL, the first group F motif in this TabZIP4 homeolog is weakly conserved with only three residues of the predicted motif being present. When TabZIP4-7DL was originally discovered in the genome sequence databases it was thought that an erroneous insertion of a thymine nucleotide was present, resulting in an early stop codon. When this nucleotide insertion was omitted the subsequent amino acid translation was closer to the translations of the homeologous genes. Full length TOPO cloning primers were therefore designed to amplify past this region, to the stop codon for the other TabZIP4 homeologs. However, cloning of this gene confirmed the presence of the early stop codon shown in red in Figure 5.4. A non-coding region at the 3' end of this gene was therefore also inserted into the pMDC32 vector, but as this is at the 3' end it is unlikely to affect the use of this vector in subsequent *Arabidopsis* complementation experiments. Figure 5.5 shows a multiple alignment of the group F TabZIPs cloned in this section with AtbZIP19 and AtbZIP23, where the less conserved group F motif 1 present in TabZIP3b-7BL and TabZIP4-7DL can be seen.

In addition to the four group F bZIPs cloned and detailed in this section a bZIP from a different group was also cloned to allow for an additional control in subsequently discussed binding assays (see Section 5.3.3.2). This group G bZIP is the non-group F control used in the gene expression analysis data presented in Chapter 3. The homeolog of this gene that was cloned was shown to be TabZIPG-5DL (for full cloning workflow see Figure 5.3). This bZIP was cloned using the pGEM-T Easy cloning method outlined in Section 2.4.3. TabZIPG-5DL was not subsequently cloned into the *Arabidopsis* transformation vector pMDC32 as it was not used for functional complementation studies. Figure 5.4 shows the alignment of the amino acid translation of the TabZIPG-5DL sequence cloned with the predicted amino acid sequence based on information from genome sequence databases. Three amino acid substitutions are present which are likely the result of varietal SNPs. The three characteristic group G motifs are also shown underlined in Figure 5.4.

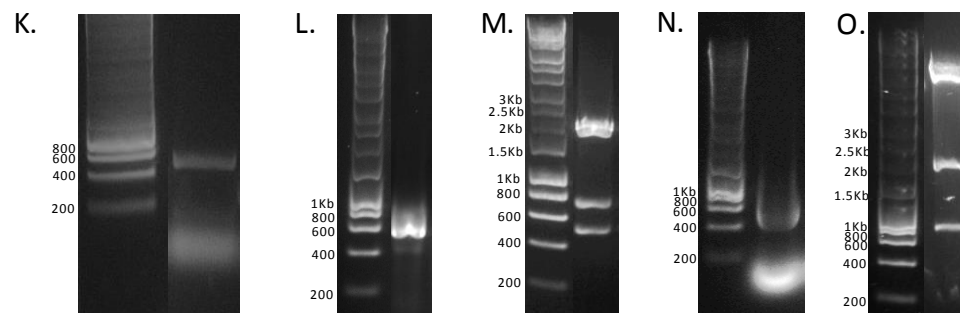
TabZIP3b-7BL



TabZIP4-7AL



TabZIP4-7DL



TabZIPG-5DL

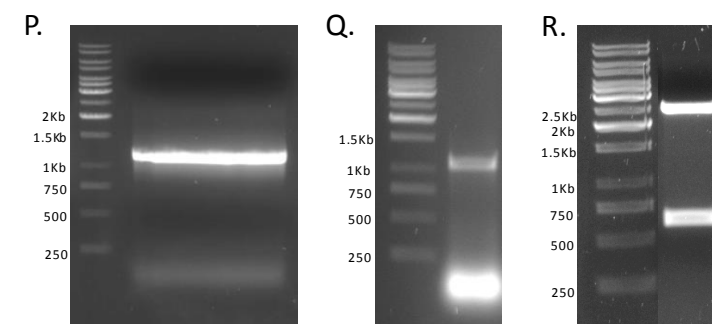


Figure 5.3. Cloning of TabZIP3b-7BL, TabZIP4-7AL, TabZIP4-7DL and TabZIPG-5DL. Composite figure showing the cloning workflow of the following TabZIPs: TabZIP3b-7BL (A.-E.). **A.** Initial amplification of a blunt ended fragment from shoot cDNA using TabZIP3bTOPO primers (expected size 531 bp). **B.** Colony PCR of a positive One Shot® TOP10 colony containing pENTRTabZIP3b screened using TabZIP3bTOPO primers. **C.** PvuII digestion of pENTRTabZIP3b with the expected fragments of 1942 and 1205 bp present. **D.** Colony PCR of a positive DH5α colony containing pMDC32TabZIP3b screened using TabZIP3bTOPO

primers. **E.** XhoI digestion of pMDC32TabZIP3b with the expected fragments of 7587, 1570, 1094 and 409 bp present.

TabZIP4-7AL (F.-J.). F. Initial amplification of a blunt ended fragment from root cDNA using TabZIP4TOPO primers (expected size 712 bp). **G.** Colony PCR of a positive One Shot® TOP10 colony containing pENTRTabZIP4-7AL screened using TabZIP4TOPO primers. **H.** PvuII digestion of pENTRTabZIP4-7AL with the expected fragments of 1942, 797 and 549 bp present. **I.** Colony PCR of a positive DH5α colony containing pMDC32TabZIP4-7AL screened using TabZIP4TOPO primers. **J.** XhoI digestion of pMDC32TabZIP4-7AL with the expected fragments of 7587, 1693, 1094 and 467 bp present.

TabZIP4-7DL (K.-O.). K. Initial amplification of a blunt ended fragment from shoot cDNA using TabZIP4TOPO primers (expected size 712 bp). **L.** Colony PCR of a positive One Shot® TOP10 colony containing pENTRTabZIP4-7AL screened using TabZIP4TOPO primers. **M.** PvuII digestion of pENTRTabZIP4-7DL with the expected fragments of 1942, 797 and 549 bp present. **N.** Colony PCR of a positive DH5α colony containing pMDC32TabZIP4-7AL screened using TabZIP4TOPO primers. **O.** XhoI digestion of pMDC32TabZIP4-7DL with the expected fragments of 7587, 2160 and 1094 bp present

TabZIPG-5DL (P.-R.). P. Initial amplification of a blunt ended fragment from root cDNA using TabZIPGTOPO primers (expected size 1167 bp). **Q.** Colony PCR of a positive DH5α colony containing pGEMTabZIPG-5DL screened using TabZIPG-5DL primers. **R.** EcoRI digestion of pGEMTabZIPG-5DL with expected fragment sizes of 2997 and 577/590 bp shown.

DNA ladder used in gels (**A.-O.**) is Bioline Hyperladder 1 kb and gels (**P.-R.**) is Thermo Scientific GeneRuler 1 kb.

TabZIP3b-7BL

A.

```
Prediction MDDGNLDCSSMGSYFDGILMDTEQVACCTHTHTCLHVHVKIAASASSDAGAETPAEFEDA
Cloned MDDGNLDCSSMGSYFDGILMDTEQVACCTHTHTCLHVHVKIAASASSDAGAETPAEFEDA
*****

Prediction HVTSRSKRRRPSGNQAAVRKYREKKAHTALLEEEAARLRAMNKELAKKVQDHAALEAEA
Cloned HVTSRSKRRRPSGNQAAVRKYREKKAHTALLEEEAARLRAMNKELAKKVQDHAALEAEA
*****

Prediction ARLHCLLVDRGRIEIGEIGAFPYQRRPAKGAGQGGAQVMSSCDFIATCEQPHTCFLZ
Cloned ARLHCLLVDRGRIEIGEIGAFPYQRRPAKGAGQGGAQVMSSCDFIATCEQPHTCFLZ
*****
```

B.

```
TabZIP3b-7DL MDDGNLDCSSMGSYFDDILMDTEQVACTHTHTCNPPAHLPHHTHTCLHVHVKIAASASSD
TabZIP3b-7BL MDDGNLDCSSMGSYFDGILMDTEQVAC-----THTHTCLHVHVKIAASASSD
*****

TabZIP3b-7DL AGAETPAEFEDAHATSRSKRRRPSGNQAAVRKYREKKAHTALLEEEAARLRAMNEQLAK
TabZIP3b-7BL AGAETPAEFEDAHVTSRSKRRRPSGNQAAVRKYREKKAHTALLEEEAARLRAMNKELAK
*****

TabZIP3b-7DL KVQDHAALEAEAARLRCLLVDRGRIEIGEIGAFPYHRRPAKGAGQGGAQVMSSCDFIATC
TabZIP3b-7BL KVQDHAALEAEAARLHCLLVDRGRIEIGEIGAFPYQRRPAKGAGQGGAQVMSSCDFIATC
*****

TabZIP3b-7DL EQPHTCFLZ
TabZIP3b-7BL EQPHTCFLZ
*****
```

TabZIP4-7AL

```
Prediction MDDGDIDFTNPETYLHPAMDSYFDDILKDPPEHLACTHTHACCNPVHRHDLAHTQTCVHV
Cloned MDDGDIDFTNPETYLHPAMDSYFDDILKGPPEHLACTHTHACCNPVHRHDLAHTQTCVHV
*****
```

Figure 5.4. figure legend overleaf

```

Prediction   HTKILREESDDVPETSESPQENNGPKKRPPGNRAAVRKYREKKKAHTTLLLEEVARLKAL
Cloned      HTKILREESDDVPETSESPQENNGPKKRPPGNRAAVRKYREKKKAHTTLLLEEVARLKVL
*****

Prediction   NKQLVRRLQSHSALEAEASRLRCLLVDIRGRIDGELGAFYKRPVKNKDLADQGSSSLGGA
Cloned      NKQLVRRLQSHSALEAEASRLRCLLVDIRGRIDGELGAFYKRPVKNKDLADQGSSSLGGA
*****

Prediction   RQVRLRCNDPPYPCSPEMQAMTMDDDVMSSEVLGQGAGDIANNQWLQGLPDDVKRZ
Cloned      RQVRLRCNDPPYPCSPEMQAMTMDDDVMSSEVLGQGAGDIANNQWLQGLPDDVKRZ
*****

TabZIP4-7DL

Prediction   MDDADIDFTNPETYPRPAMDSYFDDVLKDTQHACCNPHEVDLAHHAHTCVHVHTKIHPAE
Cloned      MDDGIDFTNPETYPRPAMDSYFDDVLKDTQHACCNPHEVDLAHHAHTCVHVHTKIHPAE
***

Prediction   SDDVAETSESPQQNSGAKKRPSGNRAAVRRYRDKRKARTALLEEEVARLKALNRQLVRKI
Cloned      SDDVAETSESPQQNSGAKKRPSGNRAAVRRYRDKRKARTALLEEEVARLKALNRQLVRKI
*****

Prediction   QSHSALQAEASRLRYLLVDIRGRIEGLGVFPCQRPMRNNDSDAQGSFLGGGAQQVRLRC
Cloned      QSHSALQAEASRLRYLLVDIRGRIEGLGVFPCQRPMRNNDSDAQGSFLGGGAQQVRLRC
*****

Prediction   NEPLYRSYAGHDNGZRWCYEWRAVGSSCRZHCKZPVAPRFARZCKEV
Cloned      NEPLYRSYAGHDNGZRWCYEWRAVGSSCRZHCKZPVAPRFARZCKEV
*****

TabZIPG-5DL

Prediction   MGSSEAETPAKANKASAPQEQPPATSSITATPTVYPDWTSFQGYPIIPPHGFFPSPVVS
Cloned      MGSSEAETPAKANKASAPQEQPPATSSITATPTVYPDWTSFQGYPIIPPHGFFPSPVVS
*****

Prediction   PQGHPYMWGPQPMMPYGSPPYVIYPPGGIYAHPSMRPGAHPFAPYTMTSPNGNPDAAGT
Cloned      PQGHPYMWGPQPMMPYGTTPPYVIYPPGGIYAHPSMRPGAHPFAPYTMTSPNGNPDAAGT
*****

Prediction   TTTAATAGGETNGKSSEGKEKSPIKRKSGSLGSLNMITGKNCVEHGKTSGASVNGTISQS
Cloned      TTTAATAGGETNGKSSEGKEKSPIKRKSGSLGSLNMITGKNCVEHGKTSGASVNGTISQS
*****

Prediction   GESGESSESSEGSEANSQND SQHKESGQEQDGDVRS SQNGVSPSPSQAQLKQTLAIMQMP
Cloned      GESGESSESSEGSEANSQND SQHKESGQEQDGDVRS SQNGVSPSPSQAQLKQTLAIMQMP
*****

Prediction   SGPVPGPTTNLNI GMDY WANTASS PALHGKVTPTAI PGAVAPTEP WMQDERELKRQKRK
Cloned      SGPVPGPTTNLNI GMDY WANTASS PALHGKVTPTAI PGAVAPTEP WMQDERELKRQKRK
*****

Prediction   QSNRDSARRSRLRKQAECEELAQRAEVLKQENASLKDEVSRI RKEYDEL LSKNSSLKDNV
Cloned      QSNRDSARRSRLRKQAECEELAQRAEVLKQENASLKDEVSRI RKEYDEL LSKNSSLKDNV
*****

Prediction   GDKQHKTDEAGLDNKLQHSGDSDQKDTNZ
Cloned      GDKQHKTDEAGLDNKLQHSGDSDQKDTNZ
*****

```

Figure 5.4. Amino acid alignments of cloned TabZIP3b-7BL, TabZIP4-7AL, TabZIP4-7DL and TabZIPG-5DL with the predicted sequences. Alignment created using Clustal omega, showing the predicted amino acid sequence of TabZIPs from the wheat genome database (Prediction, top of pairings) against the amino acid translation of the sequences cloned from the corresponding workflows presented in Figure 5.3 (Cloned, lower of pairings). In the case of TabZIP3b-7BL an alignment with the homeolog TabZIP3b-7DL is also shown (B.) the first group F motif truncated in the 7BL homeolog is highlighted in yellow. For the group F bZIPs, the two group F motifs are underlined in consensus with the sequence prediction by Jakoby et al. (2002); motif 1 C[ST]HTH[ST]CNP[PT]GPE, motif 2 H[ST]HTC[FL]H[AV]HT. For TabZIPG-5DL, The three group G motifs are underlined in consensus with the sequence prediction by Jakoby et al. (2002); motif 1 P[HP]PYMW, motif 2 MMA[PSA]YG[TA]P and motif 3 YAHP. The bZIP domain common to all bZIP groups is also underlined, the consensus of which is N-x7-R/K-x9-L-x6-L-x6-L. Red boxes indicate amino acid changes between cloned TaZIPs, with genome sequence predictions. The entire sequence of TabZIP4-7DL shown in this figure was cloned into the pMDC32 vector, however an early stop codon is present (displayed in red), as discussed further in text.

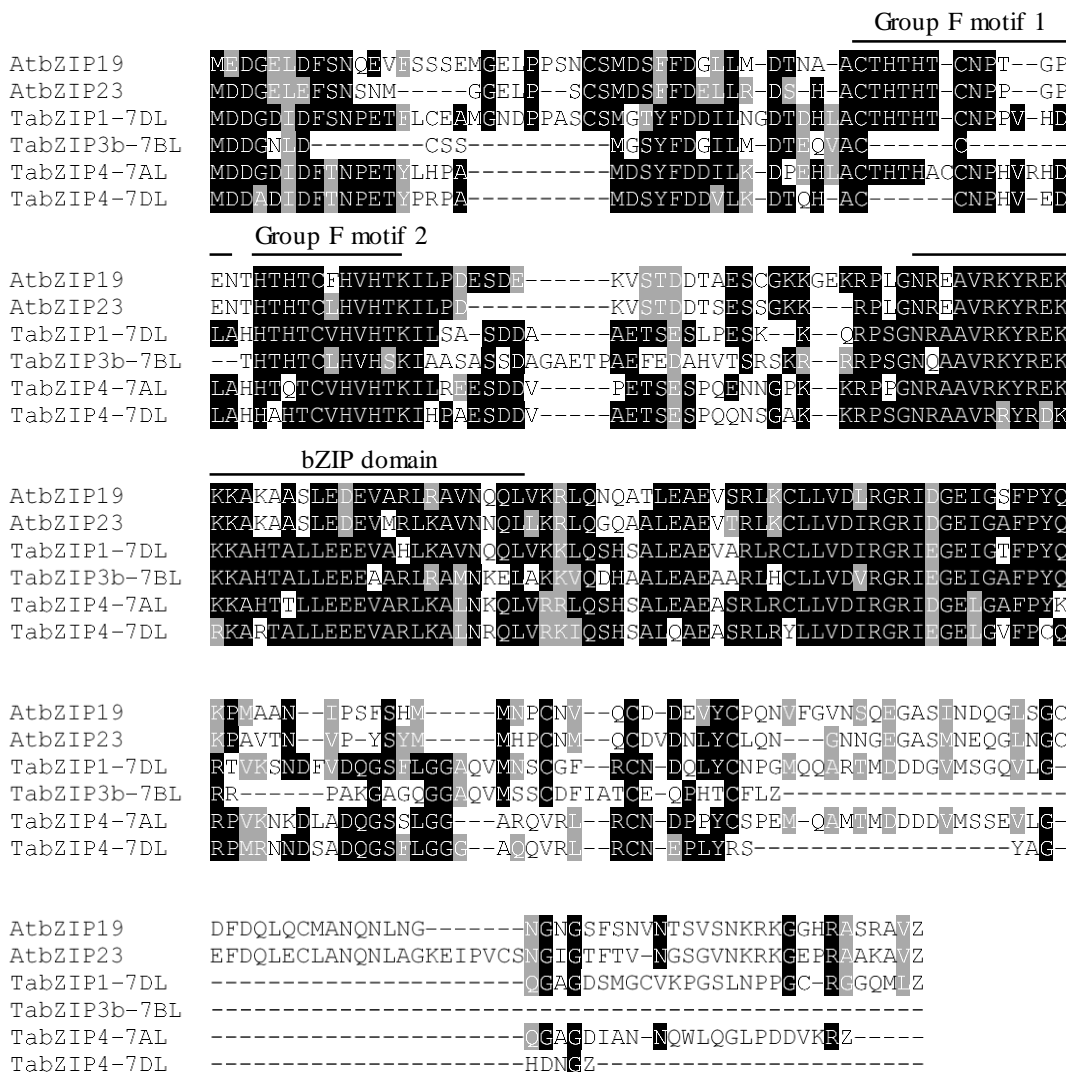


Figure 5.5. Multiple sequence alignment of cloned group F TabZIPs, AtbZIP19 and AtbZIP23. The Muscle algorithm (Edgar, 2004) was used for the alignment of sequences and the BoxShade software was used to generate this figure. The two group F motifs are labelled with lines above the alignment in consensus with the sequence prediction by Jakoby et al. (2002); motif 1 C[ST]HTH[ST]CNP[PT]GPE, motif 2 H[ST]HTC[FL]H[AV]HT. The bZIP domain common to all bZIP groups is also labelled, the consensus of which is N-x₇-R/K-x₉-L-x₆-L-x₆-L.

5.3.2 Complementation analysis of TabZIPs in the *A. thaliana* *bzip19-4bzip23-2* mutant line

In order to investigate the functional role of the cloned TabZIPs, functional complementation experiments were used to test the ability of the TabZIPs to rescue the Zn-deficient phenotype exhibited by an independently created *Arabidopsis bzip19-4bzip23-2* line (Nazri, Z and Williams, L. E., unpublished). *A. thaliana* plants (*bzip19-4bzip23-2*) were transformed with the pMDC32 *TabZIP* vector construct containing *Agrobacterium tumefaciens* cells using a floral dip method adapted from Clough and Bent, (1998) as detailed in Section 2.6.2.

Following antibiotic selection and segregation ratio analyses, multiple T3 homozygous lines were generated and two from each transformation were selected to use for phenotype assays (detailed in Sections 2.6.3 and 2.6.4).

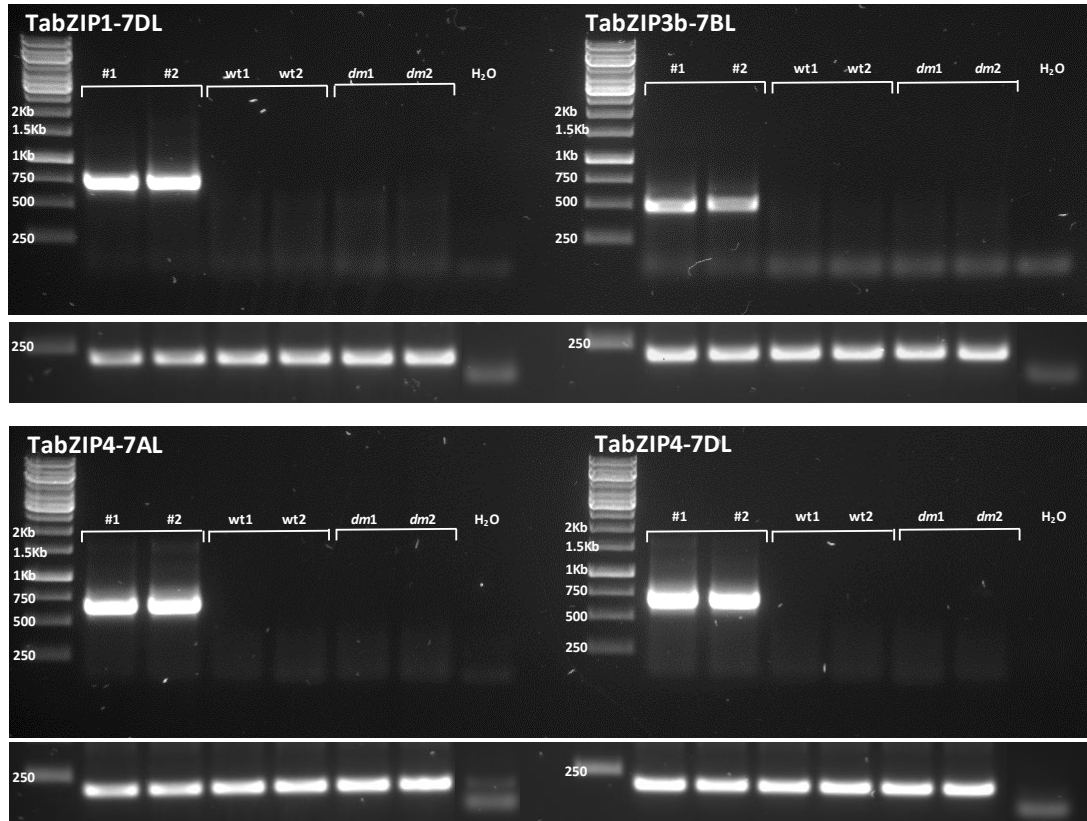


Figure 5.6. Confirmatory PCR of pMDC32TabZIP transformed *Arabidopsis* lines. Confirmatory PCR reactions showing the presence of each of the four *TabZIPs* in the transformed *Arabidopsis bzip19bzip23* line. For each *TabZIP*, cDNA from two individual lines were tested (#1 and #2). Amplifications were carried out with corresponding *TabZIPTOPO* primers, expected sizes are as follows: *TabZIP1-7DL*=757 bp, *TabZIP3b-7BL*=531 bp, *TabZIP4-7AL*=712 bp and *TabZIP4-7DL*=712 bp. Two individual wild type cDNA preparations (wt1 and wt2), two individual double mutant *bzip19-4bzip23-2* cDNA preparations (dm1 and dm2) as well as a blank water control (H₂O) were also tested with the corresponding *TabZIPTOPO* primers as control reactions. All cDNA preparations were also tested with *AtActin2* primers, these amplifications are shown below the main gels and correspond to samples in the gels as labelled directly above. Expected size of *AtActin2* primer amplicon is 201 bp. DNA ladder used in all gels is Thermo Scientific GeneRuler 1 kb.

The expression of the four group F *TabZIPs* in the transformed *Arabidopsis bzip19-4bzip23-2* line, was confirmed using PCR reactions with cDNA synthesised from whole seedling RNA preparations and is shown in Figure 5.6. Confirmation of expression for all four *TabZIPs* are shown alongside negative controls of wild-type cDNA and untransformed *Arabidopsis bzip19bzip23* cDNA. Additionally, the *AtActin2* housekeeping control gene was used to confirm the quality of all cDNA samples and verify the negative controls used. Each of the two confirmed transformed lines were used in the subsequent phenotype experiments reported in this Chapter.

Clear visible phenotypes were observable between the *Arabidopsis bzip19-4bzip23-2* double mutant line and the wild-type when grown on the -Zn (0 μ M Zn) media (Figure 5.7). The *bzip19-4bzip23-2* line exhibited greatly reduced growth, with seedlings only developing to the two leaf stage. This phenotype is in keeping with that reported by Assunção et al. (2010) where the *bzip19-1bzip23-1* mutant line showed significant growth reduction when grown on -Zn medium. TabZIP1-7DL and TabZIP4-7AL transformation of the *bzip19-4bzip23-2* resulted in rescue of the phenotype, with drastic growth improvements conferred by either of these TabZIPs when grown under -Zn conditions (Figure 5.7A, C). The rescue ability of TabZIP3b-7BL was less evident (Figure 5.7B) and TabZIP4-7DL transformation resulted in no rescue of the *bzip19-4bzip23-2* Zn-deficient phenotype (Figure 5.7D).

Analysis of the fresh weight results from both the TabZIP1-7DL and TabZIP4-7AL complementation experiments revealed there was a highly significant interaction between Zn treatment and the *Arabidopsis* line for both TabZIPs examined ($F_{3,30}=304.49$ and 401.56 respectively, $P<0.001$). Comparisons of means of interest using the least significant difference (LSD) at the 5% level of significance revealed no significant differences in fresh weight across the lines examined when grown on +Zn media (15 μ M Zn). However, when grown on the -Zn treatment (0 μ M Zn) the *bzip19-4bzip23-2* mutant showed a significantly reduced fresh weight compared to the wild-type and lines #1 and #2 of both the TabZIP1-7AL and TabZIP4-7AL transformed *bzip19-4bzip23-2* mutant line. Full complementation of *bzip19-4bzip23-2* by TabZIP1-7AL and TabZIP4-7AL was not observed as transformed lines displayed significantly reduced growth compared to the wild-type on -Zn media, although growth was significantly increased compared to the untransformed *bzip19-4bzip23-2* line.

Transformation of the *bzip19-4bzip23-2* line with TabZIP3b-7BL resulted in no clear rescue of the Zn-deficient phenotype. Of the two TabZIP3b-7BL transformed *bzip19-4bzip23-2* lines, #2 had a slightly increased growth ability on -Zn (0 μ M Zn), compared to #1, however neither line was able to rescue the mutant to the extent seen by TabZIP1-7DL or TabZIP4-7AL. Analysis of the fresh weight results from the TabZIP3b-7BL complementation experiment revealed there was a highly significant interaction between Zn treatment and the *Arabidopsis* line ($F_{3,30}=199.9$, $P<0.001$). When grown on the -Zn treatment (0 μ M Zn), the *bzip19-4bzip23-2* mutant and the TabZIP3b-7BL transformed *bzip19-4bzip23-2* lines #1 and #2, showed a significantly reduced fresh weight compared to the wild-type. Although significant increases in fresh weight were observed between the TabZIP3b-7BL transformed *bzip19-4bzip23-2* lines #1 and #2, and the *bzip19-4bzip23-2* mutant when grown on the -Zn treatment (0 μ M Zn), complementation of the mutant was far less evident with this gene compared to TabZIP1-7DL or TabZIP4-7AL. Interestingly, there were significant differences in average fresh weight between the two TabZIP3b-7BL transformed *bzip19-4bzip23-2* lines, with #2 having a significantly higher

fresh weight than #1 when grown on the -Zn treatment (0 μM Zn). This may be due to the differential insertion sites of the TabZIP3b-7BL gene in the *Arabidopsis* genome.

Analysis of the fresh weight results from the TabZIP4-7DL complementation experiment revealed there was a highly significant interaction between Zn treatment and the *Arabidopsis* line ($F_{3,30}=361.4$, $P<0.001$). Wild-type fresh weights were significantly higher than the untransformed *bzip19-4bzip23-2* line and the TabZIP4-7DL transformed *bzip19-4bzip23-2* lines #1 and #2. No significant differences were present between the untransformed *bzip19-4bzip23-2* line and the TabZIP4-7DL transformed *bzip19-4bzip23-2* lines.

Both TabZIP3b-7BL and TabZIP4-7DL have a completely truncated or poorly conserved group F motif 1 present in the coding region (see Figure 5.5). The reduction in rescue ability of both TabZIP3b-7BL and TabZIP4-7DL compared to TabZIP1-7DL and TabZIP4-7AL suggests this motif has an important function in the Zn-regulatory response.

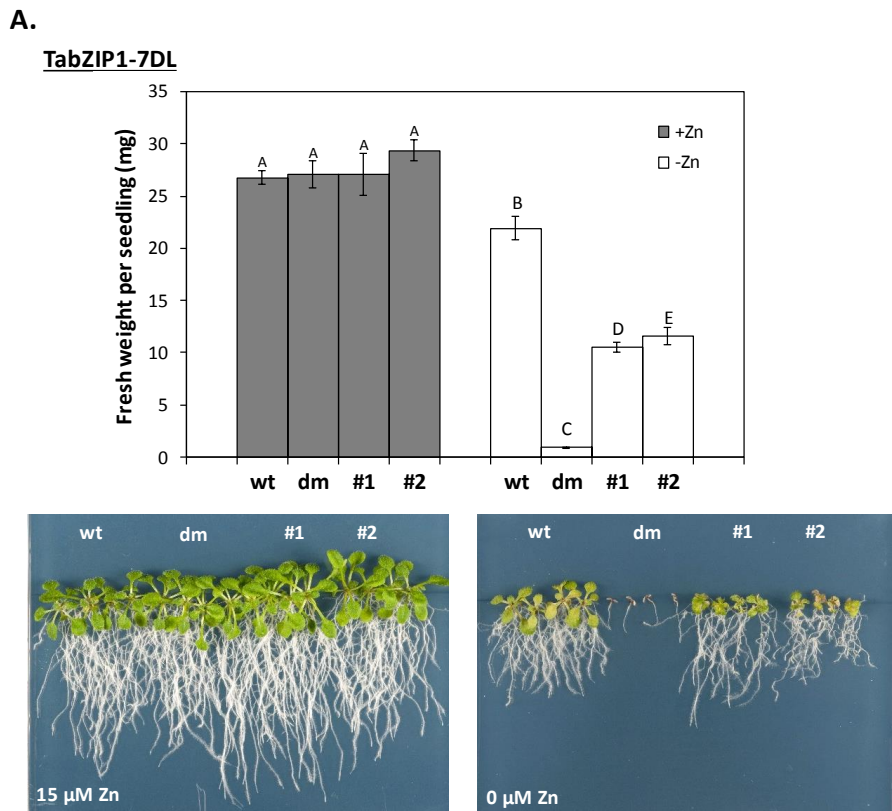
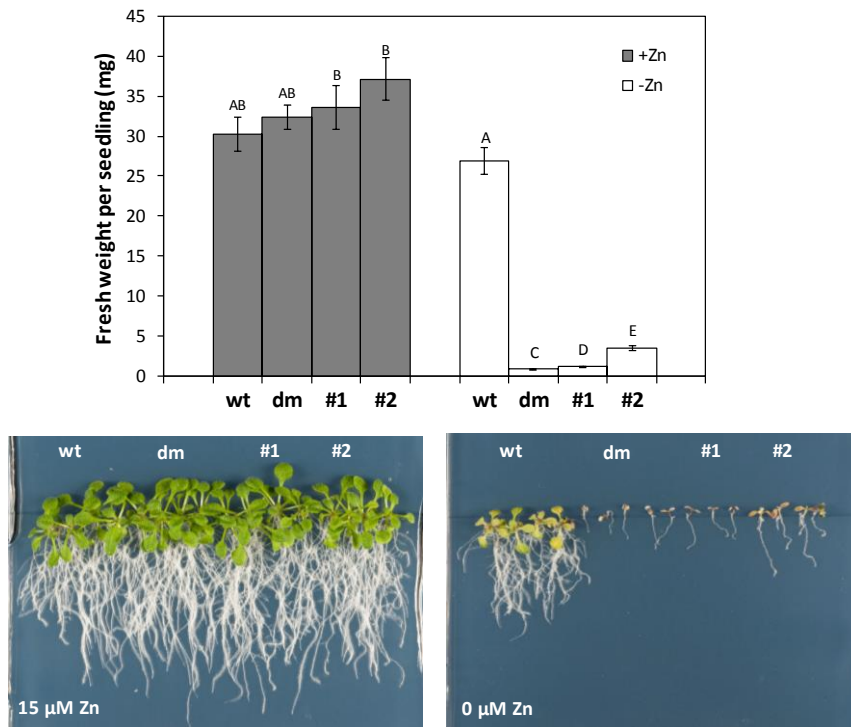


Figure 5.7 continued overleaf

B.

TabZIP3b-7BL



C.

TabZIP4-7AL

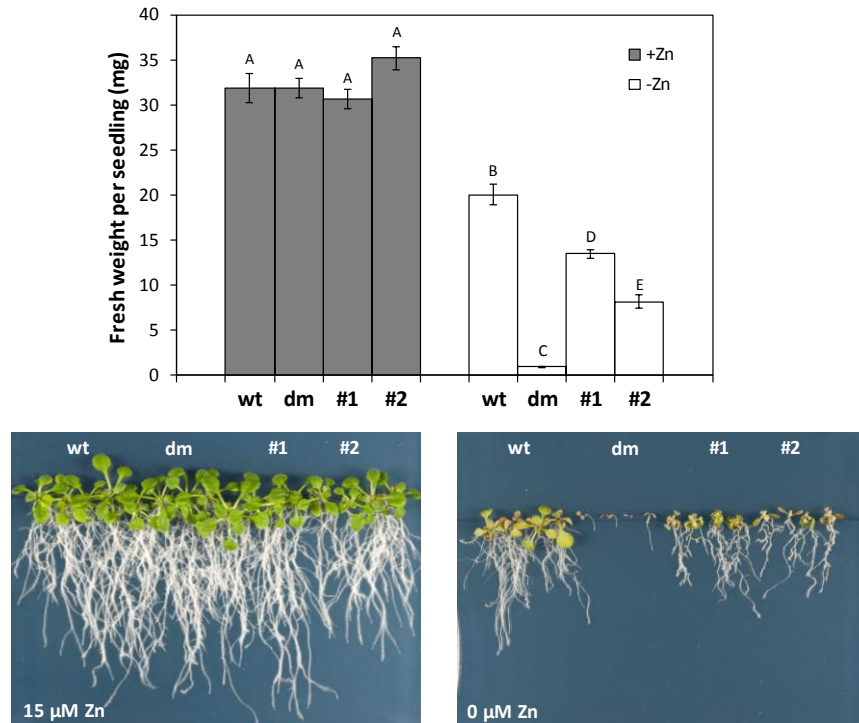


Figure 5.7. continued overleaf

D.

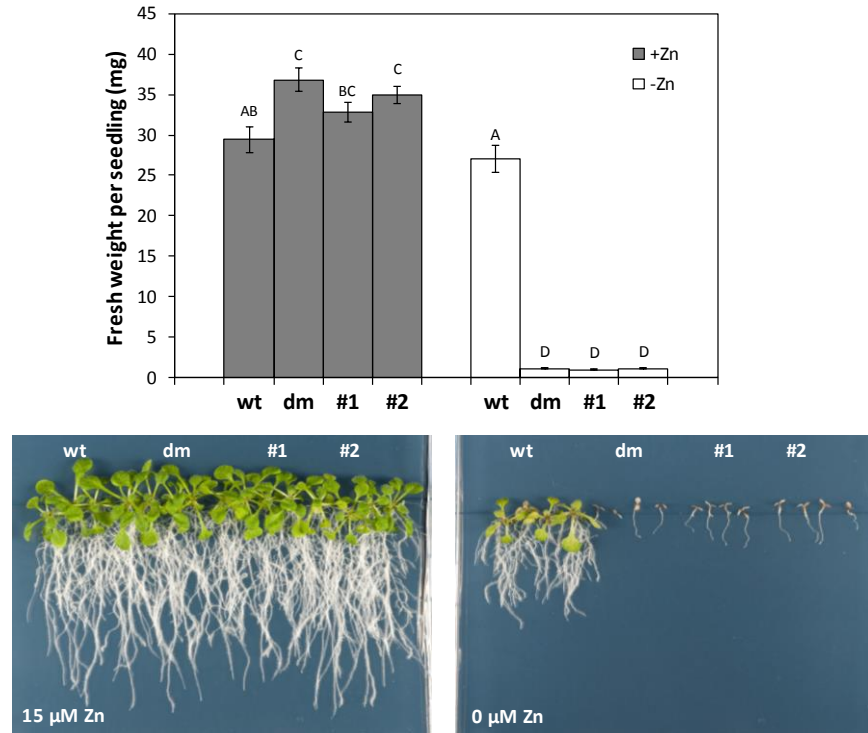
TabZIP4-7DL

Figure 5.7. Functional complementation of the *Arabidopsis bzip19-4bzip23-2* mutant with group F TabZIPs. The fresh weight analysis results shown for the four TabZIP complementation experiments are mean average fresh weights per seedling \pm S.E.M. from 6 plates with 4 seedlings per plate, per line (n=24). Bars with different letters indicate a significant difference ($P < 0.05$) tested on log-transformed data using Fisher's LSD. +Zn = 15 μ M Zn and -Zn = 0 μ M Zn. Representative plates at both the +Zn (15 μ M Zn) and -Zn (0 μ M Zn) media concentrations are shown. wt indicates the wild-type line. *bzip19+23* indicates the untransformed *bzip19-4bzip23-2* line. #1 and #2 are two independent TabZIP transformed *bzip19-4bzip23-2* lines. 4 seedlings of each line are grown per plate. All plates illustrated are 18 days post germination.

5.3.3 Interaction and binding ability of bZIPs with ZDRE motifs

The current Zn regulatory model, proposed by Assunção et al. (2010, 2013) in *Arabidopsis*, involves the binding of AtbZIP19 and AtbZIP23 in homodimer or heterodimer formation to the ZDRE regions found in the promoter of region of Zn-responsive genes. This bZIP binding enhances transcription thus elevating expression of key Zn-responsive genes including ZIP family members. It has been shown experimentally that AtbZIP19 and AtbZIP23 are able to bind to a three or two copy repeat of the ZDRE found in the promoter of *AtZIP4* (Assunção et al., 2010). To ascertain whether the TabZIPs identified here are able to bind to potentially analogous ZDREs found in the promoter regions of some *TaZIPs*, binding assays using the EMSA technique are reported in this section.

EMSAs work on the premise that a bound/interacting protein will slow the migration of a labelled probe compared to a free, unbound probe when electrophoresed in a native (non-

denaturing) polyacrylamide gel system. As detailed in Section 2.7.1 and 2.7.2, TabZIP proteins used in the following EMSAs were generated by PCR amplification from *TabZIP* containing vectors (cloned in Section 5.3.1), before being synthesised *in-vitro* using a coupled transcription-translation kit (TNT® SP6 High-Yield Wheat Germ Protein Expression System). The binding ability of the synthesised bZIP proteins was tested on a range of ZDRE containing biotinylated probes, including those used previously by Assunção et al. (2010) containing *Arabidopsis* ZDREs as well as novel biotinylated probes containing putative wheat ZDRE motifs identified in the promoter regions of TaZIPs.

5.3.3.1 ZDRE motif presence in TaZIPs

Regions upstream of the start codon (up to 2000 bp where possible) of previously identified *TaZIPs* (Chapter 3) were analysed for the presence of potential ZDREs. Motifs identified were counted as ZDREs if they had no more than one mismatch to the ZDRE consensus reported by Assunção et al. (2010). As detailed in Table 5.1 ZDREs were present in the promoter regions of *TaZIP1*, 3, 4, 5, 7, 8 and 11 across all three homeologs of each gene. Analysis revealed that all other *TaZIPs* have at least one motif that has two or more mismatches to the ZDRE consensus.

TaZIP ZDRE probes were designed based on the motifs found in *TaZIP1*, 4, 5, 6 and 7 (the *TaZIPs* with existing expression analysis data, Chapter 3). Probes were designed with the same non-native ZDRE flanking sequence as used by Assunção et al. (2010), with ZDREs adjacent to one another. The exception was the *TaZIP1*ZDRE probe, where due to the proximity of the two ZDREs present in the promoter, the probe was designed with native flanking sequence as well as the single nucleotide separating the two ZDREs. For full probe descriptions see Table 5.2.

Table 5.1. Overview of ZDREs. The number, sequence and position in relation to start codon of ZDREs in *TaZIPs* and *AtZIP4*. ZDREs with up to one mismatch from the consensus described by (Assunção et al., 2010) of RTGTCGACAY were included in the number of ZDREs present column. If no ZDREs with only one mismatch were present in a promoter, ZDREs with two mismatches are shown in the putative ZDRE sequence column. Red letters indicate nucleotide mismatches from the proposed ZDRE sequence, an asterisk after any putative ZDRE indicates it is palindromic. (N.C.) indicates a non-complete sequence, (N.F.) indicates a likely non-functional translation caused by a frameshift in the coding sequence.

Gene name	No. of ZDRE	Putative ZDRE sequences	ZDRE position from start codon	Length of promoter analysed
<i>AtZIP4</i>	2	ATGTCGACAC + ATGTCGACAT (*)	118 bp and 246 bp	597 bp
<i>TaIRT1-4AL</i>	0	GTGTCTACAA	820 bp	2000 bp
<i>TaIRT1-4BS</i>	0	AAGTCGAGAT	1770 bp	2000 bp
<i>TaIRT1-4DS</i>	0	TTGTCAACAT + GTGTCTACAA + CTGTGGACAT	344 bp, 565 bp and 726 bp	2000 bp
<i>TaZIP1-2AL</i>	2	GTGTCAACAC + ATGACGACAT, (separated by one T)	489 bp and 500 bp	2000 bp
<i>TaZIP1-2BL</i>	2	GTGTCAACAC + ATGACGACAT, (separated by one T)	570 bp and 581 bp	2000 bp
<i>TaZIP1-2DL</i>	2	GTGTCAACAC + ATGACGACAT, (separated by one T)	554 bp and 565 bp	2000 bp
<i>TaZIP2-6AS</i>	0	GTGCCTACAT + GTGTCGAGCC + ATCTCGTCAT	296 bp, 550 bp and 1005 bp	2000 bp
<i>TaZIP2-6BS</i>	0	TTGTCTACAC	1252 bp	2000 bp
<i>TaZIP2-6DS</i>	0	GTGTGCACAC (*) + ATCTCGTCAT	291 bp and 798 bp	2000 bp
<i>TaZIP3-7AL</i>	2	ATGACGACAC + GTGTCGACAT	280 bp and 528 bp	838 bp
<i>TaZIP3-7BL (N.C.)</i>	-	-	-	None available
<i>TaZIP3-7DL</i>	2	ATGACGACAC + GTGTCGACAT	393 bp and 639 bp	2000 bp
<i>TaZIP4-4AS</i>	3	ATGTGACAT + GTGTCGACAC (*) + GTGTCGACAC (*)	123 bp, 765 bp and 985 bp	2000 bp
<i>TaZIP4-4BL</i>	3	ATGTGACAT + GTGTCGACAC (*) + GTGTCGACAC (*)	121 bp, 1076 bp and 1294 bp	2000 bp
<i>TaZIP4-4DL</i>	3	ATGTGACAT + GTGTCGACAC (*) + GTGTCGACAC (*)	121 bp, 830 bp and 1051 bp	2000 bp
<i>TaZIP5-2AL</i>	2	ATGTCGTCAC + GTGTCGTCAT	229 bp and 373 bp	2000 bp
<i>TaZIP5-2BL</i>	2	ATGTCGTCAC + GTGTCGTCAT	231 bp and 374 bp	2000 bp
<i>TaZIP5-2DL</i>	1	ATGTCGTCAC	245 bp	2000 bp
<i>TaZIP6-1AS</i>	1	ATGTCGACAC	1107 bp	2000 bp
<i>TaZIP6-1BS</i>	0	ATGTCGTTACAC	1916 bp	2000 bp
<i>TaZIP6-1DS</i>	0	GTCTCACAT	643 bp	2000 bp

Table 5.1. continued

Gene name	No. of ZDRE	Putative ZDRE sequences	ZDRE position from start codon	Length of promoter analysed
<i>TaZIP7-1AS</i> (N.F.)	2	ATGACGACAC + ATGTCGACAT (*)	163 bp and 640 bp	2000 bp
<i>TaZIP7-1BS</i>	2	ATGACGACAC + ATGTCGACAT (*)	163 bp and 644 bp	2000 bp
<i>TaZIP7-1DS</i>	2	ATGACGACAC + ATGTCGACAT (*)	163 bp and 625 bp	2000 bp
<i>TaZIP8-2AS</i>	1	GTGTCGTCAT	378 bp	2000 bp
<i>TaZIP8-2BS</i>	2	ATGTCGTCAC + GTGTCGTCAT	241 bp and 376 bp	2000 bp
<i>TaZIP8-2DS</i>	2	ATGTCGTCAC + GTGTCGTCAT	234 bp and 370 bp	2000 bp
<i>TaZIP11-3AL</i>	1	GTCTCGACAT	488 bp	2000 bp
<i>TaZIP11-3BL</i>	1	GTCTCGACAT	621 bp	2000 bp
<i>TaZIP11-3DL</i>	2	ATCTCGACAT + ATGTCAACAC	921 bp and 1590 bp	2000 bp
<i>TaZIP12-1AS</i>	2	ATGTCGACTT + ATGGCGACAG	175 bp and 1846 bp	2000 bp
<i>TaZIP12-1BS</i>	0	ATGTCGGCTT + GCGTCGTCAT	175 bp and 284 bp	2000 bp
<i>TaZIP12-1DS</i>	1	ATGTCGACTT	175 bp	2000 bp
<i>TaZIP14-3AS</i>	0	ATGTTGAAAT + ATGTCCATAT	408 bp and 573 bp	2000 bp
<i>TaZIP14-3BS</i>	0	ATGTTGAAAT + ATTTTGACAT + AGGTCAACAC	441 bp, 905 bp and 1629 bp	2000 bp
<i>TaZIP14-3DS</i>	0	ATGTCATAT + GTGTCGCAT + ACGGCGACAC	559 bp, 1450 bp and 1627 bp	2000 bp
<i>TaZIP16-6AS</i>	0	ATGATGACAT	498 bp	2000 bp
<i>TaZIP16-6BS</i>	0	AGTTGACAT	1642 bp	2000 bp
<i>TaZIP16-6DS</i>	0	ATTTCAACAT + ATGTGGACTT	253 bp and 1600 bp	2000 bp

Table 5.2. ZDRE probe overview. Sequences of ZDRE probes used in EMSA assays with descriptions of their design and specific details of the putative ZDRE motifs they contain.

Probe name	Sequence 5' to 3' (all 5' biotin labelled)	Probe description
Ass3Z	aattcATGTCGACATATGTCGACATATGTCGACACgagct	Non-native sequence (lower case) at 5' and 3' end. Three ZDRE motifs present: two copies of -246 bp positioned AtZIP4 ZDRE followed by one copy of -118 bp AtZIP4 positioned ZDRE. As designed and used by Assunção et al. (2010) where both AtbZIP19 and AtbZIP23 were shown to bind to this.
Ass3Zmut	aattcATGTAGACATATGTAGACATATGTAGACACgagct	Same as Ass3Z (above) just with mutation in core of ZDRE (shown in red). AtbZIP19 and AtbZIP23 have both been shown to not bind to this (Assunção et al., 2010)
Ass2Z	aattcATGTCGACATATGTCGACACgagct	Non-native sequence (lower case) at 5' and 3' end. Two ZDRE motifs present: one copy of -246 bp positioned AtZIP4 ZDRE followed by one copy of -118 bp positioned AtZIP4 ZDRE. As designed and used by Assunção et al. (2010) where both AtbZIP19 and AtbZIP23 were shown to bind to this.
TaZIP1ZDRE	gaccgATGACGACATtGTGTCAACACtgcac	Native sequence (lower case) at 5' and 3' end, and the t as found in the middle (lower case). This probe is the same design as ZDREs are found in the promoter of TaZIP1 homeologs.
TaZIP4ZDRE	aattcGTGTCGACACGTGTCGACACATGTTGACATgagct	Same non-native sequence on either end as Assunção probes (lower case). Tandem repeat of GTGTCGACAC next to ATGTTGACAT. All three of these ZDREs are found in the promoter of all TaZIP4 homeologs.
TaZIP5ZDRE	aattcGTGTCGTCATATGTCGTCACgagct	Same non-native sequence on either end as Assunção probes (lower case). Then GTGTCGTCAT + ATGTCGTCAC adjacent to one another. Both GTGTCGTCAT + ATGTCGTCAC are found in the promoter region of TaZIP5-2AL and TaZIP5-2BL.
TaZIP6ZDRE	aattcATGTCGAGACATGTCGAGACgagct	Same non-native sequence on either end as Assunção probes (lower case). Then two tandem repeats of ATGTCGAGAC adjacent to one another. One copy of ATGTCGAGAC is found in TaZIP6-1AS, but neither of the other two TaZIP6 homeologs.
TaZIP7ZDRE	aattcATGTCGACATATGACGACACgagct	Same non-native sequence on either end as Assunção probes (lower case). Then ATGTCGACAT + ATGACGACAC adjacent to one another. Both ATGTCGACAT + ATGACGACAC are found in the promoter regions of all TaZIP7 homeologs

5.3.3.2 EMSAs

Following the design of biotin labelled probes detailed in Section 5.3.3.1, the ability of six bZIPs to bind to these probes was investigated using EMSAs. Initially, AtbZIP19 was synthesised using an *AtbZIP19* containing vector as a template, kindly provided by Nazri, Z. and Williams, L., E. The binding ability of AtbZIP19 to the probes detailed in Table 5.2 was tested and the EMSA blot is shown in Figure 5.8. Figure 5.8 shows a full EMSA membrane blot, at the bottom of the membrane the unbound, free probes are shown, these have migrated furthest as they are not interacting with proteins present. Their migration distances correspond to their size as detailed in Table 5.2. Towards the top of the blot and across all lanes except C2, a line of bands can be seen labelled endogenous protein. These bands are caused by protein present in the coupled transcription-translation kit that is being non-specifically detected. Lane C3 contains only the TNT wheat germ mix with no template, thus no synthesised bZIP proteins are present, and this non-specific band can be seen, therefore these are not due to the bZIPs being produced during the transcription-translation reaction. They are likely due to detection of a biotin containing protein endogenously present in the wheat germ coupled transcription-translation kit. Below the endogenous protein bands in Figure 5.8, in accordance with results previously published by Assunção et al. (2010), AtbZIP19 created a band shift when two (Ass2Z) or three copies (Ass3Z) of the AtZIP4 ZDRE are present, however with the mutated three copy AtZIP4 ZDRE probe (Ass3Zmut), AtbZIP19 does not produce a band shift, indicating an absence of binding. AtbZIP19 also produced band shifts with the previously untested TaZIPZDRE probes 1, 4, 5 and 7. No band shift was observed with the TaZIP6ZDRE probe suggesting AtbZIP19 does not interact with the putative ZDRE identified in the promoter of *TaZIP6*. Additionally, at the top of the blot, above the endogenous protein region, in lanes where a band shift occurs (Ass3Z, Ass2Z and TaZIPZDREs 1, 4, 5 and 7) additional bands are observed (labelled biotin containing complex). These may be caused by larger biotin containing complexes being present. These are most likely either complexes of multiple AtbZIP19 proteins binding to the multiple copies of ZDREs present in the probes which causes their migration to slow considerably. Alternatively, these bands may be labelled ZDRE probes with AtbZIP19 bound and other general transcription factors and even polymerase machinery that is present in the transcription-translation kit forming a complex.

Figure 5.9 displays a composite showing EMSAs of the five TabZIPs tested. As observed in Figure 5.8, endogenous protein detection is present across lanes containing the transcription-translation kit. The TabZIP1-7DL blot shows the TabZIP1-7DL protein created a band shift with Ass3Z and Ass2Z, which are based on *AtZIP4* ZDREs. As previously observed, a mutated version of these ZDREs (Ass3Zmut) does not produce a band shift. TaZDRE probes 1, 4, 5 and 7 all produced a band shift indicating an interaction of TabZIP1-7DL with these ZDREs. As with AtbZIP19 however TaZIP6ZDRE did not produce a band shift, suggesting an interaction does not

occur between TaZIP1-7DL and the ZDRE present in the promoter of *TaZIP6-1AS*. As observed with AtbZIP19 in Figure 5.8, a band above the endogenous protein is visible in lanes where a band shift occurred. As previously noted, this is most likely due to a biotin containing complex, containing either additional TabZIP1-7DL proteins, general transcription factors or polymerase machinery which further slows the migration of the biotin labelled probes.

TabZIP3b-7BL contains only one of the two group F motifs, see Section 5.3.1.2, and is unable to rescue the *bzip19-4bzip23-2* Zn-deficiency phenotype, Section 5.3.2. Figure 5.9 shows that TabZIP3b-7BL is unable to bind to any of the TaZIPZDRE probes investigated. TabZIP3b-7BL is also unable to bind to the two AtZDRE copy containing probe, Ass2Z. However, TabZIP3b-7BL produces a band shift when incubated with the three AtZDRE containing probe Ass3Z. The band shift observed shows migration is further for TabZIP3b-7BL than AtbZIP19 and TabZIP1, this is explained due to the smaller size of the TabZIP3b-7BL transcript and subsequent protein. Ass3Z is in fact an exaggeration of the ZDREs present in the promoter of *AtZIP4*, as only two ZDREs are actually present in the promoter region and these are spaced 128 bp apart in the promoter rather than adjacent to each other as in the Ass3Z probe. The increase from two ZDREs to three as well as their adjacency could possibly accentuate the native binding ability of TabZIP3b-7BL and cause the shift observed in Figure 5.9.

Previously, TabZIP4-7AL was shown to partially rescued the *Arabidopsis bzip19-4bzip23-2* Zn-deficiency phenotype (Section 5.3.2). When the binding ability of TabZIP4-7AL was examined through two independent EMSAs, binding was not observed to any of the TaZIPZDRE probes tested. Figure 5.9 shows that no band shifts were produced across all probes tested with TabZIP4-7AL. The ability of TabZIP4-7AL to rescue the *bzip19-4bzip23-2* mutant line strongly suggests this bZIP functions in the Zn-deficiency response of wheat, however the lack of binding observed in this assay suggests it acts either through a different binding mechanism, or potentially the binding is not observed due to one or more experimental factors as discussed in Section 5.4.

TabZIP4-7DL was unable to rescue the mutant Zn-deficient phenotype of *bzip19-4bzip23-2* (Section 5.3.2). The first group F motif of TabZIP4-7DL is poorly conserved (Figure 5.5). TabZIP4-7DL does not bind to any of the ZIPZDRE probes tested (Figure 5.9). The lack of binding supports the previously discussed inability of TabZIP4-7DL to complement the *Arabidopsis* mutant. It seems plausible to speculate that TabZIP4-7DL is redundant perhaps due to the hexaploid nature of wheat.

The final TabZIP in which the binding ability was investigated was TabZIPG-5DL. This TabZIP is from the group G bZIPs, thus does not contain the same motifs as the group F motifs previously investigated. The complementation ability of TabZIPG-5DL to rescue the *bzip19-4bzip23-2* mutant was not determined. Surprisingly, TabZIPG-5DL produced a faint band shift

with one of the TaZIPZDREs tested; TaZIP4ZDRE. TaZIP4ZDRE is the only TaZIPZDRE where three ZDRE copies are present as *TaZIP4* is the only gene investigated with three ZDRE copies identified within the promoter region (see Table 5.1).

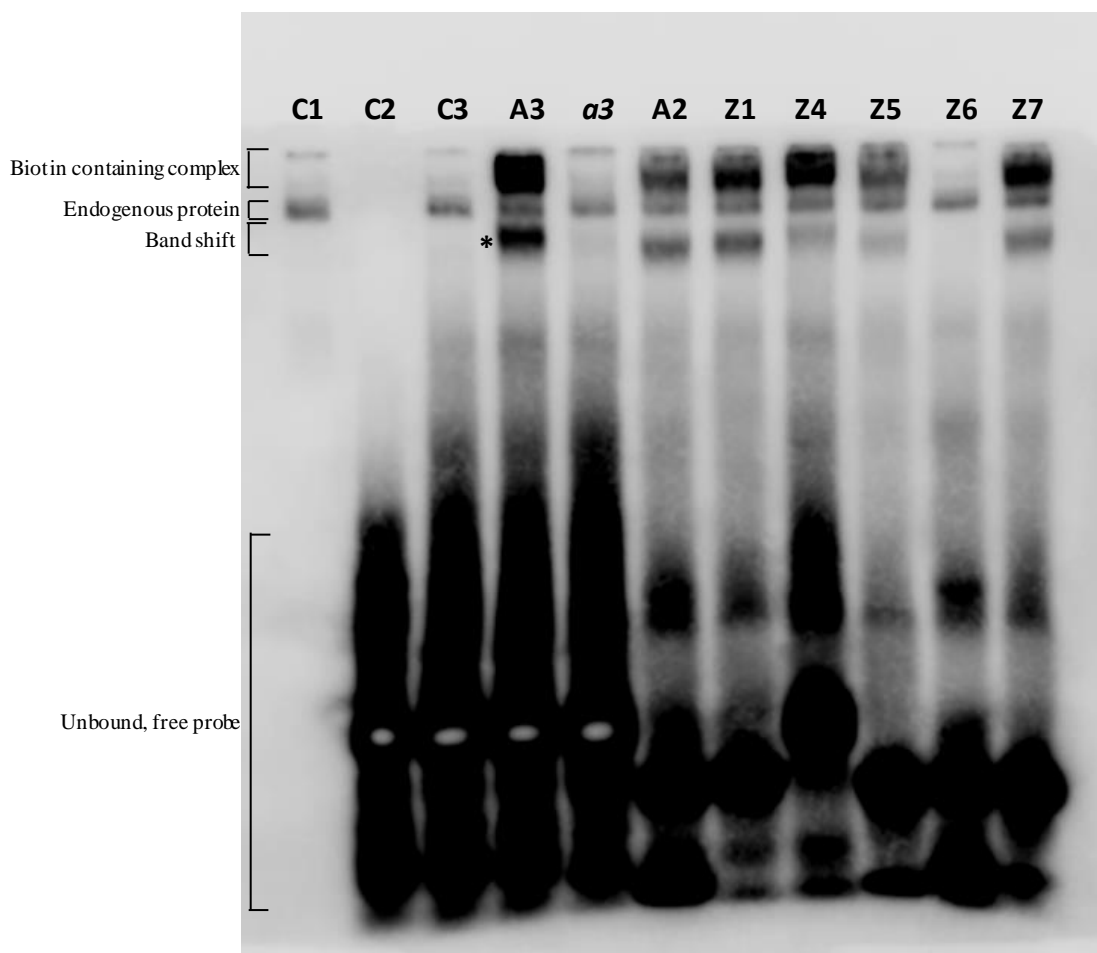


Figure 5.8. EMSA of AtbZIP19 with ZDRE containing probes. EMSA assay used to investigate the binding ability of AtbZIP19 to *Arabidopsis* ZDRE containing probes and wheat ZDRE containing probes. C1 to C3 are control lanes: C1 is AtbZIP19 protein only, no probe. C2 is probe (Ass3Z), no protein. C3 is probe (Ass3Z) with TNT wheat germ mix (no template). All other lanes contain *in-vitro* synthesised AtbZIP19 with the following probes: lane A3 is Ass3Z, *a3* is Ass3Zmut (mutated Ass3Z) and A2 is Ass2Z which all contain *Arabidopsis* ZDREs. Z1 to Z7 are TaZIP1ZDRE to TaZIP7ZDRE which all contain wheat ZDREs. Probe sequences are provided in Table 2.11 and 5.2. The band shift region is labelled with an asterisk indicating a band shift caused by the synthesised AtbZIP19 interacting with the biotin labelled probe. The biotin containing complex region is labelled, this region is caused by either: more than one AtbZIP19 binding to the labelled ZDRE probe, or other transcription machinery binding and causing a slowed migration. The endogenous protein region is labelled showing detection of non-specific biotin containing proteins present in the TNT wheat germ mix. The unbound, free probe region labelled shows the further migration of biotin labelled probes that are not interacting and binding to proteins present.

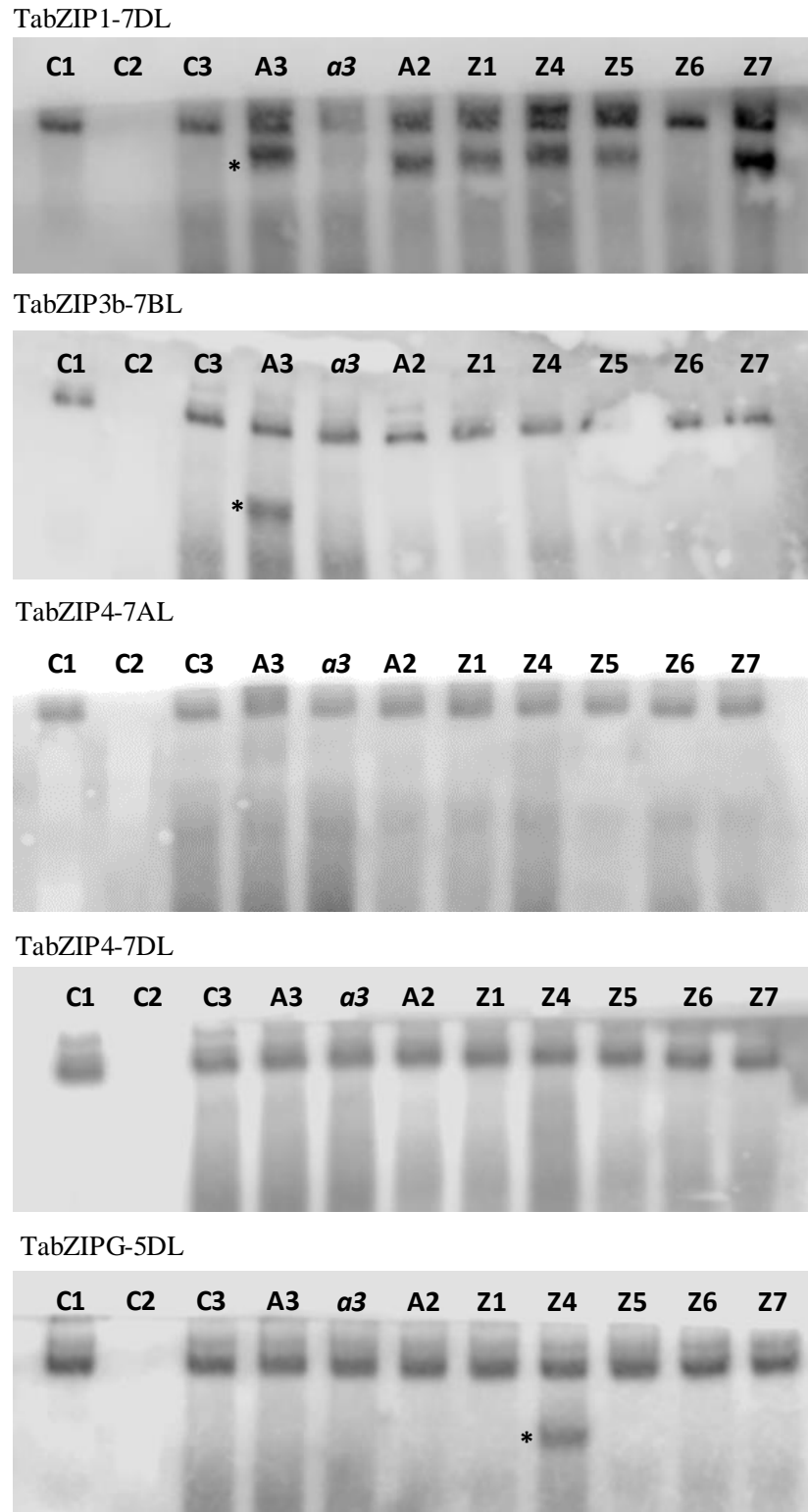


Figure 5.9. Composite of five EMSAs using different wheat bZIPs. Upper blot regions from EMSAs used to investigate the binding ability of five TabZIPs to *Arabidopsis* ZDRE containing probes and wheat ZDRE containing probes. C1 to C3 are control lanes: C1 is TabZIP1-7DL (or other corresponding protein) only, no probe. C2 is probe (Ass3Z), no protein. C3 is probe (Ass3Z) with TNT wheat germ mix (no template). All other lanes contain *in-vitro* synthesised TabZIPs (as labelled) with the following probes: lane A3 is Ass3Z, *a3* is Ass3Zmut (mutated Ass3Z) and A2 is Ass2Z which all contain *Arabidopsis* ZDREs. Z1 to Z7 are TaZIP1ZDRE to TaZIP7ZDRE which all contain wheat ZDREs. Probe sequences are provided in Table 2.11 and 5.2. Asterisks indicate band shift.

5.4 Discussion

5.4.1 TabZIPs have differential abilities to complement the *A. thaliana bzip19-4bzip23-2* mutant line grown under Zn-deficient conditions

Cloning of the five TabZIPs described in this Chapter confirms the sequence predictions made from the genome databases. The confirmation of the predicted motif 1 truncation in TabZIP3b-7BL offers the chance to investigate how important this group F motif is in the Zn-regulatory response. The cloned copy of TabZIP4-7DL had a poorly conserved motif 1 and additionally had an early stop codon which was a result of a T insertion in the nucleotide sequence. The importance these features in both TabZIP3b-7BL and TabZIP4-7DL was functionally assessed using complementation assays of the *Arabidopsis bzip19-4bzip23-2* line, as subsequently discussed. The *TabZIP* cloning workflow resulted in the cloning of two *TabZIP4* homeologs; *TabZIP4-7AL* and *TabZIP4-7DL*. Both homeologs were cloned from cDNA synthesised from different regions of the plant, *TabZIP4-7AL* from root cDNA and *TabZIP4-7DL* from shoot cDNA. It seems likely that the cloning process will amplify and clone the most prevalent homeolog present in any given tissue. As different homeologs were cloned from different plant portions it could be suggested that individual homeologs of *TabZIPs* operate at specific regions within the plant. This could be further tested using homeolog specific real time PCR expression analyses. If unique regions between the homeologs are identified this may allow the design of homeolog specific primers and subsequent homeolog expression to be analysed.

Following the cloning of the four group F *TabZIPs* they were each transformed into the *Arabidopsis bzip19bzip23* double mutant. Growth experiments confirmed that when grown on -Zn media (0 μM Zn), the *bzip19-4bzip23-2* double mutant was unable to bring about a Zn-deficiency response and growth was severely limited compared to wild-type plants grown on the same conditions. This phenotype is in agreement with studies published previously by Assunção et al. (2010) where a double mutant with different T-DNA insertion sites was used (*bzip19-1bzip23-1*) and Inaba et al. (2015) where single mutants (*bzip19-1* and *bzip23-1*) were examined. TabZIP1-7DL and TabZIP4-7AL showed partial complementation of the *bzip19-4bzip23-2* line; seedling growth was drastically improved under the -Zn treatment compared to the untransformed *bzip19-4bzip23-2* double mutant line. This indicates that the role of these genes in wheat is highly likely to be in the Zn-deficiency response and that a similar mechanism exists in wheat as in *Arabidopsis*. Both TabZIP1-7DL and TabZIP4-7AL were unable to completely rescue the *bzip19-4bzip23-2* mutant. This may be due to slight differences in the binding ability of these TabZIPs to Zn in the proposed sensing mechanism, compared to AtbZIP19 and AtbZIP23. Assunção et al. (2010, 2013) proposed that the two group F motifs which are rich in cysteine and histidine residues are the binding sites of Zn^{2+} and act as Zn-sensors in *Arabidopsis*. Perhaps TabZIP1-7DL

and TabZIP4-7AL have slightly higher binding affinities to Zn and therefore do not upregulate the suite of Zn-responsive genes under -Zn conditions to the same extent as AtbZIP19 and AtbZIP23. Another reason for the partial, yet not full complementation observed could be that the binding ability of TabZIP1-7DL and TabZIP4-7AL to the ZDREs in the promoters of Zn-responsive genes such as *AtZIP1*, 3, 4, 5, 9 and 12 may be altered perhaps due to divergent evolution. Evidence provided by individual mutant studies of *bzip19-1* and *bzip23-1* has shown they each have the individual ability to control the expression of specific ZIPs (Inaba et al., 2015). This indicates an intricate level of control is present on the ZIPs from two closely related bZIPs. It seems logical that the more distantly related TabZIP1-7DL and TabZIP4-7AL are unlikely to possess this level of control across all the Zn-responsive *Arabidopsis* genes and thus are unable to fully complement the *Arabidopsis* double mutant.

All *Atbzip19bzip23* complementation assays with TabZIPs in this Chapter used the dual 35S cauliflower mosaic virus promoter present in the pMDC32 transformation vector (Curtis and Grossniklaus, 2003). This is a strong, constitutive promoter causing expression throughout the entire plant. This constitutive expression may lead to a less tailored response to Zn-deficiency than the native *AtbZIP19* and *AtbZIP23* genes which may display a more tissue specific upregulation. This potentially less controlled response in the transformed *bzip19-4bzip23-2* mutant may go some way to explaining the substantial, yet not full complementation ability of TabZIP1-7DL and TabZIP4-7AL. The differential complementation ability exhibited by the two TabZIP4-7AL *bzip19-4bzip23-2* transformed lines may be due to different insertion sites in the *Arabidopsis* genome. It could be that the insertion site of line #2 disrupts other fundamental processes involved in the growth of *Arabidopsis* under Zn-deficient conditions. Further lines from this transformation could be tested to see how variable additional individual transformed lines are with regard to fresh weight performance under Zn-deficiency.

Transformation with TabZIP3b-7BL resulted in a far reduced rescue response compared to both TabZIP1-7DL and TabZIP4-7AL. The reduced ability of TabZIP3b to rescue the Zn-deficient phenotype of *Atbzip19bzip23* could be due to the absence of the group F motif 1 in the translation of this gene. Assunção et al. (2010, 2013) have postulated that the cysteine-histidine rich group F motif 1 and 2 are likely binding sites of Zn²⁺. Both cysteine and histidine act as ligands due to a lone pair of electrons on the sulphur atom of cysteine residues and a lone pair of electrons on the nitrogen of the imidazole side chain of histidine. Zn²⁺ forms tetrahedral complexes with these ligands (Pace and Weerapana, 2014), and the binding of Zn²⁺ to these ligands present in the group F motifs of the bZIPs is suggested to be fundamental in the sensing and response to Zn-deficiency of the group F bZIPs. Given the current model, where Zn²⁺ dissociation under Zn-deficient conditions leads to bZIP binding to ZDREs and subsequent Zn-responsive gene upregulation, the absence of one of the cysteine-histidine rich group F motifs

however may be expected to reduce the sensitivity to Zn-deficiency. Feasibly Zn²⁺ will be less able to bind to a bZIP with only one of these motifs, possibly causing the bZIP to become functionally active at a higher Zn concentration than bZIPs containing both predicted Zn²⁺ binding motifs. The reduced lack of rescue shown by TabZIP3b-7BL and the complete inability of TabZIP4-7DL (also lacking the group F motif 1) to rescue the mutant however possibly suggests additional factors may be at play and these motifs may be important in more than just binding and sensing of Zn²⁺ ions. The entire 3-dimensional structure of the bZIP may be altered by the lack of this group F motif 1; its absence may reduce the binding ability to ZDRE motifs (discussed in next section).

The presence of group F bZIPs in the wheat genome that have a reduced ability to rescue the mutant phenotype of the *bzip19-4bzip23-2* mutant (TabZIP3b-7BL and TabZIP4-7DL) is in itself intriguing. Their presence could be a result of genetic redundancy due to the hexaploidy of wheat (*T. aestivum*), perhaps in some sets of homeologs evolutionary pressure for conservation of function is not present on all three homeologs. Another explanation is that perhaps the group F TabZIPs lacking a full group F motif 1 have another role. Perhaps they are important in the fine tuning of the Zn regulatory mechanism at very specific plant tissue locations, or alternatively these bZIPs may only bind and regulate specific Zn-responsive genes in wheat and are unable to bind to ZDREs present in the promoter regions of *Arabidopsis* Zn-responsive genes and sufficiently upregulate their expression in response to Zn-deficiency.

5.4.2 The binding ability of bZIPs to ZDRE motifs and the implications for the Zn homeostatic mechanism of *T. aestivum*

As detailed in Section 5.3.3.1, all of the *TaZIPs* identified had at least one motif that had two or more mismatches to the ZDRE consensus proposed by Assunção et al. (2010). In *TaZIP1*, 3, 4, 5, 7, 8 and 11, all homeolog members had at least one ZDRE with only a single mismatch to the ZDRE consensus, however the majority had multiple ZDRE copies in the promoter regions. The presence of motifs with strong consensus to the ZDRE investigated previously (Assunção et al., 2010), indicates a similar mechanism for Zn-regulation may be present in wheat as in *Arabidopsis*. In order to supplement the gene expression analyses presented in Chapter 3, the ZDRE motifs present in the promoters of *TaZIP1*, 4, 5, 6 and 7 were used in the binding assays. These five genes were all upregulated under Zn-deficient conditions (Chapter 3) however, notably in a shorter time course experiment *TaZIP6* was only upregulated in the shoot and not in the root. *TaZIP6* was also the slowest of the five *TaZIPs* to respond to Zn-deficient conditions. Additionally, the ZDRE motif patterning of *TaZIP6* homeologs is markedly different from *TaZIP1*, 4, 5 and 7, with different motifs present across the three homeologs and only *TaZIP6-1AS* containing a ZDRE motif with a single mismatch to the consensus. Furthermore, homeologs

of *TaZIP1*, 5, 6 and 7 have all been shown to transport Zn in the *zrt1/zrt2* yeast mutant (Chapter 4). In order to consolidate and further understand the roles and interactions of these TaZIPs with the TabZIPs characterised in the *Arabidopsis* complementation section of this Chapter, EMSAs were used to investigate the binding ability of TabZIPs to the ZDRE motifs identified.

Initially, the binding ability of AtbZIP19 was tested. Assunção et al. (2010) have previously shown that AtbZIP19 can bind to a two and three ZDRE containing probe (Ass2Z and Ass3Z), however mutation of TCGA core to TAGA (Ass3Zmut) prevented binding of AtbZIP19. The AtbZIP19 results in this study are in accordance with their findings, with these three probes behaving as previously described. Of the five TaZIPZDRE probes tested, AtbZIP19 produced a band shift with TaZIPZDREs: 1, 4, 5 and 7, but not TaZIP6ZDRE. This preservation of binding shows that there is a conservation of the Zn-regulatory processes between wheat and *Arabidopsis*. It was interesting that TaZIP6ZDRE could not produce a band shift despite having a TCGA core, this indicates there is something elsewhere in this ZDRE motif that results in a lack of binding. Comparisons between the probes suggests the nucleotide following the core sequence is important. At this point, all other ZDRE probes tested had a cytosine nucleotide, whereas TaZIP6ZDRE has a guanine nucleotide (nucleotide position shown underlined as follows: ATGTCGAGAC). The results from the binding assay with AtbZIP19 show the importance of this position in the ZDRE motif.

The EMSA with TabZIP1-7DL had very similar results to that of AtbZIP19, with band shifts at the two non-mutated *Arabidopsis* probes and at all TaZIPZDRE probes except for TaZIP6ZDRE. As presented in this Chapter, TabZIP1-7DL is able to complement the *bzip19-4bzip23-2* mutant, indicating a role in the Zn-regulatory network of wheat. When the ability of TabZIP1-7DL to bind to the ZDREs present in the promoters of four confirmed Zn transporting *TaZIPs* (Chapter 4) is added to this, the evidence for this being the mechanistic basis of the Zn-regulatory network in wheat is very robust. The inability of TabZIP1-7DL to bind to a tandem repeat of the ZDRE motif found in the promoter region of the confirmed Zn transporting *TaZIP6* is surprising. Perhaps the actual ZDRE of this gene is further than 2000 bp from the start codon, or perhaps the ZDRE identified in the upstream region of *TaZIP6-1AS* is only a functional target when surrounded by the native sequence found in this upstream region.

Across the EMSAs of TabZIP3b-7BL, TabZIP4-7AL and TabZIP4-7DL, only one single band shift was observed, this was TabZIP3b-7BL binding to the three copy *Arabidopsis* ZDRE (Ass3Z). The fact that TabZIP3b-7BL did not bind to the two copy *Arabidopsis* ZDRE (Ass2Z) indicates this may not be a specific binding. It may be that a threshold in biochemical attraction between the bZIP protein and the ZDRE double strand DNA is achieved, this level of interaction may not occur naturally in the wheat genome. However, the tested *TaZIP4* promoter did have three ZDRE copies which were spaced apart across ~1000 bp (probe used was TaZIP4ZDRE),

although only two combined TCGA core sequences were present due to the third in TaZIP4ZDRE being TTGA, so this could be the difference between binding occurring or being prevented, this may be interesting to test further using different ZDRE probe permutations. Overall the lack of binding ability of TabZIP3b-7BL and TabZIP4-7DL is unsurprising given both had little ability to complement the *bzip19-4bzip23-2*. However, the complete absence of any band shift and therefore no binding across any of the TabZIP4-7AL and probe combinations tested does not support the *bzip19-4bzip23-2* complementation ability this bZIP showed. There are several hypotheses for this: firstly, the physical distance between ZDREs that is naturally found in the promoter regions may make a difference to binding. Perhaps some TabZIPs are sensitive to this binding parameter. This is supported by the lack of binding shown by TabZIP4-7AL to any of the *Arabidopsis* ZDRE probes despite their likely being interactions between them *in-planta* due to the rescue ability of TabZIP4-7AL in the *bzip19-4bzip23-2* mutant. The *Arabidopsis* ZDRE probes are not actually as they appear in the promoter of *AtZIP4* as there are gaps between the ZDREs and also different flanking sequence. These binding parameters may be important for some *TabZIPs*. It could be suggested that this differential sensitivity to the spacing of probes is part of the intricate Zn-regulatory framework in wheat and perhaps allows specific subsets of Zn-responsive genes to be upregulated rather than a global upregulation of all Zn-responsive genes as appears to likely be the case with TabZIP1-7DL. This additional level of intricacy may be more important to wheat than *Arabidopsis*, at very specific regions and at specific time points the remobilisation and redistribution of Zn in wheat may be more complex than in *Arabidopsis*.

The second hypothesis for the lack of binding exhibited in the EMSA of TabZIP4-7AL (and also perhaps TabZIP3b-7BL and TabZIP4-7DL) could be that they interact with Zn-responsive genes not tested in this study. Perhaps they have specific roles in upregulating *TaZIP* genes identified yet not tested, or even other Zn-responsive gene families such as the nicotianamine synthases which have been shown to harbour ZDREs in their promoter in *Arabidopsis* (Assunção et al., 2010). The final hypothesis for this lack of binding could be that some TabZIPs operate at very narrow Zn concentration ranges perhaps facilitating specific Zn regulation at a scale smaller than the whole plant. In the binding reaction mix during the EMSA protocol, although no Zn is added, there must be a level of Zn in the *in-vitro* coupled transcription-translation kit. Perhaps this small level of Zn is bound by TabZIP4-7AL, yet not TabZIP1-7DL which renders TabZIP4-7AL functionally inactive and prevents binding of this TabZIP. It would be interesting to both eliminate all Zn from the EMSA binding mix as well as add additional to see if binding of TabZIP4-7AL could be achieved if less Zn is present and also if the binding of both AtbZIP19 and TabZIP1-7DL is lost at higher Zn concentrations.

The final TabZIP tested was the group G TabZIPG. TabZIPG produced a band shift with one probe; TaZIP4ZDRE. It remains unclear why TabZIPG-5DL binds to this probe. It is possible

that increasing *TaZIP4* expression may be an adaptive response provided by TabZIPG-5DL. TabZIPG has been shown to be involved in numerous stress responses and possibly an upregulation of *TaZIP4* is linked to these (Zhang et al., 2008). However, another possible explanation is that it could be the DNA binding domain found across the entire bZIP family is quite similar. The presence of three TaZDRE motifs as present in the TaZIP4ZDRE probe may be biochemically irresistible when presented *in-vitro* thus creating the faint band shift observed.

In summary, thus far in this Thesis the *TaZIP* family and group F *TabZIPs* have been identified and their expression response profiles to Zn-deficiency have shown they are Zn-regulated (Chapter 3). The ability of Zn-responsive TaZIPs to transport Zn was shown in Chapter 4. The functional ability of certain TabZIPs to rescue the Zn-deficiency response of the *bzip19-4bzip23-2* mutant line has been reported in this Chapter, as well as mechanistically linking the TaZIPs and TabZIPs through interaction assays of TabZIP proteins binding to ZDRE motifs present in the promoters of the *TaZIPs*. The results provided thus far give a valuable delineation of the Zn-regulatory network in wheat. In order to move toward the end goal of developing breeding programmes and biofortification strategies, variation in Zn performance across a diverse wheat germplasm is reported in the next Chapter. An attempt is made to link the knowledge of the wheat Zn-regulatory network acquired thus far with the differential Zn performance of individual varieties to further the understanding of this intricate regulatory process.

Chapter 6. Examining differences in Zn characteristics using a diverse wheat germplasm

6.1 Introduction

Surveys examining mineral concentration in wheat (*Triticum* spp.) lines have shown that extensive variation is present. For instance, Monasterio & Graham (2010), examined 324 lines which included wild species, landraces (a traditional variety with historic origin, often locally adapted and associated with traditional farming systems), high-yielding bread wheat, durum wheat and triticale (a cross between wheat and rye). The study showed that substantial variation existed in Zn and Fe concentration in the grain, with grain Zn concentration ranging from 25-92 mg/kg and Fe from 25-73 mg/kg. Within the top 12 performers in terms of grain Zn concentration, three genotypes were wild relatives, three were pre-breeding lines from a CIMMYT project, three were landraces and three were commercial cultivars showing enhanced micronutrient accumulation in the grain. In this study, Monasterio & Graham (2010) found that seven of the top 12 performers in terms of Zn concentration in the grain were also in the top 12 in terms of Fe concentration in the grain, suggesting that it may be relatively easy to combine high-Fe and high-Zn traits during breeding programmes. However, in this study the size of the grain or yield was not accounted for when examining the grain concentrations. These parameters are vital when investigating any micronutrient concentration. Larger grains will likely contain lower concentrations of micronutrients; this is an effect of concentration-dilution by the dry matter accumulated in the grain and is not useful in terms of biofortification (White and Broadley, 2005).

In another large field study, Zhao et al. (2009) examined variation in micronutrient concentration of 150 bread wheat (*T. aestivum*) lines. Zn grain concentrations ranged from 13-34.5 mg/kg. The range in Zn concentrations is lower than that reported in Monasterio and Graham (2010), but this was suggested to be due to the high soil pH (8.0) at the trial site reducing Zn availability to the plants. It has been predicted that for a measurable biological impact on human health, grain Zn concentration should be increased by 10 mg/kg from existing levels (~30 mg/kg to ~40 mg/kg) (Graham et al., 2007). However, critically not all of the Zn consumed in any food can be absorbed and utilised by the body; antinutrients such as phytate can dramatically reduce the amount of Zn that is absorbable (the bioavailability) from a food product. Given the variation existing in both bread wheat (*T. aestivum*) and other wheat relatives (see Table 1.1) this target increase of 10 mg/kg seems feasible if variation is heritable. In order to identify lines of particular interest, further studies must take into account grain yield to avoid any concentration-dilution effects. Once lines of interest are identified that show increased Zn accumulation parameters

independent of yield, unravelling the molecular basis for this variation will be an important step in the development of breeding or biofortification strategies to enhance the Zn concentration of wheat.

QTL analyses have previously been conducted to establish the chromosomal location of genes involved in the increased grain concentration of Zn. *Gpc-B1* on chromosome 6B of wild emmer wheat (*T. dicoccoides*) was identified as a candidate for grain protein content, as well as Zn, Fe and Mn concentrations in the grain, however modern wheat cultivars carry a non-functional allele of this NAC transcription factor coding gene (Distelfeld et al., 2007). Distelfeld et al. (2007) used recombinant chromosome substitution lines (RSLs) (used previously to map the *Gpc-B1* gene) to investigate this further. An increase in grain Zn, Mn and Fe concentration was observed when the RSL carried the functional *Gpc-B1* allele from *T. dicoccoides*, compared to the non-functional *Gpc-B1* allele from *T. durum*. No significant difference was present in 1000 kernel weights between lines, suggesting the increases in protein and micronutrient concentrations were not due to the dilution-effect of grain size discussed previously. This data supports the hypothesis that the wild-type *Gpc-B1* allele is involved in a more efficient remobilisation of protein, Zn, Mn and Fe from leaves to the grains. The integration of this allele in commercial wheat cultivars may provide an option to increase the protein and micronutrient concentration of the grain and is an example of how understanding genes underlying key Zn traits can be used to breed lines with increased Zn concentration.

Another QTL analysis examining grain Zn concentration using a double haploid population derived from a cross between RAC875-2 (Zn-inefficient line) and Cascades (moderately efficient Zn line) was carried out by Genc et al. (2009). In this study four QTL were identified situated on chromosomes 3D, 4B, 6B and 7A that mapped well to grain Zn concentration which ranged from 29 to 43 mg/kg throughout the population. Interestingly, Genc et al. (2009) observed no significant difference in grain yield among the lines examined and there were no phenotypic or genetic correlations between grain yield and grain Zn content, which indicates the variations observed in grain Zn content are independent of a dilution effect from increased grain size and that further, genetic variation exists that may allow the enhancement of wheat grain Zn content without reducing yield.

In this Chapter, germplasm from the WISP (Wheat Improvement Strategic Programme) project is utilised. The WISP project, comprised of five UK research teams (Rothamsted Research, John Innes Centre, University of Nottingham, University of Bristol and NIAB (National Institute of Agricultural Botany)) aims to generate, genotype and phenotype novel wheat germplasm. An aspect of this programme is the screening of selected field grown germplasm for efficient mineral nutrient capture and partitioning between grain and straw at final harvest. The datasets generated from this programme contain a range of micronutrients including

Zn. This presents an excellent opportunity to investigate variation in Zn uptake, accumulation and partitioning to the grain across the germplasm. Rothamsted Research (Harpenden, UK) has grown a diverse germplasm within the WISP project from 2011 to 2015. This germplasm consists of a subset of the Watkins Collection (Miller et al., 2001), a selection of the Gediflux Collection (Reeves et al., 2004), synthetic hexaploid wheats (SHW) provided by NIAB and a number of modern bread wheat cultivars grown commercially throughout the UK (here on referred to as modern cultivars). The Watkins collection consists of a genetically diverse collection of wheat landraces collected from around the globe during the 1920s and 1930s. The SHW lines are derived crosses between *T. turgidum* (AABB) with the ancient D genome progenitor *Aegilops tauschii* in an attempt to introduce extensive D genome variation. In this Chapter lines are identified that both overperform and underperform in terms of Zn uptake and partitioning within the WISP donor germplasm and are investigated further in an attempt to link differential Zn performance with the existing knowledge of wheat Zn homeostatic mechanisms.

6.2 Aims

The aims of the experiments reported in this chapter were to:

- Investigate micronutrient datasets from the WISP donor germplasm experiment and identify a selection of lines that consistently exhibit Zn characteristics of interest. Lines will be selected independently of yield to prevent any concentration-dilution effects.
- Sample selected lines in the field at multiple time points before harvest and examine their Zn concentrations to determine how Zn uptake varies in identified lines before harvest.
- Link existing molecular knowledge of the Zn homeostasis network discovered in wheat, with differential in-field Zn performance using gene expression studies and a QTL analysis of an appropriate biparental mapping population.

6.3 Results

The WISP donor germplasm was used to select lines of interest based on Zn uptake and partitioning parameters; the selection process is outlined in this section. The datasets used for initial line selection were from the 2011 and 2012 field seasons (courtesy of Riche A.). Additionally, as part of this study, samples were taken at two time points before harvest in the 2013 field season and subjected to ICP-OES mineral analysis and gene expression analysis of *TaZIP1* and *TabZIP1* (see Section 6.3.6). Samples were subsequently taken at a single time point before harvest in 2014 and subjected to ICP-OES mineral analysis. These Zn concentrations taken during the growing season were compared to Zn concentration at final harvest across 2011, 2012, 2013 and 2014. Based on Zn concentrations and Zn uptake measurements across the dataset, two lines with consistently contrasting Zn uptake and partitioning were selected to investigate further

using a hydroponic Zn-deficiency experiment; reported in Section 6.3.7. Phenotypic data and gene expression analysis was used to investigate if differential ability to maintain growth existed under Zn-deficient conditions. Finally, in Section 6.3.8 a mapping population of a Watkins Collection line shown to have high Zn uptake and grain Zn concentration, which was also studied in the comparative hydroponic experiment, was analysed to identify QTLs associated with Zn concentration and partitioning within the plant.

6.3.1 General variation in Zn concentration

Initially, variation in Zn concentration of above ground tissue (wheat straw and grain combined, now on referred to as 'total biomass') was examined. Figure 6.1A shows the variation in Zn concentration of total biomass. A large variation exists across the germplasm. For example, the modern cultivar Oakley had an average total biomass Zn concentration of only 17.5 mg/kg. In comparison, Watkins Collection line 729 (WC729) showed a much higher average total biomass Zn concentration of 39.3 mg/kg. It is however important to note that lines of interest cannot be determined without considering the effect of concentration-dilution by yield variation. It is possible that lines producing lower total biomass will have higher mineral concentrations due to a reduced dilution effect; this has been previously reported in some trials (Oury et al., 2006; Garvin et al., 2006; Morgounov et al., 2006). Evidence supporting this is present in Figure 6.1A, as the Zn concentrations of total biomass from the 2011 field trial appear in general higher than those from the 2012 trial. This may be explained by the lower total biomass yields recorded in 2011 versus 2012 (2011 average yield=17.3 t/ha DM (dry matter), 2012 average yield=18.4 t/ha DM). The reduced total biomass yields experienced in 2011 result in less physical biomass to dilute the minerals present, thus contributing to the higher mineral concentrations observed. Figure 6.1A indicates that Zn concentration of above ground biomass remains quite stable across the harvest years of 2011 and 2012, as lines display a similar rank order across both years, indicated by the positive correlation observed.

When the grain Zn concentration of the germplasm was examined, considerable variation was also observed within the 2011 and 2012 datasets, see Figure 6.1B. The modern cultivars examined in this germplasm grouped at the lower end of the concentration range in both years examined, due to their increased grain yield diluting Zn present in the grain and reducing the overall Zn concentration in final grain Zn concentration measurements. The same trend in higher overall grain Zn concentration can be observed in the 2011 samples compared to the 2012 samples as seen in the Zn concentration of total biomass. The range in grain Zn concentrations in 2011 was 26.1 to 70.3 mg/kg (Oakley and WC694 respectively) with an average of 45 mg/kg. 2012 grain Zn concentrations ranged from 24.4 to 52.2 mg/kg (Oakley and WC468 respectively) with an average of 37.0 mg/kg.

These results show that the germplasm contains substantial variation in terms of total biomass and grain Zn concentrations, however in order to identify lines of interest, the data may be further examined taking the individual yield of lines into account.

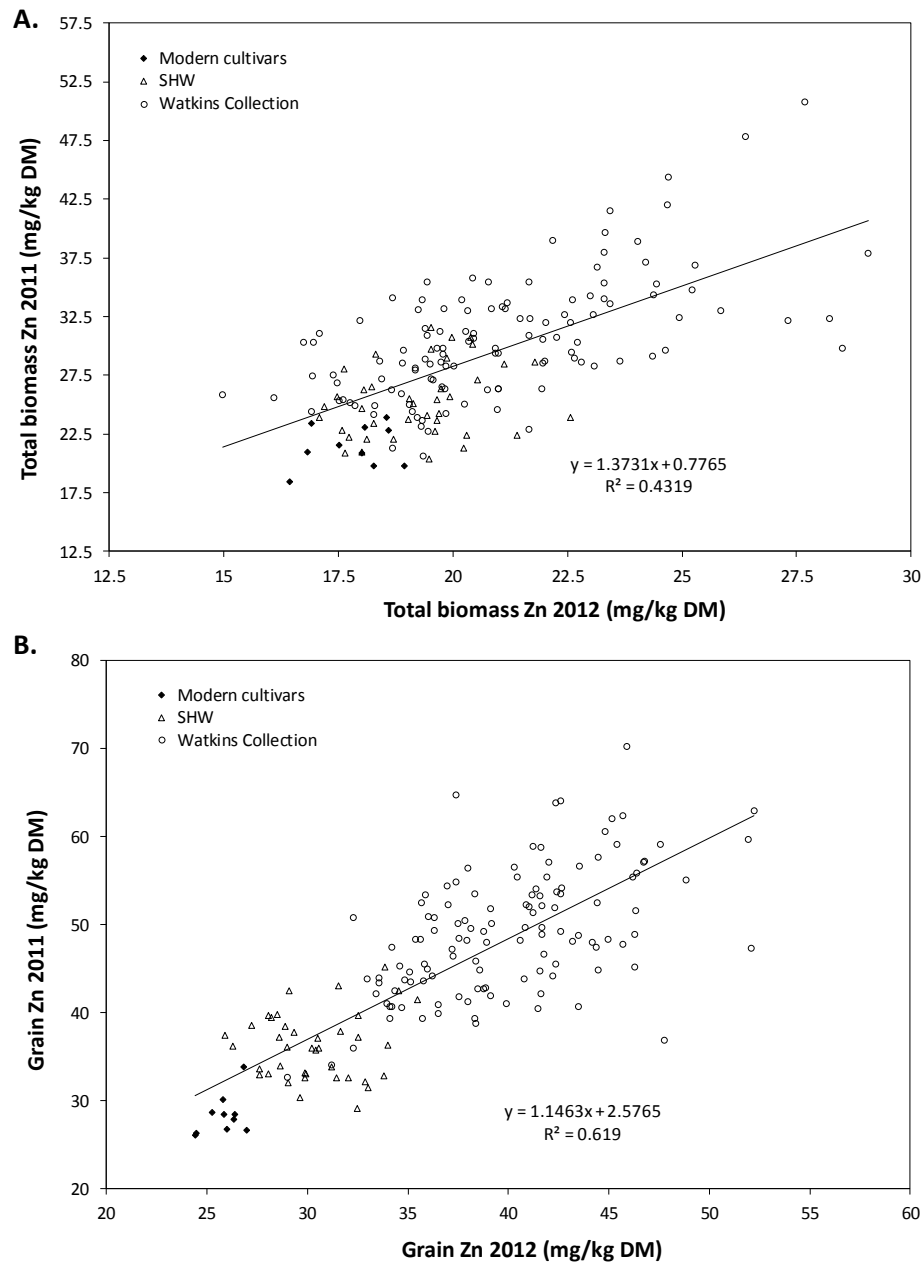


Figure 6.1. Extensive variation in Zn concentration exists across the WISP donor germplasm. Variation in the mean Zn concentration (mg/kg DM) of **A.** total biomass and **B.** grain across the 2011 and 2012 WISP germplasm datasets. Modern cultivars, synthetic hexaploid wheats (SHW) and Watkins Collection lines are given different symbols as shown in the included legend.

6.3.2 Variation in the Zn uptake of total above ground biomass

The first parameter examined when screening for lines of interest within the WISP germplasm was the total uptake of Zn in the total biomass (grain plus straw). As discussed previously, when examining micronutrient traits of interest, it is imperative that the relevant yield function is considered. In this case of total biomass Zn uptake, we must consider results alongside the total yields. Figure 6.2 shows how Zn uptake in the total biomass varied with total yield in 2011 and 2012. An increased Zn uptake can be seen with increasing total yield across both years. This is as expected; higher yielding lines will accumulate more Zn due to their increased size. However, the interesting variation lies in the deviation from this line of best fit, shown in Figure 6.2 as the blue and orange arrow annotations. The blue arrows show variation from the line of best fit and indicate lines that show a lower Zn accumulation in their total biomass than would be predicted based on their total biomass yield. Conversely the orange arrows show lines with a higher Zn accumulation than would be expected given their total yield.

This deviation from the line of best fit was calculated and is referred to in this Chapter as the ‘residual’. These residual values were plotted for 2011 and 2012 see Figure 6.3. This figure gives a clear indication of how consistent the performance of lines was across both 2011 and 2012 for total Zn uptake. Lines in the upper right quarter showed total Zn uptake values that were higher (above the line of best fit) than expected based on their total yield in both 2011 and 2012. Conversely, those lines in the lower left quarter showed total Zn uptake values lower (below the line of best fit) than expected based on their total yield in both 2011 and 2012. The calculation of residuals to identify consistent performers was also conducted with grain Zn concentration as a function of grain yield (see Section 6.3.3). Using the residual plots of these parameters ten lines were identified as consistently overperforming or underperforming in terms of Zn uptake and accumulation and are shown in graphs throughout this Chapter with orange and blue data labels respectively. The selection of the ten lines was made before the 2013 and 2014 datasets were available, so their performance in these latter years gives an indication of the robustness of the selection.

Figure 6.4 shows the 2013 and 2014 variation in total Zn uptake with total yield. The lines selected based on the 2011 and 2012 datasets are labelled and in all but one case (WC507 in 2013) performed as predicted in the amount of total Zn uptake relative to total yield. This consistency is examined further in Figure 6.5. Here the average residual measurement across the four years of datasets is shown. It is clear that the lines selected using only the 2011 and 2012 datasets consistently underperform or overperform in total Zn uptake relative to total biomass yield.

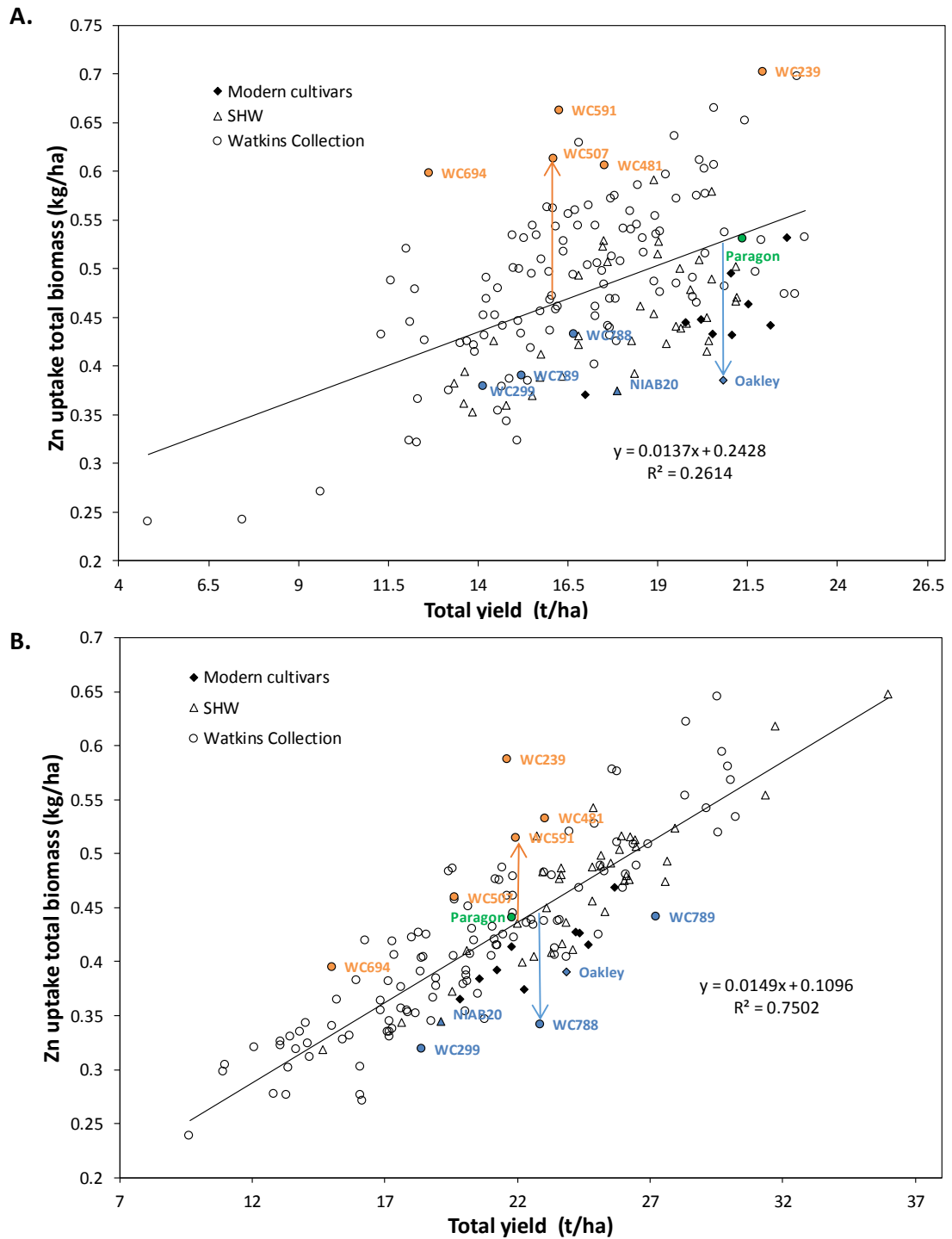


Figure 6.2. Total biomass Zn uptake increases with total yield in 2011 and 2012 field grown germplasm datasets. Total biomass Zn uptake (kg/ha) increases with total yield (t/ha) in 2011 (A.) and 2012 (B.). Arrows indicate the direction of potentially interesting deviation from the expected Zn uptake value (the residual); lines above the line of best fit (orange arrow) have higher Zn uptake levels than the trend of average total yield suggests and those below (blue arrow) have lower than expected Zn uptake levels than the total yield trend suggests. Modern cultivars, SHW and Watkins Collection lines are given different symbols as shown in the included legend.

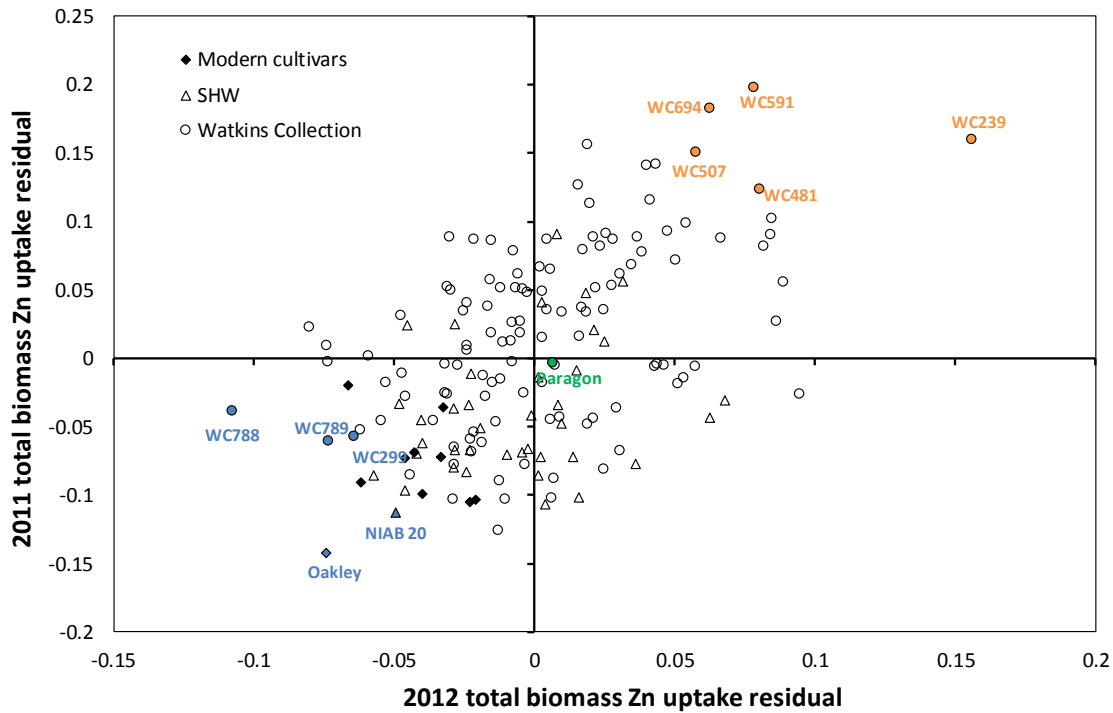


Figure 6.3. Residual values (differences between trendline predictions and actual measurements of total Zn uptake) for 2011 and 2012. The upper right quarter shows lines with higher total Zn uptake values than expected based on their total yield in both 2011 and 2012. Conversely lines in the lower left quarter showed total Zn uptake values lower than expected based on their total yield in both 2011 and 2012. The ten selected lines that are being investigated further are shown labelled in blue and orange, along with the spring wheat cv. Paragon (shown in green), which was used in the Zn-starvation experiments presented in Chapter 3.

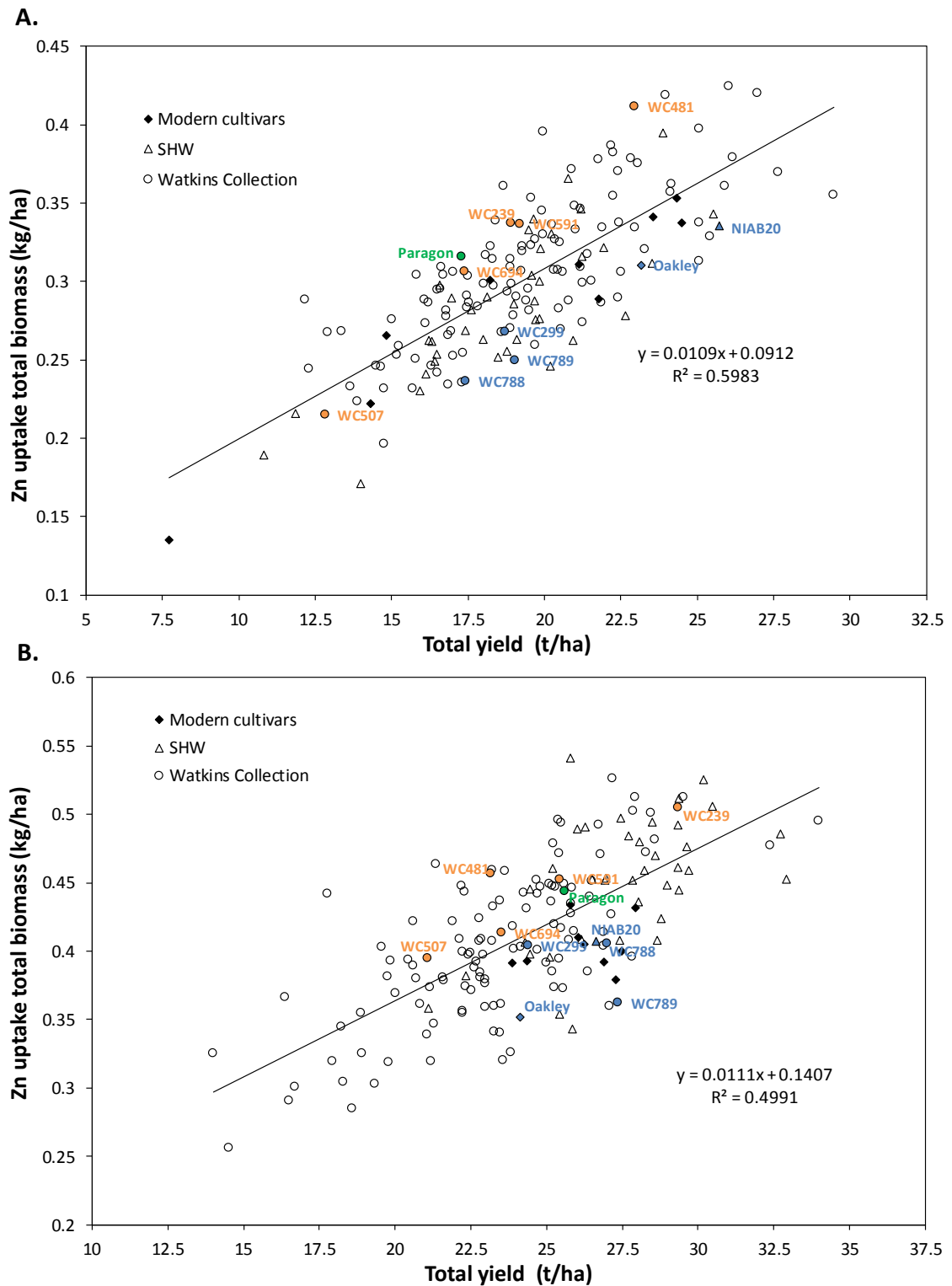


Figure 6.4. Total biomass Zn uptake increases with total yield in 2013 and 2014 field grown germplasm datasets. Total biomass Zn uptake (kg/ha) increases with total yield (t/ha) in 2013 (A.) and 2014 (B.). The lines selected for further study based on the residual measurements calculated using the 2011 and 2012 dataset are shown labelled in blue and orange. The consistency in total Zn uptake performance of these ten lines can be seen in 2013 and 2014.

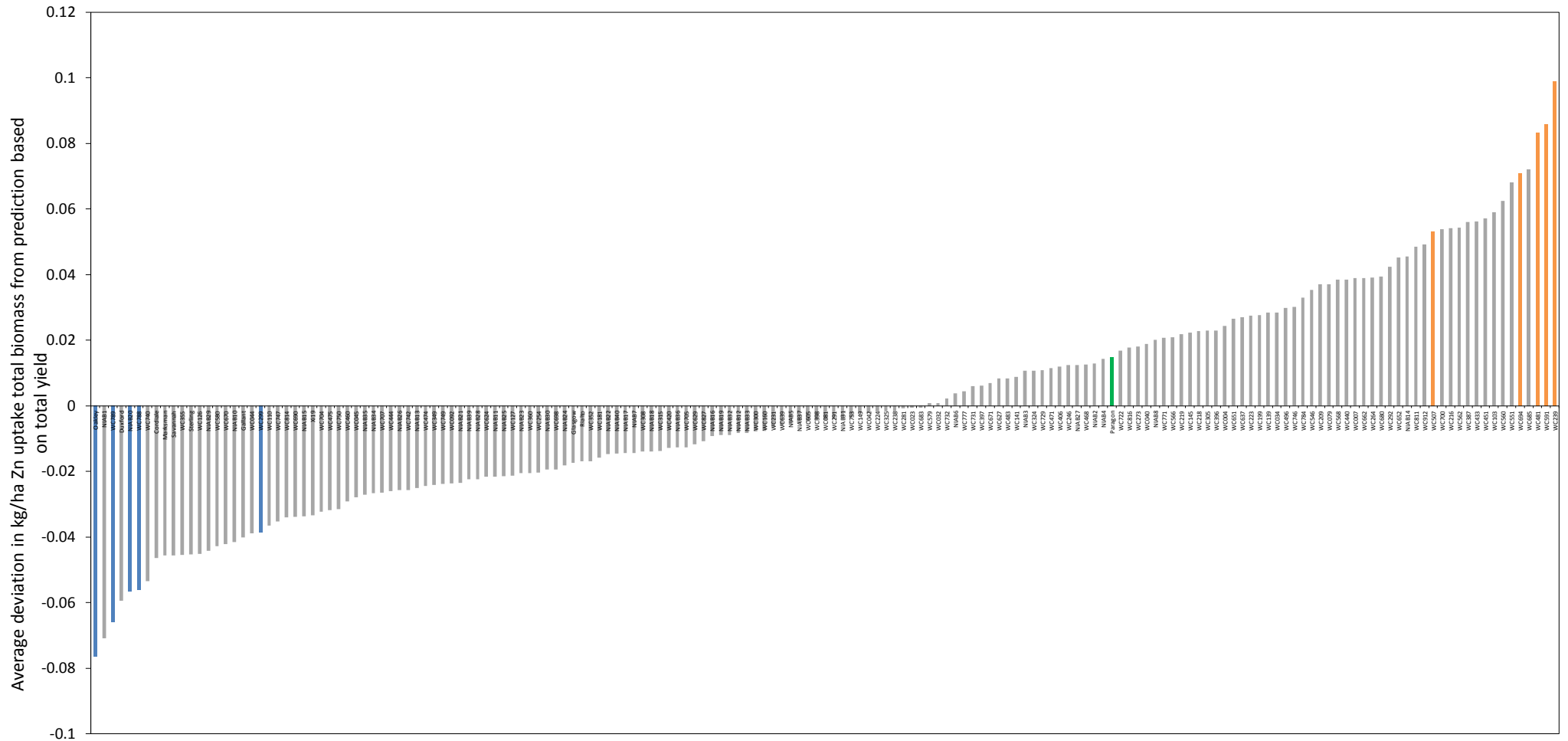


Figure 6.5. Residual values of total biomass Zn uptake vs total yield from four years of field grown WISP germplasm. Across the 2011, 2012, 2013 and 2014 datasets, average residuals were calculated. Average residuals presented are the average deviation of Zn uptake into the total biomass from the prediction based on total yield (the average deviation from the line of best fit for each line presented in Figures 6.3 and 6.4). The ten lines initially selected based only on 2011 and 2012 data are shown in blue and orange. Their consistent performance across the years is evident from their locations at the respective extremities of this figure.

6.3.3 Variation in grain Zn concentration across the germplasm

A high variation in grain Zn concentration was observed within the 2011 and 2012 grown germplasm (see Figure 6.1B). This is promising in terms of potential to increase grain Zn concentration. Figure 6.6 shows that as grain yield increases, concentration of Zn in the grain is reduced. This is as expected; the larger the grain yield, the more dilution of micronutrients that will take place. Figure 6.6 shows this relationship clearly, especially in the case of the modern cultivars examined. Across the four years examined the modern cultivars consistently grouped at the highest point in terms of grain yield but were low in terms of grain Zn concentration.

Using the same principles outlined in Figure 6.2, the residuals were calculated for grain Zn concentration plotted against grain yield for the 2011 and 2012 datasets. This was used in the selection of the ten lines of interest before the 2013 and 2014 datasets were available. Figure 6.6(C, D) shows the performance of the ten lines was less easily predicted for grain Zn concentration than previously for total Zn uptake. Nevertheless, in 2013 (Figure 6.6C) the performances aligned with predictions, however in 2014 (Figure 6.6D) the performances of WC239, 299, 507 and 788 did not align with predictions based on previous years.

Figure 6.7 shows the four-year average residual value for grain Zn concentration based on grain yield predictions. Lines on the left of this figure showed lower grain Zn concentrations than expected based on their grain yield. Conversely lines on the right of the figure consistently showed higher grain Zn concentrations than is expected given their grain yield. The performance of the ten lines across the four years is consistent and again for this parameter the lines selected appear interesting and worthy of further investigation.

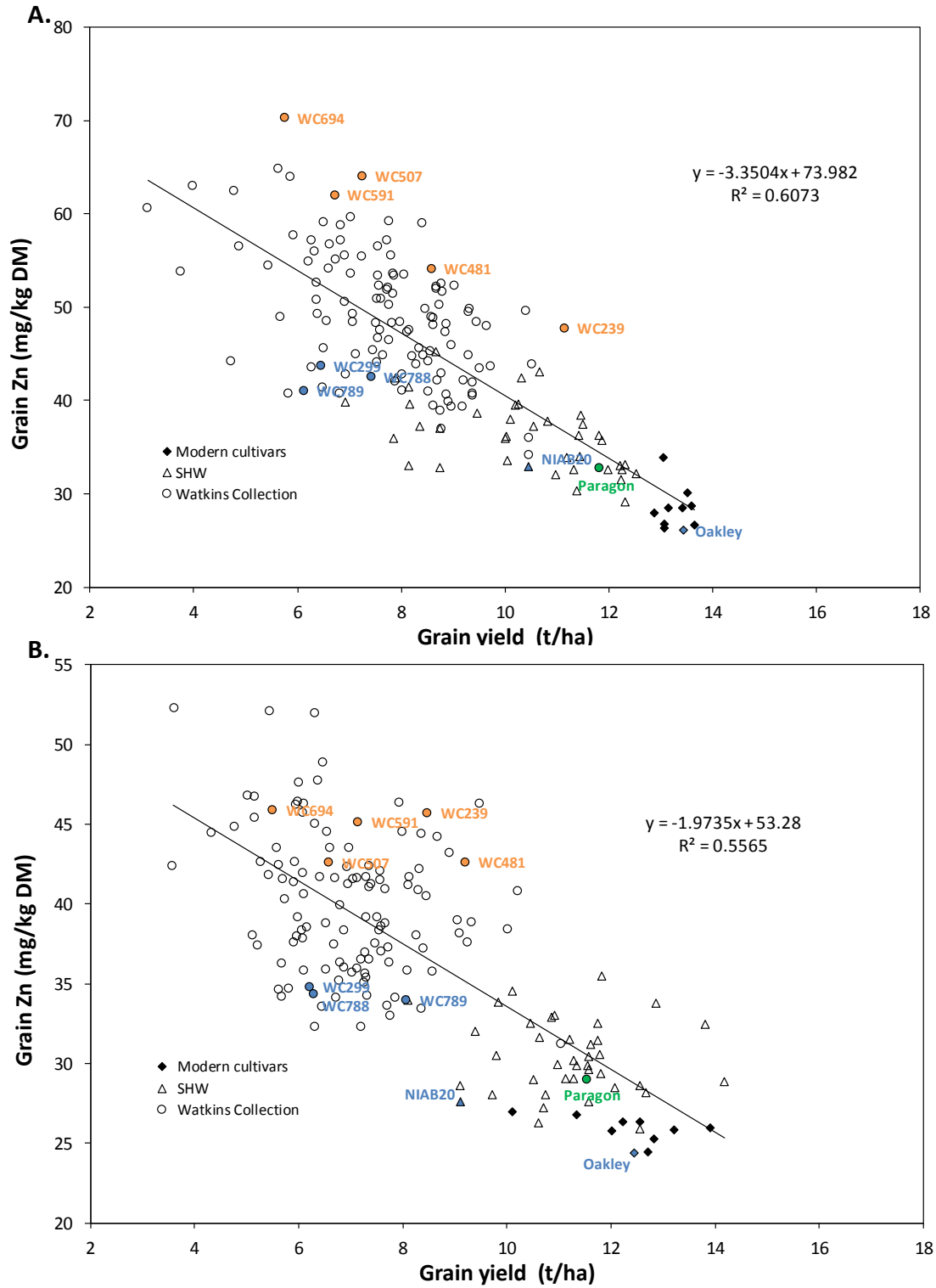


Figure 6.6. continued overleaf

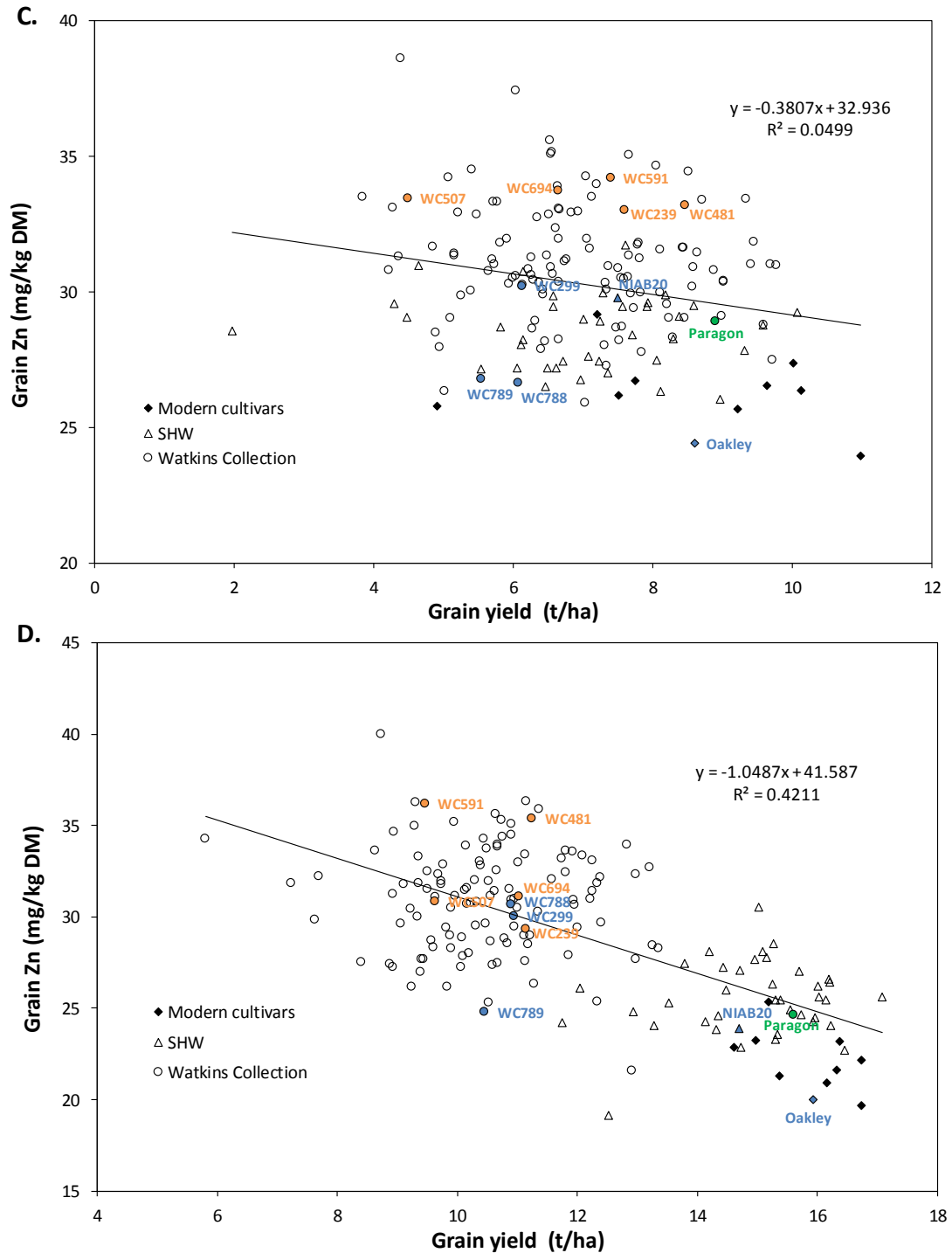


Figure 6.6. Grain Zn concentration reduces with increasing grain yield across four-years of field grown germplasm datasets. Grain Zn concentration (mg/kg DM) decreases with increasing grain yield (t/ha) in 2011 (A.), 2012 (B.), 2013 (C.) and 2014 (D.). Residual values were calculated (vertical deviation from line of best fit) for each line (see Figure 6.7). The lines selected for further study based on the residual measurements calculated using the 2011 (A.) and 2012 (B.) dataset are shown labelled in blue and orange. The consistency of the grain Zn concentrations of these ten lines can be seen in 2013 (C.) and 2014 (D.).

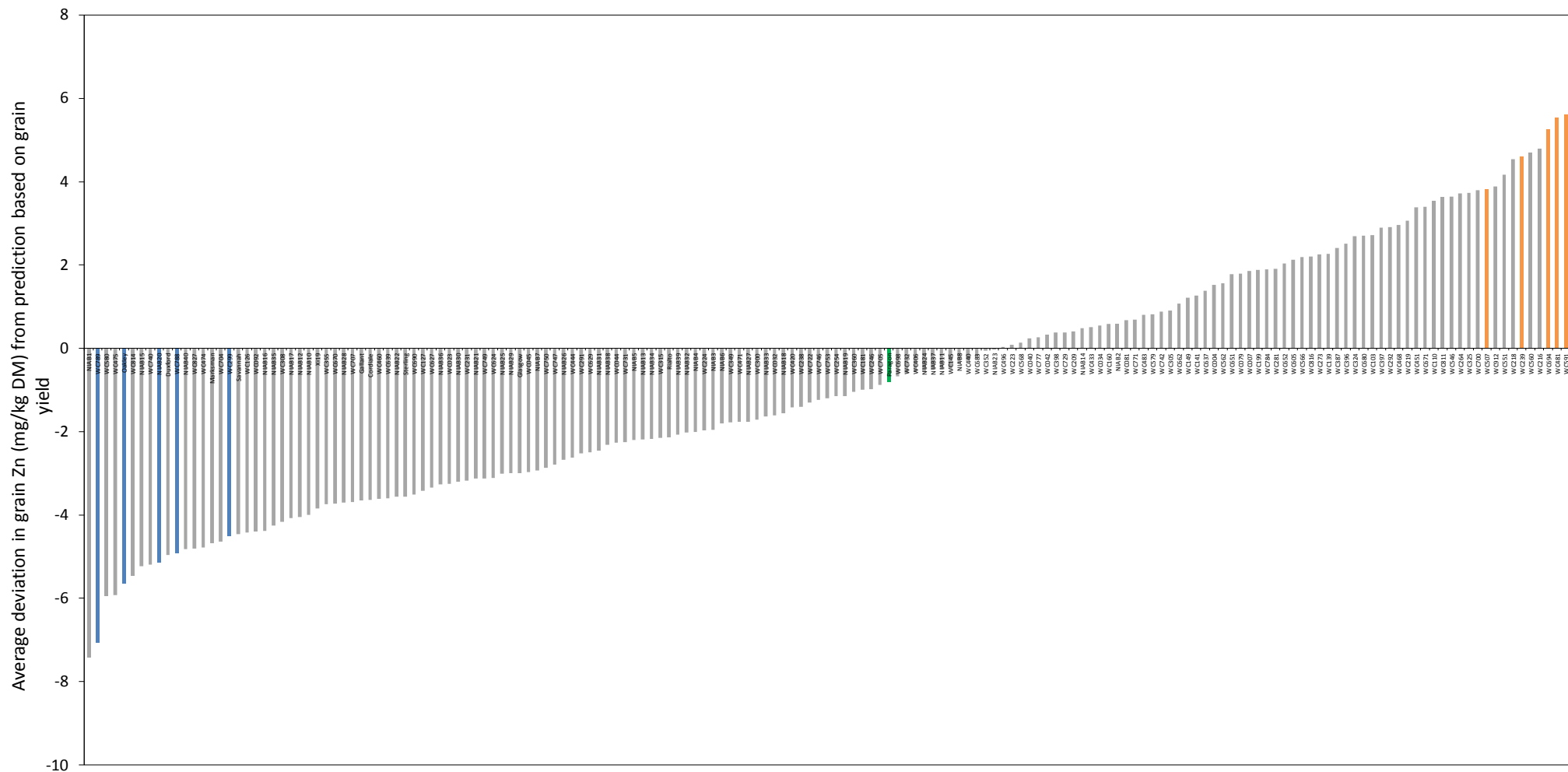


Figure 6.7. Residual values of grain Zn concentration vs grain yield from four years of field grown WISP germplasm. Across the 2011, 2012, 2013 and 2014 datasets average residuals were calculated. Average residuals presented are the average deviation of grain Zn concentration from the prediction based on grain yield (the average deviation from the line of best fit for each line presented in Figure 6.6). The ten lines initially selected based only on 2011 and 2012 data are shown in blue and orange. Their consistent performance across the years is evident from their locations at the respective extremities of this figure.

6.3.4 The variation in total yield and grain Zn partitioning across the germplasm

The four-year average total yield (straw and grain combined) of the varieties studied within the germplasm varied from a low of 13.03 t/ha in Watkins line WC729 to a high of 26.35 t/ha in Watkins line WC110. Figure 6.8 shows the range across the germplasm and the rankings of the ten lines selected for further analysis. Trends were not apparent in the total yields shown by the ten lines selected. This is favourable as if for instance lines selected as underperformers were all high yielding or tall lines, these could be factors in their differential performance. Figure 6.8 shows this is not the case and further enforces the selection of the ten lines and their subsequent use to further understand the molecular basis of differential Zn performance across the germplasm.

In order to assess Zn-partitioning efficiency across the Zn harvest index was examined. Zn harvest index is a measure of the proportion of Zn in the above ground biomass (the straw and grain combined) that is partitioned to the grain and is calculated at final harvest. The Zn harvest index average across the four years is shown in Figure 6.9. The ten lines selected show no obvious trend in terms of Zn harvest index and are spread throughout the germplasm indicating their performance in grain Zn concentration is not based solely on Zn-partitioning efficiency. Interestingly, it appears that the modern cultivars examined are efficient Zn partitioners as they cluster at the upper end of Figure 6.9, shown in yellow.

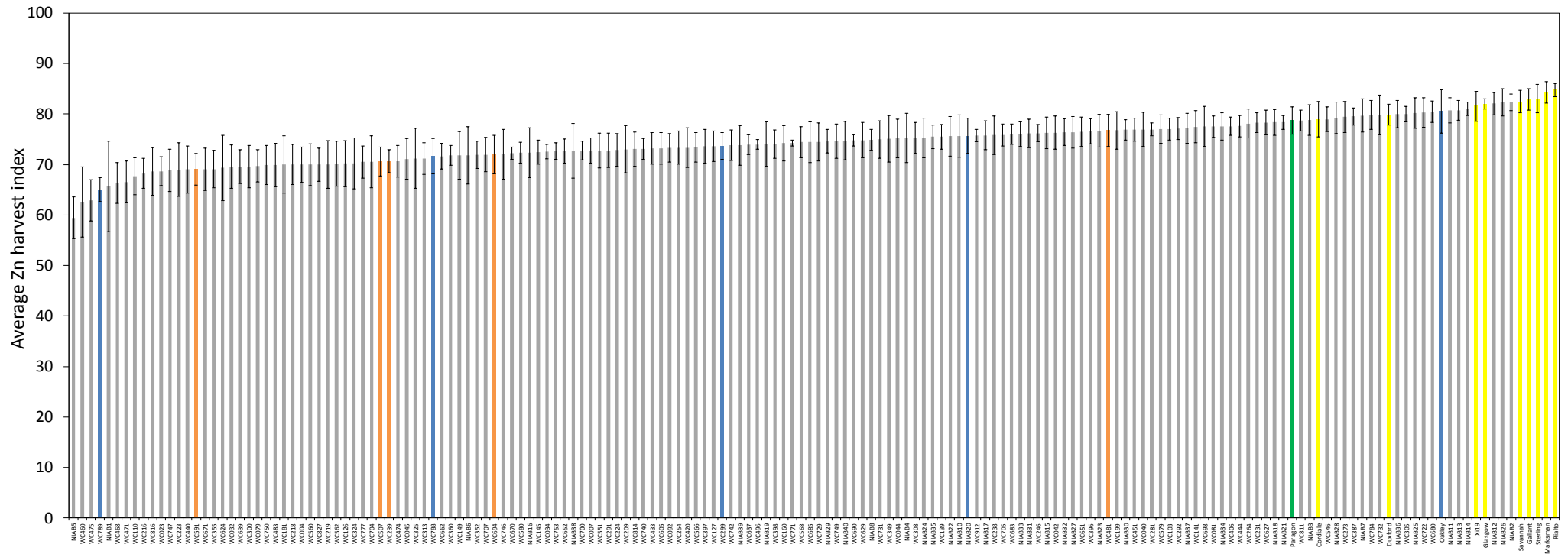


Figure 6.9. Four-year mean Zn harvest index across the field-grown WISP germplasm. Across the 2011, 2012, 2013 and 2014 datasets, Zn harvest index was calculated ($n=12$). Bars shown are \pm S.E.M. Zn harvest index is the proportion of Zn in the above ground biomass (the straw and grain combined) that is partitioned to the grain, calculated at final harvest. The ten lines initially selected based only on 2011 and 2012 data are shown in blue and orange. Trends are not visible in the total yield measurements of the ten lines selected on their differential Zn performance. The modern cultivars within the dataset are shown in yellow, their clustered presence on the right extremity of this figure indicates they are efficient Zn partitioners, partitioning a high proportion of their available Zn to the grain.

6.3.5 The performance of ten selected lines during the growing season

6.3.5.1 Zn concentrations

Having identified ten lines that show either consistently high or low Zn concentration traits at final harvest, sampling of these lines was conducted during the growing season. Shoot samples (stem and developing grain combined) were analysed using ICP-OES and Zn concentrations determined, see Figure 6.10. At the two time points sampled in 2013, a significant effect of cultivar was present at the booting growth stage ($F_{9,18} = 4.62$, $p < 0.01$ (Figure 6.10A), but not at grain filling stage ($F_{9,18} = 1.48$, $p = 0.227$) (see Figure 6.10B). At booting during the 2013 season, Watkins lines WC788 and WC789 had significantly lower Zn concentrations than the predicted overperforming lines WC239 and WC481. However, these trends were not observed at the second time point of sampling in 2013 where there was little difference between the five predicted underperformers and the five predicted overperformers.

Sampling was carried out at the booting growth stage during the 2014 field season (Figure 6.10C). No significant effect of line was observed at this time point in 2014 ($F_{9,18} = 1.13$, $p = 0.391$). There was however a noticeable difference between the predicted overperforming line WC239 and the underperforming line WC789.

Figure 6.11 shows both the total biomass Zn concentrations (mg/kg DM) and the total biomass yields at final harvest of the ten differentially performing lines from the 2011, 2012, 2013 and 2014 field seasons. The 2011 and 2012 datasets were used to select these overperforming and underperforming lines, so it is not surprising that there was a significant effect of line in these two years and the two performance groups had Zn concentrations as expected. The performance of these lines was consistent in 2013 and 2014, again with both years showing a significant effect of line in the Zn concentration measurements and both groups performing as expected in terms of total biomass Zn concentrations. When the final harvest Zn concentrations of the ten lines across the four field seasons are compared to the final harvest total yield measurements (t/ha), the trends in total yield were less evident between the two predicted Zn performance groups. This suggests that the consistent variation observed in Zn concentration and partitioning observed across the ten lines selected was not entirely due to the biomass of the lines chosen and these are interesting candidates to examine further.

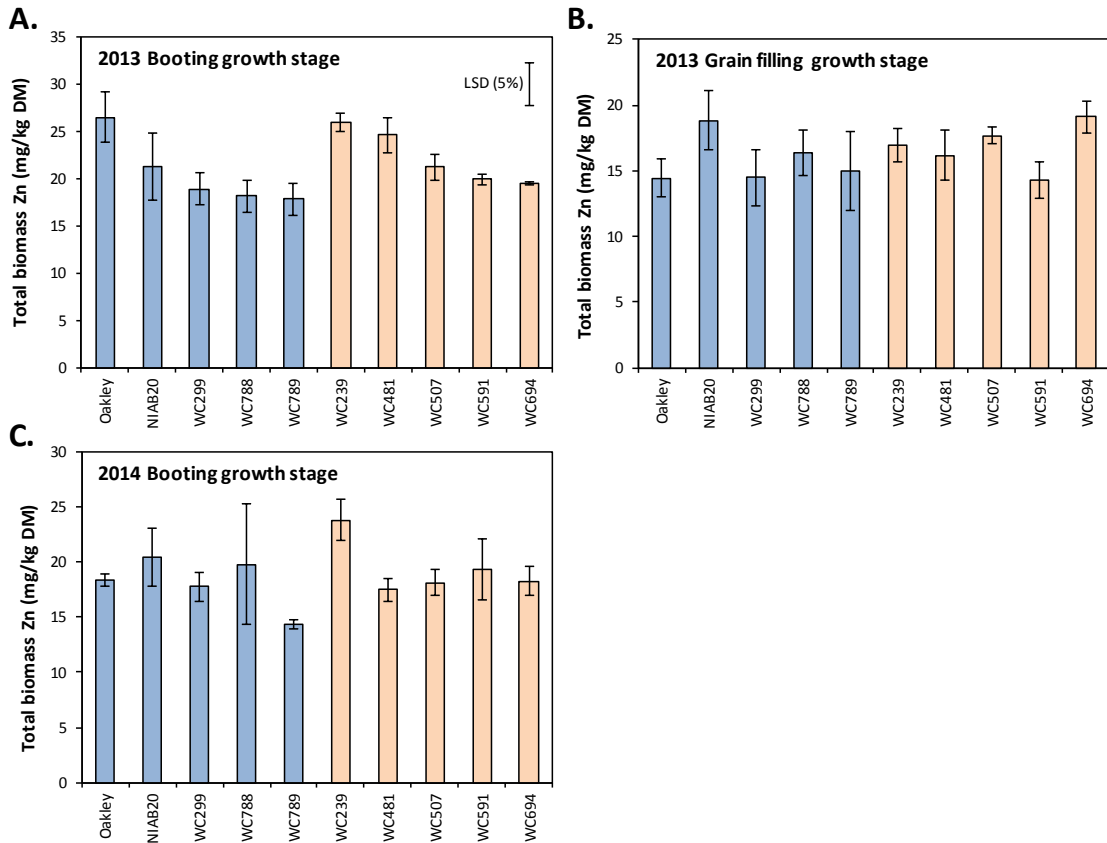


Figure 6.10. Zn concentrations of ten field grown wheat lines during the growing season. The five Zn-overperforming (orange bars) and five Zn-underperforming lines (blue bars) were sampled at two time points in 2013 (**A. Booting** and **B. Grain filling**) and one time point in 2014 (**C. Booting**). Means of three biological replicates are given (\pm S.E.M). In individual graphs where LSD bars are shown a significant effect of line was present ($P < 0.05$, F-test). LSD shown is the Fisher's LSD test value at the 5% significance level.

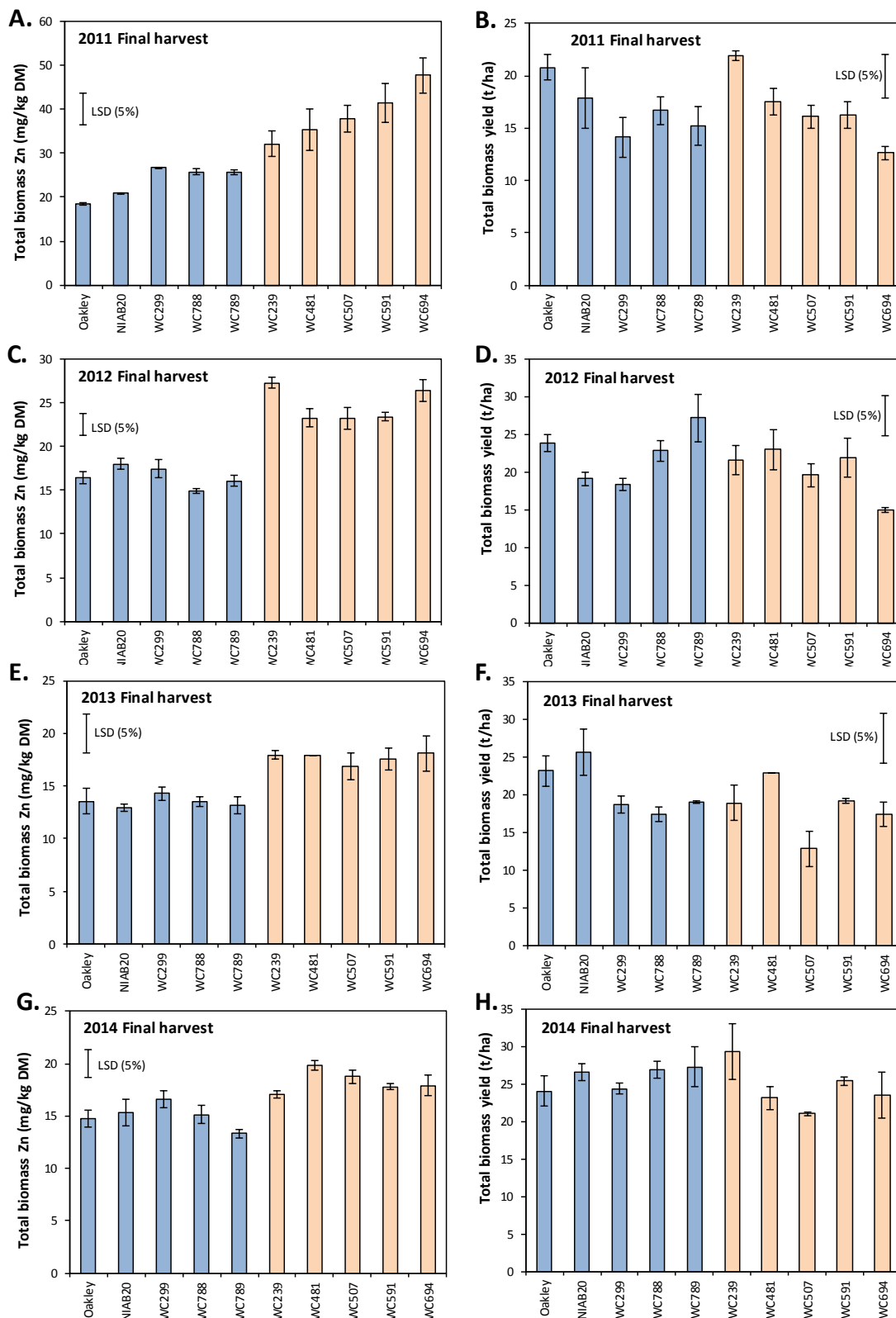


Figure 6.11. Zn concentrations and total biomass yield of ten field grown wheat lines at final harvest across four years of field trials. The Zn concentrations and total biomass yields of the five Zn-overperforming (orange bars) and five Zn-underperforming lines (blue bars) at final harvest in 2011 (A. and B.), 2012 (C. and D.), 2013 (E. and F.) and 2014 (G. and H.). Means of three biological replicates are given (\pm S.E.M.). In individual graphs where LSD bars are shown a significant effect of line was present ($P < 0.05$). LSD shown is the Fisher's LSD test value at the 5% significance level.

6.3.5.2 Gene expression

Root samples from the ten differentially performing lines taken during the 2013 field season at the time point of booting (for corresponding shoot Zn concentrations see Figure 6.10A) were analysed to determine gene expression levels of both *TaZIP1* and *TabZIP1*. Previously, *TaZIP1-2AL* was shown to transport Zn (Chapter 4), additionally, *TaZIP1* expression is Zn regulated (Chapter 3). The transcription factor, *TabZIP1-7DL* has been shown to complement the *Arabidopsis bzip19bzip23* double mutant and rescue the Zn-deficient phenotype (Chapter 5) and is also Zn regulated (Chapter 3). In order to establish whether these genes show a differential expression pattern across both the Zn overperforming and Zn underperforming lines identified, cDNA synthesised from root samples taken during the 2013 field season were subjected to absolute quantification real-time PCR (for full details see Section 2.3.7.2). Results are shown in Figure 6.12.

A significant effect of line on gene expression levels was observed only for the expression of *TaZIP1* ($F_{9,18} = 3.31$, $p = 0.016$) and not *TabZIP1* ($F_{9,18} = 2.35$, $p = 0.062$). The only line that had a significantly different *TaZIP1* expression level was the modern cultivar Oakley, which had a significantly higher *TaZIP1* expression level than all other varieties. No other line comparisons were significant when tested post-hoc with the Fisher's LSD test at 5%. No effect of line on *TabZIP1* expression level was observed, however the *TabZIP1* expression level of Oakley was again the highest of all lines examined. Compared to *TaZIP1*, *TabZIP1* expression levels had greater within line variation between the field blocks sampled, shown by the larger error bars. Somewhat similar trends in expression of the two genes between the ten lines can be observed, for example WC481 has lowest expression of both genes whilst the expression levels of most other varieties correlate well in relation to one another between the two genes examined.

Although the shoot Zn concentrations of the lines at this time point (Figure 6.10A), as well as at final harvest (Figure 6.11E), showed differences between lines (notably the Zn-underperforming lines WC299, WC788 and WC789 and the Zn-overperforming lines WC239 and WC481), little of this observed variation could be attributed to the differential root expression of either *TaZIP1* or *TabZIP1*. This may be due to the fact that only one time point was examined and that only a single *TaZIP* transporter and *TabZIP* transcription factor were analysed.

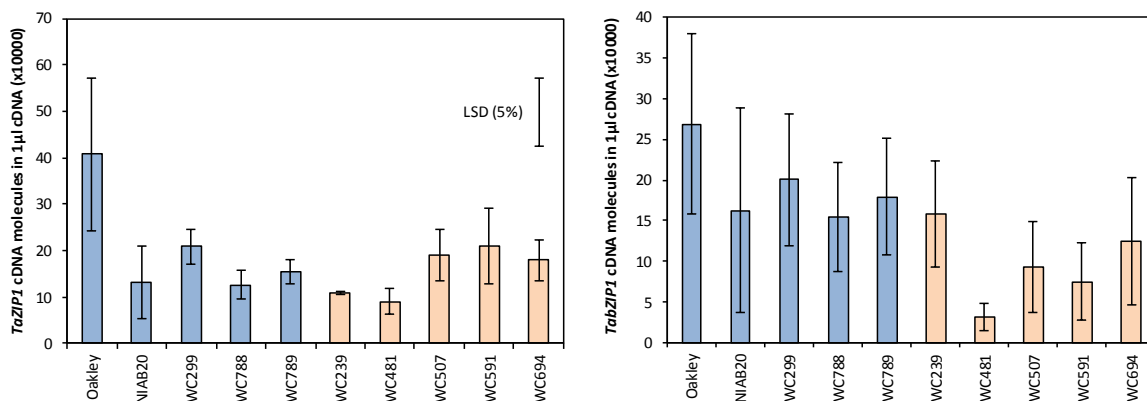


Figure 6.12. Absolute quantification of *TaZIP1* and *TabZIP1* gene expression levels in root samples obtained from ten field grown wheat lines. cDNA was synthesised from root samples of the ten differentially Zn-performing lines (five Zn-overperformers (orange bars) and five Zn-underperformers (blue bars)) taken at the booting growth stage, during the 2013 growing season. *TaZIP1* and *TabZIP1* expression levels were quantified using absolute quantification real-time PCR. Means of three biological replicates are given (\pm S.E.M.). In individual graphs where LSD bars are shown a significant effect of line was present ($P < 0.05$). LSD shown is the Fisher's LSD test value at the 5% significance level.

6.3.6 Comparative hydroponics Zn-starvation experiment of Watkins lines WC789 and WC239

Following the identification of the ten lines which showed consistent, differential Zn performance across the field grown datasets, two lines were chosen to investigate further using the hydroponic methodology previously utilised in Chapter 3. The Watkins lines WC239 (consistent overperformer) and WC789 (consistent underperformer) were chosen as they displayed consistent differences in Zn concentrations, irrespective of yield across the four field seasons (Figure 6.11), as well as the three sampling points taken during the growing season (Figure 6.10). A Zn-starvation time course experiment was used to compare the performance of these lines in hydroponic culture (see Section 2.1.1 for full details).

6.3.6.1 Phenotypic data

Both lines displayed growth phenotypes in response to extended Zn-deficient conditions as previously observed in Chapter 3. After 12 days of growth in Zn ($0 \mu\text{M Zn}$) plants were reduced in stature, with chlorotic lesions on leaves symptomatic of Zn-deficiency (see Figure 6.13). As shown in Figure 6.14(A, B), both root and shoot fresh weights were significantly reduced from D7 in both lines when grown under the -Zn treatment compared to +Zn ($8 \mu\text{M Zn}$) grown plants. Root to shoot ratio increased under -Zn growth conditions (Figure 6.14A) as previously observed and discussed (see Section 3.4.2). For root and shoot fresh weight, as well as root to shoot ratio there was no differential effect of Zn treatment between the lines as shown in Table 6.1 and no

interactions containing the line term were significant for these phenotypic measurements. SPAD readings, which allow relative chlorophyll levels to be measured, were significantly reduced in the -Zn grown treatment, and were shown to produce a significant ($p = 0.040$) interaction with the lines examined. This indicated that Zn-deficient conditions affected the reduction of chlorophyll differentially between the two lines. The overperforming line WC239 maintained chlorophyll concentration to a greater extent than the underperforming line WC789. Zn concentrations of both root and shoot samples were analysed using ICP-OES. Zn concentrations in both the root and shoot samples were significantly reduced under -Zn conditions from D7 for both lines. There was no significant differential effect of the -Zn treatment on the Zn concentrations of either root or shoot between the lines.

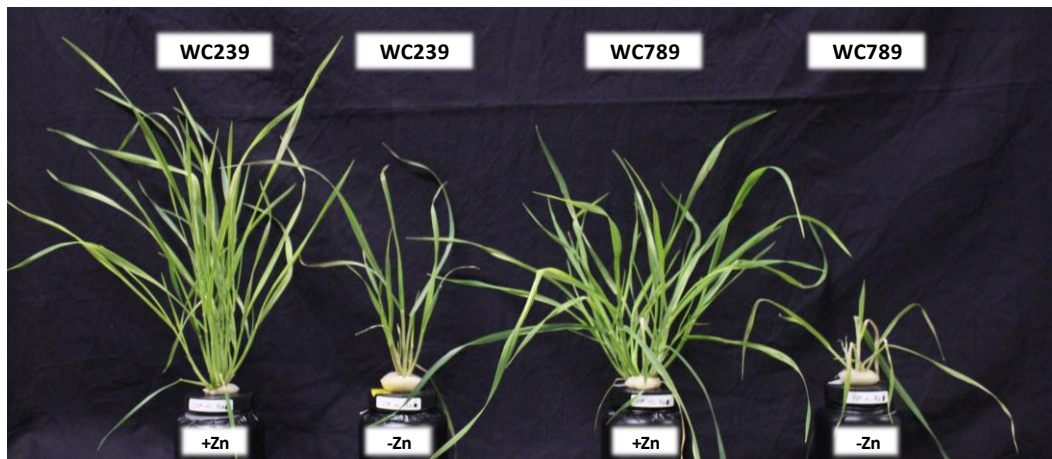


Figure 6.13. Visible phenotypic effects of Zn starvation on two Watkins Collection wheat lines. Watkins Collection lines 239 (WC239) and 789 (WC789) were tested due to differential in-field Zn-performance. The -Zn treatment caused a visible phenotype in both lines, shown here after 12 days of treatment. +Zn = 8 μ M Zn, -Zn = 0 μ M Zn.

Table 6.1. The effect and interactions of line, treatment and time point on fresh weight, SPAD value and Zn concentration of root and shoot samples from two differentially Zn-performing Watkins Collection lines throughout a 12-day Zn starvation period. p-values displayed are the result of individual three-way ANOVAs for each phenotype measurement. Three-way ANOVAs were conducted on datasets containing three biological replicates for each line (WC239) and (WC789) grown in both +Zn and -Zn at each time point. Boxes shaded in grey indicate a significant effect of the treatment or associated treatment interaction.

Treatment/Interaction	Fresh weight		Root:Shoot	SPAD	[Zn] (mg/kg DW)	
	Root	Shoot	ratio		Root	Shoot
Line	<0.001	0.143	<0.001	<0.001	0.12	0.119
Treatment	<0.001	<0.001	<0.001	<0.001	<0.001	<0.001
Time point	<0.001	<0.001	<0.001	0.008	<0.001	<0.001
Line.Treatment	0.264	0.248	0.974	0.040	0.218	0.142
Line.Time point	0.985	0.8	0.521	0.597	0.228	0.509
Treatment.Time	<0.001	<0.001	<0.001	0.010	<0.001	<0.001
Line.Treatment.Time	0.791	0.46	0.672	0.149	0.389	0.75

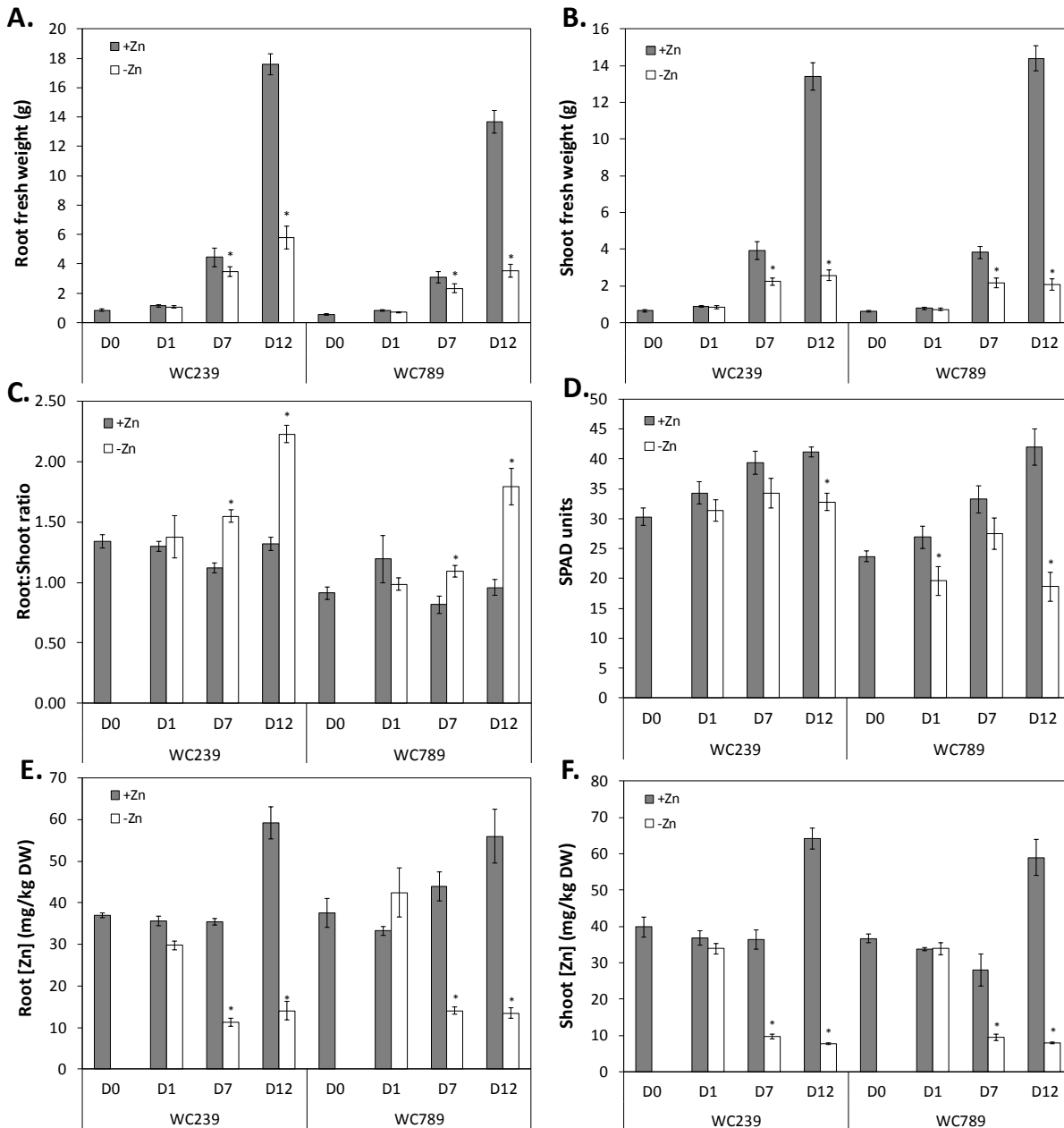


Figure 6.14. Fresh weights, SPAD value and Zn concentration of wheat root and shoot samples from two differentially Zn-performing Watkins Collection lines throughout a 12-day Zn starvation period. Results shown are means \pm S.E.M. (n = 3). * indicates a significant difference ($P < 0.05$) between treatments, within a given time point, tested using Fisher's LSD. For full significance of treatments and treatment interactions see Table 6.1.

6.3.6.2 Gene expression

Following phenotypic measurements, cDNA synthesised from both root and shoots of the hydroponically grown plants was analysed using absolute quantification real-time PCR (see Section 2.3.7.2) to investigate gene expression of *TaZIP1* and *TabZIP1*. As shown in Figure 6.15, expression levels of the Zn-transporter *TaZIP1* were significantly upregulated under Zn-deficient

conditions in both the root and the shoot. This trend supports results presented in Chapter 3. As previously noted, a significant upregulation of *TaZIP1* occurred at an earlier time point than significant differences in Zn concentrations were observed in both the root and the shoots of the plants examined. In the shoot samples, *TaZIP1* upregulation dropped between D7 and D12 in the underperforming line WC789, whereas in the Zn-overperforming line WC239 upregulation remained constantly high. For *TaZIP1* expression there was only one differential effect of line, which was a significant interaction in the root samples with time point (Table 6.2). This indicates that *TaZIP1* expression varied across the time course differently between the two lines, as was seen with the +Zn grown material, in which *TaZIP1* expression reduced from D1 in WC789, but increased from D1 in WC239. There was no interaction of line with treatment, indicating no significant differential effect of the -Zn treatment between the two lines.

When examining the group F bZIP transcription factor, *TabZIP1*, significant upregulation was present under -Zn conditions, though this was more variable than the upregulation of *TaZIP1*. Significant upregulation levels were reached faster in the overperforming line WC239 in both the root and the shoot compared to WC789. In the shoot, there was a significant interaction of treatment with line, indicating a differential response in upregulation of *TabZIP1* under Zn-deficient conditions. As is seen in Figure 6.15, although WC789 showed a slower response in the shoot, the level of upregulation was much higher than for WC239 at D7 and D12. In the root however a three-way interaction was observed between line, treatment and time point (see Table 6.2). This indicates that the lines respond differently to the Zn treatments over time. *TabZIP1* root expression levels appeared inherently higher under +Zn conditions in WC789, compared to WC239, though this decreased drastically at D12. WC239 roots responded to Zn-deficiency at least seven days earlier compared to WC789, however at the latter time point (D12), the magnitude of *TabZIP1* upregulation was much higher in WC789 compared to WC239.

Overall, little variation in response to Zn-deficiency was present between the two lines in terms of Zn concentrations and fresh weight parameters. Nonetheless, expression patterns of *TabZIP1* between the lines were different in response to Zn-deficient conditions, most notably in the root. The results showed that WC789 appeared slower at upregulating *TabZIP1* in response to the -Zn treatment in both the root and the shoot, but once upregulated it was to a greater extent than that shown by WC239.

Table 6.2. The effect and interactions of line, treatment and time point on the absolute quantification of *TaZIP1* and *TabZIP1* from root and shoot cDNA samples from two differentially Zn-performing Watkins Collection lines throughout a 12-day Zn starvation period. p-values displayed are the result of individual three-way ANOVAs for each gene in either root or shoot material. Three-way ANOVAs were conducted on datasets containing three biological replicates for each line (WC239) and (WC789) grown in both +Zn and -Zn at each time point. Boxes shaded in grey indicate a significant effect of the treatment or associated treatment interaction.

Factor/Interaction	<i>TaZIP1</i> quantification		<i>TabZIP1</i> quantification	
	Root	Shoot	Root	Shoot
Line	0.005	0.162	0.013	<0.001
Treatment	<0.001	<0.001	<0.001	<0.001
Time point	<0.001	<0.001	<0.001	0.109
Line.Treatment	0.297	0.402	0.994	<0.001
Line.Time point	<0.001	0.113	0.06	0.01
Treatment.Time	<0.001	<0.001	<0.001	<0.001
Line.Treatment.Time	0.114	0.876	0.001	<0.001

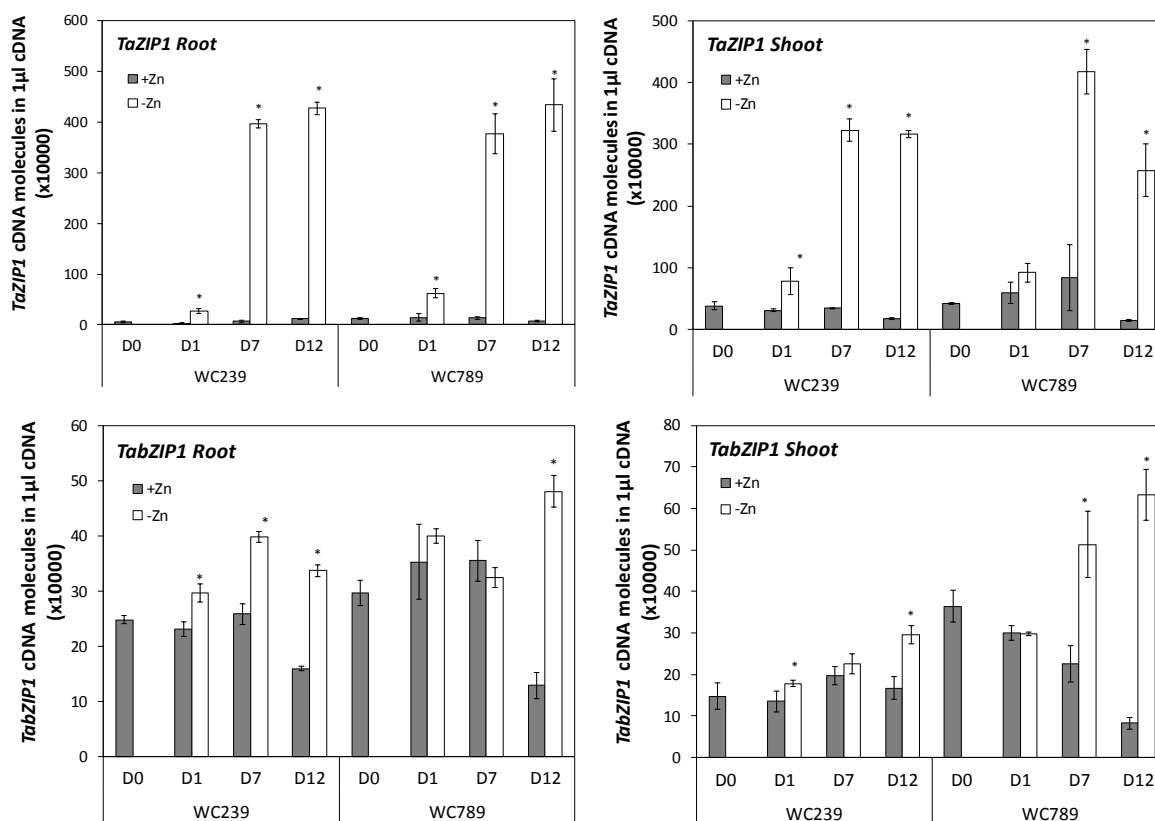


Figure 6.15. Absolute quantification of *TaZIP1* and *TabZIP1* gene expression levels in root and shoot samples of two contrasting Watkins Collection wheat lines throughout a 12-day Zn starvation period. *TaZIP1* and *TabZIP1* expression levels were quantified using absolute quantification real-time PCR. Means of three biological replicates are given (\pm S.E.M.). * indicates a significant difference ($P < 0.05$) between treatments, within a given time point, tested using Fisher's LSD. For full significance of treatments and treatment interactions see Table 6.2.

6.3.7 Using a field grown mapping population (Paragon x WC239) to identify QTL associated with Zn uptake and partitioning

In order to further investigate the genetic basis of the differential Zn performance observed across the WISP donor germplasm (see Sections 6.3.1-6.3.4) a mapping population of Watkins line WC239 x cv. Paragon was analysed for QTLs associated with yield and Zn characteristics in a field trial. WC239 consistently overperformed in Zn characteristics across the 2011-2014 field datasets, whereas Paragon is the spring wheat cultivar used in the gene expression studies of Chapter 3 and also the variety used in all wheat cloning procedures presented in this thesis.

The phenotypic values of the mapping population and parent lines, Paragon and WC239, are presented in Table 6.3. This dataset was generated from the 2015 field grown mapping population fertilised with nitrogen applications totalling 50 kg/ha over the season. WC239 had a lower grain yield compared to Paragon, but a higher total biomass yield due to an increased straw yield in this taller line. Paragon partitioned a higher proportion of biomass to the grain (harvest index), but had a lower Zn concentration in the grain and straw components than WC239. Figure 6.16 shows the frequency distributions of the measured traits. The distributions showed continuous variation across the mapping population and the distributions were approximately normal.

Table 6.3. Phenotypes of parents and the mapping population. The mean averages presented for the mapping population are averages from three replicate plots of 91 lines grown during the 2015 field season (\pm S.D.).

Traits	Parents		Mapping population		
	Paragon	WC239	Mean \pm SD	Minimum	Maximum
Grain yield (t/ha)	11.187	8.721	10.015 \pm 0.922	7.910	12.019
Straw yield (t/ha)	20.352	24.918	25.026 \pm 2.541	19.293	30.909
Total biomass yield (t/ha)	31.539	33.639	35.046 \pm 2.943	28.203	42.243
Harvest index	36.027	26.072	28.730 \pm 2.396	23.148	33.986
Grain Zn (mg/kg DM)	26.507	36.125	31.74 \pm 2.901	23.763	39.955
Straw Zn (mg/kg DM)	9.870	11.266	9.930 \pm 1.832	6.293	15.758
Total biomass Zn (mg/kg DM)	15.771	17.710	16.18 \pm 1.854	12.552	22.611
Grain Zn uptake (kg/ha)	0.297	0.315	0.317 \pm 0.034	0.241	0.403
Straw Zn uptake (kg/ha)	0.201	0.281	0.248 \pm 0.049	0.147	0.418
Total biomass Zn uptake (kg/ha)	0.497	0.596	0.566 \pm 0.072	0.422	0.795
Zn harvest index	59.615	52.882	56.335 \pm 4.430	46.639	68.598

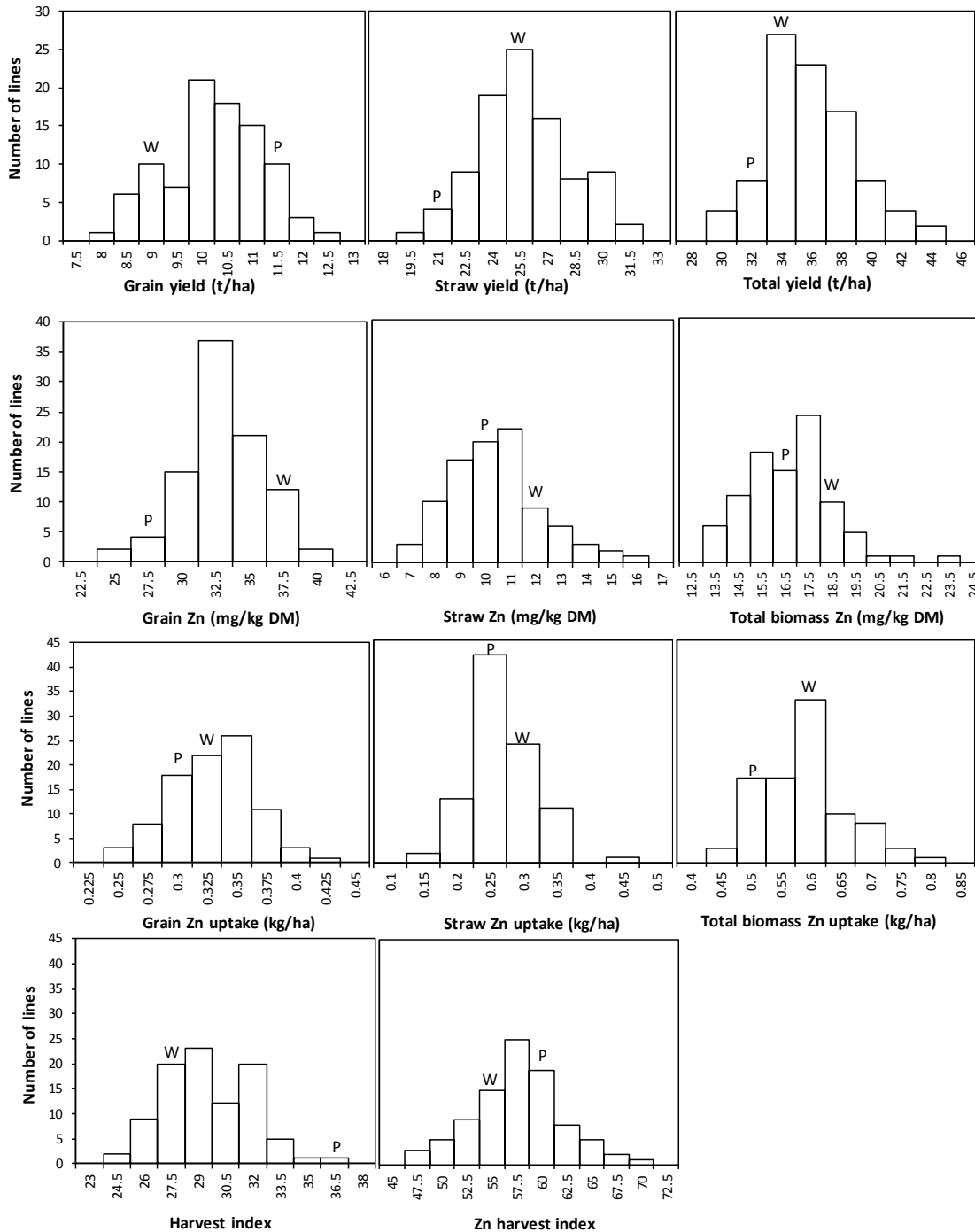


Figure 6.16. Frequency distribution of yield and Zn traits across the Paragon x WC239 mapping population. Histograms showing frequency distributions for yield parameters and Zn characteristics across the mapping population, bars with P above indicate the position of the parent paragon in each histogram and bars with W above indicate the position of the Watkins Collection line WC239.

A total of six QTLs were identified for the yield and Zn traits across the mapping population (see Table 6.4). Three of these were for yield characteristics, three for Zn characteristics. A QTL was identified on chromosome 5A that explains 15.6% of the variation observed in straw yield (t/ha). This same QTL also explains 13.35% of total biomass yield (t/ha) variation observed, presumably by accounting for differential yield of the straw component. The allele that contributes to the increased straw yield was from the WC239 parent. A different QTL explaining 21.55% of variation in harvest index was present on chromosome 6A. This same QTL on chromosome 6A also explained 12.85% of variation observed in Zn harvest index (% of Zn partitioned to the grain). The allele underlying a positive increase in harvest index mapped to this QTL is from the Paragon parent. Two separate QTLs were detected for grain Zn uptake (kg/ha) on chromosomes 2D and 5B, together explaining 16.92% of variation observed. A final QTL was detected for total biomass Zn uptake (kg/ha) on chromosome 5B at a different locus to that for grain Zn uptake.

Table 6.4. QTLs identified using the Paragon x WC239 mapping population for yield and Zn traits. QTLs are listed by trait and were identified using composite interval mapping using data from the 2015 field grown mapping population. Marker intervals are shown, with markers underlined nearest to the QTL. Positions are given in cM from the start of the respective chromosome. LR (likelihood ratios) are included with the R^2 (%) variation explained values. Additive effects are also provided, positive values indicate the positive alleles come from the Paragon parent (P), negative values indicate the positive alleles come from the WC239 parent (W).

Traits	Chromosome	Marker interval	Position	LR	R^2 (%)	Additive effects
Straw yield (t/ha)	5A	BS00070270 - <u>BS00023076</u>	23.31	15.60	14.72	-0.99 W
Total yield (t/ha)	5A	BS00070270 - <u>BS00023076</u>	23.31	14.33	13.35	-1.11 W
Harvest index	6A	<u>BS00023089</u> - BS00010221	23.71	28.41	21.55	1.08 P
Grain Zn uptake (kg/ha)	2D	BS00023211 - <u>BS00040318</u>	65.61	15.31	12.34	-0.01 W
	5B	BS00098292 - <u>BS00098520</u>	14.71	7.39	4.58	0.01 P
Total biomass Zn uptake (kg/ha)	5B	<u>BS00074804</u> - BS00084528	23.51	22.85	18.91	0.03 P
Zn harvest index	6A	<u>BS00023089</u> - BS00010221	34.71	16.10	12.85	1.68 P

6.4 Discussion

6.4.1 Extensive and consistent variation exists in Zn traits across the WISP donor germplasm

Substantial variation in grain Zn concentration was observed across the WISP donor germplasm when grown in the field, with values ranging from 24 mg/kg (4-year average for the modern cultivar Oakley) to 46 mg/kg (4-year average of Watkins Collection line WC468). This was less than the 25-92 mg/kg range reported by Monasterio & Graham (2010), but was in keeping with the ranges reported by Zhao et al. (2009) 29-51 mg/kg, Morgounov et al. (2006) 25-56 mg/kg and Oury et al. (2006) 14-43 mg/kg.

The initial data mining of the 2011 and 2012 datasets resulted in the identification of 10 wheat lines of interest. These wheat lines showed consistent variation in the amount of Zn accumulated in the total biomass and grain Zn concentrations, with five lines consistently overperforming in these parameters and five consistently underperforming. The 10 lines chosen were well spread in terms of yield and all characteristics identified were consistent in each of the ten lines over the 2011 and 2012 datasets. The known effects of concentration-dilution were also taken into account through the use of residual measurements, which calculated the difference from the expected trend based on the respective yield. The predicted Zn performances of these ten lines was consistent in 2013 and 2014 with regard to total Zn uptake and, although to a lesser extent, grain Zn concentration. These consistent performances indicate a robust choice of lines.

An analysis of Zn-partitioning efficiency across the germplasm revealed that the modern cultivars examined allocated a high percentage of their total above ground Zn to the grain by maturity (Zn harvest index). As previously noted by Fan et al. (2008) and Shewry et al. (2016), grain Zn concentrations have decreased over the past 50 years. This decrease was evident across the WISP donor germplasm; modern cultivars had lowest grain Zn concentrations. Despite their low grain Zn concentrations, modern cultivars partitioned a high percentage of above ground Zn present to the grain. The reason this may not be producing a grain Zn concentration as high as may be expected, given the proportion diverted to the grain, is likely a function of grain yield; larger grains diluting the Zn present. This demonstrates that modern cultivars are able to very efficiently partition Zn to the grain; this is important from a biofortification perspective. By increasing the amount of Zn present in the above ground biomass of modern varieties, the grain Zn concentration should be efficiently increased. Therefore, if root uptake and translocation of Zn can be increased this will result in increased grain Zn concentrations. Further understanding of the molecular basis of root Zn uptake from the rhizosphere as well as Zn translocation from the root to the shoot will be important steps in improving the above ground Zn content.

6.4.2 Zn concentrations and expression levels of *TaZIP1* and *TabZIP1* during the growing season do not reflect Zn traits at final harvest

The ten selected lines were sampled during the growing seasons of 2013 and 2014. At these time points the ten lines did not exhibit Zn concentrations in agreement with their performances at final harvest, as recorded in 2011-2014. Samples taken at the booting growth stage showed better agreement to final harvest trends of total Zn concentration than the samples taken at the later stage of grain filling. Performance across the ten lines sampled at grain filling was not clearly divided into underperformers and overperformers. This may be a function of biomass, although at sampling points within the growth season total biomass was not recorded as only a small number of plants were destructively sampled and the extrapolation to t/ha would be unreliable. This change in Zn concentration, relative to the expected performance rankings within the ten selected lines could also be due to differential uptake and/or redistribution dynamics of Zn. Zn remobilisation within the plant has been shown to be the major component contributing to Zn content of barley grains (Hegelund et al., 2010). Throughout the growth season, wheat lines may exhibit different dynamics in continued uptake from the soil and redistribution from the (unmeasured) root systems throughout growth stages, particularly during late season development. As mineral analysis of the root portions of plants was not carried out, due to the contamination of soil attached to the roots, this was not assessed.

A final explanation for the lack of agreement in Zn measurements taken during the growing season compared to those at final harvest is leaf drop. Leaves shed in the period between grain filling and final harvest may have an influence on the final harvest total Zn concentration of the above ground biomass, possibly explaining the lack of agreement between the Zn concentration results at 2013 grain filling and 2013 final harvest.

The root expression levels of *TaZIP1* and *TabZIP1* from samples taken during the 2013 growing season (booting growth stage) did not reveal clear differences between the performance groups. Gene expression levels of the two genes correlated fairly well across the ten lines, however only the modern cultivar Oakley had a significant increase in expression of the Zn transporter *TaZIP1* compared to the other varieties at this time point. Future analysis of these lines could be conducted utilising more time points and analysing specific tissues throughout development. It seems likely that any information present at this one growth stage of development may have been lost as analysis was restricted to roots. Precise regulation of these genes in specific tissues and organs may play important roles in differential Zn performance. Additionally, studying a range of *TaZIPs* and *TabZIPs* may provide further understanding of how these genes relate to Zn uptake and partitioning in wheat.

6.4.3 WC239 and WC789 display similar phenotype responses to hydroponic Zn-deficient conditions, but expression of *TabZIP1* varies between the lines in response to Zn-deficiency

To examine the performance of the Watkins lines WC239 and WC789, identified as Zn overperforming and underperforming lines respectively, a Zn-deficiency hydroponic experiment was undertaken. In response to the Zn-deficient treatment, both lines displayed characteristic Zn-deficient phenotypes. Only one phenotypic parameter, chlorophyll concentration (measured using a SPAD meter), was differential in response to the -Zn treatment between the two lines. WC239 was able to maintain a higher chlorophyll concentration in response to Zn-deficient conditions compared to WC789. Previously Chen et al. (2008) reported that the Zn-inefficient rice cultivar (Erjiufeng) had a greater decline in chlorophyll concentration under Zn-deficient conditions than the Zn-efficient rice cultivar (IR8192). This reduction in chlorophyll is likely due to an increase in reactive oxygen species (ROS) associated with Zn-deficiency (Cakmak, 2000) and subsequent damage of the chloroplast ultrastructure (Chen et al., 2008). Zn has a functional role in Copper (Cu)/Zn superoxide dismutase (SOD) which plays an important role in protecting plants against oxidative damage catalysed by ROS (Marschner and Cakmak, 1989). Cu/Zn SOD levels have been shown experimentally to be lower in the Zn-inefficient wheat cultivar (BDME) compared to the Zn-efficient cultivars (Dagdas and Kirgiz) (Hacisalihoglu et al., 2003). It seems plausible that varying levels of Cu/Zn SOD and the associated protection against ROS may be related to Zn uptake and partitioning efficiency throughout the plant, especially under low Zn conditions. Cellular Zn redistribution from vacuoles may also be an important component of Zn-efficiency. If a wheat line is better adept at redistributing Zn from vacuolar stores upon Zn-deficiency it may enhance performance under Zn-deficient conditions, allowing key enzymes such as Cu/Zn SOD to be maintained at high enough levels to counteract cellular stresses imposed by Zn-deficiency. An interesting avenue for further research in this area would be the study of vacuolar Zn export proteins such as members of the natural resistance-associated macrophage protein (NRAMP) family. It would be interesting to see if differential field Zn performance or tolerance to Zn-deficiency is correlated with the expression of members of this family.

There was no differential effect of the Zn-deficient treatment between the two Watkins lines on root or shoot fresh weight, nor root or shoot Zn concentrations. A possible future experiment to investigate this further would be the use of an intermediate Zn-solution concentration between the two concentrations (0 μ M Zn and 8 μ M Zn) used in the experiment presented in this Chapter. It may be revealing to grow the plants for longer, although this would likely have to be in a different hydroponics system or in a pot based system due to the root systems being constrained by pot volume in the existing hydroponics system. A longer-term, milder Zn-

deficiency may allow differential Zn performance between the Watkins lines to be explored more fully.

In the comparative hydroponics experiment, both *TaZIP1* and *TabZIP1* were upregulated under Zn-deficiency in the root and shoot in both WC239 and WC789. This upregulation of *TaZIP1* and *TabZIP1* in response to Zn-deficiency was in accordance with the findings presented in Chapter 3. *TaZIP1* expression levels in the roots of WC239 and WC789 were similar, with significant upregulation from the first time point after initiating the -Zn treatment. In the shoot, *TaZIP1* expression was upregulated to significant levels faster in WC239 compared to WC789, although particularly interesting is the fact that WC789 expression decreased between D7 and D12, whereas WC239 remained constant. In the longer Zn-deficiency experiments presented in Chapter 3, a common feature across the *TaZIPs* investigated was a reduction in upregulation in the final time points; this was presumed most likely due to the severe physiological stress at these latter time points. It was interesting that WC789 exhibited a clear decrease at D12; this may have been due to the plant being physiologically more stressed than the WC239 line and this was somewhat supported by the SPAD measurements of these two lines at the latter time point of D12. Previously, Durmaz et al. (2011) reported that the wild emmer wheat (*Triticum turgidum* ssp. *dicoccoides*) homolog of *TaZIP1*, *TdZIP1* was differentially upregulated across four lines examined, when grown in different Zn conditions. A Zn-inefficient line (19-36) showed an upregulation of *TdZIP1* greater than two Zn-efficient lines (24-39 and MM5/4) and another Zn-inefficient line (33-48). Durmaz et al. (2011) hypothesised that Zn-inefficiency of the line (19-36) resulted in plant Zn-deficiency at higher Zn concentrations compared to the other more Zn-efficient lines, thus causing upregulation of *TdZIP1*. The data presented in this Chapter does not agree with this hypothesis. It appears WC239 may be faster at sensing and responding to Zn-deficiency in the shoot and because of this may not have to upregulate *TaZIP1* to the same extent as WC789 does at D7. Although more studies are needed to confirm this, as previously suggested, an intermediate Zn-deficiency treatment with more sampling points and more *TaZIP* genes investigated may help to further this hypothesis.

TabZIP1 expression was shown to be Zn-regulated, again as previously observed in the hydroponic experiments conducted in Chapter 3. In both the root and shoot, *TabZIP1* was upregulated at earlier time points in WC239 compared to WC789, however at D12 upregulation was higher in WC789 than WC239. These results correlated well with those of *TaZIP1* expression in the shoot. Under +Zn conditions in the shoot *TabZIP1* levels reduced throughout the time course in WC789, yet not in WC239; it remains unclear why this occurred. As with *TaZIP1*, it appeared that the Zn-overperforming line WC239 was able to upregulate the Zn-responsive *TabZIP1* gene at an earlier time point than the Zn-underperforming line WC789, although the phenotypic data suggests this had little differential effect on both fresh weight, or Zn

concentration parameters. More research would be valuable in this area to further understand how key Zn transporter genes such as members of the *TaZIP* family and gene regulators such as *TabZIP1* contribute to differential Zn performance. Further hydroponic experiments using the ten lines identified may provide valuable insights. It may be beneficial to clone known Zn transporter genes from the different wheat lines and test Zn transport kinetics and affinities, which may help explain Zn variation observed across the germplasm. Additionally, cloning known group F members from the differentially performing lines, and analysing both their sequence (with particular attention to the predicted cysteine-histidine rich Zn binding sites) and their ability to bind to ZDREs may prove insightful. Transcriptome analyses using an RNA-seq approach may also reveal differences within the transcriptome profile that explain differential Zn performances between lines. As lines within the Watkins collection have come from very diverse geographical locations, they may have adapted differently to local Zn circumstances and consequently may have altered 'Zn-homeostasis windows' upregulating key Zn membrane transporters at different plant Zn concentrations. These suggestions for future research areas would undoubtedly further our understanding of the Zn-regulatory network in wheat, specifically on how differences present lead to altered in-field performance, which is the ultimate goal of any genetic biofortification strategy.

6.4.4 QTL analysis of the Paragon x WC239 mapping population leads to the identification of loci associated with differential Zn performance

The QTL analysis of the Paragon x WC239 mapping population identified four QTLs associated with Zn traits. Two QTLs associated with grain Zn uptake (kg/ha) were identified on both chromosomes 2D and 5B. Three of the *TaZIP* genes (*TaZIP1*, *TaZIP5* and *TaZIP8*) shown to transport Zn in Chapter 4 have a homeolog present on chromosome 2D. Further fine mapping to assign candidate genes to this 2D QTL will need to be carried out to determine if these *TaZIPs* reside in the loci identified. For example five *ZIP* bean (*Phaseolus vulgaris*) genes have been shown to be located within or near to QTLs for seed Zn concentration in beans (Astudillo et al., 2013). A QTL associated with Zn harvest index (as well as overall harvest index) was identified on chromosome 6A in the present QTL analysis. The bioinformatics analysis presented in Chapter 3 reports that *TaZIP2* and *TaZIP16* are located on this chromosome, although the Zn responsiveness or transporting capabilities of these genes and the proteins they encode has not yet been tested. A further QTL associated with total biomass Zn uptake (kg/ha) was identified on chromosome 5B. The only gene from the *TaZIPs* and *TabZIPs* identified located on chromosome 5B is a homeolog of *TabZIP2*; again this has not been tested with either gene expression studies or *Arabidopsis* complementation. The QTL analysis did not identify any loci associated with grain, straw or total biomass Zn concentrations (mg/kg DM), only grain and total biomass Zn

uptake (kg/ha). Grain and total biomass Zn uptake are functions of yield as they describe the amount of Zn taken up and subsequently accumulated per hectare.

Previously in wheat, QTLs linked with Zn grain concentration have been identified on chromosome 6B of wild emmer wheat (*Gpc-B1* locus) identified by Olmos et al. (2003) as well as loci on chromosomes 3D, 4B, 6B and 7A (Genc et al., 2009). No QTL corresponding to these positions were identified in our analysis. This is likely due to the QTL analysis being conducted only on a single year of data. Processing of the same field grown mapping population grown in the 2015 field season is underway and QTL analyses will be repeated with this replicated dataset when available. It would be useful to clone the *TaZIP* genes located on chromosome 2D (*TaZIP1-2DL*, *TaZIP5-2DL* and *TaZIP8-2DL*) from WC239 and compare them to the existing cloned alleles of the same genes from Paragon, to see if notable differences are present that alter key residues in the amino acid sequences which may contribute to differential Zn performance.

The confirmation of key genes underlying the traits that contribute to differential Zn performance in field grown wheat plants is required. If confirmed, this would suggest that the crossing of these genes into new breeding lines would improve the grain Zn concentrations as well as potentially performance under Zn-deficient conditions. Both of these characteristics are, and will be to an ever-increasing extent, essential objectives given the need to produce a more nutritious and safe food source for the growing population using increasingly marginal land.

Chapter 7. General discussion

7.1 The pressing need to increase wheat Zn content

With world population estimates predicting there will be over nine billion people to feed by 2050 (Godfray et al., 2010), the need for continued improvements in global food systems is essential. Enhancements in cropping system productivity, sustainability, resilience and distribution will be vital in meeting this increasing demand in the face of resource scarcity and environmental challenges, to achieve global food security (Garnett et al., 2013). Furthermore, food security requires that not only access to food be sufficient in terms of quantity, but also nutritional quality (FAO et al., 2015). Micronutrient malnutrition is prevalent throughout the world (WHO, 2002). A substantial cause of this is the reliance on micronutrient poor staple foods, such as cereal grains, by much of the world's population. Rural areas of developing countries obtain high proportions of their daily calorie intake from cereals, including wheat, contributing to widespread micronutrient-deficiency.

Zn is an essential micronutrient for both human and plant nutrition. Zn is required in a wide range of plant enzymes (Sinclair and Krämer, 2012) and adequate crop Zn nutrition is vital for yield maintenance (Rengel and Graham, 1995a). Widespread human Zn-deficiency could be addressed through the Zn biofortification of extensively cultivated crops such as wheat. Current Zn biofortification strategies fall into three categories: dietary supplementation /fortification/diversification, agronomic biofortification and genetic biofortification. Whilst these approaches do not appear feasible in isolation, genetic biofortification holds great potential in improving the Zn status of human populations at risk of Zn-deficiency. However, to harness the full potential of this biofortification approach, a detailed understanding of the molecular processes underlying and controlling Zn uptake from the soil and Zn partitioning throughout wheat is required. The research described in this thesis has addressed this requirement and is an important step in unravelling the molecular basis of Zn uptake and regulation in wheat. This will be valuable in the development and breeding of wheat varieties with higher Zn content as well as varieties better adapted to growing in Zn-deficient soils.

With the exception of foliar Zn-fertiliser applications (Kutman et al., 2010), Zn is taken up by plants from the soil. The journey of Zn from soil to seed is a long, complex and intricately controlled process. Zn uptake occurs from the soil directly in the form of Zn^{2+} (Marschner, 1995) and must cross the selectively permeable plasma membrane either directly upon uptake (for symplastic transport) or after apoplastic transport through the root, before penetrating and advancing past the casparian strip. Additionally, the cell plasma membrane must be crossed at further locations as the plant transports Zn from the soil, through the roots, to the shoot. In order

to cross any plasma membrane, Zn requires membrane transport proteins; the regulation of which allows the plant to control how much Zn is taken up and partitioned to specific regions. A considerable number of these key Zn membrane transporter families, as well as individual members, have been characterised in the model plant *Arabidopsis* and key crop species including barley, maize and rice. The importance of the ZIPs at key Zn transport ‘bottlenecks’ has been elucidated (Palmgren et al., 2008), however there has been little published research regarding wheat ZIP members. This thesis has identified and characterised members of the ZIP family in wheat. This is an important contribution to the field as previously, progress on the identification and characterisation of Zn transporters in wheat has lagged behind other species. This is most likely due to the complex hexaploid wheat genome (IWGSC, 2014) and the inherent difficulties of wheat transformation to investigate aspects of gene function (Jones, 2005). The identification and characterisation of the *TaZIP* family as reported in Chapters 3, 4 and 6 is summarised and considered in the following section.

Due to the variable nutrient demands of plants at different growth stages and across different tissues, as well as the variation found in the growth medium, plants have developed specialised homeostatic mechanisms to cope with variations in nutrient requirements (Pinto and Ferreira, 2015). The regulatory mechanism underlying the response to Zn-deficiency has been partly-elucidated in *Arabidopsis*, where two group F bZIP transcription factors are essential for this response. As was the case with the wheat TaZIPs, no previously published research has been conducted on this bZIP group in wheat. This thesis has identified the group F TabZIPs and demonstrated their role in the Zn-regulatory mechanism of wheat. The findings from Chapters 3, 5 and 6, and the resulting suggested adaptations to the existing regulatory model of Zn in plants are discussed in Sections 7.3 and 7.4.

7.2 Specific members of the *TaZIP* family are promising targets for Zn biofortification strategies

Through the use of heterologous yeast expression studies, membrane transporters from the ZIP family have been shown to transport a wide range of cations including Zn, Fe, Mn, Cu and Cd (Grotz et al., 1998; Milner et al., 2013; Lee et al., 2010a; Yang et al., 2009b; Li et al., 2013; Pedas et al., 2008, 2009; Tiong et al., 2015). The most studied ZIPs are those in *Arabidopsis*. Zn is the most common substrate transported by the 18 *Arabidopsis* ZIP family members with at least nine showing Zn transport ability (*AtIRT1*, 2, 3, *AtZIP1*, 2, 3, 7, 11 and 12) (Korshunova et al., 1999; Vert et al., 2001; Lin et al., 2009; Grotz et al., 1998; Milner et al., 2013), although not all members have been characterised. Ten of the 18 members have been shown to be Zn-responsive in expression: *AtIRT3*, *AtZIP1*, 2, 3, 4, 5, 7, 8, 9 and 12 are all upregulated under Zn-deficient conditions in either the root, the shoot or both (Grotz et al., 1998;

Lin et al., 2009; Jain et al., 2013; Milner et al., 2013). This widespread upregulation indicates the importance of this family in the Zn transport pathway.

ZIP transporters have been identified previously and studied in key crop species including soybean (*G. max*) (Moreau et al., 2002), bean (*P. vulgaris*) (Astudillo et al., 2013), maize (*Z. mays*) (Li et al., 2013, 2015a) and rice (*O. sativa*) (Ramesh et al., 2003; Bashir et al., 2012). Additionally, and most relevantly for wheat research, is the work carried out in barley (Pedas et al., 2009; Tiong et al., 2013, 2015). 13 ZIPs have been identified in the barley genome, of those investigated, *HvZIP3*, 5, 6, 7, 8, 10 and 13 are all Zn-responsive (Pedas et al., 2009; Tiong et al., 2013, 2015). Moreover, HvIRT1, HvZIP3, 5 and 8 rescue the *zrt1/zrt2* yeast mutant (Pedas et al., 2009). To date only one wheat ZIP has been studied, *TdZIP1*, which is a homolog of *TaZIP1* from wild emmer wheat *Triticum turgidum* ssp. (Durmaz et al., 2011). *TdZIP1* was Zn-responsive in expression and shown to transport Zn using a yeast expression system.

In this thesis, the results from a bioinformatics analysis of the existing wheat genome are presented (Chapter 3). This analysis identified 13 *TaZIPs*, each with three homeologs, this is more than the previous most comprehensive analysis conducted by Tiong et al. (2015), where 11 were discovered. The phylogenetic analysis of the 13 *TaZIPs*, identified two distinct clades, one containing three *TaZIPs* (*TaZIP12*, 14 and 16) the other containing the remaining ten. The *Arabidopsis* homologs of *TaZIP12*, 14 and 16 are *AtPutZnT*, *AtIAR1* and *AtZTP29* respectively. It seems likely that these three *AtZIP* family members are involved more in Zn regulation within the ER (Lasswell et al., 2000; Wang et al., 2010). The *TaZIP* homeologs may have a similar function. Although no gene expression or characterisation of these three *TaZIPs* was done, it can be speculated that *TaZIP12*, 14 and 16 may have a different role to that of Zn uptake across the plasma membrane given their phylogenetic location. Neither *TaZIP14* and 16 contain ZDRE motifs in their promoter regions (Table 5.1) and their divergence from the other *TaZIPs* identified suggests they may have an adapted role in the Zn regulatory framework. *AtZTP29* (homolog of *TaZIP16*) has been hypothesised to be involved in regulating Zn levels in the ER in response to excess salt (Wang et al., 2010), the closely related *TaZIP14* and also *TaZIP12* may have a similar role. Although speculative, it is suggested the third member of the *Arabidopsis* group F bZIP transcription factor family, *AtbZIP24* which is involved in salt tolerance (Yang et al., 2009a) may be involved in responding to Zn concentration fluctuations in response to salt stresses and may bind to the promoters of *AtPutZnT*, *AtIAR1* and *AtZTP29*. If this is the case, a similar mechanism may exist in wheat. Further understanding the role of the ZIPs and bZIPs in salt tolerance mechanisms may be valuable in an increasingly salinized world (Rozema and Flowers, 2008). This may be particularly useful if examined in rice, due to the overlap of rice cultivation area with regions most affected by soil salinity (Rao et al., 2013).

The larger clade of the *TaZIPs* identified in the phylogenetic analysis contained the remaining ten *TaZIPs*. Five of these *TaZIPs* (*TaZIP1*, 4, 5, 6 and 7) were shown to be Zn regulated (Chapter 3), with higher expression under Zn-deficient conditions. *TaZIP* upregulation in response to Zn-deficiency occurred in both the root and shoot. Results showed *TaZIP* upregulation response times varied both between genes and also within genes and between root and shoot material. For example, *TaZIP1* was upregulated under Zn deficiency to a similar magnitude and responded at a similar rate in both the root and the shoot. This is in agreement with results of the barley homolog, *HvZIP3*, which showed upregulation during Zn-deficient growth, as well as upon Zn resupply, in both root and shoots of barley seedlings (Tiong et al., 2015). *TaZIP4* was significantly upregulated at D1 in the roots, but only from D3 onwards in the shoot. Barley has two close homologs of *TaZIP4*: *HvZIP5* and *HvZIP8*. Both showed Zn regulation in previous studies, however upon Zn resupply (following -Zn growth) upregulation of *HvZIP5* and 8 occurred only in the roots (Pedas et al., 2009; Tiong et al., 2015). This suggests *HvZIP5*, *HvZIP8* and the wheat homolog *TaZIP4* may play an important role specifically in Zn uptake and less in translocation to the shoot and vascular transport throughout the plant. Of the five *TaZIPs* investigated in this thesis, *TaZIP6* was the slowest to respond to Zn-deficient conditions, with upregulation being faster in the shoot than the root. Interestingly, the *TaZIP6* barley homolog: *HvZIP6* showed no response to -Zn treatment in the shoots of barley plants, but was upregulated in the roots during a Zn-deficiency treatment. This suggests these wheat and barley homologs may have divergent roles; *TaZIP6* is a particularly interesting candidate to study further.

These specific spatiotemporal expression patterns indicate individual *TaZIPs* likely have precise roles within the plant, warranting further study. Individual *TaZIPs* may have important Zn transport roles at specific regions of the root or the shoot. Feasibly the Zn requirement of different regions in the root and shoot varies, which may explain the differential pattern of upregulation initiation and magnitude observed through the gene-expression studies. As precise regions are likely to reach critical Zn concentration thresholds at different times upregulation patterns vary. In order to investigate this further, it would be beneficial to undertake gene localisation experiments using in-situ hybridisation or GFP-fusion techniques on prepared sections of specific tissues. Additionally, homeolog specific gene expression studies to examine the regulation patterns of specific *TaZIP* homeologs in response to Zn-deficiency may be worthwhile.

The gene expression patterns of *TaZIP1* were investigated in roots of field grown wheat lines that displayed differential Zn uptake and partitioning. No trends were observed at the single time point examined, however this would be an area to explore more thoroughly. By using both root and shoot samples taken throughout the growing season, trends in *TaZIP* regulation may emerge that reveal the contribution of individual *TaZIPs*. Furthermore, examining *TaZIP*

expression in the field across different Zn treatment plots may provide further information; this would require a low Zn soil with Zn fertiliser applied at different rates. The gene expression studies from such an experiment would enhance the results obtained from the hydroponical culture system and verify the transferability between the two growth systems in regards to Zn-deficiency studies in wheat.

In addition to the expression of *TaZIP1* in field grown root samples of ten wheat lines from the WISP donor germplasm, two specific lines were chosen to examine in detail based on their consistently different Zn concentrations when grown across multiple field seasons (WC239-overperformer and WC789-underperformer). Hydroponic Zn-deficiency experiments demonstrated that both lines upregulated *TaZIP1* in response to Zn-deficiency. However, the levels of this upregulation were similar between the lines. This contradicts findings by Durmaz et al. (2011) which showed that *TdZIP1* expression varied across four wild emmer wheat lines with different Zn-efficiencies, in response to a Zn-deficient treatment. For the most inefficient line they studied (19-36), *TdZIP1* was upregulated to a greater extent. This was not observed with the *TaZIP1* homolog investigated in this thesis. By further testing *TaZIPs* as well as using a more intermediate Zn-deficiency treatment, the role of *TaZIPs* in conveying differential Zn performance between lines may be established.

Five of the identified *TaZIPs* were characterised using a yeast complementation approach. *TaZIP1*, 5, 6, 7 and 8 were all shown to transport Zn using the *zrt1/zrt2* mutant yeast strain. None were able to rescue the Fe uptake mutant *fet3/fet4* (Chapter 4). During yeast complementation studies, it was observed that individual *TaZIPs* displayed varying abilities to complement the *zrt1/zrt2* mutant strain, notably *TaZIP5* was able to restore growth to a greater extent under low Zn conditions. This suggests that either *TaZIP5* is expressed in a more Zn-sensitive yeast compartment or it acts as a high-affinity transporter. A potential role as a high-affinity Zn transporter is supported by previous results from Hacısalihoglu et al. (2001) where the presence of two Zn uptake systems, high and low-affinity, was observed using $^{65}\text{Zn}^{2+}$ isotope uptake studies. The exact proteins underlying these two uptake systems were not investigated in this thesis. However, given the results from the yeast heterologous expression studies presented in Chapter 4, *TaZIP5* seems likely to be one of, if not the underlying transporter of this high-affinity Zn uptake system. *TaZIPs* 1, 6, 7 and 8 may also be key players in the low-affinity Zn uptake system in wheat. However, these speculations should be tested further to investigate specific properties and kinetics using a vesicle system, as rescue ability does not necessarily correlate with affinity.

A QTL analysis of a biparental mapping population of a Watkins line that exhibits relatively high Zn concentrations (WC239) crossed with cv. Paragon, identified a locus associated with grain Zn concentration on chromosome 2D. Three of the *TaZIP* genes (*TaZIP1*, 5 and 8)

shown to transport Zn have a homeolog that resides on this chromosome. One or more of these *TaZIPs* may be vital in contributing to grain Zn content, further QTL analyses and downstream fine mapping of this locus will prove valuable in furthering the understanding of this process. Examining the gene expression of additional *TaZIPs* across the Watkins lines WC239 and WC789, as well as cloning these genes specifically from these lines and investigating subsequent allelic variation, may reveal how these membrane transporters contribute to differential Zn performance across germplasm.

The identification of the *TaZIPs* reported in Chapter 3, taken with their expression profiles in response to Zn-deficiency (Chapters 3 and 6) and their specific Zn transport abilities (Chapter 4) demonstrates their potential as breeding targets to create lines with both improved tolerances to Zn-deficient soils as well as enhanced Zn uptake and partitioning. Specific uses for the *TaZIP* information assembled throughout this thesis are proposed in Section 7.4.

7.3 Group F *TabZIPs* are important in the Zn-regulatory mechanism of wheat and regulate *TaZIP* expression

The importance of two group F bZIP transcription factors, AtbZIP19 and AtbZIP23 in the Zn-regulatory response of *Arabidopsis* has been demonstrated previously (Assunção et al., 2010). The current model proposed by Assunção et al. (2013, 2010) (as depicted in Figure 1.11) suggests that under normal cellular Zn conditions, bZIP19 and bZIP23 are present in the cytosol and have a Zn²⁺ ion bound at the cysteine-histidine group F motifs. The binding of this Zn²⁺ renders them inactive, however when cytosolic Zn concentrations decrease, the Zn²⁺ ion is released and conformational changes make the bZIPs functional. These active bZIPs then bind to ZDRE motifs found in the promoter regions of Zn regulatory genes, such as the ZIPs, resulting in their upregulation and initiating the Zn-deficiency response of the plant.

In the present study, the role of the previously unstudied group F bZIPs in wheat has been investigated. A bioinformatics analysis of the wheat genome (Chapter 3) identified seven group F *TabZIPs*, each with three homeologs. This is an improvement on the previous analysis undertaken by Li et al. (2015b), where only six of the seven *TabZIPs* were identified and incomplete homeolog sets identified were reported as individual *TabZIPs*. A conservation of the general bZIP domain was revealed across the group F bZIPs (see Figure 3.5). The two cysteine-histidine rich group F bZIP motifs predicted by Jakoby et al. (2002) were also conserved, though to a lesser degree across the group F *TabZIPs* identified. Gene-expression analyses showed that all four of the *TabZIPs* investigated (*TabZIP1*, *3a*, *3b* and *4*) are Zn-regulated (Chapter 3). Upregulation varied between the *TabZIPs* examined, with *TabZIP1* being consistently less

upregulated than the other three *TabZIPs* tested. Previously Assunção et al. (2010), similarly reported a minor upregulation of both *AtbZIP19* and *AtbZIP23* occurring during Zn deficiency. This upregulation does not entirely support the existing Zn-deficiency regulation model however there are three adaptations to this model that may explain the upregulation of *TabZIPs* observed. Firstly, a feedback loop that causes upregulation of *bZIPs* after Zn-deficiency is sensed may be present in order to increase the speed of downstream Zn-responsive gene upregulation and perhaps respond faster to Zn-deficiency. Secondly, it may be that there is an upstream signalling pathway a level higher than the *bZIPs* that senses Zn-deficiency and brings about a transcriptional response of both *bZIPs* and *ZIPs*. Lastly it is possible that certain *bZIPs* (notably the less Zn-deficiency induced members, such as *TabZIP1*) are ‘master regulators’ of the other *bZIPs*.

Four *TabZIP* homeologs were cloned and investigated using an *Arabidopsis* complementation approach (Chapter 5). Both *TabZIP1-7DL* and *TabZIP4-7AL* were shown to provide a good level of rescue to the *Arabidopsis bzip19-4 bzip23-2* mutant in response to Zn-deficiency, indicating they are able to bind to the promoter regions of key *Arabidopsis* Zn-responsive genes allowing upregulation. *TabZIP3b-7BL* and *TabZIP4-7DL* (both lacking the group F motif 1), were unable to complement the mutant to the same extent. The binding ability of these *TabZIPs* to the ZDREs identified in the promoter regions of the *TaZIPs* was tested using EMSAs (Chapter 5). Results showed that *TabZIP1-7DL* was able to bind to a range of probes containing ZDRE sequences found in the promoters of *TaZIP1*, 4, 5 and 7 as well as *AtZIP4*. *TabZIP3b-7BL*, *TabZIP4-7AL* and *TabZIP4-7DL* showed a complete lack of binding ability to the *TaZIP* ZDRE containing probes.

When examined in combination, the results allow an adaptation to the existing Zn-regulatory model to be proposed, specifically in relation to wheat. Certain *TabZIPs* (*TabZIP1* for example) may act as ‘master regulators’ of other *TabZIPs*. This may allow fine tuning responses to different levels of Zn-deficiency to be achieved. Homeologs of *TabZIPs* (such as *TabZIP3a*, *3b* and *4*) which are unable to bind to a selection of ZDREs (as shown in EMSAs), unable to rescue the *Atbzip19-4 bzip23-2* mutant (*TabZIP4-7AL* is an exception) and contain less conserved group F motifs (notably *TabZIP3b-7BL* and *TabZIP4-7DL*) may be the first response in bringing about wheat Zn-deficiency responses. If the group F motifs are proven to be the Zn-binding site, having less conserved motifs may lower the Zn-binding affinity compared to those with conserved motifs; the ‘master regulator’ *TabZIPs*. It is suggested that Zn²⁺ ions will dissociate from these less conserved motifs at a lower cellular Zn concentration than those bound to *TabZIP1* for example. This may allow an initial response of a select number of Zn-response genes to be upregulated at moderate Zn-deficiency. *TabZIP4-7AL* was able to rescue the *Atbzip19bzip23* mutant, yet did not bind to any probes presented in the EMSA, suggesting it has a more selective

binding pattern than TabZIP1-7DL. This may allow a limited and specific set of genes to be upregulated at a moderate level of Zn-deficiency (Figure 7.1).

In contrast, *TabZIP1* upregulation was noted to be lower in response to Zn-deficiency compared to *TabZIPs 3a, 3b* and *4*. *TabZIP1-7DL* also rescued the *Atbzip19-4 bzip23-2* to the greatest extent and bound to a range of ZDRE containing probes. The group F motifs are more conserved in *TabZIP1* homeologs to AtbZIP19 and 23, particularly when compared to *TabZIP3b-7BL* and *TabZIP4-7DL*. This conservation may provide a higher affinity between this TabZIP and Zn²⁺. If this is the case Zn²⁺ ions may not dissociate and render this TabZIP conformationally active until lower cytosolic Zn concentrations are reached; such as those occurring under a more severe Zn-deficiency regime. At this point the global upregulation of a large suite of Zn-responsive genes would be advantageous, and *TabZIP1* may upregulate other *TabZIPs* by an as yet unknown mechanism. This may explain the lower level of *TabZIP1* upregulation compared to other *TabZIPs* examined. These adaptations to the existing model allow for a response to moderate Zn-deficiency to be included and also provide an explanation for the upregulation of group F *TabZIPs* in response to Zn-deficiency as reported in this study.

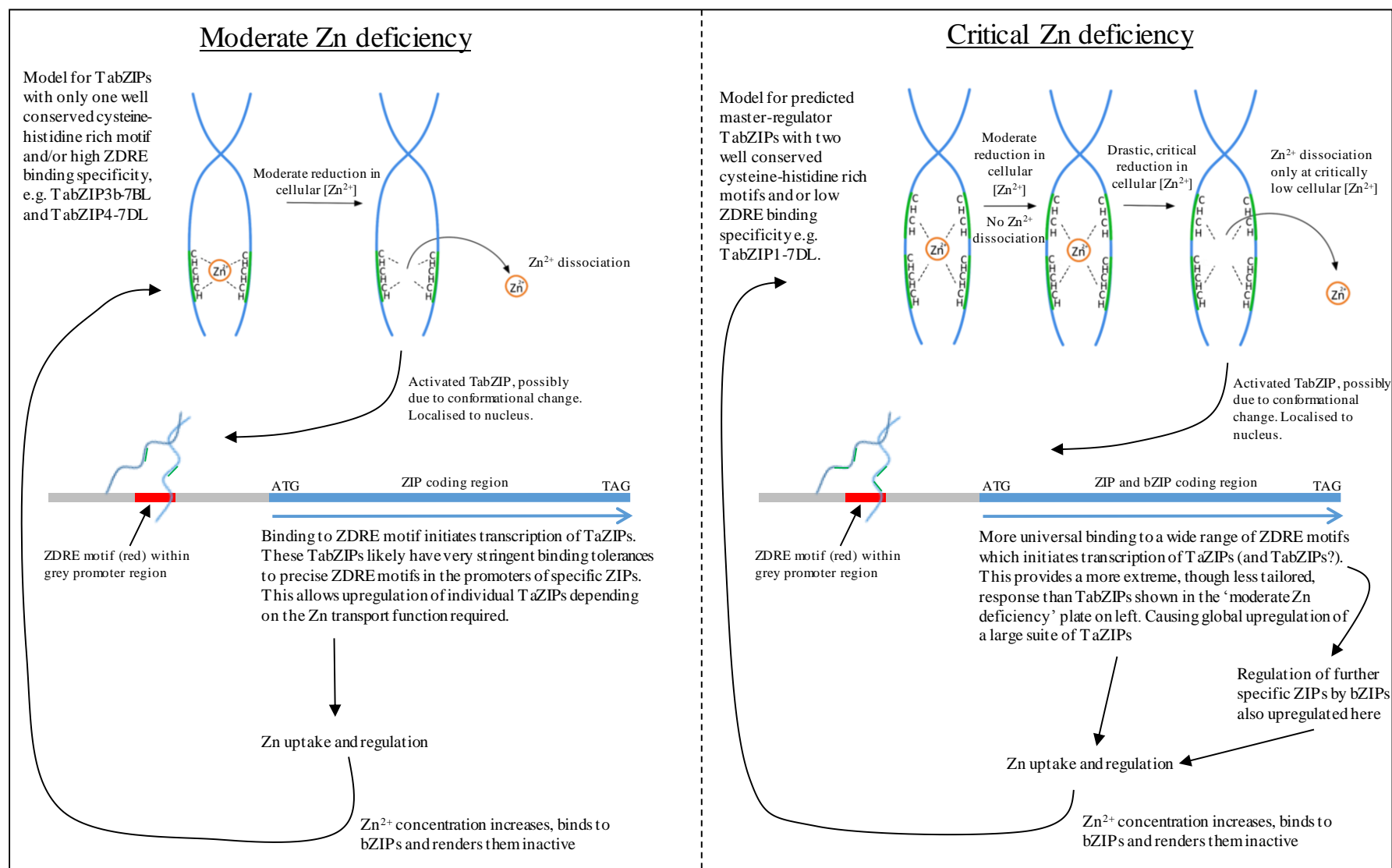


Figure 7.1. Model of Zn-regulation in wheat (*T. aestivum*). Schematics representing the response to moderate and critical Zn deficiency in *T. aestivum* mediated by group F TabZIPs.

7.4 The prospects for future research and wheat improvement

The importance of both *TaZIPs* and *TabZIPs* with regards to Zn regulation has been reported in this thesis. Overall, the results presented in this study provide a good foundation for further characterisation of the wheat Zn regulatory mechanism. Potential areas for future research are as follows:

Gene expression analyses

Undertaking further gene expression analysis of the *TaZIPs* and *TabZIPs* identified in Chapter 3, but not studied in this thesis, to determine if upregulation occurs across all genes identified will be valuable. Notably, their regulation at an intermediate Zn-deficiency treatment may provide further understanding of their role in Zn-regulation. In addition, an assessment of tissue specificity of expression is required, for example assessing gene expression at specific longitudinal root zones or more precise shoot locations such as the stem, nodes or individual leaves. Furthermore, gene expression analyses of individual homeologs may be useful to identify important alleles, although this may prove difficult for some genes, due to the conservation of sequences across homeologs. Also, additional genes should be examined in the material from the comparative hydroponic experiment of the Watkins lines WC239 and WC789 as currently only *TaZIP1* and *TabZIP1* have been assessed.

Localisation studies

In situ hybridization could be used to identify the specific plant location of both *TaZIP* and *TabZIP* expression. Information of the roles of individual *TaZIPs* may be identified using this technique, for instance which *TaZIPs* are involved in translocation from the root to the shoot and which are involved directly in Zn uptake from the rhizosphere. Additionally, overlap in expression location between *TabZIPs* and *TaZIPs* may further conclusions made on interactions of specific *TabZIPs* with *TaZIP* promoters. Also, cellular localisation studies using GFP tags downstream of full length *TaZIPs* and *TabZIPs* in yeast, wheat or *Arabidopsis* expression vectors would allow expression and subsequent cellular localisation to be determined in yeast cells, wheat cells or *Arabidopsis* protoplasts.

TaZIP characterisation

To supplement the yeast heterologous expression studies detailed in Chapter 4, a Mn uptake mutant yeast strain (such as *smf1/smf2*) could be tested for rescue ability when transformed with the *TaZIPs*. Additionally, further Fe-dependent strains could be assessed to confirm the lack of rescue observed by the *TaZIPs* in the *fet3/fet4* Fe-uptake yeast mutant. Point mutations that alter residues identified in Chapter 4 as being different between the closely related, yet

differentially performing, TaZIP5-2BL and TaZIP8-2BS (notably the HGAISS amino acid sequence between TMs III and IV) would allow an assessment of how this region changes transport ability between TaZIPs and may provide useful information.

Cloning *TaZIPs* from differentially performing (in relation to Zn uptake and utilisation) wheat lines, such as those identified in the WISP donor germplasm and comparing amino acid sequences of homologs would be an effective approach to determine if evolutionary divergence exists between alleles in different wheat lines that explains the differential performance. Cloning *TaZIP1*, 5 and 8 from Watkins line WC239 would be a good start as the QTL analysis of the Paragon x WC239 mapping population revealed a QTL on chromosome 2D associated with grain Zn uptake and homeologs of these three *TaZIPs* have been identified on this chromosome. By comparing the amino acid translations of the *TaZIPs* between cv. Paragon (already cloned in this study) and WC239 (as well as other wheat lines suggested in Chapter 6), the roles of *TaZIPs* in the differential Zn uptake and partitioning parameters exhibited by these lines would be further understood.

TabZIP characterisation

Cloning additional *TabZIPs* and transforming the *Arabidopsis bzip19bzip23* mutant line will allow further assessment of their importance in the Zn regulatory network in wheat. Additionally, mutating residues in the group F motif and comparing *bzip19bzip23* rescue ability with non-mutated *TabZIPs* may allow the importance of these motifs in Zn sensing and binding to be further analysed. A wheat RNAi approach to silence key *TabZIPs* identified and characterised, notably *TabZIP1* homeologs may prove worthwhile. Finally, assessing sequence differences between *TabZIPs* cloned from additional wheat lines that show different Zn uptake levels and relating this to observed field Zn performance may be useful.

Wheat improvement strategies

Given the evidence discovered so far, several opportunities to develop wheat lines with improved tolerance to Zn-deficient soils and/or enhanced Zn concentrations may be tested. Firstly, the constitutive overexpression of *TabZIPs*, notably *TabZIP1* should be tested, assessing performance under both Zn-deficient and replete conditions, gene expression analyses of *TaZIPs* and mineral nutrient capture (especially Zn and Cd) of developed lines will need to be evaluated. Additionally, the constitutive, as well as endosperm targeted, overexpression of identified and characterised *TaZIPs* (*TaZIP1*, 5, 6, 7 and 8) should be tested. If differences in amino acid sequences are found to exist in *TaZIPs* and *TabZIPs* between varieties, with differential Zn uptake and partitioning parameters, specific genes could be bred into modern elite cultivars, or genetic transformation approaches used in an attempt to incorporate this genetic potential into modern high-yielding varieties. Emerging genome editing technologies may also prove valuable for

integrating the genetic potential that exists throughout wheat germplasm in an effort to develop wheat cultivars with enhanced Zn uptake, partitioning as well as tolerance to Zn-deficient soils.

7.5 Conclusion

Human Zn-deficiency is an issue of global concern and may be addressed through biofortification strategies of widely consumed crop species, such as wheat (Chapter 1). The identification of genes underlying Zn uptake and partitioning in wheat is an important contribution to future Zn biofortification approaches. Zn-responsive, *TaZIP* membrane transporters were identified and shown to transport Zn (Chapters 3 and 4). Additionally, genetic regulators of these *TaZIPs* were identified; group F *TabZIPs* were shown to play a similar role in wheat as the homologs *AtbZIP19* and *AtbZIP23* do in the Zn-regulatory mechanism of *Arabidopsis*. Members of the group F *TabZIPs* bind to specific elements in the promoters of *TaZIPs* causing upregulation in response to Zn-deficiency (Chapter 5). Wheat lines with consistently varied Zn uptake and partitioning were identified within a diverse germplasm collection. Expression patterns of *TaZIP1* and *TabZIP1* did not explain their differential Zn performance (Chapter 6). To ascertain how these *TaZIPs* and *TabZIPs* contribute to differential Zn uptake and partitioning, further investigation of gene expression patterns and allelic variation is required. This study represents an important and original contribution to understanding the Zn-regulatory network of wheat.

References

- Abreu, I.A. and Cabelli, D.E.** (2010). Superoxide dismutases: A review of the metal-associated mechanistic variations. *Biochim. Biophys. Acta* **1804**: 263–274.
- Allen, A.M. et al.** (2011). Transcript-specific, single-nucleotide polymorphism discovery and linkage analysis in hexaploid bread wheat (*Triticum aestivum* L.). *Plant Biotechnol. J.* **9**: 1086–1099.
- Alloway, B.J.** (2008). Zinc in Soils and Crop Nutrition Second Edi. (IZA: Brussels, Belgium).
- Alves, M.S., Dadalto, S.P., Gonçalves, A.B., De Souza, G.B., Barros, V.A., and Fietto, L.G.** (2013). Plant bZIP transcription factors responsive to pathogens: a review. *Int. J. Mol. Sci.* **14**: 7815–7828.
- Andreini, C., Banci, L., Bertini, I., and Rosato, A.** (2006a). Counting the zinc-proteins encoded in the human genome. *J. Proteome Res.* **5**: 196–201.
- Andreini, C., Banci, L., Bertini, I., and Rosato, A.** (2006b). Zinc through the three domains of life. *J. Proteome Res.* **5**: 3173–3178.
- Arrivault, S., Senger, T., and Krämer, U.** (2006). The *Arabidopsis* metal tolerance protein AtMTP3 maintains metal homeostasis by mediating Zn exclusion from the shoot under Fe deficiency and Zn oversupply. *Plant J.* **46**: 861–879.
- Aschner, J.L. and Aschner, M.** (2005). Nutritional aspects of manganese homeostasis. *Mol. Aspects Med.* **26**: 353–362.
- Assunção, A.G.L., Herrero, E., Lin, Y., Huettel, B., Talukdar, S., and Smaczniak, C.** (2010). *Arabidopsis thaliana* transcription factors bZIP19 and bZIP23 regulate the adaptation to zinc deficiency. *Proc. Natl. Acad. Sci. U. S. A.* **107**: 10296–10301.
- Assunção, A.G.L., Martins, P.D.A.C., Folter, S.D.E., Vooijs, R., Schat, H., and Aarts, M.G.M.** (2001). Elevated expression of metal transporter genes in three accessions of the metal hyperaccumulator *Thlaspi caerulescens*. *Plant, Cell Environ.* **24**: 217–226.
- Assunção, A.G.L., Persson, D.P., Husted, S., Schjørring, J.K., Alexander, R.D., and Aarts, M.G.M.** (2013). Model of how plants sense zinc deficiency. *Metallomics* **5**: 1110–1116.
- Astudillo, C., Fernandez, A.C., Blair, M.W., and Cichy, K.** (2013). The *Phaseolus vulgaris* ZIP gene family: identification, characterization, mapping, and gene expression. *Front. Plant Sci.* **4**: 1–14.
- Axelsen, K.B. and Palmgren, M.G.** (1998). Evolution of substrate specificities in the P-type ATPase superfamily. *J. Mol. Evol.* **46**: 84–101.
- Bagci, S.A., Ekiz, H., Yilmaz, A., and Cakmak, I.** (2007). Effects of zinc deficiency and drought on grain yield of field-grown wheat cultivars in Central Anatolia. *J. Agron. Crop*

References

- Sci. **193**: 198–206.
- Baker, A.J.M. and Proctor, J.** (1990). The influence of cadmium, copper, lead, and zinc on the distribution and evolution of metallophytes in the British Isles. *Plant Syst. Evol.* **173**: 91–108.
- Banziger, M. and Long, J.** (2000). The potential for increasing the iron and zinc density of maize through plant-breeding. *Food Nutr. Bull.* **21**: 397–400.
- Baqui, A.H.** (2002). Effect of zinc supplementation started during diarrhoea on morbidity and mortality in Bangladeshi children: community randomised trial. *BMJ* **325**: 1059–1059.
- Barber, S.** (1995). *Soil Nutrient Bioavailability* (John Wiley and Sons: New York).
- Bartel, D.P.** (2004). MicroRNAs: Genomics, biogenesis, mechanism, and function. *Cell* **116**: 281–297.
- Bashir, K., Ishimaru, Y., and Nishizawa, N.K.** (2012). Molecular mechanisms of zinc uptake and translocation in rice. *Plant Soil* **361**: 189–201.
- Bashir, K., Takahashi, R., Nakanishi, H., and Nishizawa, N.K.** (2013). The road to micronutrient biofortification of rice: progress and prospects. *Front. Plant Sci.* **4**: 1–7.
- Bhatnagar, S. et al.** (2012). Zinc as adjunct treatment in infants aged between 7 and 120 days with probable serious bacterial infection: a randomised, double-blind, placebo-controlled trial. *Lancet* **379**: 2072–2078.
- Black, R.E. et al.** (1999). Prevention of diarrhea and pneumonia by zinc supplementation in children in developing countries: pooled analysis of randomized controlled trials. *J. Pediatr.*: 689–697.
- Black, R.E., Allen, L.H., Bhutta, Z.A., Caulfield, L.E., de Onis, M., Ezzati, M., Mathers, C., and Rivera, J.** (2008). Maternal and child undernutrition: global and regional exposures and health consequences. *Lancet* **371**: 243–260.
- Brennan, R.F.** (1992). The effect of zinc fertilizer on take-all and the grain yield of wheat grown on zinc-deficient soils of the Esperance region, Western Australia. *Fertil. Res.* **31**: 215–219.
- Brinch-Pedersen, H., Hatzack, F., Stöger, E., Arcalis, E., Pontopidan, K., and Holm, P.B.** (2006). Heat-stable phytases in transgenic wheat (*Triticum aestivum* L.): deposition pattern, thermostability, and phytate hydrolysis. *J. Agric. Food Chem.* **54**: 4624–4632.
- Brown, K.H., Hambidge, K.M., and Ranum, P.** (2010). Zinc fortification of cereal flours: current recommendations and research needs. *Food Nutr. Bull.* **31**: 62–74.
- Brown, P., Cakmak, I., and Zhang, Q.** (1993). Form and function of zinc in plants. In *Zinc in Soils and Plants*, K.A. Publishers, ed (Dordrecht, The Netherlands), pp. 93–106.
- Bughio, N., Yamaguchi, H., Nishizawa, N.K., Nakanishi, H., and Mori, S.** (2002). Cloning an iron-regulated metal transporter from rice. *J. Exp. Bot.* **53**: 1677–1682.

- Buttriss, J.** (2000). Nutrient requirements and optimisation of intakes. *Br. Med. Bull.* **56**: 18–33.
- Cakmak, I.** (2008). Enrichment of cereal grains with zinc: agronomic or genetic biofortification? *Plant Soil* **302**: 1–17.
- Cakmak, I.** (2000). Possible roles of zinc in protecting plant cells from damage by reactive oxygen species. *New Phytol.* **146**: 185–205.
- Cakmak, I. and Marschner, H.** (1988). Increase in membrane permeability and exudation in roots of zinc deficient plants. *J. Plant Physiol.* **132**: 356–361.
- Cakmak, I. and Marschner, H.** (1989). Mechanism of phosphorus-induced zinc deficiency in cotton. I. Zinc deficiency-enhanced uptake rate of phosphorus. *Physiol. Plant.* **68**: 483–490.
- Cakmak, I., Sari, N., Marschner, H., Ekiz, H., Kalayci, M., Yilmaz, A., and Braun, H.J.** (1996a). Phytosiderophore release in bread and durum wheat genotypes differing in zinc efficiency. *Plant Soil* **180**: 183–189.
- Cakmak, I., Torun, A., Millet, E., Feldman, M., Fahima, T., Korol, A., and Nevo, E.** (2004). *Triticum dicoccoides* : an important genetic resource for increasing zinc and iron concentration in modern cultivated wheat. *Soil Sci. Plant Nutr.* **50**: 1047–1054.
- Cakmak, I., Yilmaz, A., Kalayci, M., Ekiz, H., Torun, B., Erenoglu, B., and Braun, H.J.** (1996b). Zinc deficiency as a critical problem in wheat production in Central Anatolia. *Plant Soil* **180**: 165–172.
- Caulfield, L.E., de Onis, M., Blössner, M., and Black, R.E.** (2004). Undernutrition as an underlying cause of child deaths associated with diarrhea, pneumonia, malaria, and measles. *Am. J. Clin. Nutr.* **80**: 193–198.
- Chen, W., Yang, X., He, Z., Feng, Y., and Hu, F.** (2008). Differential changes in photosynthetic capacity, 77 K chlorophyll fluorescence and chloroplast ultrastructure between Zn-efficient and Zn-inefficient rice genotypes (*Oryza sativa*) under low zinc stress. *Physiol. Plant.* **132**: 89–101.
- Cheng, L., Wang, F., Shou, H., Huang, F., Zheng, L., He, F., Li, J., Zhao, F.-J., Ueno, D., Ma, J.F., and Wu, P.** (2007). Mutation in nicotianamine aminotransferase stimulated the Fe(II) acquisition system and led to iron accumulation in rice. *Plant Physiol.* **145**: 1647–1657.
- Chou, K.C. and Shen, H.B.** (2010). Plant-mPLOC: A top-down strategy to augment the power for predicting plant protein subcellular localization. *PLoS One* **5**: e11335.
- Claus, J. and Chavarría-Krauser, A.** (2012). Modeling regulation of zinc uptake via ZIP transporters in yeast and plant roots. *PLoS One* **7**: e37193.
- Clough, S.J. and Bent, A.F.** (1998). Floral dip: A simplified method for *Agrobacterium*-

References

- mediated transformation of *Arabidopsis thaliana*. *Plant J.* **16**: 735–743.
- Colangelo, E.P. and Guerinot, M.L.** (2004). The essential basic helix-loop-helix protein FIT1 is required for the iron deficiency response. *Plant Cell* **16**: 3400–3412.
- Collins, J.F. and Klevay, L.M.** (2011). Nutrient information: Copper. *Adv. Nutr.* **2**: 520–522.
- Conklin, D., McMaster, J., Culbertson, M., and Kung, C.** (1992). COT1, a gene involved in cobalt accumulation in *Saccharomyces cerevisiae*. *Mol. Cell. Biol.* **12**: 3678–3688.
- Cook, J.D., Skikne, B.S., Lynch, S.R., Reusser, M.E., Lynch, S.R., and Skikne, B.S.** (1986). Estimates of iron sufficiency in the US population. *Blood* **68**: 726–731.
- Corrêa, L.G.G., Riaño-Pachón, D.M., Schrago, C.G., dos Santos, R.V., Mueller-Roeber, B., and Vincentz, M.** (2008). The role of bZIP transcription factors in green plant evolution: adaptive features emerging from four founder genes. *PLoS One* **3**: e2944.
- Curtis, M.D. and Grossniklaus, U.** (2003). A Gateway cloning vector set for high-throughput functional analysis of genes in planta. *Plant Physiol.* **133**: 462–469.
- Davletova, S., Schlauch, K., Coutu, J., and Mittler, R.** (2005). The zinc-finger protein Zat12 plays a central role in reactive oxygen and abiotic stress signaling in *Arabidopsis*. *Plant Physiol.* **139**: 847–856.
- Demirezen, D. and Uruç, K.** (2006). Comparative study of trace elements in certain fish, meat and meat products. *Meat Sci.* **74**: 255–60.
- Desbrosses-Fonrouge, A.-G., Voigt, K., Schröder, A., Arrivault, S., Thomine, S., and Krämer, U.** (2005). *Arabidopsis thaliana* MTP1 is a Zn transporter in the vacuolar membrane which mediates Zn detoxification and drives leaf Zn accumulation. *FEBS Lett.* **579**: 4165–4174.
- Distelfeld, A., Cakmak, I., Peleg, Z., Ozturk, L., Yazici, A.M., Budak, H., Saranga, Y., and Fahima, T.** (2007). Multiple QTL-effects of wheat Gpc-B1 locus on grain protein and micronutrient concentrations. *Physiol. Plant.* **129**: 635–643.
- Dix, D.R., Bridgham, J.T., Broderius, M.A., Byersdorfer, C.A., and Eide, D.J.** (1994). The FET4 gene encodes the low affinity Fe(II) transport protein of *Saccharomyces cerevisiae*. *J. Biol. Chem.* **269**: 26092–26099.
- Drew, M.C. and Saker, L.R.** (1984). Uptake and long-distance transport of phosphate, potassium and chloride in relation to internal ion concentrations in barley; evidence of non-allosteric regulation. *Planta* **160**: 500–507.
- Duchateau, J., Delepesse, G., Vrijens, R., and Collet, H.** (1981). Beneficial effects of oral zinc supplementation on the immune response of old people. *Am. J. Med.* **70**: 1001–1004.
- Durmaz, E., Coruh, C., Dinler, G., Grusak, M.A., Peleg, Z., Saranga, Y., Fahima, T., Yazici, A., Ozturk, L., Cakmak, I., and Budak, H.** (2011). Expression and cellular localization of ZIP1 transporter under zinc deficiency in wild emmer wheat. *Plant Mol.*

- Biol. **29**: 582–596.
- Eckardt, N.A.** (2001). Move it on out with MATEs. *Plant Cell* **13**: 1477–1480.
- Eckhardt, U., Mas Marques, A., and Buckhout, T.J.** (2001). Two iron-regulated cation transporters from tomato complement metal uptake-deficient yeast mutants. *Plant Mol. Biol.* **45**: 437–448.
- Edgar, R.C.** (2004). MUSCLE: Multiple sequence alignment with high accuracy and high throughput. *Nucleic Acids Res.* **32**: 1792–1797.
- Eide, D., Broderius, M., Fett, J., and Guerinot, M.L.** (1996). A novel iron-regulated metal transporter from plants identified by functional expression in yeast. *Proc. Natl. Acad. Sci. U. S. A.* **93**: 5624–5628.
- Eide, D.J.** (2005). The ZIP Family of Zinc Transporters. In *Zinc Finger Proteins* (Landes Bioscience and Kluwer Academic), pp. 261–264.
- Erenoglu, B., Eker, S., Cakmak, I., Derici, R., and Römheld, V.** (2000). Effect of iron and zinc deficiency on release of phytosiderophores in barley cultivars differing in zinc efficiency. *J. Plant Nutr.* **23**: 1645–1656.
- Fan, M.-S.S., Zhao, F.-J.J., Fairweather-Tait, S.J., Poulton, P.R., Dunham, S.J., and McGrath, S.P.** (2008). Evidence of decreasing mineral density in wheat grain over the last 160 years. *J. Trace Elem. Med. Biol.* **22**: 315–24.
- FAO, IFAD, and WFP** (2015). *The State of Food Insecurity in the World: Meeting the 2015 international hunger targets: taking stock of uneven progress.*
- FAO and WHO** (2001a). *Codex Alimentarius Commission, Report of the thirty-third session of the Codex Committee on Food additives and Contaminants.*
- FAO and WHO** (2001b). *Human Vitamin and Mineral Requirements.*
- Farooq, M., Wahid, A., and Siddique, K.H.M.** (2012). Micronutrient application through seed treatments - a review. *J. Soil Sci. Plant Nutr.* **12**: 125–142.
- Foley, J. et al.** (2011). Solutions for a cultivated planet. *Nature* **478**: 337–342.
- Franco-Zorrilla, J.M., López-Vidriero, I., Carrasco, J.L., Godoy, M., Vera, P., and Solano, R.** (2014). DNA-binding specificities of plant transcription factors and their potential to define target genes. *Proc. Natl. Acad. Sci. U. S. A.* **111**: 2367–2372.
- Gainza-Cortés, F., Pérez-Díaz, R., Pérez-Castro, R., Tapia, J., Casaretto, J. a, González, S., Peña-Cortés, H., Ruiz-Lara, S., and González, E.** (2012). Characterization of a putative grapevine Zn transporter, VvZIP3, suggests its involvement in early reproductive development in *Vitis vinifera* L. *BMC Plant Biol.* **12**: 111–121.
- Gaither, L.A. and Eide, D.J.** (2000). Functional expression of the human hZIP2 zinc transporter. *J. Biol. Chem.* **275**: 5560–5564.
- Garnett, T. et al.** (2013). *Sustainable Intensification in Agriculture: Premises and Policies.* Sci.

References

- Mag. **341**: 33–34.
- Garvin, D.F., Welch, R.M., and Finley, J.W.** (2006). Historical shifts in the seed mineral micronutrient concentration of US hard red winter wheat germplasm. *J. Sci. Food Agric.* **86**: 2213–2220.
- Genc, Y., Verbyla, A.P., Torun, A.A., Cakmak, I., Willmore, K., Wallwork, H., and McDonald, G.K.** (2009). Quantitative trait loci analysis of zinc efficiency and grain zinc concentration in wheat using whole genome average interval mapping. *Plant Soil* **314**: 49–66.
- Ghaffar, S.H. and Fan, M.** (2015). Revealing the morphology and chemical distribution of nodes in wheat straw. *Biomass and Bioenergy* **77**: 123–134.
- Giglione, C., Serero, A., Pierre, Á., and Boisson, B.** (2000). Identification of eukaryotic peptide deformylases reveals universality of N - terminal protein processing mechanisms. *EMBO J.* **19**: 5916–5929.
- Glover-Cutter, K.M., Alderman, S.C., Dombrowski, J.E., and Martin, R.C.** (2014). Enhanced Oxidative Stress Resistance through Activation of a Zinc Deficiency Transcription Factor in *Brachypodium distachyon*. *Plant Physiol.* **166**: 1492–1505.
- Godfray, H.C.J., Beddington, J.R., Crute, I.R., Haddad, L., Lawrence, D., Muir, J.F., Pretty, J., Robinson, S., Thomas, S.M., and Toulmin, C.** (2010). Food security: the challenge of feeding 9 billion people. *Science* (80-.). **327**: 812–818.
- Goos, R.J., Johnson, B.E., and Thiollet, M.** (2000). A comparison of the availability of three zinc sources to maize (*Zea mays* L.) under greenhouse conditions. *Biol. Fertil. Soils* **31**: 343–347.
- Graham, R., Senadhira, D., Beebe, S., Iglesias, C., and Monasterio, I.** (1999). Breeding for micronutrient density in edible portions of staple food crops: conventional approaches. *F. Crop. Res.* **60**: 57–80.
- Graham, R., Welch, R., Saunders, D., Ortiz-Monasterio, I., Bouis, H., and Twomlow, S.** (2007). Nutritious Subsistence Food Systems. In *Advances in Agronomy*, pp. 1–73.
- Gregorio, G.B.** (2002). Progress in breeding for trace minerals in staple crops. *J. Nutr.* **8**: 500–502.
- Gregorio, G.B., Senadhira, D., Htut, H., and Graham, R.D.** (2000). Breeding for trace mineral density in rice. *Food Nutr. Bull.* **21**: 382–386.
- Grotz, N., Fox, T., Connolly, E., Park, W., Guerinot, M.L., and Eide, D.** (1998). Identification of a family of zinc transporter genes from *Arabidopsis* that respond to zinc deficiency. *Proc. Natl. Acad. Sci. U. S. A.* **95**: 7220–7224.
- Guerinot, M.L.** (2000). The ZIP family of metal transporters. *Biochim. Biophys. Acta* **1465**: 190–198.

- Guo, J., Bai, P., Yang, Q., Liu, F., Wang, X., Huang, L., and Kang, Z.** (2013). Wheat zinc finger protein TaLSD1, a negative regulator of programmed cell death, is involved in wheat resistance against stripe rust fungus. *Plant Physiol. Biochem.* **71**: 164–172.
- Guzmán, C., Medina-Larqué, A.S., Velu, G., González-Santoyo, H., Singh, R.P., Huerta-Espino, J., Ortiz-Monasterio, I., and Peña, R.J.** (2014). Use of wheat genetic resources to develop biofortified wheat with enhanced grain zinc and iron concentrations and desirable processing quality. *J. Cereal Sci.* **60**: 617–622.
- Hacisalihoglu, G., Hart, J.J., and Kochian, L. V** (2001). High- and low-affinity zinc transport systems and their possible role in zinc efficiency in bread wheat. *Plant Physiol.* **125**: 456–463.
- Hacisalihoglu, G., Hart, J.J., Wang, Y., Cakmak, I., and Kochian, L. V** (2003). Zinc efficiency is correlated with enhanced expression and activity of zinc-requiring enzymes in wheat. *Plant Physiol.* **131**: 595–602.
- Haldar, M. and Mandal, L.** (1979). Influence of soil moisture regimes and organic matter application on the extractable Zn and Cu content in rice soils. *Plant Soil* **213**: 203–213.
- Hall, T., Biosciences, I., and Carlsbad, C.** (2011). BioEdit: An important software for molecular biology. *GERF Bull. Biosci.* **2**: 60–61.
- Hambidge, K.M., Krebs, N.F., Westcott, J.L., Sian, L., Miller, L. V, Peterson, K.L., and Raboy, V.** (2005). Absorption of calcium from tortilla meals prepared from low-phytate maize. *Am. J. Clin. Nutr.* **82**: 84–87.
- Harvestplus** (2010). HarvestPlus Statement on the Potential Benefits of Biofortification on the Nutritional Status of Populations.
- Haydon, M.J., Kawachi, M., Wirtz, M., Hillmer, S., Hell, R., and Krämer, U.** (2012). Vacuolar nicotianamine has critical and distinct roles under iron deficiency and for zinc sequestration in *Arabidopsis*. *Plant Cell* **24**: 724–737.
- Heglund, J.N., Pedas, P., Schiller, M., Husted, S.S., Schjoerring, J.K., Schiller, M., and Schjoerring, J.K.** (2010). Zinc fluxes into the developing barley grain: use of stable Zn isotopes to separate root uptake from remobilization in plants with contrasting Zn status. *Plant Soil* **361**: 241–250.
- Hell, R. and Stephan, U.W.** (2003). Iron uptake, trafficking and homeostasis in plants. *Planta* **216**: 541–551.
- Hess, S.Y., Lönnerdal, B., Hotz, C., Rivera, J.A., and Brown, K.H.** (2009). Recent advances in knowledge of zinc nutrition and human health. *Food Nutr. Bull.* **30**: 5–11.
- Hotz, C. and Brown, K.H.** (2004). Contents International Zinc Nutrition Consultative Group (IZiNCG) Technical Document # 1 Assessment of the Risk of Zinc Deficiency in Populations and Options for Its Control (United Nations University Press).

References

- Hu, H. and Sparks, D.** (1991). Zinc deficiency inhibits chlorophyll synthesis and gas exchange in “Stuart” pecan. *HortScience* **26**: 267–268.
- Huang, C., Barker, S.J., Langridge, P., Smith, F.W., and Graham, R.D.** (2000). Zinc deficiency up-regulates expression of high-affinity phosphate transporter genes in both phosphate-sufficient and -deficient barley roots. *Plant Physiol.* **124**: 415–422.
- Huang, L., Drake, V., and Ho, E.** (2015). Nutrient information: Zinc. *Adv. Nutr.* **6**: 224–226.
- Huff, J., Keung, Y., Thakuri, M., Beaty, M., Hurd, M., Owen, J., and Molnair, I.** (2007). Copper deficiency causes reversible myelodysplasia. *Am. J. Hematol.* **82**: 625–630.
- Hurrell, R.F.** (1997). Preventing iron deficiency through food fortification. *Nutr. Rev.* **55**: 210–222.
- Hurst, H.C.** (1995). Transcription factors 1: bZIP proteins. *Protein Profile* **2**: 101–168.
- Hussain, D., Haydon, M.J., Wang, Y., Wong, E., Sherson, S.M., Young, J., Camakaris, J., Harper, J.F., and Cobbett, C.S.** (2004). P-Type ATPase Heavy Metal Transporters with Roles in Essential Zinc Homeostasis in *Arabidopsis*. *Plant Cell* **16**: 1327–1339.
- Inaba, S., Kurata, R., Kobayashi, M., Yamagishi, Y., Mori, I., Ogata, Y., and Fukao, Y.** (2015). Identification of putative target genes of bZIP19, a transcription factor essential for *Arabidopsis* adaptation to Zn deficiency in roots. *Plant J.* **84**: 323–334.
- Ishimaru, Y. et al.** (2006). Rice plants take up iron as an Fe³⁺-phytosiderophore and as Fe²⁺. *Plant J.* **45**: 335–346.
- Ishimaru, Y., Suzuki, M., Kobayashi, T., Takahashi, M., Nakanishi, H., Mori, S., and Nishizawa, N.K.** (2005). OsZIP4, a novel zinc-regulated zinc transporter in rice. *J. Exp. Bot.* **56**: 3207–3214.
- Islam, F.M.A., Basford, K.E., Jara, C., Redden, R.J., and Beebe, S.** (2002). Seed compositional and disease resistance differences among gene pools in cultivated common bean. *Genet. Resour. Crop Evol.* **49**: 285–293.
- IWGSC** (2014). A chromosome-based draft sequence of the hexaploid bread wheat (*Triticum aestivum*) genome. *Science* (80-.). **345**: 1–11.
- Jain, A., Sinilal, B., Dhandapani, G., Meagher, R.B., and Sahi, S. V** (2013). Effects of deficiency and excess of zinc on morphophysiological traits and spatiotemporal regulation of zinc-responsive genes reveal incidence of cross talk between micro- and macronutrients. *Environ. Sci. Technol.* **47**: 5327–5335.
- Jakoby, M., Weisshaar, B., Dröge-Laser, W., Vicente-Carbajosa, J., Tiedemann, J., Kroj, T., and Parcy, F.** (2002). bZIP transcription factors in *Arabidopsis*. *Trends Plant Sci.* **7**: 106–111.
- Jones, H.D.** (2005). Wheat transformation: current technology and applications to grain development and composition. *J. Cereal Sci.* **41**: 137–147.

- Jones, R., Oughan, H., Thomas, H., and Waaland, S.** (2013). *The Molecular Life of Plants* (Wiley-Blackwell).
- Joy, E.J.M., Ahmad, W., Zia, M.H., Kumssa, D.B., Young, S.D., Ander, E.L., Watts, M.J., Stein, A.J., and Broadley, M.R.** (2016). Valuing increased zinc (Zn) fertiliser-use in Pakistan. *Plant Soil*.
- Joy, E.J.M., Stein, A.J., Young, S.D., Ander, E.L., Watts, M.J., and Broadley, M.R.** (2015). Zinc-enriched fertilisers as a potential public health intervention in Africa.: 1–24.
- Kavitha, P., Kuruvilla, S., and Mathew, M.** (2015). Functional characterization of a transition metal ion transporter, OsZIP6 from rice (*Oryza sativa* L.). *Plant Physiol. Biochem.* **97**: 165–174.
- Kawachi, M., Kobae, Y., Mori, H., Tomioka, R., Lee, Y., and Maeshima, M.** (2009). A mutant strain *Arabidopsis thaliana* that lacks vacuolar membrane zinc transporter MTP1 revealed the latent tolerance to excessive zinc. *Plant Cell Physiol.* **50**: 1156–1170.
- Kearse, M. et al.** (2012). Geneious Basic: An integrated and extendable desktop software platform for the organization and analysis of sequence data. *Bioinformatics* **28**: 1647–1649.
- Kobayashi, T., Itai, R.N., Aung, M.S., Senoura, T., Nakanishi, H., and Nishizawa, N.K.** (2012). The rice transcription factor IDEF1 directly binds to iron and other divalent metals for sensing cellular iron status. *Plant J.* **69**: 81–91.
- Kobayashi, T., Itai, R.N., Ogo, Y., Kakei, Y., Nakanishi, H., Takahashi, M., and Nishizawa, N.K.** (2009). The rice transcription factor IDEF1 is essential for the early response to iron deficiency, and induces vegetative expression of late embryogenesis abundant genes. *Plant J.* **60**: 948–961.
- Kobayashi, T., Nakayama, Y., Itai, R.N., Nakanishi, H., Yoshihara, T., Mori, S., and Nishizawa, N.K.** (2003). Identification of novel cis-acting elements, IDE1 and IDE2, of the barley IDS2 gene promoter conferring iron-deficiency-inducible, root-specific expression in heterogeneous tobacco plants. *Plant J.* **36**: 780–793.
- Kobayashi, T. and Nishizawa, N.K.** (2012). Iron uptake, translocation, and regulation in higher plants. *Annu. Rev. Plant Biol.* **63**: 131–152.
- Kobayashi, T., Ogo, Y., Aung, M.S., Nozoye, T., Itai, R.N., Nakanishi, H., Yamakawa, T., and Nishizawa, N.K.** (2010). The spatial expression and regulation of transcription factors IDEF1 and IDEF2. *Ann. Bot.* **105**: 1109–1117.
- Kobayashi, T., Ogo, Y., Itai, R.N., Nakanishi, H., Takahashi, M., Mori, S., and Nishizawa, N.K.** (2007). The transcription factor IDEF1 regulates the response to and tolerance of iron deficiency in plants. *Proc. Natl. Acad. Sci. U. S. A.* **104**: 19150–19155.
- Kong, W.W. and Yang, Z.M.** (2010). Identification of iron-deficiency responsive microRNA

References

- genes and cis-elements in *Arabidopsis*. *Plant Physiol. Biochem.* **48**: 153–159.
- Korshunova, Y.O., Eide, D., Clark, W.G., Guerinot, M.L., and Pakrasi, H.B.** (1999). The IRT1 protein from *Arabidopsis thaliana* is a metal transporter with a broad substrate range. *Plant Mol. Biol.* **40**: 37–44.
- Kumssa, D.B., Joy, E.J.M., Ander, E.L., Watts, M.J., Young, S.D., Walker, S., and Broadley, M.R.** (2015). Dietary calcium and zinc deficiency risks are decreasing but remain prevalent. *Sci. Rep.* **5**: 1–11.
- Kutman, B., Cakmak, I., Pfeiffer, W.H., and McClafferty, B.** (2010). Biofortification of durum wheat with zinc through soil and foliar applications of nitrogen. *Cereal Chem.* **87**: 10–20.
- Lasswell, J., Rogg, L.E., Nelson, D.C., Rongey, C., and Bartel, B.** (2000). Cloning and characterization of IAR1, a gene required for auxin conjugate sensitivity in *Arabidopsis*. *Plant Cell* **12**: 2395–2408.
- Lee, S., Jeong, H.J., Kim, S.A., Lee, J., Guerinot, M. Lou, and An, G.** (2010a). OsZIP5 is a plasma membrane zinc transporter in rice. *Plant Mol. Biol.* **73**: 507–517.
- Lee, S., Kim, S.A., Lee, J., Guerinot, M. Lou, and An, G.** (2010b). Zinc deficiency-inducible OsZIP8 encodes a plasma membrane-localized zinc transporter in rice. *Mol. Cells* **29**: 551–558.
- Levine, M. and Tijan, R.** (2003). Transcription regulation and animal diversity. *Nature* **424**: 147–151.
- Li, S., Zhou, X., Chen, J., and Chen, R.** (2016). Is there a strategy I iron uptake mechanism in maize? *Plant Signal. Behav.*: Advance online publication. DOI: 10.1080/15592324.
- Li, S., Zhou, X., Huang, Y., Zhu, L., Zhang, S., Zhao, Y., Guo, J., Chen, J., and Chen, R.** (2013). Identification and characterization of the zinc-regulated transporters, iron-regulated transporter-like protein (ZIP) gene family in maize. *BMC Plant Biol.* **13**: 1–14.
- Li, S., Zhou, X., Li, H., Liu, Y., Zhu, L., Guo, J., Liu, X., Fan, Y., Chen, J., and Chen, R.** (2015a). Overexpression of ZmIRT1 and ZmZIP3 enhances iron and zinc accumulation in transgenic *Arabidopsis*. *PLoS One* **10**: e0136647.
- Li, X., Gao, S., Tang, Y., Li, L., Zhang, F., Feng, B., Fang, Z., Ma, L., and Zhao, C.** (2015b). Genome-wide identification and evolutionary analyses of bZIP transcription factors in wheat and its relatives and expression profiles of anther development related TabZIP genes. *BMC Genomics* **16**: 1–21.
- Liang, J., Han, B., Han, L., Nout, M.J.R., and Hamer, R.J.** (2007). Iron, zinc and phytic acid content of selected rice varieties from China. *J. Sci. Food Agric.* **510**: 504–510.
- Lin, Y.F., Liang, H.M., Yang, S.Y., Boch, A., Clemens, S., Chen, C.C., Wu, J.F., Huang, J.L., and Yeh, K.C.** (2009). *Arabidopsis* IRT3 is a zinc-regulated and plasma membrane

- localized zinc/iron transporter. *New Phytol.* **182**: 392–404.
- Ling, H.Q., Bauer, P., Berczky, Z., Keller, B., and Ganai, M.** (2002). The tomato fer gene encoding a bHLH protein controls iron-uptake responses in roots. *Proc. Natl. Acad. Sci. U. S. A.* **99**: 13938–13943.
- Liu, H., Wang, Z.H., Li, F., Li, K., Yang, N., Yang, Y., Huang, D., Liang, D., Zhao, H., Mao, H., Liu, J., and Qiu, W.** (2014). Grain iron and zinc concentrations of wheat and their relationships to yield in major wheat production areas in China. *F. Crop. Res.* **156**: 151–160.
- Liu, X. and Chu, Z.** (2015). Genome-wide evolutionary characterization and analysis of bZIP transcription factors and their expression profiles in response to multiple abiotic stresses in *Brachypodium distachyon*. *BMC Genomics* **16**: 1–15.
- Lombardi-Boccia, G., Lanzi, S., and Aguzzi, A.** (2005). Aspects of meat quality: trace elements and B vitamins in raw and cooked meats. *J. Food Compos. Anal.* **18**: 39–46.
- Lombnaes, P. and Singh, B.R.** (2003). Varietal tolerance to zinc deficiency in wheat and barley grown in chelator-buffered nutrient solution and its effect on uptake of Cu, Fe, and Mn. *J. Plant Nutr. Soil Sci.* **166**: 76–83.
- Loneragan, J., Grunes, D., Welch, R., Aduayi, E., Tengah, A., Lazar, V., and Cary, E.** (1982). Phosphorous accumulation and toxicity in relation to zinc supply. *Soil Sci. Soc. Am. J.* **46**: 345–352.
- Lucca, P., Hurrell, R., and Potrykus, I.** (2001). Genetic engineering approaches to improve the bioavailability and the level of iron in rice grains. *Theor. Appl. Genet.* **102**: 392–397.
- MacDiarmid, C.W., Milanick, M.A., and Eide, D.J.** (2003). Induction of the ZRC1 metal tolerance gene in zinc-limited yeast confers resistance to zinc shock. *J. Biol. Chem.* **278**: 15065–15072.
- Macnair, M.R., Bert, V., Huitson, S.B., Saumitou-Laprade, P., and Petit, D.** (1999). Zinc tolerance and hyperaccumulation are genetically independent characters. *Proc. Biol. Sci.* **266**: 2175–2179.
- Maidment, J.M., Moore, D., Murphy, G.P., Murphy, G., and Clark, I.** (1999). Matrix metalloproteinase homologues from *Arabidopsis thaliana*. Expression and activity. *J. Biol. Chem.* **274**: 34706–34710.
- Maret, W.** (2009). Molecular aspects of human cellular zinc homeostasis: redox control of zinc potentials and zinc signals. *Biometals* **22**: 149–157.
- Maret, W.** (2013). Zinc biochemistry: from a single zinc enzyme to a key element of life. *Adv. Nutr.* **4**: 82–91.
- Marino, G. and Funk, C.** (2012). Matrix metalloproteinases in plants: A brief overview. *Physiol. Plant.* **145**: 196–202.

References

- Marschner, H.** (1995). *Mineral Nutrition of Higher Plants* (Academic Press: London).
- Marschner, H. and Cakmak, I.** (1989). High light intensity enhances chlorosis and necrosis in leaves of Zn, K and Mg deficient bean plants. *J. Plant Physiol.* **138**: 308–315.
- Marschner, H. and Romheld, V.** (1994). Strategies of plants for acquisition of iron. *Plant Soil* **165**: 261–274.
- Martelli, A, Rousset, E., Dycke, C., Bouron, A., and Moulis, J.-M.** (2006). Cadmium toxicity in animal cells by interference with essential metals. *Biochimie* **88**: 1807–1814.
- Martens, D. and Westerman, D.** (1991). Fertilizer application for correcting micronutrient deficiencies. In *Micronutrients in Agriculture* (Soil Science of America, Madison), pp. 89–112.
- Maziya-Dixon, B., Kling, J.G., Menkir, A., and Dixon, A.** (2000). Genetic variation in total carotene, iron, and zinc contents of maize and cassava genotypes. *Food Nutr. Bull.* **21**: 419–422.
- McDermid, J. and Lonnerdal, B.** (2012). Nutrient information: Iron. *Adv. Nutr.* **3**: 532–533.
- Menguer, P.K., Farthing, E., Peaston, K., Ricachenevsky, F.K., Fett, J.P., and Williams, L.E.** (2013). Functional analysis of the rice vacuolar zinc transporter OsMTP1. *J. Exp. Bot.* **64**: 2871–2883.
- Meriardi, M., Caulfield, L.E., Zavaleta, N., Figueroa, A., and DiPietro, J.A.** (1999). Adding zinc to prenatal iron and folate tablets improves fetal neurobehavioral development. *Am. J. Obstet. Gynecol.* **180**: 483–490.
- Miller, T., Ambrose, M., and Reader, S.** (2001). The Legacy of John Percival. In *The Legacy of John Percival*, P. Caligari and P. Brandham, eds (Academic Press: London), pp. 113–120.
- Mills, R.F., Francini, A., Ferreira Da Rocha, P.S.C., Baccarini, P.J., Aylett, M., Krijger, G.C., and Williams, L.E.** (2005). The plant P1B-type ATPase AtHMA4 transports Zn and Cd and plays a role in detoxification of transition metals supplied at elevated levels. *FEBS Lett.* **579**: 783–791.
- Mills, R.F., Krijger, G.C., Baccarini, P.J., Hall, J.L., and Williams, L.E.** (2003). Functional expression of AtHMA4, a P1B-type ATPase of the Zn/Co/Cd/Pb subclass. *Plant J.* **35**: 164–176.
- Mills, R.F., Peaston, K., Runions, J., and Williams, L.E.** (2012). HvHMA2, a P(1B)-ATPase from barley, is highly conserved among cereals and functions in Zn and Cd transport. *PLoS One* **7**: e42640.
- Milner, M., Seamon, J., Craft, E., and Kochain, L.** (2013). Transport properties of members of the ZIP family in plants and their role in Zn and Mn homeostasis. *J. Exp. Bot.* **64**: 369–381.

- Monasterio, I. and Graham, R.D.** (2010). Breeding for trace minerals in wheat. *Food Nutr. Bull.* **21**: 392–396.
- Moore, P.A. and Patrick, W.H.** (1988). Effect of zinc deficiency on alcohol dehydrogenase activity and nutrient uptake in rice. *Agron. J.* **80**: 882–885.
- Moreau, S., Thomson, R.M., Kaiser, B.N., Trevaskis, B., Guerinot, M.L., Udvardi, M.K., Puppo, A., and Day, D.A.** (2002). GmZIP1 encodes a symbiosis-specific zinc transporter in soybean. *J. Biol. Chem.* **277**: 4738–4746.
- Morgounov, A., Gómez-Becerra, H.F., Abugalieva, A., Dzhunusova, M., Yessimbekova, M., Muminjanov, H., Zelenskiy, Y., Ozturk, L., and Cakmak, I.** (2006). Iron and zinc grain density in common wheat grown in Central Asia. *Euphytica* **155**: 193–203.
- Moursi, M.** (2015). Efficacy and other nutrition evidence for zinc crops. In *The 2nd Global Conference on Biofortification: Getting Nutritious Foods to People*, pp. 37–38.
- Murashige, T. and Skoog, F.** (1962). A revised medium for rapid growth and bio assays with Tobacco tissue cultures. *Physiol. Plant.* **15**: 473–497.
- Neal, A.L., Geraki, K., Borg, S., Quinn, P., Mosselmans, J.F., Brinch-Pedersen, H., and Shewry, P.R.** (2013). Iron and zinc complexation in wild-type and ferritin-expressing wheat grain: implications for mineral transport into developing grain. *J. Biol. Inorg. Chem.* **18**: 557–570.
- Nijhawan, A., Jain, M., Tyagi, A.K., and Khurana, J.P.** (2008). Genomic survey and gene expression analysis of the basic leucine zipper transcription factor family in rice. *Plant Physiol.* **146**: 333–350.
- Norvell, W.A. and Welch, R.M.** (1993). Growth and nutrient uptake by barley (*Hordeum vulgare* L. cv Herta). *Plant Physiol.* **101**: 619–625.
- Nozoye, T., Nagasaka, S., Kobayashi, T., Takahashi, M., Sato, Y., Sato, Y., Uozumi, N., Nakanishi, H., and Nishizawa, N.K.** (2011). Phytosiderophore efflux transporters are crucial for iron acquisition in graminaceous plants. *J. Biol. Chem.* **286**: 5446–5454.
- Ogo, Y., Itai, R.N., Kobayashi, T., Aung, M.S., Nakanishi, H., and Nishizawa, N.K.** (2011). OsIRO2 is responsible for iron utilization in rice and improves growth and yield in calcareous soil. *Plant Mol. Biol.* **75**: 593–605.
- Ogo, Y., Itai, R.N., Nakanishi, H., Inoue, H., Kobayashi, T., Suzuki, M., Takahashi, M., Mori, S., and Nishizawa, N.K.** (2006). Isolation and characterization of IRO2, a novel iron-regulated bHLH transcription factor in graminaceous plants. *J. Exp. Bot.* **57**: 2867–2878.
- Ogo, Y., Itai, R.N., Nakanishi, H., Kobayashi, T., Takahashi, M., Mori, S., and Nishizawa, N.K.** (2007). The rice bHLH protein OsIRO2 is an essential regulator of the genes involved in Fe uptake under Fe-deficient conditions. *Plant J.* **51**: 366–377.

References

- Ohki, K.** (1976). Effect of zinc nutrition on photosynthesis and carbonic anhydrase activity in cotton. *Physiol. Plant.* **38**: 300–304.
- Olmos, S., Distelfeld, A., Chicaiza, O., Schlatter, A.R., Fahima, T., Echenique, V., and Dubcovsky, J.** (2003). Precise mapping of a locus affecting grain protein content in durum wheat. *Theor. Appl. Genet.* **107**: 1243–1251.
- Olsen, L.I. et al.** (2016). Mother-plant-mediated pumping of zinc into the developing seed. *Nat. Plants* **2**: 1–6.
- Olsen, L.I. and Palmgren, M.G.** (2014). Many rivers to cross: the journey of zinc from soil to seed. *Front. Plant Sci.* **5**: 1–6.
- Oparak, K. and Gates, P.** (1984). Sink anatomy in relation to solute movement in rice (*Oryza sativa* L.): A summary of findings. *Plant Growth Regul.* **307**: 297–307.
- Oury, F.-X., Leenhardt, F., Révész, C., Chanliaud, E., Duperrier, B., Balfourier, F., and Charmet, G.** (2006). Genetic variability and stability of grain magnesium, zinc and iron concentrations in bread wheat. *Eur. J. Agron.* **25**: 177–185.
- Ozturk, L., Yazici, M.A., Yucel, C., Torun, A., Cekic, C., Bagci, A., Ozkan, H., Braun, H.-J., Sayers, Z., and Cakmak, I.** (2006). Concentration and localization of zinc during seed development and germination in wheat. *Physiol. Plant.* **128**: 144–152.
- Pace, N. and Weerapana, E.** (2014). Zinc-Binding Cysteines: Diverse Functions and Structural Motifs. *Biomolecules* **4**: 419–434.
- Palmgren, M.G., Clemens, S., Williams, L.E., Krämer, U., Borg, S., Schjørring, J.K., and Sanders, D.** (2008). Zinc biofortification of cereals: problems and solutions. *Trends Plant Sci.* **13**: 464–473.
- Parr, R.M. and Fjeld, C.R.** (1994). Human health and nutrition: how isotopes are helping to overcome “hidden hunger.” *IAEA Bull.* **4**: 18–27.
- Paterson, J., Berndt, G., Cameron, D., and Rowbottom, W.** (1991). Investigation into the response of barley to applied zinc. *J. Sci. Food Agric.* **54**: 387–392.
- Patrick, J.W. and Offler, C.E.** (1996). Post-sieve element transport of photoassimilates in sink regions. *J. Exp. Bot.* **47**: 1165–1177.
- Pedas, P., Schjoerring, J.K., and Husted, S.** (2009). Identification and characterization of zinc-starvation-induced ZIP transporters from barley roots. *Plant Physiol. Biochem.* **47**: 377–383.
- Pedas, P., Ytting, C.K., Fuglsang, A.T., Jahn, T.P., Schjoerring, J.K., and Husted, S.** (2008). Manganese efficiency in barley: identification and characterization of the metal ion transporter HvIRT1. *Plant Physiol.* **148**: 455–466.
- Pennington, J. and Young, B.** (1990). Iron, zinc, copper, manganese, selenium, and iodine in foods from the United States total diet study. *J. Food Compos. Anal.* **3**: 166–184.

- Pilon, M., Cohu, C.M., Ravet, K., Abdel-Ghany, S.E., and Gaymard, F.** (2009). Essential transition metal homeostasis in plants. *Curr. Opin. Plant Technol.* **12**: 347–357.
- Pineau, C., Loubet, S., Lefoulon, C., Chalies, C., Fizames, C., Lacombe, B., Ferrand, M., Loudet, O., Berthomieu, P., and Richard, O.** (2012). Natural variation at the FRD3 MATE transporter locus reveals cross-talk between Fe homeostasis and Zn tolerance in *Arabidopsis thaliana*. *PLoS Genet.* **8**: e1003120.
- Pinto, E. and Ferreira, I.** (2015). Cation transporters/channels in plants: tools for nutrient biofortification. *J. Plant Physiol.* **179**: 64–82.
- Podar, D., Scherer, J., Noordally, Z., Herzyk, P., Nies, D., and Sanders, D.** (2012). Metal selectivity determinants in a family of transition metal transporters. *J. Biol. Chem.* **287**: 3185–3196.
- Pourabed, E., Ghane Golmohamadi, F., Soleymani Monfared, P., Razavi, S.M., and Shobbar, Z.S.** (2015). Basic leucine zipper family in barley: genome-wide characterization of members and expression analysis. *Mol. Biotechnol.* **57**: 12–26.
- Prask, J.A. and Plocke, D.J.** (1971). A role for zinc in the structural integrity of the cytoplasmic ribosomes of *Euglena gracilis*. *Plant Physiol.* **48**: 150–155.
- Public Health England** (2014). National Diet and Nutrition Survey Results from Years 1 , 2 , 3 and 4 (combined) of the Rolling Programme (2008/2009-2011/2012) Executive Summary.
- Ramesh, S.A., Choimes, S., and Schachtman, D.P.** (2004). Over-expression of an *Arabidopsis* zinc transporter in *Hordeum vulgare* increases short-term zinc uptake after zinc deprivation and seed zinc content. *Plant Mol. Biol.* **54**: 373–385.
- Ramesh, S.A., Shin, R., Eide, D.J., and Schachtman, D.P.** (2003). Differential metal selectivity and gene expression of two zinc transporters from rice. *Plant Physiol.* **133**: 126–134.
- Randall, P.J. and Bouma, D.** (1973). Zinc deficiency, carbonic anhydrase, and photosynthesis in leaves of spinach. *Plant Physiol.* **52**: 229–232.
- Rao, P.S., Mishra, B., and Gupta, S.R.** (2013). Effects of soil salinity and alkalinity on grain quality of tolerant, semi-tolerant and sensitive rice genotypes. *Rice Sci.* **20**: 284–291.
- Rayman, M.P.** (2000). The importance of selenium to human health. *Lancet* **356**: 233–241.
- Reeves, J.C., Chiapparino, E., Donini, M., Ganal, M., Guiard, J., Hamrit, S., Malysheva, L., Melchinger, A., and Orf, S.** (2004). Changes over time in the genetic diversity of four major European crops: a report from the Gediflux Framework 5 project (Tulin-Austria).
- Remy, E., Cabrito, T.R., Batista, R.A., Hussein, M.A.M., Teixeira, M.C., Athanasiadis, A., Sá-Correia, I., and Duque, P.** (2014). Intron retention in the 5' UTR of the novel ZIF2 transporter enhances translation to promote zinc tolerance in *Arabidopsis*. *PLoS Genet.* **10**: 15–19.

References

- Rengel, Z.** (1999a). Physiological responses of wheat genotypes grown in chelator-buffered nutrient solutions with increasing concentrations of excess HEDTA. *Plant Soil* **215**: 193–202.
- Rengel, Z.** (1999b). Zinc deficiency in wheat genotypes grown in conventional and chelator-buffered nutrient solutions. *Plant Sci.* **143**: 221–230.
- Rengel, Z. and Graham, R.D.** (1995a). Importance of seed Zn content for wheat growth on Zn-deficient soil I. Vegetative growth. *Plant Soil* **173**: 259–266.
- Rengel, Z. and Graham, R.D.** (1995b). Wheat genotypes differ in Zn efficiency when grown in chelate-buffered nutrient solution. *Plant Soil* **176**: 307–316.
- Ricachenevsky, F.K., Menguer, P.K., Sperotto, R.A., Williams, L.E., and Fett, J.P.** (2013). Roles of plant metal tolerance proteins (MTP) in metal storage and potential use in biofortification strategies. *Front. Plant Sci.* **4**: 1–16.
- Ricachenevsky, F.K. and Sperotto, R.A.** (2014). There and back again, or always there? The evolution of rice combined strategy for Fe uptake. *Front. Plant Sci.* **5**: 1–5.
- Richter, S. and Lamppa, G.K.** (2003). Structural properties of the chloroplast stromal processing peptidase required for its function in transit peptide removal. *J. Biol. Chem.* **278**: 39497–39502.
- Riechmann, J.L.** (2000). *Arabidopsis* transcription factors: genome-wide comparative analysis among eukaryotes. *Science.* **290**: 2105–2110.
- Rieu, I. and Powers, S.J.** (2009). Real-time quantitative RT-PCR: design, calculations, and statistics. *Plant Cell* **21**: 1031–1033.
- Robinson, N.J., Procter, C.M., Connolly, E.L., and Guerinot, M.L.** (1999). A ferric-chelate reductase for iron uptake from soils. *Nature* **397**: 694–697.
- Rogers, E.E., Eide, D.J., and Guerinot, M.L.** (2000). Altered selectivity in an *Arabidopsis* metal transporter. *Proc. Natl. Acad. Sci. U. S. A.* **97**: 12356–12360.
- Rozema, J. and Flowers, T.** (2008). Crops for a salinized world. *Science* (80-.). **322**: 1478–1480.
- Ruel, M.T., Rivera, J.A., Santizo, M.-C., Lonnerdal, B., and Brown, K.H.** (1997). Impact of zinc supplementation on morbidity from diarrhea and respiratory infections among rural Guatemalan children. *Pediatrics* **99**: 808–813.
- Ruijter, J.M., Ramakers, C., Hoogaars, W.M.H., Karlen, Y., Bakker, O., Van Den Hoff, M.J.B., and Moorman, A.F.M.** (2009). Amplification efficiency: linking baseline and bias in the analysis of quantitative PCR data. *Nucleic Acids Res.* **37**: e45.
- Rutherford, J.C., Jaron, S., Ray, E., Brown, P.O., and Winge, D.R.** (2001). A second iron-regulatory system in yeast independent of Aft1p. *Proc. Natl. Acad. Sci. U. S. A.* **98**: 14322–14327.

- Sadeghzadeh, B. and Rengel, Z.** (2011). Zinc in Soils and Crop Nutrition. In *The Molecular and Physiological Basis of Nutrient Use Efficiency in Crops*, M. Hawkesford and P. Barraclough, eds (John Wiley and Sons), pp. 335–375.
- Salt, D.E., Prince, R.C., Baker, A.J.M., Raskin, I., and Pickering, I.J.** (1999). Zinc ligands in the metal hyperaccumulator *Thlaspi caerulescens* as determined using X-ray absorption spectroscopy. *Environmental Sci. Technol.* **33**: 713–717.
- Sandmann, G. and Boger, P.** (1983). The enzymatological function of heavy metals and their role in electron transfer processes of plants. In *Encyclopedia of Plant Physiology*, New Series, Springer-Verlag, ed (Berlin and New York), pp. 563–593.
- Sasaki, A., Yamaji, N., Mitani-Ueno, N., Kashino, M., and Ma, J.F.** (2015). A node-localized transporter OsZIP3 is responsible for the preferential distribution of Zn to developing tissues in rice. *Plant J.* **84**: 374–384.
- Satoh-Nagasawa, N., Mori, M., Nakazawa, N., Kawamoto, T., Nagato, Y., Sakurai, K., Takahashi, H., Watanabe, A., and Akagi, H.** (2012). Mutations in rice (*Oryza sativa*) heavy metal ATPase 2 (OsHMA2) restrict the translocation of zinc and cadmium. *Plant Cell Physiol.* **53**: 213–224.
- Schaaf, G., Ludewig, U., Erenoglu, B.E., Mori, S., Kitahara, T., and von Wirén, N.** (2004). ZmYS1 functions as a proton-coupled symporter for phytosiderophore- and nicotianamine-chelated metals. *J. Biol. Chem.* **279**: 9091–9096.
- Shankar, A., Genton, B., Baisor, M., Paino, J., Tamja, S., Adiguma, T., Wu, L., Rare, L., Bannon, D., Tielsch, J., West KP, and Alpers, M.** (2000). The influence of zinc supplementation on morbidity due to *Plasmodium falciparum*: a randomized trial in preschool children in Papua New Guinea. *Am J Trop Med Hyg* **62**: 663–669.
- Sharma, P.N., Chatterjee, C., Agarwala, S.C., and Sharma, C.P.** (1990). Zinc deficiency and pollen fertility in maize (*Zea mays*). *Plant Soil* **124**: 221–225.
- Shewry, P.R., Pellny, T.K., and Lovegrove, A.** (2016). Is modern wheat bad for health? *Nat. Plants* **2**: 1–3.
- Shuman, L.M.** (1998). Micronutrient fertilizers. *J. Crop Prod.* **1**: 165–195.
- Siddiqui, I., Shaikat, S.S., and Hamid, M.** (2002). Role of zinc in *Rhizobacteria*-mediated suppression of root-infecting fungi and root-knot nematode. *J. Phytopathol.* **150**: 569–575.
- Sillanpää, M.** (1982). Micronutrients and the nutrient status of soils: a global study. *FAO soils Bull.* No. 48.
- Sinclair, S.A. and Krämer, U.** (2012). The zinc homeostasis network of land plants. *Biochim. Biophys. Acta* **1823**: 1553–1567.
- Singh, K.** (2002). Transcription factors in plant defense and stress responses. *Curr. Opin. Plant Biol.* **5**: 430–436.

References

- Somasundar, P., Riggs, D.R., Jackson, B.J., Cunningham, C., Vona-Davis, L., and McFadden, D.W.** (2005). Inositol hexaphosphate (IP6): a novel treatment for pancreatic cancer. *J. Surg. Res.* **126**: 199–203.
- Song, W.-Y., Choi, K.S., Kim, D.Y., Geisler, M., Park, J., Vincenzetti, V., Schellenberg, M., Kim, S.H., Lim, Y.P., Noh, E.W., Lee, Y., and Martinoia, E.** (2010). *Arabidopsis* PCR2 is a zinc exporter involved in both zinc extrusion and long-distance zinc transport. *Plant Cell* **22**: 2237–2252.
- Song, W.Y., Lee, H.S., Jin, S.R., Ko, D., Martinoia, E., Lee, Y., An, G., and Ahn, S.N.** (2015). Rice PCR1 influences grain weight and Zn accumulation in grains. *Plant, Cell Environ.* **38**: 2327–2339.
- Sparrow, D.H. and Graham, R.D.** (1988). Susceptibility of zinc-deficient wheat plants to colonization by *Fusarium graminearum* Schw. Group 1. *Plant Soil* **112**: 261–266.
- Strebel, O. and Duynisveld, W.H.M.** (1989). Nitrogen supply to cereals and sugar beet by mass flow and diffusion on a silty loam soil. *Z. Pflanzenernahr. Bodenk* **152**: 135–141.
- Streeter, T.C., Rengel, Z.Z., Graham, R.D., Neate, S.M., and Graham, R.D.** (2001). Zinc fertilisation increases tolerance to *Rhizoctonia solani* (AG 8) in *Medicago truncatula*. *Plant Soil* **228**: 233–242.
- Suzuki, M., Takahashi, M., Tsukamoto, T., Watanabe, S., Matsuhashi, S., Yazaki, J., Kishimoto, N., Kikuchi, S., Nakanishi, H., Mori, S., and Nishizawa, N.K.** (2006). Biosynthesis and secretion of mugineic acid family phytosiderophores in zinc-deficient barley. *Plant J.* **48**: 85–97.
- Suzuki, M., Tsukamoto, T., Inoue, H., Watanabe, S., Matsuhashi, S., Takahashi, M., Nakanishi, H., Mori, S., and Nishizawa, N.K.** (2008). Deoxymugineic acid increases Zn translocation in Zn-deficient rice plants. *Plant Mol. Biol.* **66**: 609–617.
- Talke, I.N.** (2006). Zinc-dependent global transcriptional control, transcriptional deregulation, and higher gene copy number for genes in metal homeostasis of the hyperaccumulator *Arabidopsis halleri*. *Plant Physiol.* **142**: 148–167.
- Tan, J., Wang, J., Chai, T., Zhang, Y., Feng, S., Li, Y., Zhao, H., Liu, H., and Chai, X.** (2013). Functional analyses of TaHMA2, a P(1B)-type ATPase in wheat. *Plant Biotechnol. J.* **11**: 420–431.
- Tauris, B., Borg, S., Gregersen, P.L., and Holm, P.B.** (2009). A roadmap for zinc trafficking in the developing barley grain based on laser capture microdissection and gene expression profiling. *J. Exp. Bot.* **60**: 1333–1347.
- Timmer, C.P.** (2003). Biotechnology and food systems in developing countries. *J. Nutr.* **133**: 3319–3322.
- Tinker, P. and Nye, P.** (2000). *Solute Movement in the Rhizosphere* (Oxford University Press).

- Tiong, J., McDonald, G., Genc, Y., Shirley, N., Langridge, P., and Huang, C.Y.** (2015). Increased expression of six ZIP family genes by zinc (Zn) deficiency is associated with enhanced uptake and root-to-shoot translocation of Zn in barley (*Hordeum vulgare*). *New Phytol.* **207**: 1097–1109.
- Tiong, J., McDonald, G.K., Genc, Y., Pedas, P., Hayes, J.E., Toubia, J., Langridge, P., and Huang, C.Y.** (2013). HvZIP7 mediates zinc accumulation in barley (*Hordeum vulgare*) at moderately high zinc supply. *New Phytol.* **201**: 131–143.
- Tusnády, G.E. and Simon, I.** (2001). The HMMTOP transmembrane topology prediction server. *Bioinformatics* **17**: 849–850.
- Uauy, C., Distelfeld, A., Fahima, T., Blechl, A., and Dubcovsky, J.** (2006). A NAC Gene regulating senescence improves grain protein, zinc, and iron content in wheat. *Science.* **314**: 1298–1301.
- Velu, G. et al.** (2012). Performance of biofortified spring wheat genotypes in target environments for grain zinc and iron concentrations. *Field Crop. Res.* **137**: 261–267.
- Velu, G., Ortiz-Monasterio, I., Singh, R.P., and Payne, T.** (2011). Variation for grain micronutrients concentration in wheat core-collection accessions of diverse origin. *Asian J. Crop Sci.* **3**: 43–48.
- Velu, G., Singh, R., Balasubramaniam, A., Mishra, V.K., Chand, R., Tiwari, C., Joshi, A., Virk, P., Cherian, B., and Pfeiffer, W.** (2015). Reaching out to farmers with high zinc wheat varieties through public-private partnerships – An experience from Eastern-Gangetic Plains of India. *Adv. Food Technol. Nutr. Sci.* **1**: 73–75.
- Verret, F., Gravot, A., Auroy, P., Leonhardt, N., David, P., Nussaume, L., Vavasseur, A., and Richaud, P.** (2004). Overexpression of AtHMA4 enhances root-to-shoot translocation of zinc and cadmium and plant metal tolerance. *FEBS Lett.* **576**: 306–312.
- Vert, G., Briat, J.F., and Curie, C.** (2001). *Arabidopsis* IRT2 gene encodes a root-periphery iron transporter. *Plant J.* **26**: 181–189.
- Vert, G., Grotz, N., Dedaldechamp, F., Gaymard, F., Guerinot, M., Briat, J., and Curie, C.** (2002). IRT1, an *Arabidopsis* transporter essential for iron uptake from the soil and for plant growth. *Plant Cell* **14**: 1223–1233.
- Verwoerd, T., Dekker, B., and Hoekema, A.** (1989). A small-scale procedure for the rapid isolation of plant RNAs. *Nucleic Acids Res.* **17**: 2362.
- Walker, E.L. and Connolly, E.L.** (2008). Time to pump iron: iron-deficiency-signaling mechanisms of higher plants. *Curr. Opin. Plant Biol.* **11**: 530–535.
- Wang, A.S., Angle, J.S., Chaney, R.L., Delorme, T. a., and Reeves, R.D.** (2006). Soil pH effects on uptake of Cd and Zn by *Thlaspi caerulescens*. *Plant Soil* **281**: 325–337.
- Wang, H., Offler, C.E., and Patrick, J.W.** (1994). The cellular pathway of photosynthate

References

- transfer in the developing wheat grain. II. A structural analysis and histochemical studies of the pathway from crease phloem to the endosperm cavity. *Plant, Cell Environ.* **18**: 378–388.
- Wang, L., Ying, Y., Narsai, R., Ye, L., Zheng, L., Tian, J., Whelan, J., and Shou, H.** (2013). Identification of OsbHLH133 as a regulator of iron distribution between roots and shoots in *Oryza sativa*. *Plant, Cell Environ.* **36**: 224–236.
- Wang, M., Xu, Q., Yu, J., and Yuan, M.** (2010). The putative *Arabidopsis* zinc transporter ZTP29 is involved in the response to salt stress. *Plant Mol. Biol.* **73**: 467–479.
- Waters, B.M. and Grusak, M.A.** (2008). Whole-plant mineral partitioning throughout the life cycle in *Arabidopsis thaliana* ecotypes Columbia, Landsberg erecta, Cape Verde Islands, and the mutant line ysl1ysl3. *New Phytol.* **177**: 389–405.
- Weaver, C. and Peacock, M.** (2011). Nutrient information: Calcium. *Adv. Nutr.* **2**: 290–292.
- Welch, R.M. and Graham, R.D.** (2004). Breeding for micronutrients in staple food crops from a human nutrition perspective. *J. Exp. Bot.* **55**: 353–364.
- Wenzel, A. and Mehlhorn, H.** (1995). Zinc deficiency enhances ozone toxicity in bush beans (*Phaseolus vulgaris* L. cv. Saxa). *J. Exp. Bot.* **46**: 867–872.
- Wessells, K.R. and Brown, K.H.** (2012). Estimating the global prevalence of zinc deficiency: results based on zinc availability in national food supplies and the prevalence of stunting. *PLoS One* **7**: e50568.
- White, P.J. and Broadley, M.R.** (2005). Biofortifying crops with essential mineral elements. *Trends Plant Sci.* **10**: 586–593.
- White, P.J. and Broadley, M.R.** (2011). Physiological limits to zinc biofortification of edible crops. *Front. Plant Sci.* **2**: 1–11.
- WHO** (2002). The World Health Report 2002.
- Von Wiren, N., Marschner, H., and Romheld, V.** (1996). Roots of iron-efficient maize also absorb phytosiderophore-chelated zinc. *Plant Physiol.* **111**: 1119–1125.
- Wu, J., Zhao, F.-J., Ghandilyan, A., Logoteta, B., Guzman, M.O., Schat, H., Wang, X., and Aarts, M.G.M.** (2009). Identification and functional analysis of two ZIP metal transporters of the hyperaccumulator *Thlaspi caerulescens*. *Plant Soil* **325**: 79–95.
- Xing, F., Fu, X., Wang, N., Xi, J., Huang, Y., Zhou, W., Ling, L., and Peng, L.** (2016). Physiological changes and expression characteristics of ZIP family genes under zinc deficiency in navel orange (*Citrus sinensis*). *J. Integr. Agric.* **15**: 803–811.
- Yada, S., Huang, G., and Lapsley, K.** (2013). Natural variability in the nutrient composition of California-grown almonds. *J. Food Compos. Anal.* **30**: 80–85.
- Yamaguchi, N., Ishikawa, S., Abe, T., Baba, K., Arao, T., and Terada, Y.** (2012). Role of the node in controlling traffic of cadmium, zinc, and manganese in rice. *J. Exp. Bot.* **63**:

2729–2737.

- Yamaji, N. and Ma, J.F.** (2014). The node, a hub for mineral nutrient distribution in graminaceous plants. *Trends Plant Sci.* **19**: 556–563.
- Yamaji, N., Xia, J., Mitani-Ueno, N., Yokosho, K., and Feng Ma, J.** (2013). Preferential delivery of zinc to developing tissues in rice is mediated by P-type heavy metal ATPase OsHMA2. *Plant Physiol.* **162**: 927–939.
- Yang, O., Popova, O. V., Süthoff, U., Lüking, I., Dietz, K.-J., and Gollack, D.** (2009a). The *Arabidopsis* basic leucine zipper transcription factor AtbZIP24 regulates complex transcriptional networks involved in abiotic stress resistance. *Gene* **436**: 45–55.
- Yang, X., Huang, J., Jiang, Y., and Zhang, H.S.** (2009b). Cloning and functional identification of two members of the ZIP (Zrt, Irt-like protein) gene family in rice (*Oryza sativa* L.). *Mol. Biol. Rep.* **36**: 281–287.
- Yilmaz, A., Ekiz, H., and Gültekin, I.** (1998). Effect of seed zinc content on grain yield and zinc concentration of wheat grown in zinc deficient calcareous soils. *J. Plant Nutr.* **21**: 2257–2264.
- Yu, Q. and Rengel, Z.** (1999). Micronutrient deficiency influences plant growth and activities of superoxide dismutases in narrow-leafed lupins. *Ann. Bot.* **83**: 175–182.
- Yuan, Y., Wu, H., Wang, N., Li, J., Zhao, W., Du, J., Wang, D., and Ling, H.-Q.** (2008). FIT interacts with AtbHLH38 and AtbHLH39 in regulating iron uptake gene expression for iron homeostasis in *Arabidopsis*. *Cell Res.* **18**: 385–397.
- Zeng, Z.-B.** (1994). Precision mapping of quantitative trait loci. *Genetics* **136**: 1457–1468.
- Zhang, W., Zhou, Y., Dibley, K.E., Tyerman, S.D., Furbank, R., and Patrick, J.W.** (2007). Nutrient loading of developing seeds. *Funct. Plant Biol.* **34**: 314–331.
- Zhang, Y., Xu, Y.H., Yi, H.Y., and Gong, J.M.** (2012). Vacuolar membrane transporters OsVIT1 and OsVIT2 modulate iron translocation between flag leaves and seeds in rice. *Plant J.* **72**: 400–410.
- Zhang, Y., Zhang, G., Xia, N., Wang, X.J., Huang, L.L., and Kang, Z.S.** (2008). Cloning and characterization of a bZIP transcription factor gene in wheat and its expression in response to stripe rust pathogen infection and abiotic stresses. *Physiol. Mol. Plant Pathol.* **73**: 88–94.
- Zhao, F.J., Su, Y.H., Dunham, S.J., Rakszegi, M., Bedo, Z., McGrath, S.P., and Shewry, P.R.** (2009). Variation in mineral micronutrient concentrations in grain of wheat lines of diverse origin. *J. Cereal Sci.* **49**: 290–295.
- Zhao, H. and Eide, D.** (1996a). The yeast ZRT1 gene encodes the zinc transporter protein of a high-affinity uptake system induced by zinc limitation. *Proc. Natl. Acad. Sci. U. S. A.* **93**: 2454–2458.

References

- Zhao, H. and Eide, D.** (1996b). The ZRT2 gene encodes the low affinity zinc transporter in *Saccharomyces cerevisiae*. *J. Biol. Chem.* **271**: 23203–23210.
- Zhao, J., Liu, M., Jiang, L., Ding, L., Yan, S.S., Zhang, J., Dong, Z., Ren, H., and Zhang, X.** (2014). Cucumber SUPERMAN has conserved function in stamen and fruit development and a distinct role in floral patterning. *PLoS One* **9**: e86192.
- Zheng, L., Ying, Y., Wang, L., Wang, F., Whelan, J., and Shou, H.** (2010). Identification of a novel iron regulated basic helix-loop-helix protein involved in Fe homeostasis in *Oryza sativa*. *BMC Plant Biol.* **10**: 1–9.